**CZECH UNIVERSITY OF LIFE SCIENCES PRAGUE**
**FACULTY OF TROPICAL AGRISCIENCES**
**Department of Sustainable Technologies**


# Dependence of briquettes quality on their structure and biomass material composition

Dissertation Thesis

**Author**: Ing. Veronika Chaloupková
**Chief supervisor:** doc. Ing. Tatiana Ivanova, PhD.
**Specialist supervisor:** doc. Ing. Vladimír Krepl, CSc.

Prague 2019

# Declaration

I hereby declare that I have done this Thesis entitled "Dependence of briquettes quality on their structure and biomass material composition" independently, all texts in the Thesis are original, and all the sources have been quoted and acknowledged by means of complete references and according to Citation rules of the FTA.

In Prague 23rd of August 2019

…….....

Veronika Chaloupková

# Acknowledgements

At this place I would like to thank to all persons and institutions that have helped me during the research and Thesis elaboration and throughout the whole PhD studies.

First and foremost, I would like to express my heartfelt appreciation to my supervisor doc. Ing. Tatiana Ivanova, Ph.D. who has overseen my work already from master studies. I would like to thank her very much for her time, significant help, sagacious advice and academic support throughout the research and Thesis completing. I highly appreciate the supervision of doc. Ing. Vladimír Krepl, CSc. and prof. Ing. Bohumil Havrland, CSc., as well.

My gratitude also goes to the Centre for the Development of Renewable Energy Sources (CEDER-CIEMAT) in Spain and its workers in the Laboratory of Biomass Characterization, namely Javier, María, Mari Carmen, Jaime, Yubero, Rocío and mainly Miguel Fernández Llorente, the head of the laboratory, for their time and opportunity to work on my research. Without their contributions I could never have realized this Thesis. The research experience in Spanish laboratory was enabled by the International Relation Office of FTA, where my acknowledgement goes as well, and its financial support through Erasmus+ Training Programme.

Special thanks go to Ing. Alexandru Muntean for his help with material preparation and prof. Ing. Milan Brožek, Csc. and Alexandra Nováková from the Faculty of Engineering (CULS) for the assistance with the testing of briquettes' mechanical quality. Further, I would like to heartily thank to Ing. Jan Vlček, Ph.D. from the University of Chemistry and Technology Prague (UCT), for his inestimable help with the macroscopic analysis and Research Institute of Agricultural Engineering (RIAE) for the opportunity to do material preparation.

And last but not least, my sincere gratitude is given to my family, especially to my great Mum, my dear Oscar and all friends for their patience, understanding and support throughout the whole PhD studies.

This research was also financially supported by the Internal Grant Agency of the Faculty of Tropical AgriSciences, Czech University of Life Sciences Prague, project numbers 20165012, 20175011, 20185011 and 20195010.

# Abstract

Improved knowledge about material properties together with process variables may enhance an efficiency of briquettes production and should bring densified products of higher quality with desired properties. The composition of the biomass and fraction size of a material to be pressed are key parameters in the process of densification that govern the formation of briquette structure, which has influence on the mechanical quality of produced solid biofuels. In this Thesis, the dependence of briquettes quality on their structure and material composition was investigated. The miscanthus, industrial hemp and pine sawdust, the representants of compositionally different biomass materials, were grinded by hammer mill into three differently sized test materials (4, 8 and 12 mm). Important input parameters - moisture content, particle size distribution and materials' bulk density were determined. Apart from the general particle size characterization done by traditional sieve analysis, the more precise approach – photo-optical analysis, considering the irregular shape of the biomass particles, was applied. Selected materials were pressed into the form of cylindrical briquettes by the hydraulic piston briquetting machine. The structure of briquettes was studied by microscopy and special software for image analysis to identify agglomeration and binding mechanisms and especially the locality concentration of larger particles. Effects of particle size as well as lignocellulosic structure (content of cellulose, hemicellulose and lignin) on the mechanical quality of final briquettes were evaluated. Complementary chemical analyses were included as well to present the main fuel properties of selected materials. Obtained data were summarized by descriptive statistics and the data from particle size measurement of the briquette cross-sections were tested by Kruskal-Wallis test. The results showed that there are statistically significant differences in the particle size on the briquette surface. In case of miscanthus and pine sawdust, larger particles are generally concentrated on the front side of briquettes and *vice versa* smaller are on the rear side as well as larger particles are centred in the briquette cross-sections and smaller particles are located on the briquette bottom. These two materials obtained the highest mechanical durability for the fraction 8 mm. On the other hand, the hemp briquettes exhibited more even size distribution of particles on the surface and reached greatly superior mechanical qualities for all fraction sizes, with the best results for 4 mm fraction. Mechanical quality was ensured by its fibrous nature and creation of inter-locking bonds, rather than by the content of lignin and its ability to excrete and form solid bridges during the densification, as it occurred in pine sawdust briquettes.

**Key words**: solid biofuels, agglomeration, bonding, macrostructure, particle size, image analysis, mechanical properties, durability, strength

# Content

# List of Tables

# List of Figures

# List of abbreviations

| | |
|---|---|
| BEC | Biomass Energy Centre |
| CCD | Charge-coupled device |
| CEN | European Committee for Standardization |
| CA | California |
| CEDER | Centre for the Development of Renewable Energy Sources (Soria, Spain) |
| CIEMAT | Centre for Energy, Environment and Technology Research (Madrid, Spain) |
| CO | Colorado |
| CULS | Czech University of Life Sciences Prague |
| *CV* | Calorific value |
| *D* | Diameter |
| DM | Dry matter |
| *dTG* | Derivative thermogravimetric analysis |
| *DU* | Mechanical durability |
| EC | European Commission |
| EU | European Union |
| Eq. | Equation |
| *FC* | Fixed carbon |
| FTA | Faculty of Tropical AgriSciences |
| *GCV* | Gross calorific value |
| ISO | International Organization for Standardization |
| LED | Light-emitting diode |
| *L* | Length |
| L. | Linnaeus as the authority for a species name |
| *MC* | Moisture content |
| *NCV* | Net calorific value |
| PC | Personal computer |
| POA | Photo-optical analysis |
| PSD | Particle size distribution |
| RGB | Colour model (red, green, blue) |
| RIAE | Research Institute of Agricultural Engineering |
| SA | Sieve analysis |
| SEM | Scanning electron microscopy |
| TGA | Thermogravimetric analysis |
| UCT | University of Chemistry and Technology Prague |
| USA | United States of America |
| var. | Variety |
| *VM* | Volatile matter |
| WA | Washington |
| 2D | Two-dimensional space |
| 3D | Three-dimensional space |

# List of symbols

| | |
|---|---|
| A | Ampere |
| *Al* | Aluminium |
| *As* | Arsenic |
| $A_0$ | Particle's calculated surface area |
| $A_1$ | Particle projection area |
| $A_r$ | Aspect ratio |
| *C* | Carbon |
| *Cd* | Cadmium |
| *Cr* | Chromium |
| *Cu* | Copper |
| $C_i$ | Circularity |
| *Cl* | Chlorine |
| $CO_2$ | Carbon dioxide |
| $(C_6H_{10}O_5)_n$ | Cellulose (chemical formula) |
| °C | Degree Celsius |
| dB | Decibel |
| d.b. | Dry basis (calculation basis in which a solid fuel is free from moisture) |
| $d_v$ | Diameter of an equal volume sphere |
| $E_d$ | consumed deformation energy |
| *F* | Force |
| *Fe* | Iron |
| g | Gram (unit of weight) |
| GPa | Giga pascal |
| h | Hour |
| *H* | Hydrogen |
| *Hg* | Mercury |
| *K* | Potassium |
| kN | Kilonewton |
| $kg.m^{-3}$ | Kilogram per cubic metre |
| kW | Kilowatt |
| $kWh.t^{-1}$ | Kilowatt-hour per tonne |
| $m_w$ | Total mass of wet material |
| $m_d$ | Dry matter mass of the dried material |
| mg | Milligram |
| mm | Millimetre |
| mm/"g" | Sieve shaker intensity (vibration height in mm or acceleration of the sieve in "g" – acceleration due to gravity $9.81 m.s^{-2}$) |
| *Mn* | Magnesium |
| MPa | Megapascal |
| $MJ.kg^{-1}$ | Mega joule per kilogram |
| $m.s^{-1}$ | Meter per square second (acceleration) |
| *N* | Nitrogen |
| N | Newton |
| $N.mm^{-1}$ | Newton per millimetre |
| *Ni* | Nickel |
| $NO_x$ | Nitrogen oxides |
| n | Number of observations |
| nm | Nanometre |
| *O* | Oxygen |
| *Pb* | Lead |
| px | Pixel |
| rpm | Revolution per minute |
| $R_d$ | Particle roundness |
| $R_{lw}$ | Length/width ratio |
| $r_{max}$ | Radius of the maximum inscribed circle |
| $r_1$ | The smallest radius |
| $r_2$ | The largest radius |
| $R^2$ | Coefficient of determination (R-squared) |
| *S* | Sulphur |
| *Se* | Selenium |
| $SiO_2$ | Silicon dioxide |
| $S_m$ | Particle symmetry |
| $T_g$ | Glass transition temperature |
| Ti | Titanium |
| $T_i$ | Initial degradation temperature |
| *Tl* | Thallium |
| $t.h^{-1}$ | Ton per hour |
| $t.ha^{-1}$ | Ton per hectare |
| µm | Micrometre |

| | | | |
|---|---|---|---|
| $\mu m^2$ | Square micrometre | $X_{min}$ | Minimum feret diameter of particle |
| $\mu m.px^{-1}$ | Micrometre per pixel | | |
| $U_p$ | Perimeter of particle | $\alpha$ | Significance level |
| $V$ | Vanadium | $\sigma_t$ | Compressive strength |
| V | Volt | $\varrho$ | Density |
| $V_b$ | Volume | $\varepsilon$ | Porosity |
| $W_{max}$ | Maximum width | $(1 - \varepsilon)$ | Solids content |
| w.b. | Wet basis (calculation basis in which a solid fuel is wet) | $\pi$ | Mathematical constant approx. equals to 3.14159 |
| $X$ | Feret diameter | $\psi$ | Sphericity of particle |
| $X_a$ | Equivalent diameter | $\Sigma$ | Summation |
| $X_m$ | Martin-diameter | $\sigma_t$ | Compressive strength |
| $X_{max}$ | Maximum feret diameter of particle | $\sim$ | Equivalence relation |

# 1. Introduction

Energy plays a vital role in a socio–economic development and raising standards of human beings. Nowadays an energy sector faces to several serious problems due to the population expansion and related increasing energy demand and consumption (Hiloidhari et al. 2014). These factors along with the gradually depleting supplies of fossil fuels and their adverse environmental impact have led the population to seek for an alternative and sustainable energy sources to meet its basic needs (Zhang & Guo 2014; Bajwa et al. 2018). Therefore, the use of biomass has become a feasible possibility and important part of the global energy mix thanks to its huge potential for the substitution of fossil fuels with significant reduction of $CO_2$ emissions without causing negative effects on ecosystems (Cheng 2017). Biomass including various energy crops and agricultural & forest organic residues has a great potential capacity for an energy production (Gokcol et al. 2009), however in its original form the biomass faces many limitations because of its high moisture content, irregular shape and sizes, low volumetric energy density and diverse chemical composition (Puig-Arnavat et al. 2016; Shuma & Madyira 2017; Dhyani & Bhaskar 2018). One of the promising methods overcoming above-mentioned limitations is a densification and especially briquetting technology which converses biomass into solid biofuels of uniform form (Tumuluru et al. 2010; Gendek et al. 2018). Compare to liquid and gaseous biofuels, solid biofuels have been leading contributor to biomass capacity since 2005 and this trend will certainly continue in next years (Scarlat et al. 2015; Bajwa et al. 2018).

Increased interest in bio-energy goes hand in hand with demand for quality biofuels with appropriate mechanical, chemical and energy features (Shaw 2008), so better and more comprehensive knowledge of feedstock material properties and other variables influencing densification process is generally needed (Ramírez-Gómez et al. 2014). Up-to-date data about material properties together with process variables may enhance efficiency of densification processes and thus may bring optimal densified products of higher quality with desired properties (Ndindeng et al. 2015).

Purpose of densification process is to create dense, strong and durable bonding between particles and efficiency of this process can be determined by evaluation of briquette strength and durability (Pietsch 2002; Kaliyan & Morey 2009). These parameters of quality may be influenced by the structural and rheological behaviour of feedstock material and variables that govern development of a briquette structure (Pietsch 2002). The structure rests on the processes engaged in formation of final agglomerate and various parameters related to particles composition and morphology including particle size and its distribution, macroscopic as well as microscopic shape of particle and roughness (Pietsch 2002; Muntean et al. 2013). Generally,

particle size and particle size distribution are counted among the major factors affecting many properties of particulate as well as densified materials and are useful indicators of material performance and quality (Pietsch 2002; Tumuluru et al. 2011b; Guo et al. 2012; Zhang & Guo 2014). They play important roles in bulk density, compressibility of bulk solid material and durability of densified products (Ganesan et al. 2008; Kaliyan & Morey 2009).

One of the methods by which structural properties of densified biofuels can be nowadays rapidly, objectively and precisely visualized and evaluated is computer vision and image analysis. It is a highly useful and effective technique with versatile range of application in industry and science (Davies 2018), where increase of efficiency, quality and performance of controlled objects is highly demanded. It includes tasks, among others, visual inspection of prescribed parameters, estimation of size, shape, structure and texture and object counting and defects identification (Gongal et al. 2018; Manish et al. 2018; Smith et al. 2018; Su et al. 2018). Development of machine vision and image analysis is still on the rise and its applications have got into research of biomass materials for energy purposes, where it has been used for observation of surface and interior structures of agglomerates (Yang et al. 2009; Miao et al. 2015) and for identification of particle size and particle size distribution from loose samples (Igathinathane et al. 2009a; Igathinathane et al., 2009b; Souza & Menegalli 2011; Kumara et al. 2012; Guo et al. 2012; Gil et al. 2014; Pothula et al. 2014; Pons & Dodds 2015; Febbi et al. 2015) or directly from the image of compact's cross sections (Chaloupková et al. 2018a). In case of solid biofuels, it was used only for basic observations and as complementary part to a research (Kaliyan & Morey 2010; Stelte et al. 2011b; Muntean et al. 2013; Zhang & Guo 2014). Hence, the purpose of this theoretical and experimental study is to provide more complex insight into this actual topic.

In this Thesis, the dependence of briquettes quality on their structure and material composition was investigated. The miscanthus, industrial hemp and pine sawdust, the representant of compositionally different biomass materials, were grinded into three different size fractions (4, 8 and 12 mm) and pressed into the form of cylindrical briquettes by the hydraulic piston briquetting press. The structure of briquettes was studied by computer vision and image analysis to identify agglomeration and binding rules and especially the location(s) of concentration of the larger particles. Particle size and shape were deeply studied using traditional and modern method and their effect as well as lignocellulosic structure (content of cellulose, hemicellulose and lignin) on the mechanical quality (density, mechanical durability and compressive strength) of final briquettes was evaluated. Complementary chemical analyses were included as well to present the main fuel properties of selected materials. The study results are a part of the comprehensive knowledge required for the designing an optimal and efficiency production of quality biomass briquettes as a renewable energy resource.

# 2. Literature review

## 2.1. Biomass as a source of energy

Biomass is one of the renewable energy sources with a greater capacity for energy production (Gokcol et al. 2009; Bahng et al. 2009) and nowadays, there is worldwide growing interest in its application and development (Kim & Dale 2015; Scarlat et al. 2015; Cheng 2017). Biofuels in solid, liquid and gaseous form have been produced and evaluated by countless authors during last 15 years (Guo et al. 2015). This interest has been caused mainly by rising energy demand, which is expected to rise by 48% to 2040 (Fournel et al. 2015) and inevitable need for decrease of dependency and use of gradually depleting fossil fuels, today's the main energy source worldwide, which burning results in many negative environmental effects that may cause global climate changes (Karunanithy et al. 2012; Zhang & Guo 2014). This trend is supported and accompanied by change of EU policy, which now assumes 20% consumption share of energy from renewable sources by 2020 (Directive 2009/28/EC 2009) and up to 2030 there is a proposal for 27% (Directive proposal COM/2016/0767 2016). Also, national strategies of countries around the world has set off towards development and higher share of bio-energy (Xu et al. 2015; Zhou et al. 2016; Agarwal et al. 2017; Kang et al. 2017). Share of renewable energy in the global final energy consumption is shown in **Figure 1**. As it can be seen the estimated share of biomass in 2016 in the total consumption was 18.2% (REN21 2018).

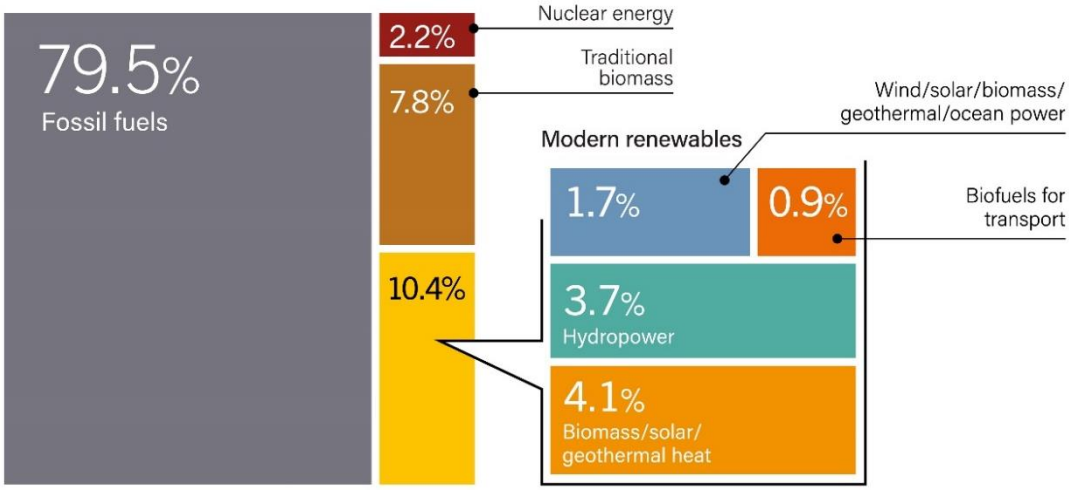


**Figure 1.** Estimated share of renewables in the total final energy consumption (2016)
Source: REN21 (2018)

Biomass energy production is more and more expanding field. It is due to its renewable and sustainable nature, abundance of materials and their versatile composition, local availability, possibility of conversion into many useful products and positive environmental effect owing to carbon-neutrality and very low sulphur content (Melero et al. 2012; Pothula et al. 2014; Kim

& Dale 2015). Biomass has a considerable advantage in terms of its capacity to produce different products, among other biofuels that can be modified according to applied technology and pathway of processing, which is absent in other energy sources, and used for various purposes (Cheng 2017). **Many bio-energy conversion pathways** are well established and fully available on commercial level, while others are so far at the development, demonstration or commercialisation stages. In 2016, the bio-energy was mainly used for heat in buildings and industry and less in electricity generation and transport sector (**Figure 2**); however, the electricity sector has experienced the highest rate of growth in bio-energy consumption (REN21 2018).

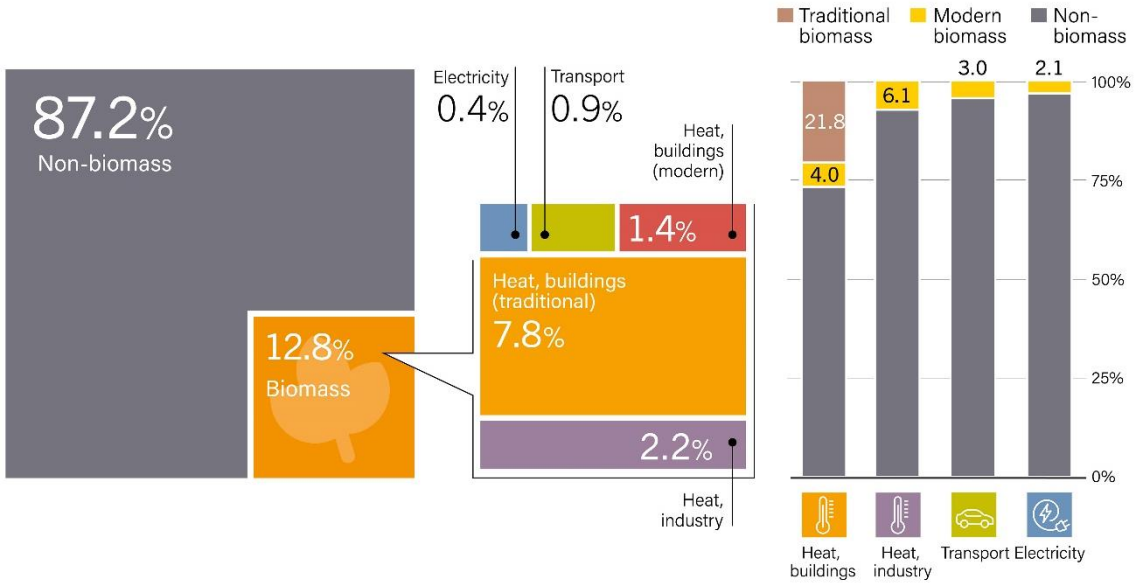


**Figure 2.** Shares of bioenergy in the total final energy consumption, overall and by end-use sector (2016) Source: REN21 (2018)

For these biomass materials and their specific composition there are **many conversion processes available** to produce energy, bio-fuels and bio-chemicals (Ganesh & Raveendran 2008; Melero et al. 2012), including but not limited to direct combustion, co-combustion, mechanical densification, gasification, pyrolysis, anaerobic digestion, hydrolysis, hydrogenation or fermentation (Agarwal et al. 2017; Cheng 2017; Akhtar et al. 2018; Arregi et al. 2018; Dhyani & Bhaskar 2018; Molino et al. 2018). Today, there are different types of solid, liquid or gaseous biofuels, but the most widely used and commonly available in the market are **densified solid biofuels** (Scarlat et al. 2015; Zhou et al. 2016; Pradhan et al. 2018). It is caused by their easier production with attractive price (Havrland et al. 2011). Solid biomass used for heating, cooling and electricity generation is the leading source of renewable energies in EU, thus solid biofuels market is still more and more developing and growing field, and this trend will continue till 2020 and may greatly contribute to achieving energy targets not only in EU countries, but also around the world (Chen et al. 2009; Scarlat et al. 2015; Xu et al. 2015; Bajwa et al. 2018). A quite varied set of industries is participating in growing, harvesting, supplying, processing and using solid

biomass to produce heat and electricity, ranging from the supply of traditional biomass (e.g. wood), to the locally based supply for small-scale heating units, to regional and worldwide subjects involved in large-scale district heating and power generation technology supply and operations (REN21 2018). Solid biofuels as a source of energy has a high potential mainly in rural areas as well as in low income regions owing to their local availability, great adaptability, low cost and sustainability (Zhou et al. 2016; Shuma & Madyira 2017).

Utilization of biomass for production of electricity and/or heat may involve the usage of biofuels close to their source, such as municipal solid waste, residues from agricultural and forestry operations and purposely grown energy crops (REN21 2018). As indicated, there is a wide range of biomass materials available for energy purposes. A solution that helps to avoid using of food-crops and firewood causing food competition, deforestation and problems associated with them, is a use of **lignocellulosic biomass** and **forest & agriculture residues** (Xu et al. 2015; Oh et al. 2018). Lignocellulosic biomasses (also called energy crops) are non-food, purposely grown crops with high energy potential and low requirements for soil conditions, nutrition and growth (Dhyani & Bhaskar 2018). It includes lignocellulosic woody crops such as poplar, willow or eucalyptus, and, lignocellulosic herbaceous crops like miscanthus, hemp, common reed, giant reed, switchgrass, cynara cardu, canary grass, bamboo or indian shrub (Tumuluru et al. 2011a; Krzyżaniak & Stolarski 2017; Dhyani & Bhaskar 2018).

Apart from the **purposely grown biomass**, huge amounts of non-edible biomass and **organic residues** are produced every year around the world (Agarwal et al. 2017; Sutrisno et al. 2017). It means materials from wood processing and forestry activities such as sawdust, wood shavings, barks, as well various urban organic residues and agricultural organic wastes, including husks and straw from cereals (e.g. rice, maize, wheat), husks from sunflower and coffee, cotton stalks, coir pith, sugar beet leaves, waste flows from bulb sector, olive pits etc. (Grover & Mishra 1996). A significant amount of waste is also produced by pruning activities of permanent crops (vineyards and orchards) in Europe (Manzone et al. 2016; Pari et al. 2018; Toscano et al. 2018). All these residues can be potentially used for energy production (Popp et al. 2014; Xu et al. 2015; García-Galindo et al. 2016; Picchi et al. 2018). More materials suitable for production of densified biofuels are cited in the Chapter 2.5.

Most of the agricultural residues available after harvest are unutilized or improperly processed (Agarwal et al. 2017; Sutrisno et al. 2017); they are used as fodder or fertilizer, just left on the field or burnt (Kumar et al. 2015). The open field burning is cheap and helps to avoid propagating fungal stem rot diseases (Kadam et al. 2000), however it is than associated with extensive air pollution due to high emission of unburned hydrocarbons and particulate matter,

and, consequent health problems as well as with decreased soil fertility (Matsumura et al. 2005; Kumar et al. 2015). Altogether, the use of waste biomass for energy purposes is not only a green technology, but it is also the technology of **proper waste management** since it eliminates problems with waste disposal (Cardozo et al., 2014; Agarwel et al. 2017; Brunerová et al. 2018).

## 2.2. Biomass composition

Biomass is a contemporaneous (non-fossil) and complex organic product generated by natural and anthropogenic processes from plant and animal materials, living or recently died (Vassilev et al. 2010). It is very porous cellular material containing mainly large organelles full of water or air in case of dry material (Stelte et al. 2011b; Dhyani & Bhaskar 2018). In case of plant-based biomass, the product of the photosynthetic process, plant cell wall consists mainly of cellulose, hemicelluloses (carbohydrate polymers) and lignin (phenolic polymers) and minor quantities of extraneous elements (Zeng et al. 2014; Cheng 2017), as it can be seen in the **Figure 3**. Proportion of these constituents differs according to both plant species and age, stage of growth and other circumstances influencing plant's life cycle, like sunlight, location, climate, soil type etc. (Sarkar et al. 2009; Vassilev et al. 2010). Divergences in plant cell walls were reported for both plant part, cell types inside one tissue and even inside one particular cell (Knox 2008; Frei 2013). In general, dry biomass contains 40–50% of cellulose, 20–25% of lignin, 15–25% of hemicellulose and 5–10% of other minor extraneous components (McKendry 2002; Faik 2013) like alkaloids, proteins, essential oils, fats, waxes, resins, glycosides, gums, terpenes, mucilages, pectins, phenolics, saponins and starches (Dhyani & Bhaskar 2018).

Relative proportion of the main compounds serves as a fundamental determining factor for suitability of particular feedstock for energy-based conversion pathway (McKendry 2002). Ganesh & Raveendran (2008) developed assessing criteria for this biomass suitability for the conversion process to produce solid, liquid and gaseous fuels. Following subchapters provide brief description of biomass main components.

### 2.2.1. Cellulose

Cellulose is the major constituent of biomass and the most copious naturally occurring material on the planet (Stelte et al. 2011b; Zeng et al. 2014). Its quantity differs from species to species (Fengel & Wegner 1983); woody biomass contains 40–50%, agricultural residues 30–45% and herbaceous biomass 25–50% (Fujita & Harada 2000; Pérez et al. 2002). High content of cellulose is found in natural fibres – cotton (up to 98%), kapok, jute, flax, hemp etc. (Cheng 2017).

In chemical terms, cellulose is a long linear polymer consisting of repeating chains of β-D-glucopyranose units connected by β-1,4 bonds with chemical formula $(C_6H_{10}O_5)_n$ (Shaw 2008; Kumar & Turner 2015; Cheng 2017). These chains, bonded by hydrogen covalent bonds and van der Waals forces (Pérez et al. 2002), are organized into strands of high crystallites, so-called microfibrils, and characterized by high mechanical strength and chemical stability (Zeng et al. 2014; Cheng 2017; Dhyani & Bhaskar 2018). In interaction with functional groups of other compounds, the microfibrils are organized into fibres – major structural elements of a plant cell wall (Stelte et al. 2011b). Cellulose is found more in the secondary cell wall, than in the primary one (Pérez et al. 2002; Zeng et al. 2014).

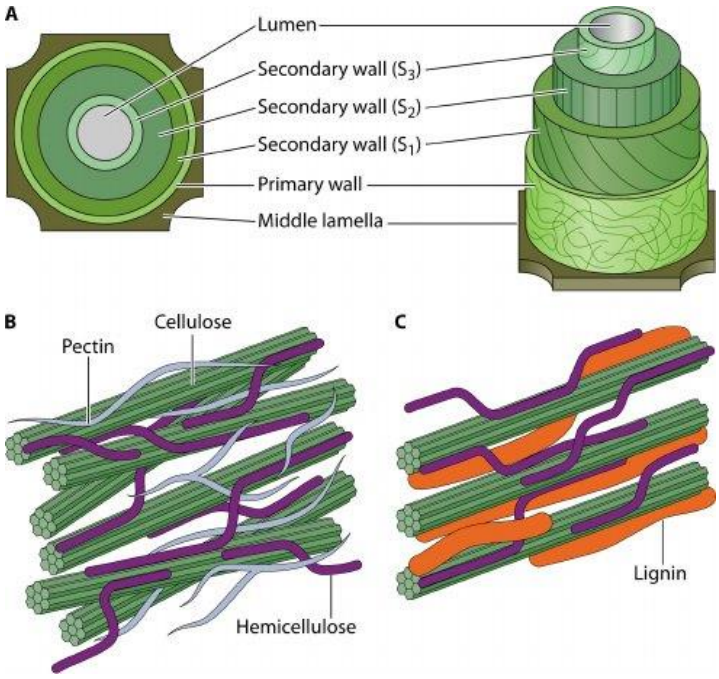


**Figure 3.** Simplified model of plant cell wall structure

(A) The structure consists of three main layers: the middle lamella and the primary and secondary walls. (A and B) The main polysaccharides and lignin which form the surrounding structure for the plasma membrane are presented in the primary (B) and secondary wall (C)
Source: Rytioja et al. (2014)

### 2.2.2. Hemicellulose

Hemicellulose, unlike cellulose, is a heterogeneous group of very branched polysaccharides of β-1,4-(and sporadically β-1,3)-linked glucose units (Stelte et al. 2011b), mainly composed of xylose, mannose, galactose, glucose, arabinose, methyl-glucuronic, galacturonic and glucuronic acids (Pérez et al. 2002; Scheller & Ulvskov 2010; Dhyani & Bhaskar 2018). Besides being heteropolymer, hemicellulose differs from cellulose in degree of polymerization, amorphous structure, molecular weight, physical strength and small thermal stability (Pérez et al. 2002). Morphology and quantity of hemicellulose varies according to species. Woody biomass

has generally 25–30%, agricultural residues 20–25% and herbaceous biomass 15–30% (Cheng 2017).

Hemicellulose is found in primary and secondary cell wall though higher quantity occurs in the primary cell wall (Scheller & Ulvskov 2010). It surrounds the cellulose fibres and acts as a joining bridge between cellulose and lignin, so it helps to strengthen the cell wall by interaction with cellulose through hydrogen bonds and by forming covalent bonds with lignin (Zeng et al. 2014; Cheng 2017).

### 2.2.3. Lignin

Lignin is a very complex insoluble three-dimensional polymer consisting of highly cross-linked phenylpropane units (mostly guaiacyl, sinapyl and p-hydroxyphenyl) bonded by aryl ether or C-C bonds (Rowell et al. 2012; Zeng et al. 2014). Lignin proportion varies (Knox 2008; Sarkar et al. 2009; Frei 2013); most herbaceous biomass and hardwood contain 15–25% and softwood up to 40% (Cheng 2017). Usually, lignin can be detected by histochemical staining, Raman microscopy or using ultraviolet light to provoke blue fluorescence (Agarwal 2006; Kaliyan & Morey 2010; Zeng et al. 2014).

From biological standpoint, lignin serves as a binder between cellulose and hemicelluloses and contributes to higher strength of the cell wall (Fujita & Harada 2000; Stelte et al. 2011b; Dhyani & Bhaskar 2018), where it has supporting, mechanical and protective function against microbial attacks and oxidative stresses (Pérez et al. 2002). Regarding to energy production, lignin plays opposing roles (Frei 2013). In case of solid biofuels, lignin softened by high temperatures performs as a **natural binding agent** during densification process. Lignin helps to bond particles together, which results in increased strength properties and makes a final product more durable (Chou et al. 2009; Kaliyan & Morey 2010; Gendek et al. 2018; Qin et al. 2018). Biomass consisting of more lignin, protein or starch has better agglomeration properties compare to a material with higher cellulosic content (Tumuluru et al. 2011b). Alaru et al. (2011) studied content of lignin in different fibre hemp plant types and sunflower and their ability to produce durable briquettes. Lignin can be extracted by steam explosion and used as binding agent, as it was studied by Gravitis et al. (2010) on wood composites. On the other hand, the lignin is one of the slowly decomposing components of a dead plant material (Tutt & Olt 2011) and it can cause difficulties in saccharification process for production of liquid biofuel (Li et al. 20113). Zeng et al. (2014) summarized the negative roles of lignin in biochemical processes for production of lignocellulosic biofuels, including microbial fermentation and enzyme hydrolysis, requiring some type of chemical pre-treatment.

## 2.3. Importance of densification

Biomass, in its original form, is characterized by high moisture content (between 10 and 70%), hygroscopic nature, diverse chemical composition, irregular dimensions, low bulk density and associated low energetic density and rapid burning (Thoreson et al. 2014; Shuma & Madyira 2017; Dhyani & Bhaskar 2018). Generally, herbaceous biomass has a bulk density of 112 to 160 $kg.m^{-3}$ and woody biomass, like wood chips, 220–265 $kg.m^{-3}$ (Tumuluru et al. 2015). These factors go hand in hand with troublesome and inefficient handling, storing, transporting, feeding into the boilers, burning properties and overall utilization in its primary state without any sort of pre-treatment, which leads to commercial limitations of biomass as a biofuel and bio-power source (Puig-Arnavat et al. 2016; Shuma & Madyira 2017; Tumuluru et al. 2018). To make the raw biomass approachable and convenient for different uses, the challenges of these feedstocks should be addressed (Ganesh & Raveendran 2008).

One of the approaches bringing up-and-coming resolution to get over the aforesaid barriers is a mechanical densification of biomass into products with **specific shape, size and volume**, such as pellets, briquettes, logs or cubes (Ahiduzzaman & Sadrul Islam 2013; Xu et al. 2015; Bajwa et al. 2018). It is a process of forcing loose particles together into harder and more compact solids by employment of external mechanical force to generate particle-to-particle bonding (Shaw 2008; Kaliyan & Morey 2010). Densification converts biomass into high-density, high-energy, saleable and aerobically stable products with great potential for heating applications (Xu et al. 2015; Antwi-Boasiako & Acheampong 2016; Tumuluru et al. 2018). It **increases bulk density** up to 600–1300 $kg.m^{-3}$ and produces homogenous products that may be easily and efficiently handled, dosed (even automatically), transported and stored (Kaliyan & Morey 2009; Tumuluru et al. 2010). It follows that expenses related to mentioned logistic operations are reduced (Karunanithy et al. 2012; Thoreson et al. 2014). Such uniform and symmetrical products may be managed without any troubles using standard logistic equipment and employed both in direct combustion, pyrolysis, gasification and in other biomass-to-energy conversion processes (Kaliyan & Morey 2009). Densified biomass relates to lower possibility of degradation since the moisture content (*MC*) is decreased during the compaction process and higher resistance to air humidity (Karunanithy et al. 2012). Up to 70% of relative humidity does not have any effect on storage conditions of commercially available briquettes (Singh 2004). Moreover, densified biomass is characterized by **improved burning properties** including uniform combustion, rate of combustion comparable to coal and reduced entrained particulate emissions as well as lower possibility of spontaneous ignition in storage place (Werther et al. 2000; Tumuluru et al. 2010).

To densify loose biomass efficiently and sustainable also issues related to biomass densification in terms of energy consumption, emissions, and costs of densification and process use of the densified biomass should be particularly considered (Puig-Arnavat et al. 2016; Muazu et al. 2017; Mladenović et al. 2018). Economic, social and/or environmental assessments of biomass densification for various feedstocks in different regions have been done e.g. by Karkania et al. (2012), Feng et al. (2013), Pirraglia et al. (2013), Stolarski et al. (2013), Hu et al. (2014), Kolaříková et al. (2015), Xu et al. (2015) and Toscano et al. (2018).

There is a wide range of **densification technologies** commercially available, including pellet press, briquette press, cuber, agglomerator, tablet press, roller press and screw extruder (Tumuluru et al. 2011b; Ahiduzzaman & Sadrul Islam 2013; Kaliyan et al. 2013). Generally, there are two main approaches: pressure agglomeration (including mechanical compression) and tumble agglomeration involving application of binding additives (Kaliyan & Morey 2009), but which is no longer commonly used in biomass densification (Tumuluru et al. 2011b). The technologies are produced with a capacity of 0.1 $t.h^{-1}$ (for smaller woodworking joinery plants) up to a performance of 5 $t.h^{-1}$ for large pellet plants following up on large power plants and heating plants. There are three systems of briquetting presses.

Before densification process itself, proper material drying and reduction of particles size are indispensable operational steps in production process (Dai et al. 2012). The purpose is to reduce *MC* as well as to decrease particle size and enlarge a number of contact points for further inter-bonding among particles (Bajwa et al. 2018) leading to higher mechanical strength of produced compacts (Zhang & Guo 2014). Size reduction also allows the loose particles to dry more rapidly (Kaliyan & Morey 2009). Such prepared material may undergo further pre-treatments to improve densification process and/or final product quality, like blending with additives and fats, preheating, steam conditioning to expand material temperature and *MC* or torrefaction (Tumuluru et al. 2010; Gaitán-Alvarez et al. 2017; Wilk & Magdziarz 2017). All life cycle of biomass densification then includes drying, size reduction, blending, densification, cooling, screening, packaging and transportation (Muazu et al. 2017) and optimisation of this biomass supply chain is essential to enhance the development and sustainability of a competitive market with densified biofuels (De Meyer et al. 2014).

## 2.4. Insight into agglomeration process

In general terms, agglomeration is a process of joining loose particles into a compact agglomerate. The process can occur naturally or with application of external actions, and, is accompanied by activity of natural short-range physical or chemical forces among particles

themselves, by physical or chemical transformations of solids or by binders, compounds that adhere chemically or physically to solid surfaces and develop stable bonds among particles (Pietsch 2003). The main purpose of agglomeration process is to create a compact with specific characteristics (defines size, shape and volume) that enhance certain physical features, including stability, dispersibility and bulk density (Tumuluru et al. 2010; Bajwa et al. 2018). Agglomeration can be carried out by heat/sintering, tumble/growth or pressure technology (Pietsch 2002); this Thesis deals only with the pressure agglomeration approach.

### 2.4.1. Process of pressure agglomeration

During any pressure densification structural, elastic and plastic stages of particle deformation occur (Pietsch 2002; Shaw 2008; Muntean et al. 2013). Firstly, when low pressures are applied, particles make rearrangement to change the shaky arrangement of loose mass and create a closely packed and stabilized formation. Further, the space between particles is continually reduced while particle properties, size and shape, retain in their original state. As pressure rises, particles move into vacant spaces, air is reduced and extended contact and interaction among particles appear. During this step, dimensional character of the input particles is still not changed or just slightly. As the pressure increases particles are forced against each other and brittle particles break, malleable particles deform and porosity is further reduced, this cause further rearrangement leading to close interaction of particles and creation of binding mechanisms like mechanical interlocks. When the temperature overcomes certain melting limit, local melting among particles arises. High pressure has influence alongside on particles themselves as well as on tissue's morphology, cell organelles, membranes, and at the atomic/molecular level (Shaw 2008). In all stages, binding agents play important role in the biomass agglomeration process. Process of particle rearrangement remains until final density is achieved. All these steps help to change elastic deformation into a permanent plastic deformation. After the pressing action, when the agglomeration is finished, elastic spring-back recovery in case of biomass can occur to some extent (Pietsch 2002; Qin et al. 2018). The porosity of final agglomerates is very important factor for the characteristics and further applications of these products (Pietsch 2003).

### 2.4.2. Binding mechanisms

When the particles are brought closer enough due to external applied (mechanical) forces, binding mechanism may develop (Sastry & Fuerstenau 1973). Binding mechanisms are physical and chemical impacts resulting in adhesion and bonding among surfaces of solid loose

particles during compaction. Based on the traditional theory, they can be classified into following major groups: **stable bridges, adhesional and cohesional forces, surface tension and capillary pressure, attraction forces between solids**, and, **mechanical interlocking bonds** (Rumpf 1962; Sastry & Fuerstenau 1973; Pietsch 2002), see **Figure 4**. Bonding mechanisms are greatly influenced by the particle structure and fraction size (Kaliyan & Morey 2009).

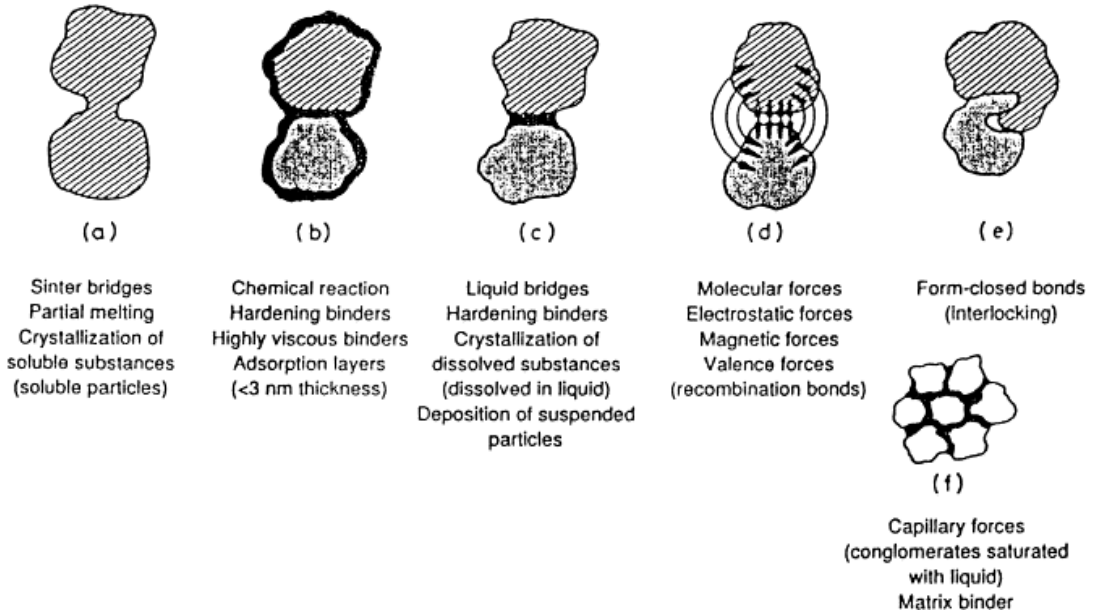


**Figure 4.** The binding mechanisms of agglomeration process
Source: Pietsch (2003)

During densification process, when the high pressures and temperatures are employed **stable solid bridges** can be created at the points where particles touch each other by molecules diffusion among particles. Solid links may be provoked by chemical reactions, hardening and plasticization of binders, crystallization of dissolved substances, partial melting or sintering (Rumpf 1962; Pietsch 2002). This mechanism is mainly formed after the final agglomerate drying or cooling (Kaliyan & Morey 2009). Very finely grinded particles attracting easily free atoms or molecules contain the gentle stable adsorption levels that can create strong bonding among adjacent particles. It is enabled due to even out surface roughness, growth of the contact space between particles or by declination of the inter-particle distance and presence of the intermolecular attractive forces involved in the bonding mechanism (Ghebre-Sellassie 1989). Greatly adhesive binders, like molasses and bitumen, adhere to the surfaces of solid particles to form strong ties, highly similar to those of solid links. Many viscous binders stiffen after cooling and create the solid bridges, too (Pietsch 2002). Presence of liquids, like free water in particles pores, induces capillary attraction between the particles owing to the air-liquid interfacial tension and thus improves adhesion (Sastry & Fuerstenau 1973; Grover & Mishra 1996). Solid particles are attracted by natural (physical) short-range forces, such as molecular (valance and van der

Waals'), magnetic or electrostatic charges, that can originate adhesion of solid particles to each other if the particles get closer enough together (Sastry & Fuerstenau 1973). During the compaction process, close bonds are created when fibres, flat or unevenly shaped and bulky particles intertwine, twist, fold and bend about each other. Since the surface of these solid particles is not smooth and is full of lock and key points at which they may be connected together, these morphological changes lead to **mechanical interlocking** effects (Pietsch 2002; Kaliyan & Morey 2009), which may contribute to adequate mechanical strength to control the destructive forces caused by elastic phenomenon after the pressing process (Rumpf 1962).

### 2.4.3. Binding agents

Binding agents (binders) play important role in densification process as well as in quality and performance of final densified products (Zhang et al. 2018). The raw biomass itself contains various own types and concentrations of naturally occurring binding agents such as water-soluble carbohydrates, **lignin**, protein, pectin, starch and fats (Chou et al. 2009; Kaliyan & Morey 2010; Tumuluru 2014; Urbanovičová et al. 2017) that are activated and released at high pressures and temperatures occurring during compression to work as a sealant of particles. Later, when pressure and temperature action cease, the natural binding agents harden or "settle down" creating links or ties between particles, resulting in compact, strength and durable products (Kaliyan & Morey 2010). It supports the necessity of adequate strength for logistic operations of these products (Pietsch 2002; Shaw 2008). Various papers have reported feedstock materials with sufficient binding features without using additional binding materials (Shaw & Tabil 2007). Li and Liou (2000) studied a high-pressure binderless compression of wood processing wastes and other organic residues, like hardwood, softwood, and bark in the forms of sawdust, mulches and chips. Kaliyan and Morey (2010) investigated the function of natural elements in switch grass and corn stover briquettes and pellets forming stable and strong particles' bonding mechanisms.

There are many additive binders that can be added extra such as organic, inorganic and compound binders offering different mechanical strength and thermal stability (Zhang et al. 2018). Inorganic ones can be represented by limestone, lime, calcite, clay, bentonite etc. (Wang et al. 2012; Zhang et al. 2018). Additives can increase particle adhesion, abrasion resistance and compressive strength and can decrease the energy cost of production (Muazu & Stegemann 2017). Briquette quality in terms of calorific value (*CV*) and ash sintering characteristics can be improved with additives too (Wang et al. 2012; Zhang et al. 2018).

Many studies investigating briquettes mixed with additives have been conducted. Thabuot et al. (2015) evaluated briquettes from palm fibre, bamboo sawdust, corn con with

additive – molasses. With the same additive Jittabut (2015) produced and assessed briquettes from rice straw and sugarcane leaves in various ratios. Rajaseenivasan et al. (2016) studied the effect of binder – neem powder on sawdust briquettes. The results showed that mixing of neem powder with sawdust significantly increased briquettes strength, but lowered *CV* compared to a briquette made of sawdust alone. Chou et al. (2009) studied rice straw briquettes with rice bran, soybean residues and *Acacia confusa* sawdust additives. Rahaman and Salam (2017) investigated binder properties of sawdust in briquetting of rice straw. Additive increased *CV* and decreased ash content. Mitan et al. (2018) evaluated addition of starch and calcium hydroxide in various ratios into durian peel briquettes. Other material like cow dung and cactus (Shuma & Madyira 2017) were studied as briquette binders. Also, **water** acts as a film type binding agent due to van der Waals' forces and increased surface interaction among particles (Grover & Mishra 1996; Pietsch 2002). Several papers reported increased strength and durability of densified products with higher *MC* (Kaliyan & Morey 2009). Yank et al. (2016) reported that adding of cassava wastewater into rice husk had positive effect on briquette quality.

## 2.5. Briquetting technology and current research

Briquetting is a well-known and broadly used technology of material compaction when fine grinded biomass is compacted, with or without additives, under high pressure and temperatures that emerge from the high friction between densified material and press matrix/die walls of a briquetting machine (Shaw 2008; Kers et al. 2010). Final products – briquettes are clean and green biofuels combustible in special furnaces, boilers or in open fire (Tumuluru et al. 2010). Given by used densification procedure and shape of a stamping/compacting/pressing channel/chamber (Pietsch 2002; Ivanova 2012) biomass can be shaped into blocks of **specific size, shape and volume** (**Figure 5**) – cylinders, prisms or hexahedrons with or without a hole in the centre and, with diameter ranging from 40 to 100 mm and length up to 300 mm (Stupavský & Holý 2010) and specific density around 600–1300 kg.m$^{-3}$ (Tumuluru et al. 2015).

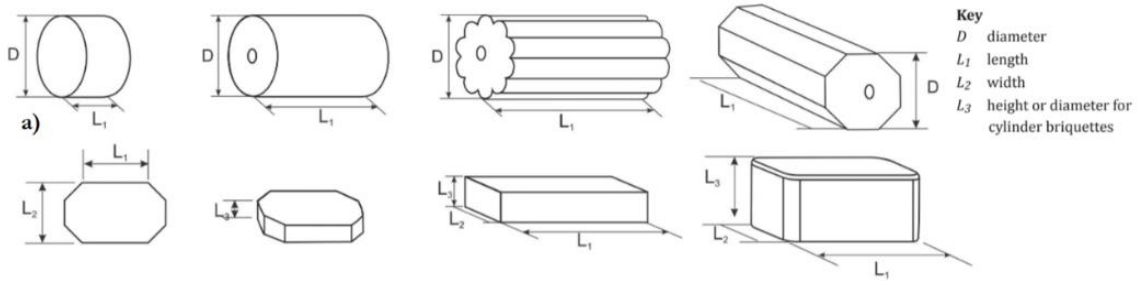


**Figure 5.** Dimensions of briquettes
Source: BS EN ISO 17225-3 (2014)

Briquetting technology has developed into two directions: hydraulic or mechanical piston press technology and screw press technology (Grover & Mishra 1996; Tumuluru et al. 2011b). In **mechanical piston press** biomass mass is pressed in an open press chamber where the material is punched through a matrix by a pressing piston. The briquette is formed by pressing the material by rectilinear reciprocating movement of the piston; each stroke of the piston forms a thin sheet - one briquette (Križan et al. 2009). The output is around 1 $t.h^{-1}$. The piston press has long life of wearing parts and low power consumption. It can be used to compress a wide range of raw biomass materials including corn straw, peanut shell, ground nut shell, cotton stalks, sun flower stalks, etc., and with *MC* 10−15% (Grover & Mishra 1996). Contrarily, the piston press needs a higher level of maintenance and the briquettes have lower quality and cannot be carbonized if compared to the screw press (Zeng et al. 2007).

On the other hand, in **hydraulic piston briquetting machine** (**Figure 6**), the energy to the piston is transferred from an electric motor (1) through a high-pressure hydraulic oil system (Grover & Mishra 1996). Briquettes are formed by each stroke of the piston (2), when the mass is pressed in closed pressing chamber (8).

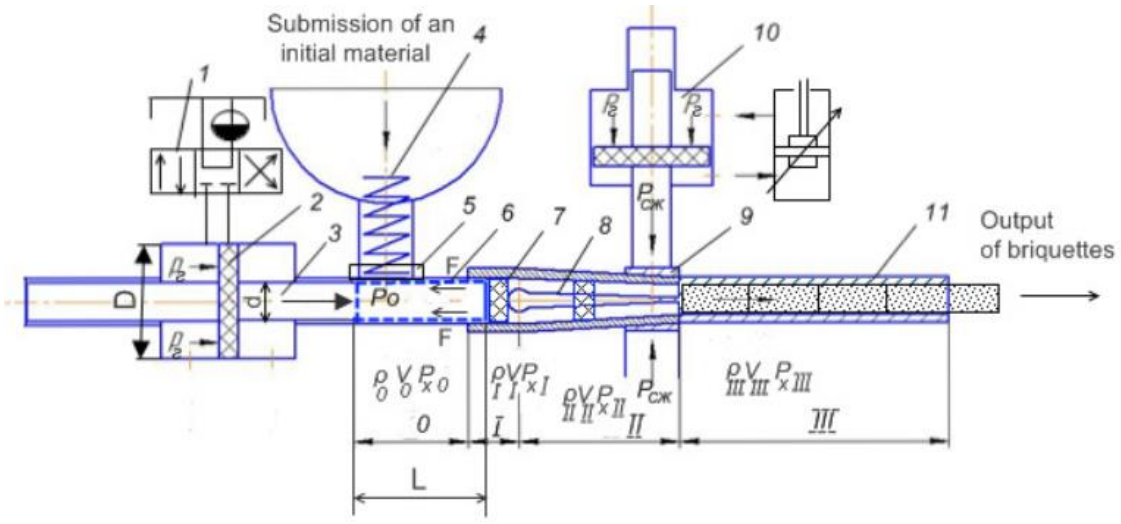


**Figure 6.** The block diagram of hydraulic piston briquetting machine BrikStar CS 50

0 - metering chamber; I and II working zones of pressing chamber and III – additional compression and strain relaxation. 1. hydraulic system provided with electric drive and adjusting elements; 2. the pressing piston of the main hydro-cylinder with a punch 3.; 4. feeder of the raw material from the bunker with screw and valve 5; 6. dosing chamber; 7. matrix with a slit; 8. pressing chamber; 9. system of a clip on the matrix with hydraulic drive 10; 11 device for additional briquette compaction and relaxations. According to it, on the scheme are shown: $\varrho_0$ - initial density of an initial material; $\varrho_{III}$ - final density of a briquette; $P_0$ - axial pressure created by a punch 3; d-diameter of a punch; Pг - pressure in a hydrosystem; D - diameter of the piston of the hydrocylinder; $P_{xI}$, $P_{xII}$, $P_{xIII}$ - axial pressure in various zones of pressing; $V_0$ - volume of an initial portion; VI, VII, VIII - volumes of briquettes portions changing during pressing; $P_{сж}$ - effort of compression of the cut part of a matrix

Source: Muntean et al. (2010) and Havrland et al. (2011)

It works with lower pressures than other briquetting types, which can cause crack formation on cylinder structure (Križan et al. 2009). Compared to the mechanical machine, it results in lower outputs (0.05 to 0.5 $t.h^{-1}$), but it can tolerate higher *MC* of agricultural residues (Zeng et al. 2007). They are generally cheaper (Havrland et al. 2011).

In a **screw press**, the biomass is extruded continuously through a heated, tapered matrix with help of rotating screw (Grover & Mishra 1996; Tumuluru et al. 2010). Screw press produces more stable and strength briquettes with smooth and noiseless operation, however, this technology is associated with higher requirements for a power consumption and maintenance (screw) compared to the piston press (Tumuluru et al. 2010). It is possible to create different shapes, from cylindrical to n-angled, with or without a hole. As the material is pressed continuously, presence of structural failures is reduced in comparison to piston presses (Križan et al. 2009). The briquettes are formed as infinite and then divided into the desired lengths. Continuous material pressing ensures a high degree of compaction and a high level of mechanical quality indicators (Havrland et al. 2011). The outer surface of the briquette from the screw press is partly carbonized which facilitates ignition and combustion. This also prevents the briquettes from catching ambient moisture (Grover & Mishra 1996).

Many studies have actively investigated densification of herbaceous and woody biomass employing piston or screw presses (Tumuluru et al. 2010). Ahiduzzaman and Sadrul Islam (2013) studied rice husks briquettes made with screw extruder. Chou et al. (2009) evaluated optimal conditions for production of rectangular briquettes from rice straw using a piston-mold process. Granada et al. (2002) investigated the biomass densification mechanism and improved hydraulic briquetting machine. Li and Liu (2000) using high-pressure piston-and-mold densification approach compressed the wood processing wastes and other residues. Thabout et al. (2015) evaluated biomass wastes briquettes produced by a manual hydraulic press. Yank et al. (2016) studied rice husk and bran briquettes densified using a manual press as well. Helwani et al. (2018) tested the manual hydraulic press on empty friut bunches with quite positive results.

As there is a wide range of feedstock materials, numberless investigations have been performed to produce biomass briquettes **from diverse agricultural and forest residues** and to evaluate their physical, mechanical and energy properties. Chin and Siddiqui (2000) compressed rice husks, peanut shells, coconut fibres and palm fruit fibres into briquettes by piston and matrix type presses. Coates (2000) and Akhmedov et al. (2017) studied briquettes from cotton plant residues. Yank et al. (2016) studied rice husk and bran briquettes under a low-pressure densification for rural applications. Brand et al. (2017) analysed briquettes from mixtures of husk and rice straw and rice husk ash. Stolarski et al. (2013) assessed briquettes from

agricultural and forest biomass residues and determined their quality and production costs. Srivastava et al. (2014) studied the energy use of briquettes from a vegetable market waste. Brunerová et al. (2017a) evaluated mechanical properties of briquettes made of straw and seed pods of poppy and wheat husks produced by the hydraulic piston press.

Other studies actively evaluated briquettes made of olive refuse (Yaman et al. 2000), olive cake (Al-Widyan et al. 2002), palm fibre and palm shell residues (Husain et al. 2002), sugarcane leaves (Jittabut 2015), sugarcane skin and bamboo fibre (Brunerová et al. 2018), wheat, barley, oat, and canola straws (Tumuluru et al. 2015), corn stalk, vine shoots, rape straw and cereal straw (Ramírez-Gómez et al. 2014), composite of mango seed shell and cashew nut shell (Huko et al. 2015), *Cerbera manghas* (Sutrisno et al. 2017), fruit wastes form durian, coconut, coffee, cacao, banana and rambutan (Brunerová et al. 2017c), corn cobs (Kaliyan & Morey 2010; Muazu & Stegemann 2015), corn stover (Yuan et al. 2010; Thoreson et al. 2014; Tumuluru 2018), banana tree waste (Ku Ahmad et al. 2018), guava fruit tree residues (Ivanova et al. 2018), cashew waste (Sawadogo et al. 2018), eucalyptus bark (Sette et al. 2018), durian peel (Mitan et al. 2018), groundnut shells and bagasse (Lubwama & Yiga 2018), cones of Scots pine, Norway spruce and European larch (Gendek et al. 2018).

Also many studies reported a potential of various types of purposely grown biomass for bio-fuels production, e.g. perennial grasses, such as *Caragana korshinskii* Kom (Zhang & Guo 2014), miscanthus (Ivanova 2012), giant knotweed, switchgrass (Kaliyan & Morey 2010; Tumuluru 2018) and giant reed (Ivanova 2012); annul plants – hemp (Alaru et al. 2011; Ivanova 2012; Kolaříková et al. 2014; Chaloupková et al. 2018a) and sunflower (Alaru et al. 2011). Urbanovičová et al. (2017) investigated briquettes from energy crops: *Spartina pectinata, Miscanthus sinensis, Sida hermaphrodita, Salix viminalis, Polygonum sachalinensis, Rosa multiflora* and *Helianthus tuberosus.*

Residual woody biomass as a traditional material for densified fuel production has been investigated by countless studies. Woody sawdust was studied, among others, by Chin and Siddiqui (2000), Lehtikangas (2001), Bergström et al. (2008), Yumak et al. (2010), Tembe et al. (2015), Antwi-Boasiako and Acheampong (2016), Lela et al. (2016). Garrido et al. (2017) produced and evaluated properties of briquettes from sawdust and date palm trunk and Križan et al. (2015) from beech biomass.

In the last years research is also focused on potential pretreatments of biomass before densification process and torrefaction is one of them. The torrefaction was recognized as improver of biomass quality in terms of decreasing moisture content and increase of heating/calorific value (Chen & Kuo 2010; Wilk & Magdziarz 2017).

## 2.6. Key variables in briquetting process

Densification process and the quality of densified product is influenced by combination of following factors: **feedstock variables** such as *MC* and particle size and shape, fibrous and non-fibrous nature, biomass composition, including protein, fat, cellulose, hemicelluloses and lignin content, usage of additional binders, and, **process variables**, i.e., matrix temperature, matrix geometry, compression pressure, speed, and retention time (Kaliyan & Morey 2009; Tumuluru et al. 2010). From this list it is obvious that the quality of final fuel is influenced not only by material and densification process itself, but also by initial pre-treatment processes such as proper material drying and particle size reduction. Particle factor is in detail described in the following Subchapter 2.6.1.

*MC* of feedstock material before the briquetting should be inside of the optimal range of 8-15%. When the *MC* is lower and, vice versa, higher, the particles are not cohesive and densified compact disintegrates. Especially residual biomass from agricultural production tends to higher *MC* (Chen et al. 2009). High *MC* can cause problems in grinding, densification and subsequent firing and excessive energy is required for drying (Grover & Mishra 1996). Type of feedstock material and its properties has the major effect on energy characteristics (*CV*, burning time, fuel ignition), content of heavy metals, volatile matter content, ash content, ash fusibility and other parameters (Davies & Abolude 2013; Poddar et al. 2014; Antwi-Boasiako & Acheampong 2016; Sutrisno et al. 2017; Monedero et al. 2018). Ratio DM/*MC* significantly affects *CV*. Water evaporates during combustion and it reduces the basic *CV* of the biomass dry matter (Werther et al. 2000). Field of solid biofuels production goes hand in hand with evaluation and control of feedstock influence on combustion facilities too (Fournel et al. 2015; Huko et al. 2015). Pressure of compaction is the most important variable with the main influence on briquette strength; with increasing pressure the density and strength of briquette increase (Križan et al. 2009; Tumuluru et al. 2010). Compacting pressure is related to compaction temperature, which determines the segregation of lignin from the cellular structure of the biomass. The optimal value of pressing temperature for lignin plastification (that corresponds to glass transition temperature of lignin) depends on the type of material which is densified, but generally it is approximately 120ºC (Križan et al. 2009). With an increasing pressing temperature, there is lower need of compacting pressure and vice versa (Kaliyan & Morey 2009; Križan et al. 2009).

An influence of mentioned variables has been actively investigated. Yank et al. (2016) studied the influence of a binder type on quality of rice husks briquettes. Jirjis (2005) evaluated the role of particle size and pile height on storage processes and fuel quality of chopped *Salix viminalis*. Yumak et al. (2010) briquetted Russian tumbleweed (*Salsola tragus)* with three moisture

levels (7%, 10%, and 13%) in hydraulic press with two dies (cylindrical and square) using three pressure levels (15.7, 19.6 and 31.4 MPa). Tumuluru et al. (2015) studied impact of briquetting pressure, hammer mill size, and *MC* on briquette quality properties of wheat, barley, oat, and canola straws briquettes. Tumuluru (2018) evaluated effect of *MC* and hammer mill screen size on briquette properties of woody (pine wood chips) and herbaceous biomass (switchgrass, corn stover). Thoreson et al. (2014) investigated the effect of compression pressure, *MC*, particle size, and material composition on quality of briquettes from raw corn stover. Kaliyan and Morey (2009) presented that achieving a temperature averaging 75 °C was essential to activate binding components of cellulosic materials and to produce stable products. Ndiema et al. (2002) densified briquettes under pressure ranging from 20 to 140 MPa and reported pressure of 80 MPa beyond which no significant gain in bonding may be achieved. Demirbas et al. (2004) produced quality briquettes made of spruce wood sawdust and pulping reject with initial *MC* of 12% (w.b.), matrix temperature of 130 °C and compression pressure of 12.5 MPa. Pampuro et al. (2018) reported that compression pressure, in the range of 40–80 MPa, significantly affected the specific compression energy requirements, the final density and the durability of the produced compacts. Al-Widyan et al. (2002) reported that retention compression times between 5 and 20 seconds did not have a significant effect on durability and density of olive cake briquettes. Further studies were done by Havrland et al. (2011), Stelte et al. (2011b), Wrobel et al. (2013), Zvicevicius et al. (2013), Rynkiewicz et al. (2013), Poddar et al., (2014), Križan et al. (2015), Miao et al. (2015), Harun and Afzal (2016), Muntean et al. (2017), Whittaker and Shield (2017).

### 2.6.1. Particle size and shape

Understanding of particle morphological and rheological behaviour as well as measuring particle size and understanding how it affects processes and final products can be critical to the success of many manufacturing businesses and industries (Shekunov et al. 2006; Vaezi et al. 2013; Agimelen et al. 2017; Cardona et al. 2018). In case of biomass it is significant in fields associated with particle handling, transportation, mixing, dosing, fluidization, possibility of densification, gasification or combustion (Dai et al. 2012; Gil et al. 2014; Ahmad et al. 2016; Holmgren et al. 2017; Trubetskaya et al. 2017; Knoll et al. 2019). In case of the biomass densification, understanding the morphological behaviour of input material is crucial to optimise design of used equipment, reduce energy consumption and improve the quality of products (Mani et al. 2014b).

Reduction of biomass size into **appropriate particle size** is an important pre-processing operation in using biomass for energy purposes (Igathinathane et al. 2010). It should lead to finer particle grind and to the breakage of compacted structure of the lignocellulose by disruption of

its microfibers to improve the availability of bioactive substances specific surface area for further processing and conversion processes (Sun & Cheng 2002). Generally, aim of size reduction is to increase an accessible surface area, size of feedstock porosity and enlarge number of contact points for further adhesion and binding between particles (Shaw 2008; Guo et al. 2012; Bajwa et al. 2018). Decreased particle size also lets the loose particles to dry more rapidly (Kaliyan & Morey 2009). Biomass size reduction decreases pressure and specific energy requirements to about 50% (Miao et al. 2015). Moreover, grinded biomass produces more stable flame, lower $CO_2$ and ash emissions and high burnout during combustion when compared briquettes to bales (Tumuluru et al. 2014).

**Efficient grinding** of biomass to an appropriate particle size fraction is one of the challenges in the development of systems based on manipulation with reduced particle size (Holmgren et al. 2017) since rather small particles are required, but conversely fine milling is high energy demanding (Mani et al. 2004; Dai et al. 2012; Wang et al. 2018a), thus balance between energy efficiency and costs should be established (Gil & Arauzo 2014). Consumed energy is influenced by material type and its physical and mechanical properties, grinding machine type and blade edge sharpness (Womac et al. 2005; Tumuluru et al. 2014). There are several types of **grinding machines** available such as hammer mill, knife mill, disk mill, crusher and roller mill (Grover & Mishra 1996; Svihus et al. 2004; Guo et al. 2012). The grinders may produce particles with different dimensional properties; **hammer mills** may produce more fines and more prolonged particles than grind from knife mill (Paulrud et al. 2002). Angular speed of hammer and mesh size are the most important variables influencing the grinding process (Gil & Arauzo 2014). Angular speed of grinders influences variability and dispersion of size; higher the angular speed of hammer, the lower the dispersion on particle size and contrarily physical conditions of the biomass have a negligible effect on particle size distribution (Gil & Arauzo 2014). There are several studies focused on milling of herbaceous, woody and agricultural residual biomass in mentioned grinding devices (Paulrud et al. 2002; Bitra et al. 2009a; Bitra et al. 2009b; Lisowski et al. 2010; Gil et al. 2012; Williams et al. 2016; Tumuluru 2019). Kirsten et al. (2016) evaluated the performance of three different grinding techniques: cutting, impact and hammer mill with different variables as mesh sizes of 2, 4, and 6 mm, with or without additional aspiration, and, found out that the hammer mill with a 4 mm screen size produced optimal feedstock for production of densified fuels with desired bulk density and durability while having the lowest specific energy input. Grinding with the hammer mill is the most effective to grind the fibrous material and produce the required wide particle size distribution (Kirsten et al. 2016)

Because of the high and varied proportion of cellulose, hemicellulose and lignin in biomass composition, which is different for all plant species, **particle morphology can be**

**greatly irregular** (Guo et al. 2012). Particles shape can be spherical (one-dimension shape – diameter of sphere) and **non-spherical**, which is in practice more probable (Dai et al. 2012). Due to the anisotropy in spatial structure, biomass particles have prolonged shape (Guo et al. 2012). There are several **shapes qualitatively described** by various studies, for instance flakes, rod-like and needle-like particle (Guo et al. 2012), or plate, slab, prism, cylinder, rod and sphere (Liliedahl & Sjoèstroèm 1998; Saastamoinen 2006). Gil et al. (2014) described particle shape as **circle, square, rectangle, rectangle fibrous, hook and hook fibrous** (**Figure 7**). Particle size and shape can be modified during the densification process itself, especially in case of brittle particles (Pietsch 2002).

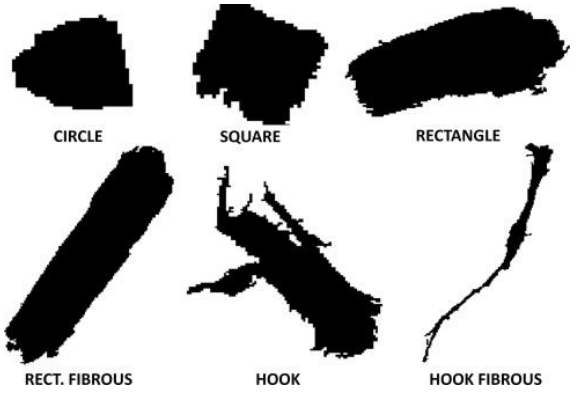


**Figure 7.** Effects of particle shape and size for poplar and corn stover
Source: Gil et al. (2014)

Particle size is a **complex parameter** (Fernlund 1998), thus at least two parameters are necessary to describe particle size/shape (Trubetskaya et al. 2017). It can be represented by several variables, such as length, width, diameter, perimeter, surface area, volume and descriptors calculated from them, like sphericity, roundness and ratios of two object dimensions (Murphy 1984; Vaezi et al. 2013; Bagheri et al. 2015; Zhao & Wang 2016). Often, particle morphology of more or less regular shapes is simplified by a single parameter size, assuming sphericity or circularity (Lu et al. 2010; Ulusoy & Igathinathane 2016). Already in 1953 Powers (1953) defined six roundness classes for characterization of sedimentary particles (**Figure 8**).

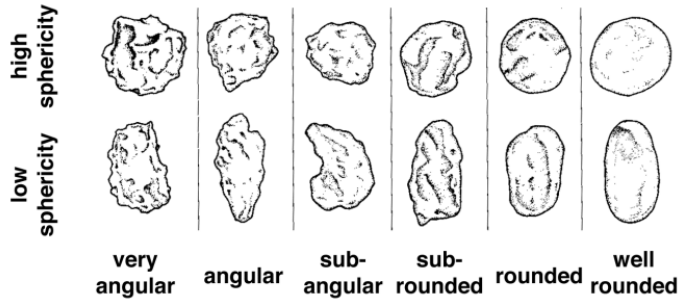


**Figure 8.** Roundness and sphericity scale for sedimentary particles
Source: Powers (1953)

Behaviour models of spherically-shaped particles have been studied for many years (Walpole 1972; Militzer et al. 1989; Tripathi et al. 1994; Riguidel et al. 1994; Niazmand & Renksizbulut 2003; Antonyuk et al. 2005). However, assuming sphericity for biomass particles may result in large errors at most biomass particle sizes (Lu et al. 2010). Slowly there is a progress in studies predicting and describing behaviour of irregular biomass particles (Bagheri et al. 2015; Dioguardi & Mele 2015; Wang et al. 2018b; Elfasakhany & Bain 2019; Knoll et al. 2019). Despite numerous studies on biomass particle morphology, there is no universal consensus on how to represent a biomass particle size and shape in some details, thus the combination of several descriptors is needed (Pons et al. 1999).

Particle size and shape measurement has long tradition in soil and sediment sciences (Cox 1927; Wadell 1932; Krumbein 1941; Koerner 1970) and core of biomass morphology characterization originates from these disciplines. Classification of particular matter/material based on dimensional properties has long been based upon sieve analysis where the material is separated by sieves of differently sized apertures into fractions of particle size distribution (Fernlund 1998). Biomass fuels rarely consist of particles of uniform size, for this reason not only a mean size should be measured, but also **particle size distribution** (hereafter referred as PSD). PSD analysis procedure serves for evaluation of dimensional and morphological properties of particulate/granular materials (Igathinathane et al. 2009a; Vaezi et al. 2013). PSD is an important characteristic in various industries as pharmaceuticals, agrochemicals, detergents, pigments and food industry (Agimelen et al. 2017). Commonly, output from PSD analysis is composed of percentage of particles retained on sieves with descending opening sizes, cumulative undersize distribution (**Figure 9**), geometric and arithmetic mean value and associated standard deviation, and many more characteristics that in specific manner describe the size distribution of particles depending on an applied method (Igathinathane et al. 2009a).

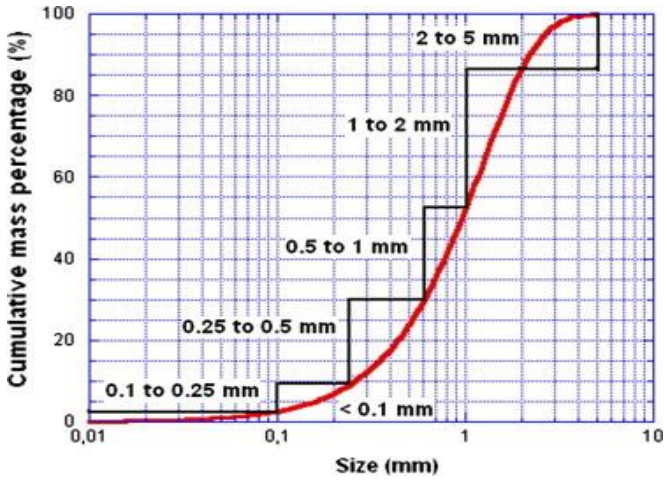


**Figure 9.** Typical cumulative PSD of milled biomass
Source: Gil et al. (2014)

To determine PSD precisely quite large numbers of particles are required. Masuda and Gotoh (1999) estimated by the application of theoretical equation that about 61000 particles are needed to obtain the mass median diameter of particles within 5% error with 95% probability for a particular material having a geometric standard deviation of 1.60.

For determination of PSD there are several approaches available, including laser diffraction, acoustic spectroscopy, light scattering, cascade impactors, traditional mechanical screening/sieve analysis whose procedure is generally standardized (e.g. EN ISO 17827-1 2016) for biomass and lately developed machine vision and image analysis (Igathinathane et al. 2009b; Gil et al. 2014). **Classical sieve analysis** separates the material by sieves of different sized apertures/openings; the approach is widely used in various fields, standardized, inexpensive, easy to perform and giving a possibility to physically separate the particle size fractions (Al-Thyabat & Miles 2006; Ulusoy & Igathinathane 2016). On the other hand, this method has several disadvantages as: limited set of available standard sieves, bounded number of sieves that can be held by a shaker, non-suitability for fine fractions under 38 μm (Persson 1998), assumption of particle spherical shape (Mora & Kwan 2000), and longer analysis time for smaller sieve openings (Persson 1998). A number of studies has reported the PSD results of different biomass materials, e.g. wheat straw, switchgrass, corn stover (Bitra et al. 2009), barley straw (Mani et al. 2006), *Cynara cardunculus* L. (Igathinathane et al. 2009b), miscanthus, pine sawdust (Igathinathane et al. 2009b; Chaloupková et al. 2016), wood sawdust and shavings mixture (Vítěz & Trávníček 2010), industrial wood particles (Li et al. 2014) and hemp (Dinh 2014; Chaloupková et al. 2016).

How **particles size affects quality and physical properties** of briquettes was investigated by several authors. Bergström et al. (2008) reported no significant effect of the PSD of Scots pine sawdust (*P. sylvestris* L.) on the briquetting process as well as on the physical and thermo-chemical characteristics of produced pellets, however, claimed that the results are not applicable to other types of biomass materials. Lisowski et al. (2010) compared PSD of seven energetic plant species, including *Miscanthus* × *giganteus*. Černá et al. (2016) evaluated influence of PSD on durability of digestate briquettes. Rahaman and Salam (2017) investigated the effect of particle size together with pressure and mold diameter on the physical characteristics of rice straw briquettes. Urbanovičová et al. (2017) evaluated effect of particle size on physical and mechanical properties of briquettes made of various energy crops. Wang et al. (2018a) investigated the effects of the particle size on the rice straw briquetting process, energy consumption, maximum extrusion force, product compressive strength and product density. Sette et al. (2018) evaluated impact of particle size on the quality of eucalyptus bark briquettes.

Basically, we can say that the particle size of the fraction affects the pressing process itself. It influences the smoothness of the pressing process and the resulting product quality. Generally, agricultural residues have poor flow characteristics that can cause problems during the pressing and principally irregular particle size and shape have significant effect on this behaviour. The granular homogeneous materials (preferentially 6–8 mm in size) that may flow easily in conveyors, feeders and storage silos, are appropriate for densification (Grover & Mishra 1996). The higher input fraction size requires more pressing power. The product has lower homogeneity and strength. As the size of the fraction increases, the bonding forces also decrease, resulting in a rapid disintegration of the compact (fast burning of the densified biofuel is undesired). The pressing pressure increases as the size of the pressed material fraction increases. In case of binder-free compaction, the surface of the feedstock particles should touch the largest surface of each other. The size of the contact surface increases with increasing fineness of the material and with increasing pressing pressure (Križan et al. 2015).

### 2.6.2. Briquette structure

Structure of briquette is an important variable affecting many briquettes properties and performance. The structure (internal structure) of a material is defined by the character and geometric arrangement of solid particles and the nature of the bonds between them. Generally, it is greatly affected by employed type of agglomeration and binding mechanisms prevailing and involved in a compact creation (Pietsch 2002). Regarding pressure agglomeration (e.g. briquetting), the structure is affected by degree of structural, elastic and plastic phase of deformation and applied pressure level (Pietsch 2002). The structure is given by the particle nature and arrangement and depends on various characteristics related to particle morphology and rheology like particle size and PSD, macroscopic and microscopic shape of particle and roughness (Pietsch 2002; Muntean et al. 2013). Composition of an input material is of a great influence on the final structure. Grind biomass material is characterized by its porosity, which considerably decreases during the compression (Miao et al. 2015) and in case of the final densified product a high porosity is undesirable. Mainly in the course of high-pressure agglomeration variables related to the input particles may modify, especially size and shape of brittle particles (Pietsch 2002). However, on micro-structural level, particles exposed to high pressures show no fractions and disruptions in the cell walls (Miao et al. 2015).

## 2.7. Computer vision & image analysis – tool for structure and particle visualization

Artificial vision and related image analysis are another method for inspection and quality evaluation. In general, machine (or computer) vision and image analysis are highly helpful and effective tools with varied scope of employment in diverse fields of industry and science (Batchelor & Bruce 2012; Davies 2018), where greater precision, efficiency, quality and performance of observed objects are highly demanded. It includes tasks as visual examination of prescribed parameters, pattern recognition, estimation of size, shape, structure and texture, colour, object counting and defects identification (Gongal et al. 2018; Manish et al. 2018; Smith et al. 2018; Su et al. 2018; Tan et al. 2018) of wide range of materials including metals (Wang et al. 2015), plastics (Kim et al. 2016), glass (Huang et al. 2018), wood (Gutzeit & Voskamp 2012), ceramics (Bao et al. 2017), rubber (Kuang et al. 2019), gravel (Kumara et al. 2012), concrete (Shah & Kishen 2011; Ozen & Guler 2014), fruit (Cubero et al. 2014; Song et al. 2014; Rady et al. 2017), vegetable (Pace et al. 2015; Pan et al. 2017), nuts (Sunoj et al. 2018), meat (Girolami et al. 2013) and other food products (Morais de Oliveira et al. 2015; Calvo et al. 2016).

Use of these artificial-vision-based techniques has expanded to biomass-to-energy applications. Artificial vision and imaging applications are suitable for assessment of briquette/pellet **structure, particle size and shape properties** (Wang 2006; Pothula et al. 2014; Pons & Dodds 2015).

There are many studies that have researched the 2D shape factors of biomass by microscopy (Guo et al. 2012), 2D digital imaging (Gil et al. 2014), and 3D particle through reconstruction algorithms to calculate particle surface area and volume (Lu et al. 2010; Bagheri et al. 2015; Williams et al. 2016). In the **Figure 10** we can see a schematic illustration of different protocols used to measure dimensions of an irregular particle.

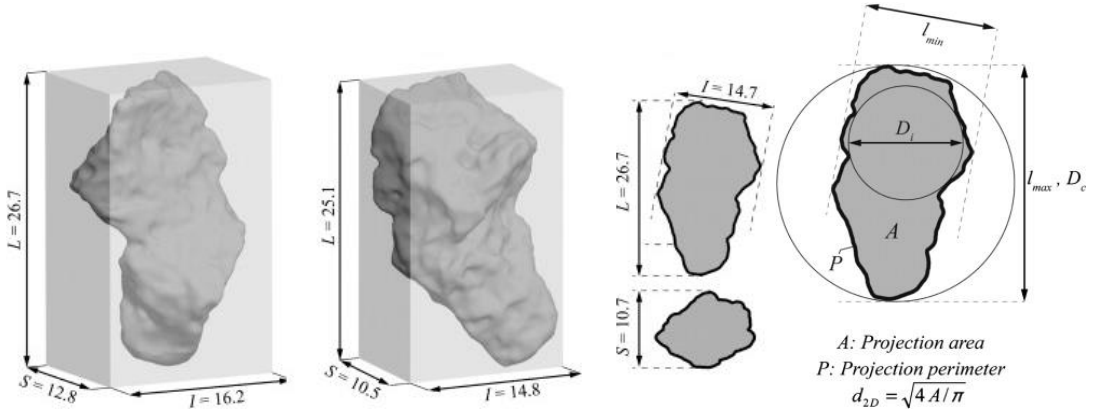


**Figure 10.** Variables determined for a particle projection using ImageJ and MATLAB software
Source: Bagheri et al. (2015)

Briquette surface and/or interior structure is possible to visualize and study by image scanning of a briquette cross-section that may bring information and knowledge on particle size and its distribution, porosity, binding mechanisms, and, with the application of appropriate specific software, a shape factor, particles' specific surface area and many other parameters. Precision may be broadened by examination of multiple cuts of the same agglomerate and further statistical data analysis (Pietsch 2002).

Computer vision algorithms evaluate images obtained usually from the interaction of visible light with the observed object or less commonly from the scanning of surface with a focused beam of electrons (Ribeiro & Shah 2006). Images can be taken with a real size of the object or with some level of **magnification**, e.g. use of microscopy. On nano- and micro-levels a **scanning electron microscopy** (SEM) is an effective technique enabling these advantages (Pietsch 2002). For example, Zhang and Guo (2014) using the SEM examined structure of briquettes from perennial grass *Caragana korshinskii* Kom regarded to their porosity (**Figure 11**). Kaliyan and Morey (2010) using SEM and light microscopy investigated structural bonding mechanisms on micro level in corn stover and switchgrass briquettes and pellets (**Figure 12**). Stelte et al. (2011b) studied fracture surfaces of beech pellets using also SEM to understand inter-particles bonding. Huang et al. (2008) studied the structures of biomass briquettes from corn stalks by microscopy. Miao et al. (2015) evaluated a particle porosity of compressed miscanthus and switchgrass using SEM. The same technique used also Okot et al. (2018) in investigation of the main bonding mechanisms in briquettes form corn cobs produced during different densification conditions. Roman and Świętochowski (2016) studied briquette structure using X-Ray analysis. Zhao et al. (2015) investigated structure of carbonized anthracite briquettes obtained at different pyrolysis temperatures by surface area measurements, SEM, Fourier transform infrared spectroscopy, Raman spectroscopy and X-ray photoelectron spectroscopy.

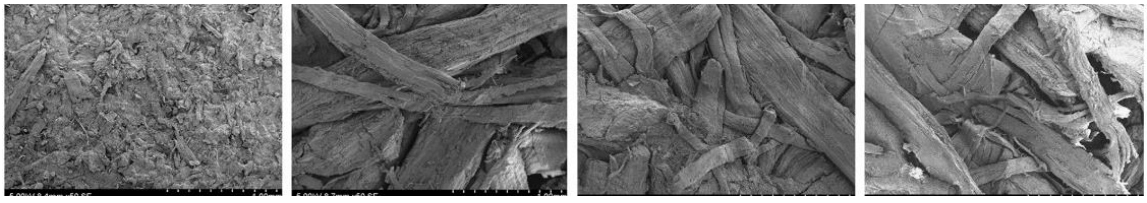

**Figure 11.** Scanning electron microscopy (magnification at 50×) images of cross-sections of briquettes.
Source: Zhang and Guo (2014)

In case of a visualization of loose particles with **real size**, the computer vision-based method can be used for PSD analysis, where it is an interesting alternative or even substitution for traditional sieve analysis method (Igathinathane et al. 2009a; Igathinathane et al. 2009b; Souza

& Menegalli 2011; Kumara et al. 2012). Unlike the sieve analysis, the image analysis is an approach sensitive to the geometrical particle shape and considering more parameters than just sphericity which leads to more precise results. Besides accuracy, PSD analysis using imaging offers time savings, individual measurement of all particles, and it gives an additional information relating to the size, shape, texture and the number of particles (Fernlund 1998; Igathinathane et al. 2009b; Shanthi et al. 2014). Souza and Menegalli (2011) suggested a number of particles required for such analysis and the statistical methodology to be used in its evaluation. Paulrud et al. (2002) studied PSD of wood particles using image analysis to compare different grinding machines. Febbi et al. (2015) used image analysis with multivariate modelling approach to construct cumulative PSD curves based on chip mass. Gil et al. (2014) compared effectiveness of PSD of poplar and corn stover via sieve method and image analysis. PSD can be also analysed using photo-optical analyser, which quantitatively measures all particles in real time (Chaloupková et al. 2018b). This method undoubtedly provides several merits, yet the material is not physically separated. On the contrary, this is offered by another method of machine vision – by sensor-based sorting, which enables physical separation of granular material into predefined classes in real time (Maier 2017). Nowadays it is used in the field of waste management (Kępys 2016), food processing (Narendra & Hareesh 2010) and mining industry (Lessard et al. 2014).

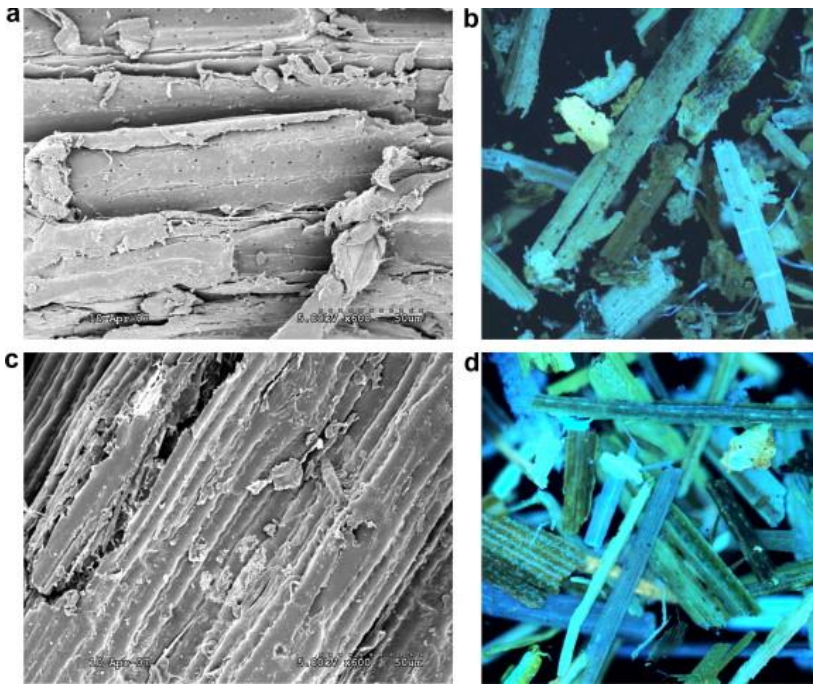


**Figure 12.** Scanning Electron Microscopy (SEM) (magnification at 600×) and UV-Auto-Fluorescence (UV-AF) (magnification at 145×) images of corn stover (Fig. 12a and b) and switchgrass (Fig. 12c and d) grinds before briquetting or pelleting. The green or yellow-green represents protein compounds and whitish fluorescence represents the cutin (cuticle).

Source: Kaliyan and Morey (2010)

## 2.8. Briquettes quality attributes

Quality requirements for woody and non-woody bio-briquettes and pellets are generally standardized, in EU for instance by EN ISO 17225-2,3,6,7 (2014). These international norms define physical, chemical and mechanical properties of briquettes/pellets. As described in the Chapter 2.6. densification process is influenced by several factors, such as feedstock and process variables (Tumuluru et al. 2010). Quality of final products is evaluated from its **chemical, physical-mechanical** and **energy aspect**.

### 2.8.1. Moisture content

Lower *MC* of the briquettes should be secured already before densification and by the briquetting process itself (Grover & Mishra 1996). Densified biomass relates to lower possibility of degradation since the *MC* is decreased during the compaction process and higher resistance to an air humidity (Karunanithy et al. 2012). Up to 70% of relative humidity does not have any effect on storage conditions of commercially available briquettes (Singh 2004). High *MC* can result in a poor ignition, decrease of combustion temperature, which in turn hinders the combustion of the reaction products and consequently affects overall the quality of combustion (Werther et al. 2000). Higher *MC* may also have effect on storage conditions since it leads to less-durable and stable products with susceptibility to spoilage (Tumuluru et al. 2010).

### 2.8.2. Chemical properties

The composition of biomass in terms of *C*, *H*, and *O* differ among different biomass sources. **Table 1** presents proximate and ultimate analyses of several types of biomass and bituminous coal (Bapat et al. 1997; Allica et al. 2001). Typical (dry) weight percentages for *C*, *H*, and *O* range 30 to 60%, 5 to 6%, and 30 to 45%, respectively (Khan et al. 2009).

*N, S* and *Cl* are found in amounts usually less than 1% dry matter, but sporadically well above this. *N* is a micronutrient for plants, and a crucial element to their growth. Some inorganic compounds may be found in higher concentration too. Compare to coal, biomass in general has lower content of *C*, more *O*, more $SiO_2$, *Cl* and *K*, less *Al, Fe, Ti* and *S*, and occasionally more *Ca* (Khan et al. 2009).

**Volatile matter** (*VM*) refers to the part of the biomass that is released when the biomass is heated. In comparison with coal and wood, agricultural residues and herbaceous biomass are characterized by higher contents of *VM* (up to 80%). This indicates that the materials are easier

to ignite and to burn, however, the combustion is supposed to be quick and difficult to control (Werther et al. 2000). Content of *VM* affects the overall combustion process.

**Table 1.** Analysis of some biofuels and bituminous coal (mass basis)

| Fuel | Proximate analysis | | | | Ultimate analysis | | | | | |
|---|---|---|---|---|---|---|---|---|---|---|
| | ***MC*** | ***VC*** | ***FC*** | **Ash** | ***C*** | ***H*** | ***O*** [d] | ***N*** | ***S*** | ***Cl*** |
| | **%** | **%** | **%** | **%** | **%** | **%** | **%** | **%** | **%** | **%** |
| **Pine pellets** | 4.9 | 80.4 | 14.5 | 0.2 | 45.5 | 6.6 | 47.7 | Lld | Lld | Lld |
| **Demolition wood pellets** | 9.1 | 69.6 | 19.7 | 1.7 | 45.7 | 6.3 | 36.2 | 0.9 | Lld | 0.1 |
| **Palm fibre** | 36.4 | 43.6 | 12.0 | 5.3 | 51.5 | 6.6 | 40.1 | 1.5 | 0.3 | - |
| **Pepper plant residue** | 6.5 | 60.5 | 19.5 | 13.5 | 33.8 | 4.0 | 39.1 | 2.5 | 0.5 | 0.1 |
| **Greenhouse residue** | 2.5 | 61.0 | 5.50 | 31.0 | 47.1 | 7.4 | 10.9 | 1.0 | Lld | 0.1 |
| **Wheat straw**[a] | 13.9 | 77.9 | 21.5 | 6.8 | 56.7 | 6.7 | 48.8 | 1.0 | 0.2 | - |
| **Sunflower pellets** | 11.2 | 65.2 | 19.5 | 4.1 | 44.1 | 5.17 | 34.6 | 0.5 | 0.1 | 0.1 |
| **Olive cake pellets** | 11.9 | 64.2 | 15.7 | 8.2 | 42.1 | 4.99 | 31.0 | 1.3 | 0.1 | 0.3 |
| **Sewage sludge** | 6.9 | 44.6 | 7.0 | 41.5 | 52.0 | 6.3 | 32.1 | 6.3 | 3.1 | - |
| **Bituminous coal** [c] | 4.9 | 32.3 | 48.1 | 14.7 | 65.7 | 5.6 | 7.7 | 1.2 | 0.5 | Lld |

[a,c] Ashing at 815 °C [d] by difference; Lld ~ below the lower detection limit; - ~ Not reported

The **ash** content is an indicator of slagging behaviour of the biomass (Grover & Mishra 1996). Generally, the higher ash content means the greater slagging behaviour and corrosion problems (Grover & Mishra 1996). Herbaceous biomass and mainly straws have higher ash content, ranging from 9 to 22% (Zevenhoven 2010; Schmitt & Kaltschmitt 2013). These negative aspects can be overcome by the addition of mineral additives or mixing with other biomass materials that can raise the melting temperature (Steenari et al. 2009; Wang et al. 2012). Biomass can contain also heavy metals, namely the harmful ones *As, Cd, Cr, Cu, Hg, Mn, Ni, Pb, Se, Tl* and *V* that remain in the ash after combustion (Nzihou and Stanmore 2013).

### 2.8.3. Calorific value

The calorific value (*CV*), also called heating value, represents the fuel energy content on a dry basis. It is one of the most significant characteristic indicators for design calculations and numerical simulations of thermal systems (Werther et al. 2000). *CV* can be expressed on two bases, as **gross calorific value** (*GCV*) or higher heating value and **net calorific value** (*NCV*) or lower heating value and can be determined experimentally by using a bomb calorimeter, which measures the enthalpy change between reactants and products. The *GCV* refers to the heat released from the mass of fuel during complete combustion with the original and generated water in a condensed (liquid) state, while the *NCV* is based on gaseous water component as the product and in practice it is calculated by subtracting the energy consumed to evaporate the *MC* of the

fuel. Biomass has usually lower heating value compared to coal (Khan et al. 2009). Generally, *C* and *H* increase the heating value while *O* decreases it. The lignin content of the lignocellulosic fuel is greatly correlated with the heating value. The *GCV* of lignin was reported to be higher than the cellulose and hemicellulose. It is because they have higher degree of oxidation (Demirbas 2005). The heating value of fuel rapidly reduces with increasing *MC* (Werther et al. 2000).

### 2.8.4. Briquettes' strength and durability

Purpose of densification process is to create dense, strong and durable bonding between particles to produce highly durable and stable products more resistant to damages during handling (Mani et al. 2006). During the logistic operations, briquettes are subjected to several forces from any directions that may cause degradation or failure (Gilvari et al. 2019). The acting forces can be divided into three main groups, namely compressive forces, shear forces, and impact forces (Kaliyan & Morey 2009).

Efficiency of briquettes' compactness can be determined by testing product's maximum strength/resistance to withstand forces and stresses (compressive resistance, impact resistance, water resistance) and durability/abrasion resistance – ability of briquette to withstand abrasion (Pietsch 2002; Kaliyan & Morey 2009).

**Compressive resistance** (strength/hardness/crushing resistance) is the maximum compressive load a briquette may withstand before cracking or breaking (Kaliyan & Morey 2009). Compressive strength tests simulate the compressive forces acting on a specimen during transportation and storage operations (Gilvari et al. 2019) with application of various devices, including universal testing machine (Kaliyan & Morey 2009). A compressive resistance can be calculated both as compressive force in cleft, i.e. force applied on briquette's side and divided by briquette length (Brožek et al. 2012; Brunerová 2018), and, compressive axial force applied on briquette's cross-section divided by area of the cross-section (Kers et al. 2010; Huko et al. 2015). The first mentioned method considers the briquette length, which varies more among the samples unlike the briquette diameter (Brožek et al. 2012).

The **impact resistance** (or shattering resistance/drop test) determines the resistance of sample when this sample is dropped from a known height onto a specific floor material (Gilvari et al. 2019). Beside others, Okot et al. (2018) used this method in evaluation of corn cob briquettes mechanical properties, Li and Liu (2000) for oak, oak bark, pine and cottonwood briquettes or Rajaseenivasan et al. (2016) for sawdust briquettes blended with neem powder. The last mentioned also tested the same material by **water resistance test**, when the briquettes were immersed in water and maintained at the atmospheric temperature for 30 seconds to determine

the percentage of water resistance to penetration. The test indicates the storage behaviour of briquettes during the contact with water, like rain etc., (Kaliyan & Morey 2009).

**Mechanical durability** (*DU*) also called abrasion resistance is defined as an ability of briquettes to remain intact, e.g. without abrasion and dust/fines production during handling and transportation (EN ISO 16559 2014) and is determined by placing a specific mass of screened briquettes into the device, which enables briquette-briquette and briquette-wall interactions during a specified time period. Then amount of fine particles (abraded matter) produced during the test is determined using sieving and finally, the *DU* is expressed as the percentage fraction of mass remained on sieve divided by the initial mass (Kaliyan & Morey 2009; Gilvari et al. 2019). Various devices of different designs are used by researchers to determine the *DU* of solid biofuels such as the rotating drum (Temmerman et al. 2006; Gendek et al. 2018), tumbling can (Rajaseenivasan et al. 2016), Holmen device (Obidziński et al. 2019), ligno tester (Obernberger & Thek 2004), and electronic friabilator (Zainuddin et al. 2014). The working principles and some examples of each test device are explained and summarized by Gilvari et al. (2019).

### 2.8.5. Volumetric mass density

Besides above-mentioned properties, volumetric mass density (or density) is another important indicator of briquette quality (Tumuluru et al. 2010) mainly from the viewpoint of manipulation, transportation, burning speed and briquette stability (Križan 2007). The final density of the produced briquettes is the major parameter characterizing the pressing process and it generally depends on height of applied pressure (Havrland et al. 2011). Higher density means desired longer burning time (Križan 2007; Kers et al. 2010).

Many researchers including Chin and Siddiqui (2000), Rabier et al. (2006), Kaliyan and Morey (2009), Ivanova (2012) evaluated the quality of the densified products in terms of briquette/pellet strength, stability and/or *DU*. Zhang and Guo (2014) studied impact of input and process variables on density, compressive strength and impact resistance of briquettes made of *Caragana korshinskii* Kom. Karunanithy et al. (2012) evaluated physio-chemical properties of briquettes made of different bio-materials. Demirbas et al. (2004) studied quality of briquettes made of spruce wood sawdust and pulping reject in term of *MC,* shatter index, water resistance, compressive strength, *CV* and combustion properties. Gaitán-Alvarez et al. (2017) studied density, internal density variation, *MC*, water absorption and compression force of torrefied biomass pellets of five wood species. Physical and mechanical properties of briquettes were further studied by Thabuot et al. (2015), Tumuluru et al. (2015), Yank et al. (2016), Urbanovičová et al. (2017).

# 3. Hypotheses and aims of the Thesis

## 3.1. Hypotheses

The research of the Thesis has been conducted under certain hypothetical considerations, based on the gained experience and observations conducted during the past studies and investigation.

**Hypothesis 1**

There are differences in particles size in different briquettes surface locations, larger particles are generally located on the front side of briquettes cross-section and vice versa smaller ones on the rear side, larger particles are centred in the middle of briquette cross-sections and smaller particles are located on the briquette bottom.

**Hypothesis 2**

Structure of briquettes influences their main mechanical properties. Particle size and particle size distribution affect the mechanical stability of briquettes as well as non-uniform distribution of particle sizes on the briquette surface has negative influence on the briquette mechanical strength.

**Hypothesis 3**

There are links between excretion of binding agents and mechanical strength of the briquettes.

## 3.2. Overall objective

The main objective of the present Thesis is to assess surface structure of briquettes in order to identify agglomeration rules and to determine relationships between briquettes structure and their mechanical properties.

## 3.3. Specific objectives

To achieve the above-mentioned goal, the overall objective of the Thesis has been supported and supplemented by specific objectives that had been defined as follows:

– to determine important input parameters (moisture content, particle size distribution and bulk density) of selected biomass materials;

– to produce briquettes of different biomass materials and fractions;

– to analyse briquette surfaces structure at various locations using microscope technique and special software for image analysis;

– to determine particles properties (their size and particle size distribution) on the briquette surface);

– to identify principles of particles agglomeration and binding mechanisms created during the compaction in the briquetting machine (pressing chamber);

– to analyse excretion and role of binding agents (lignin);

– and, to confront briquettes main mechanical properties (volumetric mass density, mechanical durability and compressive strength) with structural and compositional characteristics of feedstock materials.

# 4. Methodology

## 4.1. Materials

In this study, material and briquettes made from the following three biomass types were researched: miscanthus (*Miscanthus* × *giganteus*), industrial hemp (*Cannabis sativa* L.) and pine sawdust (*Pinus* sp.) and their **selection as study materials** was driven by the undermentioned reasons. Perennial herbaceous crop *Miscanthus* × *giganteus* was selected as it has a great energy potential and currently it attracts significant scientific attention (Brosse et al. 2012; Xue et al. 2016; Wilk & Magdziarz 2017). Industrial hemp, other representative of herbaceous biomass, is an annual fibre plant which application as a bio-energy crop is an interesting alternative (Das et al. 2017), even for production of solid biofuels (Prade et al. 2012). Both crops produce high yields of above ground biomass and are characterized by low-intensive cultivation (Alaru et al. 2011; Wilk & Magdziarz 2017). And pine sawdust as a wooden material represents a traditional input material for solid biofuels production (McKendry 2002; Deac et al. 2016), thus this residual material has been included to the study as well. The intention was to analyse three compositionally different feedstocks - herbaceous, fibrous and wooden biomass and to compare them. Brief descriptions of selected materials are presented below.

### 4.1.1. Miscanthus

Miscanthus is a large **perennial rhizomatous grass** from *Poaceae* family with C4 photosynthesis (McKendry 2002; Lewandowski et al. 2003; Clifton-Brown et al. 2004; Dufossé et al. 2014). This non-food energy crop has its origin in the East Asia, however, it is widely cultivated in temperate climates throughout the world (Lewandowski et al. 2003). It is fast-growing grass with low input requirements, easy to maintain, resistant to pathogens and estimated life time of a plantation of 20–25 years (Lewandowski et al. 2003; Wilk & Magdziarz 2017). The cultivation of miscanthus is a good option for areas that are polluted with industrial contaminants, since it is characterized by quite high uptake of heavy metals from the soil (Wanat et al. 2013; Pidlisnyuk et al 2019). Miscanthus can be also planted as an anti-erosion plant (Szulczewski et al. 2018). *Miscanthus* × *giganteus* (hereafter referred to as miscanthus) has vigorous growth up to 3–4 meters and can yield annually 20–50 $t.ha^{-1}$ of dry matter for early harvests and 10−30 $t.ha^{-1}$ for the late harvest (Clifton-Brown et al. 2004). Other study reported harvestable yield values of miscanthus on arable land of 18.1–44.2 $t.ha^{-1}$ per year and yield potential on marginal land of 2.1–32.4 $t.ha^{-1}$ per year (Xue et al. 2016). Miscanthus gives higher yields of biomass dry matter as almost twice comparing to the yields of *Miscanthus sinensis* (Ivanova 2012).

Therefore, for its high yield and good combustible properties miscanthus is a promising biomass source for renewable energy generation (Hodkinson et al. 2002; Brosse et al. 2012; Xue et al. 2016; Wilk & Magdziarz 2017). *CV* varies from 14 to 17 MJ.kg$^{-1}$ and the *MC*, depending on the time of harvest (spring/autumn) and climate conditions, varies from 15% to 30% (Szulczewski et al. 2018). In Europe, miscanthus has been used mainly for heat and electricity generation (Lewandowski et al. 2003). Even though the miscanthus is lignocellulosic material it is not used for bio-ethanol production as appropriate commercial technology is still not available (Brown & Brown 2013).

Miscanthus used in this Thesis was cultivated under the natural conditions without any additional inputs in the experimental field of CULS in Prague. The experimental field was established in 2009 from underground tufts of the two years old young plants. The energy crop biomass for the present research was harvested in the spring 2017. The harvest was done manually using the gasoline-powered hedge trimmer Husqvarna (model 123 HD 65 X, Husqvarna Group, Husqvarna, Sweden). For the study purpose all above ground parts of the plant, i.e. stem, leaves and flowers, were used.

### 4.1.2. Industrial hemp

Industrial hemp (*Cannabis sativa* L.) is an **annual herbaceous fibre crop** from *Cannabaceae* family with C3 photosynthesis originated from Western Asia and India and traditionally cultivated for its long and strong bast fibres and seeds with multipurpose application (Kyzas et al. 2015; Johnson 2018). Industrial hemp (hereinafter referred to as hemp) produces great yields of above ground biomass ranging from 10 to 20 t.ha$^{-1}$ of dry matter and as other energy crops is characterized by low-intensive and high-adaptable cultivation (Kreuger et al. 2011). Whole plants of hemp can be harvested either as a green plant in the autumn or as a plant with lower water content in early spring (Kolaříková 2017). Strašil (2005) compared different energy crops from autumn and spring harvests (**Table 2**).

**Table 2.** Moisture and yield losses according to harvest time at selected crops (average for period 2001−2004)

| | Autumn harvest | | Spring harvest | | | |
|---|---|---|---|---|---|---|
| **Crop** | *MC* (%) | DM yield (t.ha$^{-1}$) | *MC* (%) | DM yield (t.ha$^{-1}$) | *MC* loss (%) | Yield loss (t.ha$^{-1}$) |
| **Hemp** | **52** | **10.25** | **24** | **7.06** | **28** | **31.1** |
| **Miscanthus** | 50 | 15.57 | 25 | 12.11 | 25 | 22.3 |
| **Reed canary grass** | 50 | 7.21 | 19 | 5.22 | 31 | 27.3 |
| **Fescue grass** | 48 | 7.25 | 19 | 5.15 | 29 | 28.9 |
| **Bohemian knotweed** | 62 | 23.06 | 20 | 14.96 | 42 | 35.1 |

Source: Strašil (2005)

Hemp has a high potential to become a promising commodity crop for production of biofuels since its parameters are comparable with other energy crops (Das et al. 2017). The whole plant can be used to produce solid biofuels (briquettes, pellets) for heating or electricity generation purposes (Prade et al. 2012; Kolaříková 2017). In Sweden, the hemp briquettes are commercially available for households (Prade et al. 2011). In case of burning properties, it can compete with miscanthus, reed canary grass and other perennial crops; regarding to energy balance of hemp, the combustion scenarios show high net energy yields and high energy output-to-input ratios (Prade et al. 2012). The *GCV* is about 18 MJ.kg$^{-1}$ d.b. and *NCV* 13.6 MJ.kg$^{-1}$ w.b. (Kolaříková 2017). Industrial hemp fibre is one of the strongest and stiffest available natural fibres (Pickering et al. 2005); its average tensile strength is 857 MPa and a Young's modulus is 58 GPa (Pickering et al. 2007). Therefore, it has high potential for use in composite materials, thus a production of hemp briquettes may bring products with good mechanical properties.

Whole plant can be also used for bioethanol production (Tutt & Olt 2011) and biogas production (Kreuger et al. 2011). The seeds on the other hand can be utilized for production of biodiesel (Patel et al. 2014). Besides the energy carries production, hemp could play important role in bioremediation of heavy metals from contaminated soils (Kyzas et al. 2015). Tanase et al. (2014) studied phytoremediation process in soils contaminated by copper and lead using rapeseed cultivation with hemp shives (hurds) as soil natural amendments in Romania with favourable results.

Hemp for the Thesis was also cultivated under the natural conditions without any additional inputs in the experimental field in Strašín, in the Plzeň Region of the Czech Republic. The cultivation was established in 2016 and harvested in the spring 2017. After harvesting, the crops were dried out naturally to the *MC* suitable for storing. For the study purpose all above ground parts of the plant (stem, leaves and flowers) were used.

### 4.1.3. Pine sawdust

The last studied biomass material was pine sawdust, a representative of **woody biomass**. Pine (*Pinus* sp.) belong to coniferous tree species that account for the majority of harvested forest tree species (Timbal et al. 2005). Sawdust, the by-product or residual product of wood processing operations is a traditional woody feedstock material for densified biofuels production (Deac et al. 2016). Compare to herbaceous biomass, woody biomass has higher *CV*, in case of pine sawdust it is approx. 18 MJ.kg$^{-1}$ (Szyszlak-Bargłowicz & Zarajczyk 2009). **Table 3** shows comparison of *CV* of pine sawdust with other coniferous and deciduous tree species. The *CV* of coniferous species is generally a bit higher than in broadleaved or deciduous tree species (Huhtinen 2006).

This wooden material was obtained as a residual material from CULS joinery in Prague, Czech Republic thus further information about its origin was not available. The material was naturally dried out to the *MC* suitable for storage.

**Table 3.** *CV* of selected kinds of sawdust

| Material | *GCV* (MJ.kg$^{-1}$) | *NCV* (MJ.kg$^{-1}$) | *MC* (%) |
|---|---|---|---|
| **Pine (*Pinus* sp.)** | **18.40** | **18.10** | **11.8** |
| ***Pinus sylvestris* L.** | 19.96 | 18.66 | 0.0 |
| **Norway spruce** | 19.61 | 18.32 | 0.0 |
| **Silver fir** | 20.59 | 19.29 | 0.0 |
| **Oak** | 18.00 | 17.90 | 7.7 |
| **Walnut** | 16.60 | 15.90 | 2.8 |
| **Ash** | 14.60 | 13.70 | 3.2 |

Sources: Szyszlak-Bargłowicz and Zarajczyk (2009), Aniszewska and Gendek (2014)

## 4.2. Methods

All methods used in the experimental part of the Thesis are summarized in following scheme (**Figure 13**).

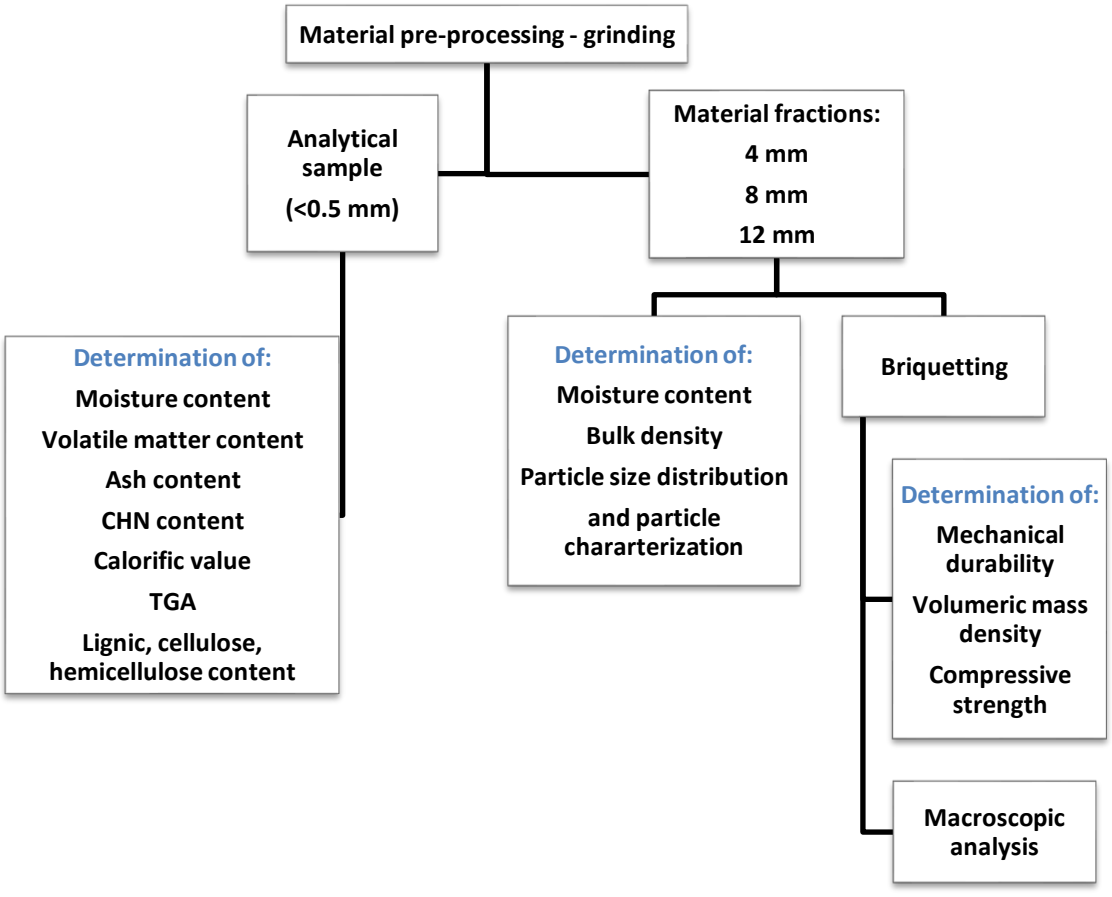


**Figure 13.** Summary of used methods in the Thesis

### 4.2.1. Pre-processing of material and sample preparation

At RIAE, the material for briquette production was grinded into **three different initial fraction sizes of 4, 8 and 12 mm** (**Figure 14**) by the hammer mill (model STOZA ŠV 15, Stoza s.r.o., Lány u Dašic, Czech Republic) with energy input 15 kW and vertical axis of rotation (more technical information is provided in the **Table 4** below). Applied grinding machine influences the properties of grinded feedstock (Paulrud et al. 2002). And specifically hammer mills are the most effective to grind the fibrous material and produce the required wide particle size distribution compared to other grinding machines (Kirsten et al. 2016). Such grinded materials (not mixed with any other materials or additives) were used besides briquette production also for determination of *MC*, bulk density and PSD.

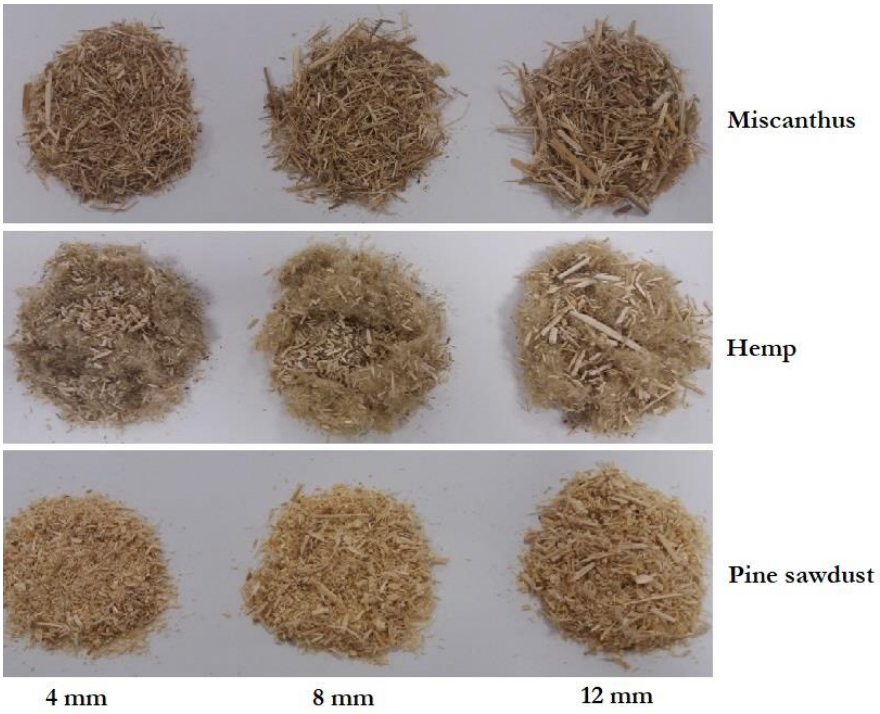


**Figure 14.** Grinded studied materials

**Table 4.** Technical specification of the used hammer mill STOZA ŠV 15

| Parameter | Unit | Value/Specification |
|---|---|---|
| **Drive method** | - | Electric motor |
| **Energy input** | kW | 15 |
| **Dimensions of inlet opening** | mm | 300 × 300 |
| **Material throughput** | $t.h^{-1}$ | 2.2–3.2 |
| **Type of grinding body** | - | 16 hammers with vertical axis of rotation |
| **Wrap angle** | ° | 360 |
| **Feeding method** | - | Manual |
| **Weight of the mill** | t | 0.4 |

Source: Souček (2008)

In accordance with EN ISO 14780 (2017) analytical samples for other analyses were prepared by further grinding using a laboratory mill (model Foss Cyclotec 1093, Foss, Denmark) and a screen with the diameter of 0.5 mm. The uniform samples were dried up at 105 ºC (more details in the Subchapter 4.2.2.1.).

## 4.2.2. Analytical methods

A concise characterisation of studied materials was carried out, based on the latest **European standards/International Organization for Standardization** for solid biofuels. Analytical standard methods used for the material characterization are summarized in the **Table 5** and described in detail in following Subchapters (4.2.2.1.–4.2.2.5). Since the topic of presented Thesis is focused on physical and mechanical aspect of input material and produced briquettes, detailed chemical analyses (content of *S, O, Cl*, inorganic elements, heavy metals, ash composition and melting behaviour etc.) have not been done, even the used chemical analyses were carried out for the materials without considering the factor of fraction size. Thus, the analytical testing samples for these analyses were prepared as the mixture of all three fractions within the material. Only the *MC* was determined also for fractions since this parameter highly influences the densification process.

**Table 5.** Summary of used analytical methods

| Parameter | Unit | Reference |
|---|---|---|
| ***Proximate analysis*** | | |
| *MC* | % w.b. | EN ISO 18134-2 (2017) |
| *VM* | % d.b. | EN ISO 18123 (2015) |
| Ash (550 °C) | % d.b. | EN ISO 18122 (2015) |
| Fixed carbon (*FC*) | % | By difference[a] |
| *FC* | % d.b. | By difference[b] |
| ***Ultimate analysis*** | | |
| *C* | % d.b. | EN ISO 16948 (2015) |
| *H* | % d.b. | EN ISO 16948 (2015) |
| *N* | % d.b. | EN ISO 16948 (2015) |
| ***Calorific value*** | | |
| *GCV* | $MJ.kg^{-1}$ d.b. | EN ISO 18125 (2017) |
| *NCV* | $MJ.kg^{-1}$ d.b. | EN ISO 18125 (2017) |

[a] *FC* is a remainder after the percentages of total moisture, ash, and volatile matter are subtracted from 100% (EN ISO 16559 2014), [b] for better comparison the *MC* was excluded, and *FC* was calculated as FC=100%−*VC* −Ash (Vassilev et al. 2010)

#### 4.2.2.1. Moisture content analysis

*MC* w.b. of materials was determined according to EN ISO 18134-2 (2017) using the **oven drying method** in the oven JP-Selecta Dry-Big (model 16/2, JP Selecta S.A., Abrera, Spain), dried out within 24 hours at 105 ºC to constant weight. For sample weighting a scale Kern (model EW 3000-ZM, Kern & Sohn GmbH, Balingen, Germany; readout d = 0.01 g) was used. MC was calculated using following formula (**Eq. 1**):

$$\boldsymbol{MC = \frac{(m_w - m_d)}{m_w} \times 100\%} \quad \text{(Eq. 1)}$$

where: $m_w$ – wet material mass (g),
$m_d$ – dry matter mass of the dried material (g).

The final results were calculated as an arithmetic means of the two measurements for each material and each fraction with respect to repeatability precision, i.e. difference between two individual results of each sample was not more than 0.2%.

#### 4.2.2.2. Volatile matter determination

Content of volatile matter (*VM*) was determined according to EN ISO 18123 (2015) standard as the loss in mass when the analytical sample placed in a crucible was **heated at 900 °C for a period of 7 minutes**. For the sample weighting a scale Mettler Toledo (model AX304, Greifensee, Switzerland; readout d = 0.1 mg) was used and for the sample heating a muffle furnace Horbesal (model JM 3/16, Ovens Hobersal SL, Caldes de Montbu, Spain) was applied. The *VC* in the samples, expressed as a % by mass on the d.b., was calculated based on following **Eq. 2**:

$$\mathrm{V}\boldsymbol{C = \frac{m_2 - m_3}{m_2 - m_1} \times 100\%} \quad \text{(Eq. 2)}$$

where: $m_1$ – mass of the empty crucible and lid (g),
$m_2$ – mass of the crucible with measured sample and lid before heating (g),
$m_3$ – mass of the crucible with measured sample and lid after heating (g).

The final result is reported as the mean of duplicate determinations with respect to repeatability precision.

#### 4.2.2.3. Ash content determination

Ash content, mass of inorganic residue remaining after sample heating under specific conditions, was determined according to EN ISO 18122 (2015) norm. The analytical samples (<0.5 mm) put in crucibles were heated up to **550 ºC in a muffle furnace LAC** (model LH

30/13, LAC, Židlochovice, Czech Republic). For sample weighting a scale Mettler Toledo (model AX304, Greifensee, Switzerland; readout d = 0.1 mg) was used. The results were expressed as % of the mass of the dry matter in the sample.

#### 4.2.2.4. CHN analysis

Amount of **carbon, hydrogen and nitrogen** (hereafter as *C, H, N*) was determined in accordance with EN ISO 16948 (2015) norms using **automated CHN analyser Leco** (model TruSpec, LECO Corporation, St. Joseph, MI, USA). Dried analytical samples of approx. 0.1 g in aluminium foils were put into the equipment and combusted to oxidize the sample into simple compounds that were then detected with thermal conductivity and infrared detectors. For sample weighting a scale Mettler Toledo (model AX304, Greifensee, Switzerland; readout d = 0.1 mg) was used. The results were expressed as % by mass.

#### 4.2.2.5. Calorific value determination

*CV* was determined according to EN ISO 18125 (2017) using **automated calorimeter IKA** (model C-5003, IKA-Werke GmbH & Co. KG, Staufen, Germany). For sample weighting a scale Mettler Toledo (model AX304, Greifensee, Switzerland; readout d = 0.1 mg) was used. The gross calorific value (*GCV*) was calculated by the calorimeter itself and net calorific value (*NCV*) was calculated according to following **Eq. 3**:

$$\boldsymbol{NCV = GCV - 24.42 \times (MC + 8.94 \times H_a)} \qquad \text{(Eq. 3)}$$

where:
- $GCV$ – gross calorific value ($J.g^{-1}$),
- 24.42 – coefficient corresponding to 1% of the water from the sample at 25 °C,
- $MC$ – water content in the sample (%),
- 8.94 – coefficient for conversion of hydrogen to the water,
- $H_a$ – hydrogen content in the sample (%).

### 4.2.3. Cellulose, hemicelluloses and lignin analysis

For evaluation of agglomeration process and its efficiency, it is important to know the composition of biomass, since several substances have higher positive effect on densification. Thus, analysis of cellulose, hemicellulose and lignin content was processed in the laboratory of CIEMAT (Madrid, Spain) according to the Laboratory Analytical Procedures (LAP) for biomass analysis, provided by the National Renewable Energies Laboratory (NREL, Golden, CO, USA). The procedure used a **two-step acid hydrolysis** to fractionate the biomass samples into forms that are more easily quantified (Sluiter et al. 2012). Results were expressed as % of dry weight mass.

### 4.2.4. Thermogravimetric analysis

It has been recognized that the lignocellulosic structure (cellulose, hemicellulose and lignin) of biomass can be qualitatively identified by means of derivative thermogravimetric analysis and can be distinguished from the course of weight loss intensity of biomass (Chen & Kuo 2010). For this purpose, the thermogravimetric analyser Setaram Setsys Evolution (model S60, Setaram Instrumentation, Tours, France) was used to study the **weight mass loss** of input materials **as a function of time and rising temperature**. For thermogravimetric analysis (*TGA*) dried analytical samples of <10 mg were put in the analyser with the heating medium being air with specific flow rate and heating rates 10 °C per minute. The samples were heated from a room temperature to 1000 °C. The outputs were expressed as *TGA* (in Annex)/*dTGA* graphs.

### 4.2.5. Bulk density determination

Bulk density (*BD*) of studied materials and fractions was determined in accordance with EN ISO 17828 (2015) **using a cylindrical container** with stated **volume of 5 l**. Material was weighted by a scale Bosch (model PE 612, Bosch, Jungingen, Germany; readout d = 1 g). Each measurement was repeated for three sample refills, within a short period of time, but not simultaneously. The *BD* was calculated by following **Eq. 4**:

$$\boldsymbol{BD} = \frac{\boldsymbol{m_2 - m_1}}{\boldsymbol{V}}, \text{ kg.m}^{-3} \qquad \text{(Eq. 4)}$$

where: $m_1$ – mass of the empty container (kg),
$m_2$ – mass of the filled container (kg),
$V$ – net volume of the measuring container ($m^3$).

The final result of bulk density for each material fraction was calculated as the mean value of three repetitions and with repeatability precision equal to a maximum 3.0%.

### 4.2.6. Sieve analysis – Particle size distribution

Particle size and its distribution is important factor for densification process and mechanical behaviour of final briquettes (Al-Thyabat & Miles 2006; Ulusoy & Igathinathane 2016). Sieve analysis (SA) was used to determine the weight and percentage representation of individual fraction sizes of each material, and, it was performed according to a valid standard EN ISO 17827-1 (2016). For this purpose, a horizontal mechanical sieve shaker Cisa (model PR 08, Mervilab, S.A., Madrid, Spain) together with the standard round sieves with diameter of 20 cm and opening size of 16, 8, 3.15, 2.8, 2.0, 1.4, 1.0, 0.5, 0.25, 0.125, 0.063 mm and bottom pan were used to sort particles in decreasing size classes. For the hemp material two more sieves (size 31.5

and 45 mm) were added because of its fibrous nature and previous testing (Chaloupková et al. 2016). For sample weighting a scale Kern (model EW 3000-ZM, Kern & Sohn GmbH, Balingen, Germany; readout d = 0.01 g) was used. A representative weighed sample was spread on the top sieve with the largest opening size and 30-minute sieve shaking time and amplitude 3.0 mm/"g" were applied. After the operation, a material retained on each sieve was weighted. The percentage of particles' weights retained on the sieves was determined by **Eq. 5**. Three repetitions were done for each material and fraction (with sieving loss error approx. 0.3%) and their average value was reported as the final result.

$$\% \textbf{ Retained} = \frac{\boldsymbol{W\ sieve}}{\boldsymbol{W\ total}} \times \mathbf{100\%} \qquad \text{(Eq. 5)}$$

where: *W sieve* – weight of aggregate in the sieve (g),
*W total* – total weight of the aggregate (g).

Cumulative percentage of material retained in the n$^{th}$ sieve was determined by **Eq. 6:**

$$\% \textbf{ Cumulative} = \boldsymbol{\Sigma}\textbf{ Retained} \qquad \text{(Eq. 6)}$$

### 4.2.7. Photo-optical analysis – Particle characterization & Particle size distribution

The conventional SA considers only one parameter: general particle shape. Thus, to obtain detailed information about particle shape and size a computerized **photo-optical particle analyser Harver** (model CPA 4-2, Haver & Boecker OHG, Oelde, Germany) was used to identify particles dimensional properties. The analyser worked under the particle measuring range from 0.091 up to 90 mm, which was selected with respect to the material character (according to the manual another measuring possibility is a range of 0.035–15 mm, but it is suitable mainly for fine materials like ash). The analyser consisted of a feeding unit with the height of 6 mm being set for the regular particles spread on a vibration channel, a vibratory channel itself, a CCD-line digital scan camera with the high-resolution (4096 pixels line resolution), which **scanned all freefalling particles** of the studied samples against the background of a LED lighting array module with a high recording frequency (up to 28000 line scans per second) (Haver & Boecker 2015). The analyser and process of gathering data can be seen in the **Figure 15**. Amplitude of the vibrating feeder was automatically regulated by the analyser. Minimum and maximum values of optical density were set as 0.5 and 2, respectively. Shape model was set as "*elongated*" and volume model as "*elliptical segment*". Control of the entire measurement process and data evaluation was performed from a portable computer equipped with a Gigabit Ethernet (GigE) interface as well as a RS 232 interface, which were connected to the analyser.

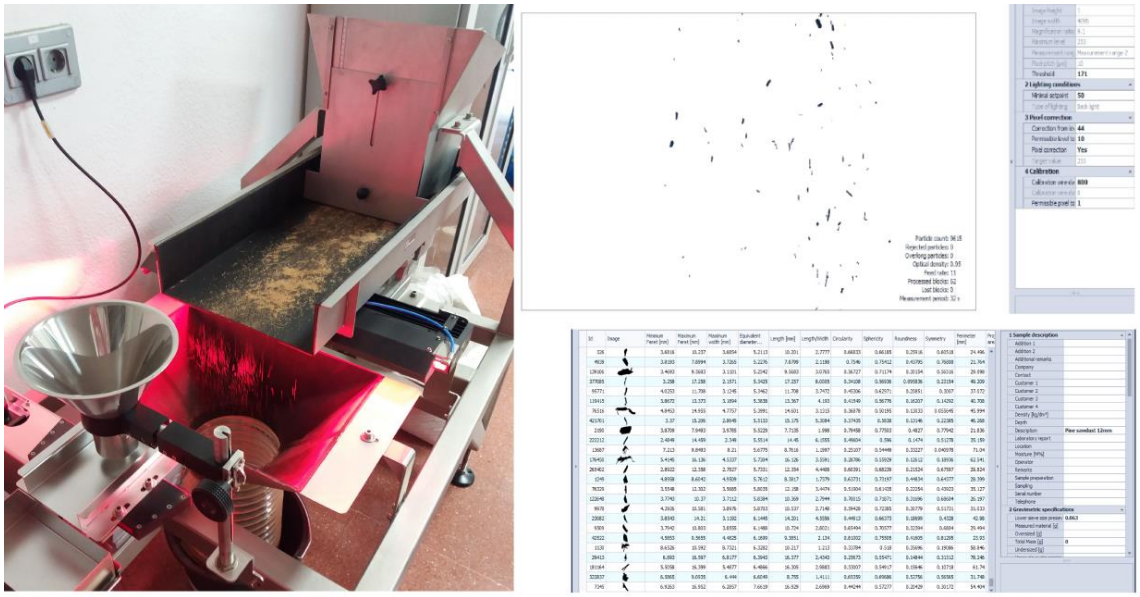

**Figure 15.** Photo-optical analyser measuring falling particles of pine sawdust 12 mm and obtained tabulated data ready for statistical processing

All passed particles were **individually recorded, measured** (in mm) **and their 2D profile parameters** were processed via Haver CpaServ software (Haver & Boecker OHG, Oelde, Germany). The data were transferred into the spreadsheet for further analyses. To compare PSD outputs from this analysis with outputs from the previous SA, **the maximum feret diameter ($X_{max}$)** was set as a measurement algorithm (see **Table 6**) for particle length (Dražić et al. 2016; Kirsten et al. 2016). This parameter gives the value of the minimum sieve size through which the particle can pass through without any obstacle (Shanthi et al. 2014). To compare PSD results with the conventional sieve method, the data were grouped into the groups in accordance with the particles' distinct lengths corresponding to the sieve sizes used in the screening method. PSD analyses were confronted as the percentages of particles' weights retained on the sieves (SA) and the percentages of particle numbers retained on virtual sieves (photo-optical analysis, POA). Beside $X_{max}$, other **significant parameters of particle size and shape were evaluated**. The scanned particles were analysed in terms of variables stated and defined in the **Table 6**.

**Table 6.** Variables measured by the photo-optical analyser used to evaluate the particle size and shape

| Variable and definition | Diagram |
|---|---|
| **Minimum feret diameter ($X_{min}$)**<br>Minimum distance of two tangents, which can be placed in parallel onto the outer particle contour (Haver & Boecker 2014) | 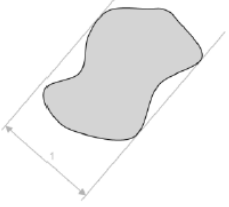 |

**Length (*L*)**
The length is determined perpendicularly to the minimum feret diameter and it corresponds to the long side of a rectangular shaped projection area; used for calculation of length/width ratio ($R_{lw}$) (Haver & Boecker 2014)

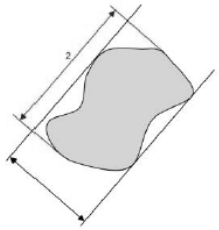


**Maximum feret diameter ($X_{max}$)**
Maximum distance between two parallel tangents of the particle contour (Haver & Boecker 2014)


**Maximum width ($W_{max}$)**
Maximum extension of the particle projection area orthogonally to the maximum length (Haver & Boecker 2014)

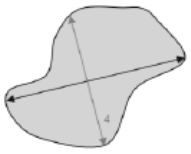


**Equivalent diameter ($X_a$)**
Diameter of a circle, the surface area of which corresponds to the projected area of the particle (Olson 2011)

$$X_a = \sqrt{\frac{4*A_1}{\pi}} \qquad \text{(Eq. 7)}$$

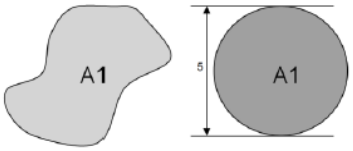


**Projection area ($A_I$)**
Sum of the areas of individual pixel (Olson 2011)

$$A_1 = \sum a_p \qquad \text{(Eq. 8)}$$

Where $a_p$ is area of each individual pixel

**Feret diameter* (*X*)**
Distance between two parallel tangents of the particle contour, vertical to the direction of measurement (Haver & Boecker 2014)

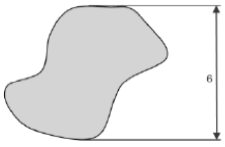


**Martin-diameter* ($X_m$)**
Length from the particle projection, it is the line that cuts the area in half, horizontally to the direction of measurement (Haver & Boecker 2014)

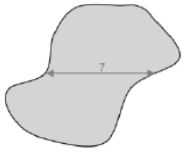


**Circularity ($C_i$)**
Degree of similarity of the particle projection area with a circle (Haver & Boecker 2014)

$$C_i = \frac{U_p}{(2*\sqrt{\pi*A_1})} \qquad \text{(Eq. 9)}$$

Where $U_p$ is measured perimeter of particle and $A_I$ measured projected area

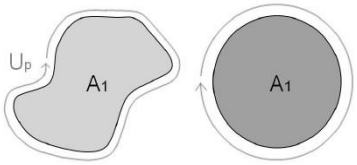

**Sphericity ($\varphi$)**

Degree of similarity of the particle with a sphere

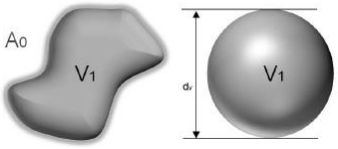


$$\psi = \frac{\pi * d_v}{A_0} \qquad \text{(Eq. 10)}$$

Where $A_0$ is the particle's calculated surface area and $d_v$ is the diameter of an equal volume sphere (Wadell 1932)

**Roundness ($R_d$)**

Degree of roundness the particle corners and edges (Wadell 1932)

$$R_d = \frac{\frac{1}{n}\sum_{i=1}^{n} r_i}{r_{max}} \qquad \text{(Eq. 11)}$$

where $r_i$ is the radius of the i-th corner curvature, $n$ the number of corners, and $r_{max}$ the radius of the maximum inscribed circle

**Length/width ratio ($R_{lw}$)**

The ratio of length to width was calculated from the ratio of length to the minimum feret diameter of the projection area (Haver & Boecker 2014)

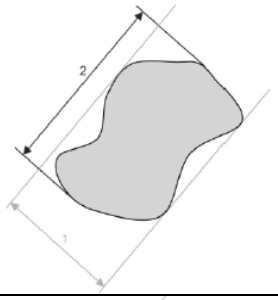


$$R_{lw} = \frac{L}{X_{min}} \qquad \text{(Eq. 12)}$$

where $L$ is length and $X_{min}$ minimum feret diameter

**Aspect ratio ($A_r$)**

Ratio of maximum ($X_{max}$) to minimum ($X_{min}$) feret diameter (Agimelen et al. 2017)

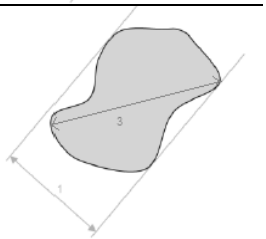


$$A_r = \frac{X_{max}}{X_{min}} \qquad \text{(Eq. 13)}$$

**Symmetry ($S_m$)**

For symmetry, the area centroid of the particle is determined. Axes of symmetry run through the centroid. These axes are rotated in 1° increments. Here the ratio of radii is computed. The smallest result is denoted as the symmetry (Haver & Boecker 2014)

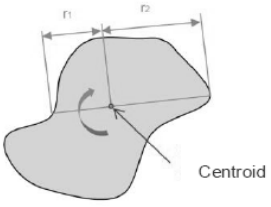


$$S_m = \frac{r_1}{r_2} \qquad \text{(Eq. 14)}$$

where $r_1$ is the smallest radius and $r_2$ the largest radius

**Perimeter ($U_p$)**

Total length of the particle boundary (Olson 2011)

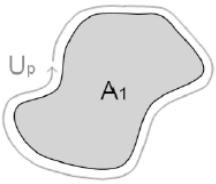


$$U_p = \frac{\pi}{N}\sum_{\alpha}^{\pi} I_\alpha \, d_L \qquad \text{(Eq. 15)}$$

Where $I$ is number of intercepts, formed by series of parallel lines, with spacing $d_L$, exploring $N$ directions, from $a$ to $\pi$

Notes: * position-dependent size
All diagrams adopted from Haver & Boecker (2014)

### 4.2.8. Briquetting of the materials

The ground materials (without any additives) were subsequently pressed to the form of briquettes by the hydraulic piston briquetting machine BrikStar (model CS 50, Briklis, Malšice, Czech Republic; **Figure 16** on the next page) with the diameter of a pressing cylinder (matrix/die) of 65 mm, which corresponds approximately to the diameter of produced briquettes.

The BrikStar press is designed for production of cylindrical briquettes from various biomass types, including sawdust and straws and works under the maximum compression pressure 18 MPa and maximum pressing temperature 60 °C (Briklis 2011), other technical parameters are listed below in the **Table 7**. From each material and fraction, five briquettes were selected for the study. The briquettes' selection was carried out in the middle of pressing process when the maximum temperature and pressure were reached out.

**Table 7.** Technical parameters and working conditions of briquetting press BrikStar CS 50

| Parameter | Value |
|---|---|
| Necessary voltage | 400 V |
| Control circuit voltage | 24 V |
| Power input required | 5.6 kW |
| Electric intensity of protection circuit breaker | 16 A |
| Pressing duration without adding hydraulic liquid | 6−8 h |
| Calculated production capacity | 50 $kg.h^{-1}$ |
| Overall equipment mass | 790 kg |
| Raw material hopper volume | 1.0 $m^3$ |
| Piston | 6 $runs.min^{-1}$ |
| Length of piston run | 180 mm |
| Level of acoustic pressure | 90 dB |
| Expected lifetime of matrix, piston and hydraulic pump | 2000 h |
| Maintenance (change of filters in the hydraulic system) | after 500 h |
| Acceptable *MC* of raw materials | 8–12% |
| Maximum working pressure | 18 MPa |
| Maximum working temperature | 60 °C |
| Optimum temperature of the environment (at pressing) | between +5 + 35 °C |

Source: Briklis (2011)

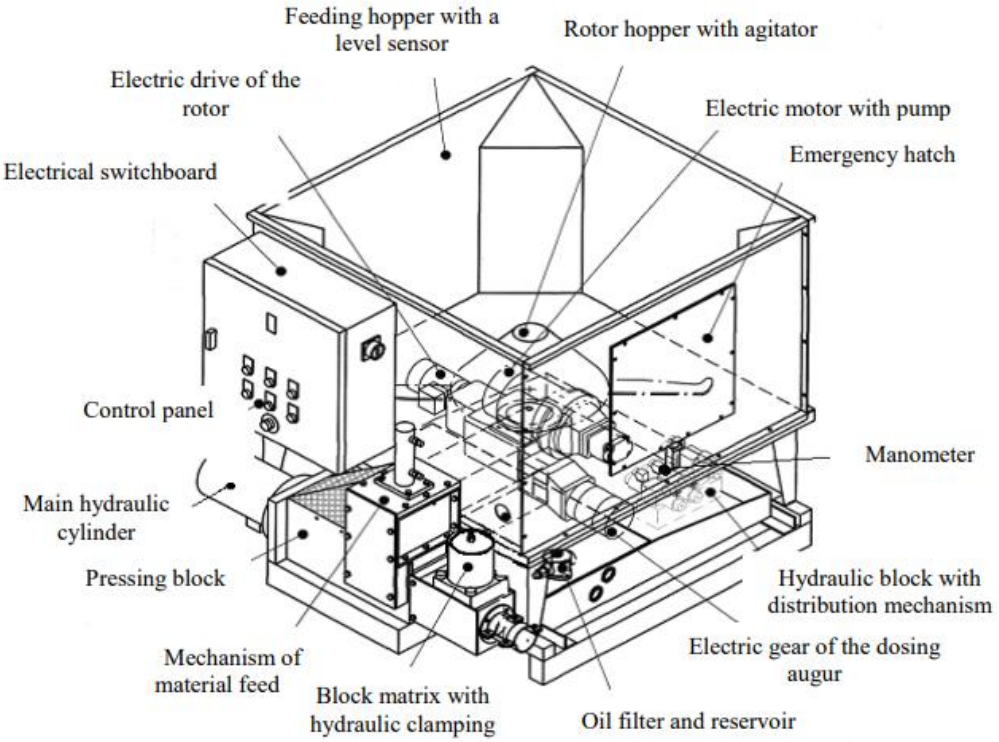


**Figure 16.** Scheme of hydraulic piston briquetting press BrikStar CS 50
Source: Havrland et al. (2011)

### 4.2.9. Briquette volumetric mass density determination

Basic parameter of investigated briquette samples related to their dimensions and mechanical quality was a volumetric mass **density** $\varrho$ (kg.m$^{-3}$). ϱ of the produced briquettes was found as a ratio of weight and volume determined from the briquette shape and dimensions. Their **length (*L*)** and **diameter (*D*)** were measured in accordance with EN ISO 17225-3:2014 and EN ISO 17225-7:2014 by the electronic digital caliper (model Mitutoyo Absolute IP66, Aurora, Illinois, USA; d = 0.01 mm) as it is seen in the **Figure 17** (the position of points A and C is explained in the Subchapter 4.2.12. "*Process of image analysis*").

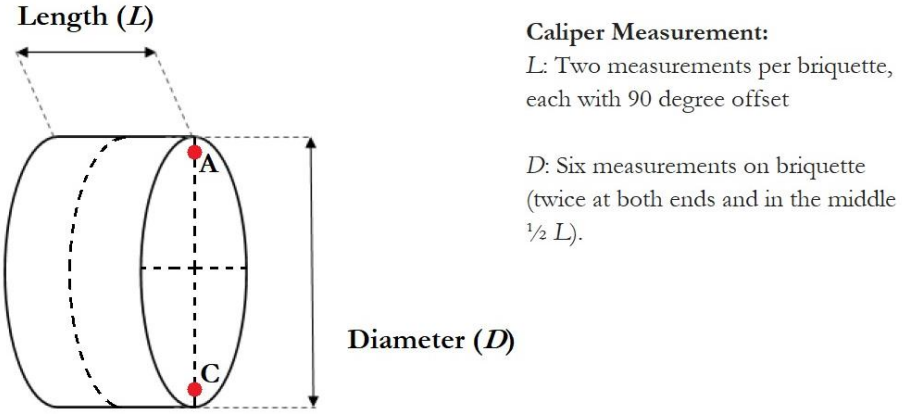


**Figure 17.** Scheme of dimensions measurement

The volume of briquette ($V_b$) was calculated according to following formula (**Eq. 16**):

$$\boldsymbol{V_b = \frac{D_a^2 \times \pi \times L}{4}}, \text{ mm}^3 \qquad \text{(Eq. 16)}$$

where: $D_a$ – average value for 6 measurements of each briquette (mm),
L – length (mm).

The **weight** of briquettes ($\boldsymbol{w_b}$) was determined by scale Kern (model EW 3000-ZM, Kern & Sohn GmbH, Balingen, Germany; d = 0.01 g) and subsequent calculations of $\boldsymbol{\varrho}$ were performed by using of following equation (**Eq. 17**).

$$\boldsymbol{\rho = \frac{w_b}{V_b}}, \text{ kg.m}^{-3} \qquad \text{(Eq. 17)}$$

where: $m_b$ – weight of the briquette (kg),
$V_b$ – volume of the briquette ($m^3$).

## 4.2.10. Mechanical durability determination

According to the standard EN ISO 17831-2 (2015) a *DU* of produced briquettes was measured using a rotation abrasion drum (**Figure 18**). The briquettes (test portion 2±0.1 kg) were subjected to shocks by collisions of briquettes against each other and against chamber's wall of the rotation drum with 21±0.1 rpm for 5 min. The *DU* was calculated from the mass remaining after a separation of abraded mass (**Eq. 18**) and the result for each material type and fraction was reported as the mean value from the results of five replications.

$$DU = \frac{m_A}{m_E} \times 100, \ \% \qquad \text{(Eq. 18)}$$

where: $m_A$ – the mass of sieved briquettes after the drum treatment (g),
$m_E$ – the mass of pre-sieved briquettes before the drum treatment (g).

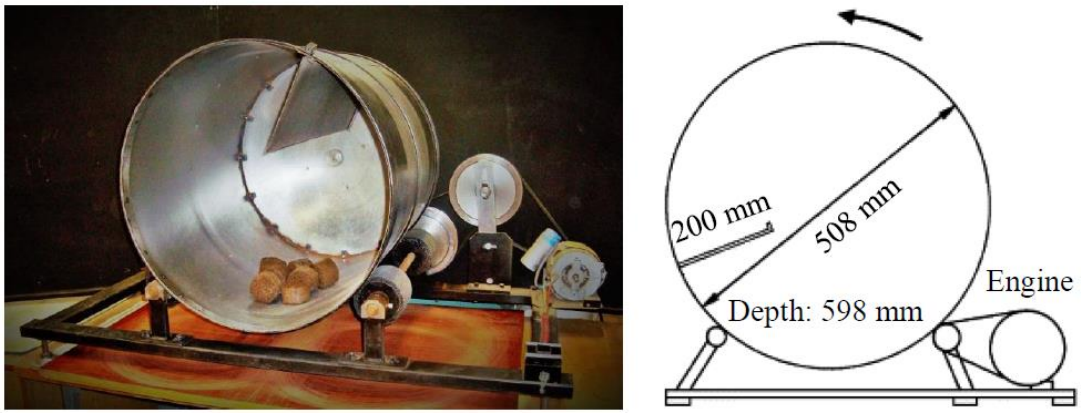


**Figure 18.** Rotation drum used for *DU* testing
Source: Brunerová (2018)

### 4.2.11. Briquette compressive strength determination

Principle and procedure of briquette compressive strength test is not defined by any valid technical standard for densified biofuels but originates from previous research works (Plíštil et al. 2005; Kers et al. 2010; Brožek et al. 2012; Mitchual et al. 2013; Brunerová 2018; Wang et al. 2018a). In case of bio–briquette fuel, the test simulates the influence of briquette transportation, handling and storage in reality and the potential damages (Gilvari et al. 2019). The product compressive strength was determined by a universal tensile strength testing machine (model ZDM 50, WPM Werkstoffprüfmaschinen Leipzig, Dresden, Germany). The briquette was placed on the test platform vertically and exposed to the action of the **force *F*** (N) which is perpendicular to the briquette axis of symmetry. The briquette was pressed at a constant rate equal to 20 mm.min$^{-1}$ and maximal force equal to 500 kN until the briquette broke (**Figure 19**). The maximum force $F$ was recorded and the compressive strength $\sigma_t$ (N.mm$^{-1}$) was calculated by dividing the maximum load $F$ by the length $L$ (mm) of the specimen; the $L$ was calculated as mean of two measurements, as indicated in the Subchapter 4.2.9.

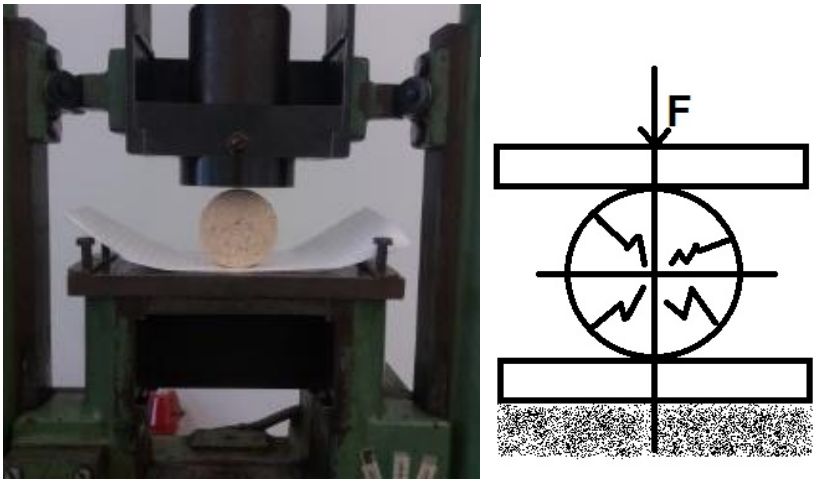


**Figure 19.** Compressive strength test

### 4.2.12. Image-based macroscopic analysis

The produced briquettes were subjected to image-based macroscopic analysis aimed to **analyse and assess the briquette cross-sectional surface structure** in order to determine particle size and its distribution and better understand the behavioural pattern of input material during agglomeration process in the pressing chamber of a briquetting machine and to identify potential principles and rules in behaviour and interaction between particles at different locations on the surface of the briquette within different sources of biomass material.

### *System setup*

Macroscopic analysis of biomass briquettes was done in laboratory of image analysis at the Department of Physics and Measurements of the UCT. Following hardware and software was employed to the research (**Figure 20**).

**Figure 20.** Equipment employed for macroscopic analysis of briquettes

**Stereomicroscope** Zeiss Stemi (model Stemi 2000, Carl Zeiss, Jena, Germany) equipped with illumination Schott VisiLED (MC1500, Schott, Mainz, Germany), Sony **digital camera** (DFW-SX 910, Sony Corp., Minato, Tokyo, Japan) with CCD detector of resolution 1392×1040 pixels, personal computer (PC), IC Capture 2.3 **image acquisition software** (The Imaging Source Europe GmbH, Bremen, Germany), and, above all **NIS-Elements Advanced Research** 3.2 (Laboratory Imaging s.r.o., Prague, Czech Republic), special software for the image analysis and data measurement.

### *Process of image analysis*

Steps of the image analysis process chain are schematically shown in the **Figure 21** below.


**Figure 21.** Scheme of macroscopic analysis process

Cross-sections of selected briquettes were observed via stereomicroscope with 6.5 times magnification and scanned by digital camera through IC Capture software. Precisely, briquettes were scanned at 10 specific points on the surface (**A, B, C, D, E, F, G, H, I, J**), see **Figure 22**. The points A, B, C, D, E were placed on the front side, which is a breaking area of the briquettes leaving from the briquetting press. Points F, G, H, I, J were located at the rear side, where the piston pressed during the compaction. Points A, C, E, D, E, F, H, I, J were placed approximately five millimetres from the briquette edges, and points B and G in the middle of the circular cross-section.

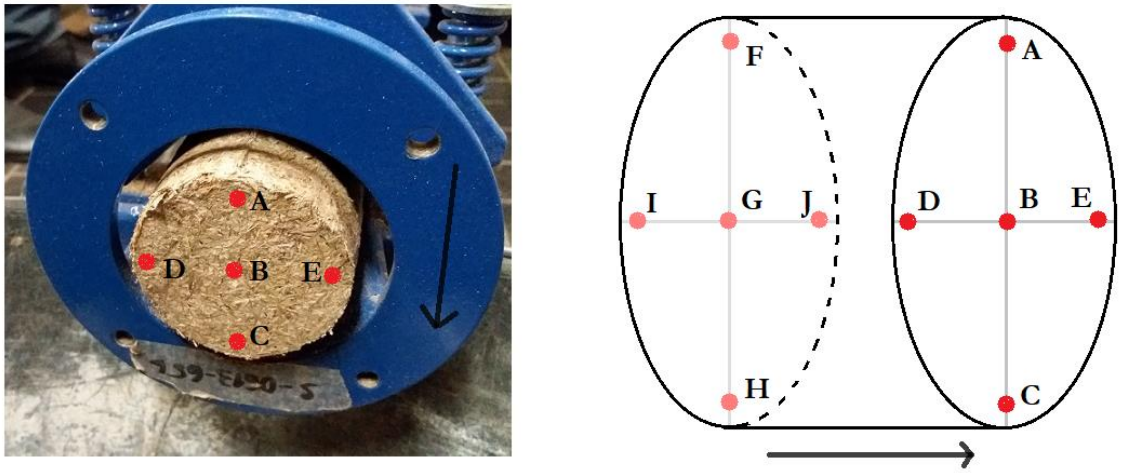


**Figure 22.** Scheme of scanned points where the particle size was measured

From each briquette ten images of each location were scanned, which means 50 images from each biomass source and fraction were obtained, thus in total **450 colour 2D images**. The taken images was analysed through the NIS-Elements software for the image processing and data measurement. Before the measurement itself, image calibration using reference object (graph paper) was done for each briquette (the calibration values range around 6.97 $\mu m.px^{-1}$). Then the manual measurements of particles' size in terms of areas were carried out along the outer edges of the particle (**Figure 23**) and with the readout 0.01 $\mu m^2$ within images. The measurements were done for particles with clearly defined edges. From manually defined particles areas, the software calculated particles' max feret diameter (in µm).

To compare behavioural pattern of specified surface locations (points A–J), 10 particle measurements for each point within one briquette was recorded, and thus 50 measured particle areas for each point/location (10 measurements × 5 briquettes). All in all, 50 measurements were obtained for each scanned point, 500 measurements (50 measurements × 10 points) for all images within one biomass material and fraction (points A, B, C, D, E and F), and totally 1500 measurements of particle's lengths and areas for one material (500 measurements × 3 fractions). In total **4500 measurements** (3 materials × 1500 measurements) were recorded.

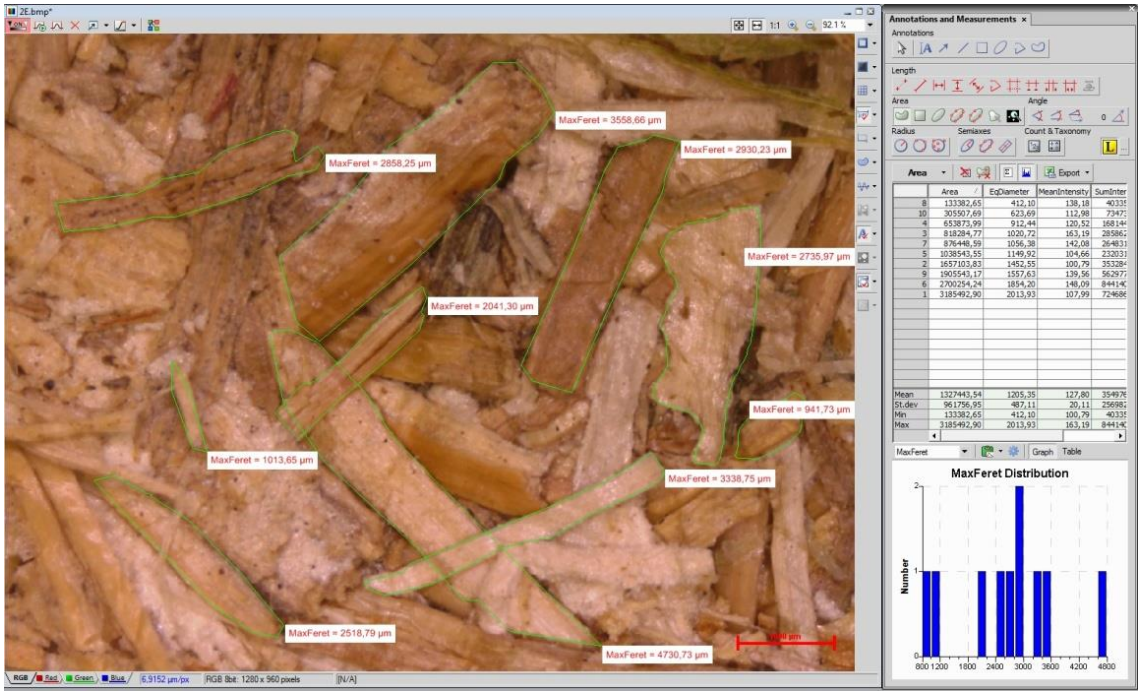


**Figure 23.** Measuring of particle size using NIS-Elements AR

Further, **lignin as the glassy coating** on the surface of particles was **detected using thresholding function** (**Figure 24**) on each image taken at the scanned locations. Thresholding (type of image segmentation) isolated the glassy coating as the same colour segments of pixel value and highlighted it in red colour. The area of the segments was bounded (highlighted in green colour), calculated and their sum gave the total area (in $\mu m^2$) of glassy coating per image.

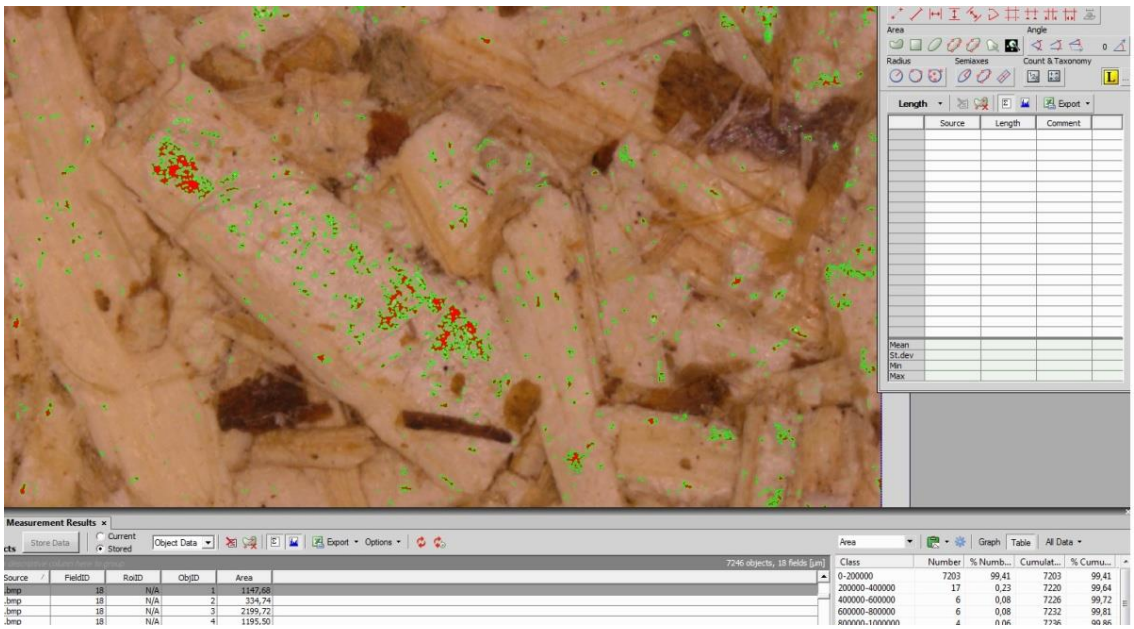


**Figure 24.** Thresholding of glassy coat on the particles

## 4.3. Data processing and analysis

Collected data from above described methods were organized, cleaned, processed and statistically analysed using Microsoft Office **Excel** (version 2013, Microsoft, Redmond, WA, USA,) and **Statistica software** (version 12, TIBCO Software Inc., Palo Alto, CA, USA).

Organized and cleaned data were analysed by **descriptive statistics**. Data were summarized by measures such as arithmetic means, medians, minimum and maximum values, variance, coefficient of variance and/or standard deviation etc. Data from macroscopic analysis (measured areas and max ferets) were described by inferential statistics and underwent statistical hypothesis testing with respect of set Thesis hypothesis and objective. For this purpose, a test ANOVA of main effects, with significance level $\alpha$ 0.05, for comparing the independent samples, i.e. particles sizes measured at different surface locations on the briquette structure, was intended to use. However, compliance of mentioned variables with the assumptions of normality (Shapiro Wilk test) and homoscedasticity of variance (Levene's test) was not verified (see Annex). Thus, the non-parametric alternative of ANOVA, **Kruskal-Wallis H test** was used ($\alpha$ 0.05) to compare particle size between materials, fractions and mainly between points at which the measurements of areas and max ferets were done, and, to make inference about the particle size distribution on the surface of the briquettes.

Obtained results were listed in tables or visualized in graphic form and subsequently interpreted, evaluated and discussed with other studies. Parameters measured according to the valid EN ISO standards were also compared with EN ISO 17225-3:2014 (pine sawdust) and EN ISO 17225-7:2014 (miscanthus and hemp) standards specifying the requirements for woody and non-woody bio-briquettes.

# 5. Results and Discussion

## 5.1. Evaluation of physical and chemical material characteristics

Proximate and ultimate analysis and *CV* is the most common method used to describe the quality of solid fuels (Khan et al. 2009). Both the **proximate and ultimate analysis of studied materials** are summarized in the **Table 8** and discussed in detail in following subchapters. In the **Table 9** the results are compared with other biomass types and conventional fuels.

**Table 8.** Physical and chemical characterization of studied materials

| Parameter | Unit | Miscanthus | Hemp | Pine sawdust |
|---|---|---|---|---|
| ***Proximate analysis*** | | | | |
| *MC* | % w.b. | **8.95** | **8.62** | **8.27** |
| *VC* | % d.b. | **79.78** | **79.70** | **83.38** |
| Ash | % d.b. | **4.46** | **4.60** | **0.26** |
| *FC* | % | **6.81** | **7.08** | **8.09** |
| *FC*[a] | % d.b. | **15.76** | **15.70** | **16.36** |
| ***Ultimate analysis*** | | | | |
| *C* | % d.b. | **45.48** | **44.11** | **50.69** |
| *H* | % d.b. | **5.89** | **5.59** | **6.14** |
| *N* | % d.b. | **0.12** | **0.72** | **0.17** |
| ***Calorific value*** | | | | |
| *GCV* | $MJ.kg^{-1}$ d.b. | **19.15** | **18.86** | **20.80** |
| *NCV* | $MJ.kg^{-1}$ d.b. | **18.39** | **18.43** | **19.13** |

[a] moisture-free values

**Table 9.** Proximate and ultimate analyses of selected types of biomass and conventional fuels

| Crop | *Proximate analysis* | | | | *Ultimate analysis* | | | *GCV* | References |
|---|---|---|---|---|---|---|---|---|---|
| | ***MC*** (%) | ***VM*** (%) | ***FC*** (%) | **Ash** (%) | ***C*** (%) | ***H*** (%) | ***N*** (%) | ($MJ.kg^{-1}$ d.b.) | |
| **Miscanthus** | 7.28 | - | - | - | - | - | - | 18.62 | Ivanova (2012) |
| ***Miscanthus sinensis*** | 8.23 | - | - | - | - | - | - | 17.70 | Ivanova (2012) |
| ***Miscanthus* × *giganteus* '*Nagara*'** | 2.0 | 87.5 | 11.7 [a] | 0.8 | 46.7 | 6.0 | 0.2 | 18.5 | Kambo and Dutta (2014) |
| **Miscanthus** | 2.0 | 80.5 | 16.0 | 1.5 | 45.52 | 5.93 | 0.13 | - | Kok and Özgür (2013) |
| **Miscanthus** | 10.2 | 72.03 | 15.63 | 2.13 | 48.75 | 5.94 | 0.39 | 19.00 | Roesch et al. (2011) |
| **Torrefied *Miscanthus* × *giganteus* '*Nagara*'** | - | 84.8 | 14.2 [a] | 0.9 | 49.6 | 5.7 | 0.1 | 20.3 | Kambo and Dutta (2014) |
| **Hemp** [b] | 7.31 | - | - | - | - | - | - | 17.55 | Ivanova (2012) |
| **Hemp** | 10.7 | 66.88 | 15.81 | 6.6 | 48.46 | 6.27 | 5.67 | 20.17 | Roesch et al. (2011) |
| **Hemp** [c] | - | 87.9 | 8.9 [a] | 3.2 | - | - | - | - | Branca et al. (2017) |
| **Switch grass** | - | 76.69 | 14.34 [a] | 8.87 | 46.68 | 5.82 | 0.77 | 18.06 | Jenkins et al. (1998) |
| **Wheat straw** | 8.87 | 82.12 | 10.98 [a] | 6.90 | 42.95 | 5.35 | - | 17.99 | Channiwala and Parikh (2002) |
| **Rape straw** | 8.68 | 76.54 | 17.81 [a] | 4.65 | 46.17 | 6.12 | 0.46 | 18.34 | Tortosa Masiá et al. (2007) |
| **Corn straw** | 7.44 | 73.15 | 19.19 [a] | 7.65 | 44.73 | 5.87 | 0.60 | 17.68 | Tortosa Masiá et al. (2007) |
| **Rice husk** | 8.47 | 61.81 | 16.95 [a] | 21.24 | 38.50 | 520 | 0.45 | 14.69 | Channiwala and Parikh (2002) |
| **Coconut shell** | 8.27 | 77.19 | 22.10 [a] | 0.71 | 50.22 | 5.70 | 43.37 | 20.50 | Channiwala and Parikh (2002) |
| **Almond shell** | - | 76.00 | 20.71 [a] | 3.29 | 49.30 | 5.97 | 0.76 | 19.49 | Jenkins et al. (1998) |
| **Palm kernels** | 11.01 | 77.28 | 17.59 [a] | 5.14 | 48.34 | 6.20 | 0.46 | 20.71 | Tortosa Masiá et al. (2007) |
| **Bamboo fibre** | 7.62 | - | - | 1.16 | 50.42 | 5.75 | 0.48 | 19.76 | Brunerová (2018) |

| | | | | | | | | | |
|---|---|---|---|---|---|---|---|---|---|
| **Bamboo wood** | 11.50 | 86.80 | 11.24 [a] | 1.95 | 48.76 | 6.32 | 0.20 | 20.55 | Channiwala and Parikh (2002) |
| **Pine bark** | 14.02 | - | - | 1.87 | - | - | - | 18.60 | Brunerová (2018) |
| **Pine chips** | 7.6 | 72.40 | 21.65 [a] | 5.95 | 49.66 | 5.67 | 0.51 | 19.79 | Tortosa Masiá et al. (2007) |
| **Pine sawdust** | 15.3 | 70.4 | 14.2 | 0.1 | 51.0 | 6.0 | 0.1 | - | Vassilev et al. (2010) |
| **Pine sawdust** | 4.55 | 84.57 | 14.82 [a] | 0.61 | 50.75 | 6.29 | 0.17 | 20.31 | Gong et al. (2016) |
| **Pine sawdust** | 1.93 | 81.59 | 15.96 | 0.52 | 46.63 | 6.43 | 0.20 | - | Muley et al. (2016) |
| **Larch sawdust** | 14.36 | - | - | 0.43 | 45.00 | 6.61 | 0.09 | 17.42 | Brunerová (2018) |
| **Willow wood** | - | 82.22 | 16.07 [a] | 1.71 | 49.90 | 5.90 | 0.61 | 19.58 | Jenkins et al. (1998) |
| **Oak wood** | 40.62 | 80.82 | 16.18 [a] | 3.00 | 48.62 | 6.52 | 2.58 | 19.24 | Miranda et al. (2009) |
| **Poplar wood** | 1.0 | 74.0 | 24.0 | 1.0 | 45.44 | 6.03 | 0.36 | - | Kok and Özgür (2013) |
| **Eucalyptus wood** | - | 75.35 | 21.30 [a] | 3.35 | 46.04 | 5.82 | 0.3 | 18.64 | Parikh et al. (2005) |
| **Coal** | 9.15 | 35.41 | 52.09 [a] | 12.50 | 71.00 | 4.85 | 1.53 | 28.55 | Tortosa Masiá et al. (2007) |
| **Bituminous coal** | 11 | 35 | 45 | 9 | 73.1 | 5.5 | 1.4 | 34 [c] | McKendry (2002) |
| **Lignite** | 34 | 29 | 31 | 6 | 56.4 | 4.2 | 1.6 [d] | 26.8 [c] | McKendry (2002) |
| **Coke** | - | 0.92 | 91.47 [a] | 7.61 | 89.13 | 0.43 | 0.85 | 31.124 | Spiers (1962) |
| **Charcoal** | - | 9.88 | 89.10 [a] | 1.02 | 92.04 | 2.45 | 0.53 | 33.04 | Rose and Cooper (1977) |
| **Peat** | 14.6 | 57.8 | 24.3 | 3.3 | 67.6 | 3.9 | 3.9 | 22.8 | Theis et al. (2006) |

- ~ not reported, [a] moisture-free value, [b] var. *Bialobrzeskie*, [c] var. *Eletta Campana*, [c] *NCV* MJ.kg$^{-1}$, [d] combinated *N* and *S*

### 5.1.1. Moisture content

One of the most important parameters of raw material that can have influence on the briquetting process and the quality of solid biofuel is *MC* (Kaliyan & Morey 2009; Tumuluru et al. 2010). Average *MC* of materials used in this research before briquetting was presented in the **Table 8**. The *MC*, quantity of water in the material, expressed as a percentage of the material's weight, of examined ground biomass materials and their fractions before compaction process is presented in the **Table 10** together with *MC* of briquettes from these materials.

From the **Table 10** it is visible that *MC* of materials before briquetting ranged between **8.13% and 9.11%.** The *MC* in biomass differs depending on biomass type, growing conditions, time of harvesting, level of drying and storage conditions (Heidenreich et al. 2016). It is important to mention that all studied materials and briquettes from this Thesis were stored under laboratory conditions at room temperature. Following authors investigated the same type of the materials as studied in this Thesis and their *MC* values are as follows: Chaloupková et al. (2018b) reported *MC* for *Miscanthus* × *giganteus,* industrial hemp and pine sawdust 9.91%, 8.82% and 10.35%, respectively, all materials grinded with a screen hole diameter of 12 mm. Miao et al. (2013) measured *MC* of *Miscanthus* × *giganteus* before densification 11.5%, Ivanova (2012) 7.28%. For hemp material Ivanova (2012) found *MC* of 7.31%. In case of pine sawdust, Stolarski et al. (2013) determined *MC* 10.85±0.02% and Guo et al. (2012) 9.3%.

**Table 10.** *MC* of studied materials and fractions

| Fraction | Unit | Miscanthus | Hemp | Pine sawdust |
|---|---|---|---|---|
| ***Material before densification*** | | | | |
| **4 mm** | % w.b. | 8.78 | 8.54 | 8.29 |
| **8 mm** | % w.b. | 8.96 | 8.65 | 8.13 |
| **12 mm** | % w.b. | 9.11 | 8.68 | 8.39 |
| ***Briquettes*** | | | | |
| **4 mm** | % w.b. | 7.34 | 7.10 | 6.52 |
| **8 mm** | % w.b. | 7.46 | 7.84 | 6.50 |
| **12 mm** | % w.b. | 8.19 | 7.82 | 6.82 |

Demirbas (2004) reported that the increasing *MC* (7–15%) of spruce wood sawdust and pulping reject resulted in stronger briquettes. Li and Liu (2000) determined ideal *MC* for wood compactions ranging from 5 to 12% and recommended optimal content 8% for ideal value of briquette density. According to Wamukonya and Jenkins (1995) and Kaliyan and Morey (2009) feedstock *MC* should be 12–20% since it may help the binding mechanisms occurring during densification process under room temperature. Kers et al. (2010) determined optimal material *MC* of 10–18%. According to Mani et al. (2006b) low *MC* of corn stover (5–10%) results in

denser, more stable and more durable briquettes than high moisture stover (15%). Tumuluru et al. (2015) produced high-quality briquettes from cereals with *MC* ranging from 9 to 12%. Okot et al. (2018) produced quality briquettes with feedstock *MC* 7–8% and small particle size (<4mm). **Particles size has effect on *MC***, since decreased particle size also lets the loose particles to dry more rapidly (Kaliyan & Morey 2009), as it was also true in case of studied materials and fractions.

In case of **briquettes' *MC***, the values are lower than *MC* of materials before densification (**7.66%**, **7.59%**, **6.61%** in average for miscanthus, hemp and pine sawdust, respectively). It was caused by the briquetting process itself since the process was accompanied by an increase of the temperature (up to 60 °C) and additional drying occurred (Muntean et al. 2017). The final moisture content of biomass briquettes is greatly dependent on processing conditions, such as already mentioned initial moisture content, further, temperature and pressure, and also, on storage conditions (Matúš et al. 2015). According to the technical norm (EN ISO 17225-1 2014) and its general requirements for solid biofuels, *MC* of quality solid biofuels should **not exceed limit of 15%**. The same value, as the critical *MC* for safe storage without microbial degradation of biomass is recommended by Kaliyan (2008). Optimum *MC* of solid biofuels intended for combustion differs from study to study. According to Chen et al. (2009) *MC* should pertain to a range of 10–15%. The same range is recommended by Grover and Mishra (1996) as well and reported the best results for 12% *MC,* since with increasing *MC* the *CV* and burning properties of fuel rapidly deteriorates (Werther et al. 2000).

To conclude, *MC* of studied biomass materials is appropriate for densification without any operating difficulties and *MC* of produced briquettes enables their safe storage with no degradation processes and offers good environment for combustion.

### 5.1.2. Volatile matter

*VM* is another factor, which may influence the combustion behaviour and thermal decomposition of biofuels (Qin et al. 2018). Samples of pine sawdust demonstrated the highest *VM* content (**85.38%**), resembling result was reported by Gong et al. (2016), see **Table 9**. Miscanthus and hemp showed similar contents, **79.78%** and **79.70%**, respectively. Kok and Özgür (2013) and Branca et al. (2017) also determined analogous values. These results correspond with general description of agricultural residues and herbaceous biomass that are characterized by higher *VM* contents up to 80% in comparison with coal and wood (Tortosa Masiá et al. 2007). This indicates that the biomass materials are easier to ignite and to burn, however, the combustion is supposed to be quick and difficult to control (Werther et al. 2000).

### 5.1.3. Ash content

As it can be seen from the **Table 8**, **hemp** demonstrated the highest ash content (**4.60%**); Roesch et al. (2011) and Tutt and Olt (2011) reported even higher values. Very similar ash content to hemp determined Tortosa Masiá et al. (2007) for rape straw. Hemp value was closely followed by miscanthus (**4.46%**). However other authors from the **Table 9** (Roesch et al. 2011; Kok & Özgür 2013; Kambo & Dutta 2014) published lower values. Both miscanthus and hemp comply the ash content requirements for briquettes from herbaceous biomass class A, which is **less than 6%** (EN ISO 17225-7 2014). Ash content of pine sawdust was the lowest from the studied materials (**0.26%**) and it corresponded with data of other authors (Vassilev et al. 2010; Gong et al. 2016; Muley et al. 2016). Wood has in general ash content less than 1% (Khan et al. 2009). The limit of **<1%** is the requirement for graded wood briquettes of category A (EN ISO 17225-3 2014). Ash, the inorganic matter left out after complete combustion of the biomass has no energy value and high ash-content may cause problems in thermochemical processes (Thy et al. 2006), like greater slagging behaviour and corrosion problems (Zevenhoven 2010; Wang et al. 2012).

### 5.1.4. Fixed carbon

*FC* is the solid combustible residue that remains after biomass is heated and the moisture and volatile matter is expelled (Vassilev et al. 2010). The *FC* content of biomass can be easily associated with the ***CV*** as it has a positive effect on the energy potential of biomass (Özyuğuran & Yaman 2017). We can see from the **Table 8** that the highest *FC* had the pine sawdust and the lowest one the hemp that also **corresponds with the results of *CV*** presented later in the Subchapter 5.1.6. *FC* of miscanthus and hemp were similar to results of Roesch et al. (2011), and *FC* of pine sawdust closely corresponds to Muley's et al. (2016) investigation.

### 5.1.5. CHN content

Elementary composition of waste biomass influences its *CV* and behaviour of subsequently produced biofuels during combustion. The higher percentage of *C* content in fuel means higher *CV* (Sutrisno et al. 2017), which corresponds with following results (Subchapter 5.1.6.). The highest content of *C* has pine sawdust (**50.69%**), which is according to Rybak (2019) characteristic value for wood in general, since dried wood contains 49.5% of *C*, 6.3% of *H*, 44.2% of *O*, 0.04−0.26% of *N* and 0.20−2.30% of mineral compounds. On the other hand, *N* element causes pollution in combustion as it can react with the surrounding air and producing $NO_x$, thus the amount of *N* should not be higher than 1% (Sutrisno et al. 2017).

The miscanthus (**0.12%**) and hemp (**0.72%**) comply the standard's quality requirement of *N* content less than 1.5% (EN ISO 17225-7 2014) and pine sawdust (**0.17%**) less than 0.3% (EN ISO 17225-3 2014).

### 5.1.6. Calorific value

*CV* is one of the main indicators of briquettes quality expressing the usability of the fuel in combustion process and the energy generated (Urbanovičová et al. 2017). From the **Table 8** it is evident that pine sawdust has the highest *CV* (*GCV* d.b. **20.80 MJ.kg$^{-1}$**) in comparison with herbaceous biomass (miscanthus **19.15 MJ.kg$^{-1}$** and hemp **18.86 MJ.kg$^{-1}$**). *CV* of dry herbaceous biomass generally lies in the range of 15 to 21 MJ.kg$^{-1}$ (McKendry 2002; Urbanovičová et al. 2017). Ivanova (2012) reported *GCV* for miscanthus 18.62 MJ.kg$^{-1}$ (*MC* 7.28%) and moisture-free sample 20.78 MJ.kg$^{-1}$ and for hemp 17.55 MJ.kg$^{-1}$ (*MC* 7.31%) and 19.18 MJ.kg$^{-1}$ d.b. Miscanthus was harvested from the same field of CULS (in 2010/2011) as the miscanthus from the Thesis. All studied materials comply the requirements of *NCV* for briquetted biofuels of category A1 (**>15.5 MJ.kg$^{-1}$**) according to the EN ISO 17225-3 (2014) and A (**> 14.5 MJ.kg$^{-1}$**) by EN ISO 17225-7 (2014).

Since the particle size does not provide a significant effect on the calorific value of briquettes (Huko et al. 2015; Tembe et al. 2017; Helwani et al. 2018), the factor of particle size versus *CV* was not examined in this Thesis.

## 5.2. Cellulose, hemicellulose & lignin content

Proportion of cellulose, hemicellulose and lignin in the biomass has **effect on agglomeration behaviour of particles** and mechanical strength of final product (Tumuluru et al. 2011b). In order to characterize the studied materials and to draw conclusions on possible binding mechanisms the analysis of these main biomass components was done. **Table 11** and **Figure 25** presents results from the lignocellulosic analysis and the **Table 12** compares these results with other authors and with other plants.

**Table 11.** Cellulose, hemicellulose and lignin content of studied materials

| | Unit | Cel. [a] | Hem. [b] | Lignin total | Lignin insol. [c] | Lignin soluble | Acids | Ash | Total |
|---|---|---|---|---|---|---|---|---|---|
| Miscanthus | % d.b | 40.26 | 21.93 | 29.69 | 24.33 | 5.36 | 3.44 | 4.46 | 99.78 |
| Hemp | % d.b | 51.82 | 17.25 | 23.68 | 19.51 | 4.17 | 0.85 | 4.60 | 98.20 |
| Pine sawdust | % d.b | 45.71 | 20.80 | 34.02 | 32.68 | 1.34 | 2.62 | 0.26 | 103.41 |

[a] cel. ~ cellulose, [b] hem. ~ hemicellulose, [c] lignin insol. ~ lignin insoluble

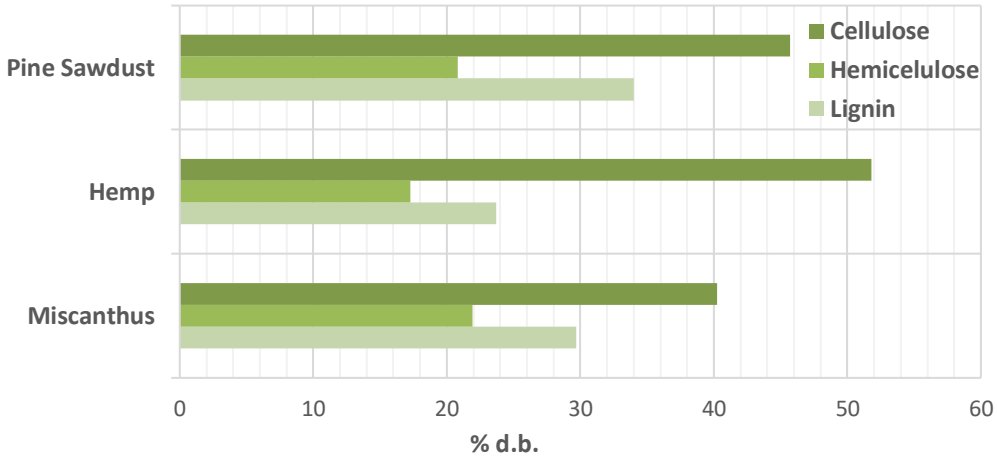


**Figure 25.** Cellulose, hemicellulose and lignin content (% d.b.) of studied materials

As it is clear from the **Table 11** and **Figure 25** the highest amount of lignin has the **pine sawdust**. It corresponds with the composition of softwood in general (Malherbe & Cloete 2002). Lignin helps to bond particles together, which results in increased strength properties and makes a final product more durable (Chou et al. 2009; Kaliyan & Morey 2010; Gendek et al. 2018; Qin et al. 2018). Biomass consisting of more lignin, protein or starch has better agglomeration properties compared to the material with higher cellulosic content (Tumuluru et al. 2011b). The more lignin is contained in the material the more of it can be released and then the briquette quality is higher as the lignin brings about higher material strength (Križan et al. 2009). These assumptions, nevertheless, do not correspond with the results of *DU* and compressive strength test presented in the Subchapter 5.8., where the hemp briquettes showed better mechanical properties than pine sawdust and miscanthus with higher lignin content.

Generally, herbaceous biomass has lower content of lignin and the increased presence of cellulose and hemicelluloses (McKendry 2002). However, in this case, miscanthus and hemp exhibited quite high content of lignin, **29.69%** and **23.68%**, respectively. Grams et al. (2019), see **Table 12**, reported similar results for miscanthus composition, although with a little bit lower value for lignin. Tutt and Olt (2011) presented even 4× lower value of lignin for *Miscanthus sacchariflori*s. In case of hemp Faruk et al. (2012) and Lavoie and Beauchet (2012) measured 2× lower content of lignin. Lignin content is related also to *CV*. Since lignin oxides less than hemicelluloses and celluloses, it has higher *CV* and this, thus wood has generally higher *CV* compared to herbaceous biomass (Demirbas 2001). This is also confirmed in the previous Subchapter (5.1.6.), pine sawdust with higher lignin content has higher *CV* than other materials.

**Table 12.** Content of ash, cellulose, hemicellulose and lignin in different biomass samples

| Crop | Ash (%) | Cel. [a] (%) | Hem. [b] (%) | Lignin (%) | *GCV* ($MJ.kg^{-1}$) | Reference |
|---|---|---|---|---|---|---|
| ***Miscanthus* × *gig.*** | 3.0 | 41.9 | 20.6 | 23.4 | 17.70 | Grams et al. (2019) |
| ***Miscanthus sacchariflori*** | 5.37 | 42.00 | 30.15 | 7.00 | - | Tutt and Olt (2011) |
| **Hemp** | 5.25 | 53.86 | 10.60 | 8.76 | - | Tutt and Olt (2011) |
| **Hemp** | - | 68 | 15 | 10 | - | Faruk et al. (2012) |
| **Hemp** | 3.2 | 40 | 26 | 19 | - | Lavoie and Beauchet (2012) |
| **Sunflower** | 9.78 | 34.06 | 5.18 | 7.72 | - | Tutt and Olt (2011) |
| **Jerusalem artichoke** | 5.15 | 20.95 | 5.48 | 5.05 | - | Tutt and Olt (2011) |
| **Tobacco leaf** | - | 43.45 | 41.54 | 15.01 | 17.70 | Demirbas (2001) |
| **Corn straw** | - | 51.53 | 30.88 | 17.59 | 18.27 | Demirbas (2001) |
| **Rice husk** | - | 35−45 | 19−25 | 20 | - | Martí-Ferrer et al. (2005) |
| **Willow** | 2.77 | 59.72 | 20.06 | 20.22 | 18.37 | Chen and Kuo (2010) |
| **Softwood** | - | 45−50 | 25−35 | 25−35 | - | Malherbe and Cloete (2002) |
| **Hardwood** | - | 40−55 | 24−40 | 18−25 | - | Malherbe and Cloete (2002) |
| **Hardwood** | - | 45.85 | 32.26 | 21.89 | 18.97 | Demirbas (2001) |
| **Oak wood** | 3.00 | 48.61 | 13.28 | 21.87 | 19.24 | Miranda et al. (2009) |
| **Pine sawdust** | 0.61 | 47.64 | 14.32 | 29.57 | 20.31 | Gong et al. (2016) |

[a] cel. ~ cellulose, [b] hem. ~ hemicellulose, - ~ not reported

Compare to the miscanthus and pine sawdust, hemp is a specific plant. Its stems are composed of about 65% woody core fibers (hurds/shives) with high lignin content and 35% bast fibers. The core fibers contain 40–48% cellulose, 18–24% hemicellulose and 21–24% lignin. On the other hand, the bast fibers contain 57–77% cellulose, 9–14% hemicellulose and 5–9% lignin (Capelle 1996). Variety "*Belobrzesky*" contains even 65–80% shives of the stalk with high lignin content (Andzs et al. 2013). The gummy polysaccharides of lignin, pectin and hemicellulose are localized on the surfaces of the hemp fibres, as can be seen in the SEM image (**Figure 26**), and they are expected to provide the direct bonding between the agglomerating particles (Väisänen et al. 2018).

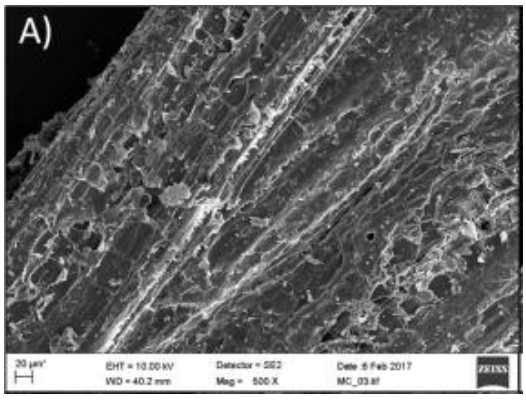


**Figure 26.** SEM micrographs of mechanically treated hemp (Väisänen et al. 2018)

## 5.3. Thermogravimetric analysis

Biomass composition based on cellulose, hemicellulose and lignin content influences the process of decomposition during combustion (Yang et al. 2006; Burhenne et al. 2013). The supplementary information about **combustion behaviour** of studied materials is presented below in *dTG* graphs (**Figures 27—29**). The blue curve represents the heat rate, green curve the weight loss (*TG*) and the orange curve the derivate weight loss (*dTG*) as a function of temperature. *TGA* graphs without derivated weight loss are enclosed in the Annex.

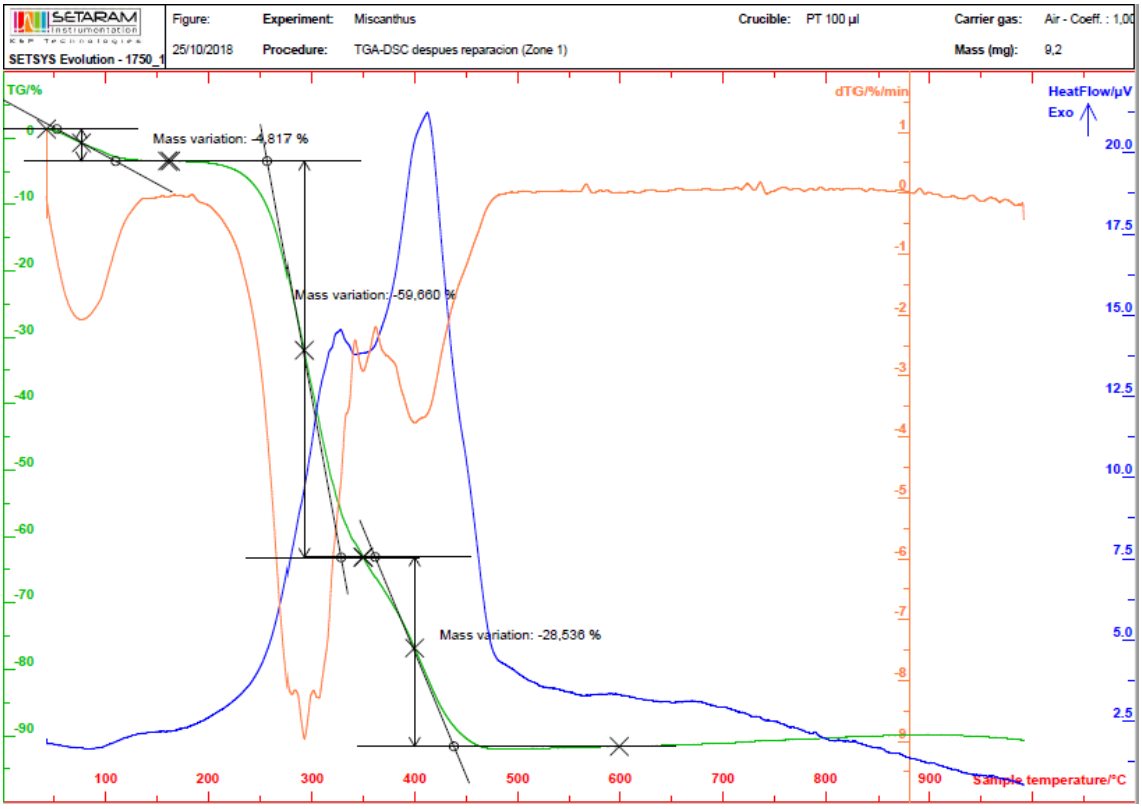


**Figure 27.** *TGA* graph of miscanthus with derivated weight loss *dTG*

The results from the thermal analysis showed three stages of combustions that are clearly seen from the peaks of the *dTG* curves. In the first stage (peak), the material lost the weight due to ***MC* removal** which started at around **35 °C** and ended at around **150 °C** (Oladokun et al. 2016). Than the devolatilization of the studied materials started at low temperatures of **200 °C** (*Ti* – initial degradation temperature) for miscanthus and hemp and of **250 °C** for pine sawdust. This first stage represents the reactivity of biomass fuels. Than the heating rate increased (blue curve on the graph) and the combustion of *FC* occurred. Around 300 °C, temperature of the maximum devolatilization rate, the devolatilization was rapid and the most significant weight losses were recorded, specifically for miscanthus approx. **59.66% at 290 °C**, for hemp **58.00%**

**at 300 ºC** and for pine sawdust **68.77% at 330 ºC**. These *dTG* peaks are associated with the decomposition of cellulose and hemicellulose (Chen & Kuo 2010; Yang et al. 2006; Burhenne et al. 2013; Oladokun et al. 2016; Farrokh et al. 2018). The process of degradation continued till approx. 450 ºC and associated with other significant weight loss **at 400 ºC** due to decomposition of lignin (Oladokun et al. 2016). Above 500 ºC the weight remained more or less constant.

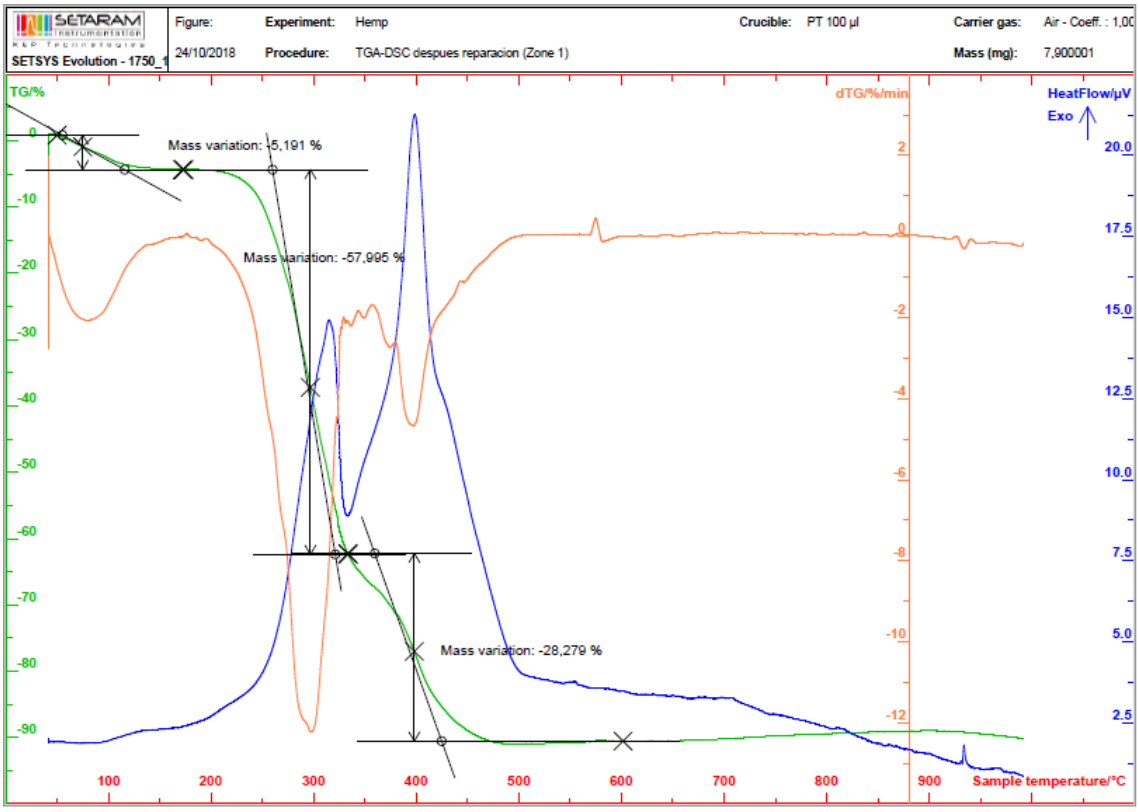


**Figure 28.** *TGA* graph of hemp with derivated weight loss *dTG*

From the weight loss curves it can be seen that the pine sawdust contained less ash than other two materials which resulted to complete combustion with almost 100% weight loss till the end of the measurement. The results revealed the highest combustibility of miscanthus, which is clear from its *Ti, dTG* peak, then it is followed by hemp and finally pine sawdust. These results indicated that pine sawdust needed a higher activation energy to decompose that can be explained by higher lignin content (Burhenne et al. 2013). *TG* results of miscanthus and hemp were similar, despite the fact that the miscanthus has higher content of lignin.

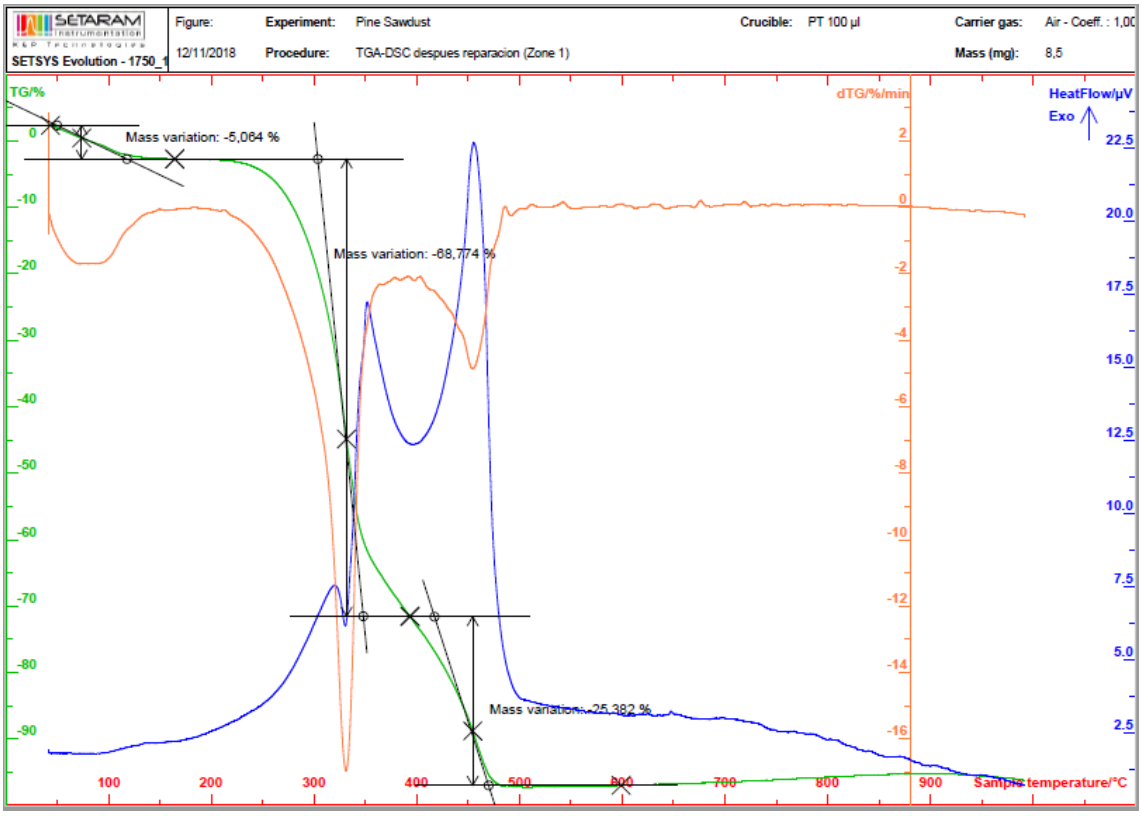


**Figure 29.** *TGA* graph of pine sawdust with derivated weight loss *dTG*

## 5.4. Bulk density of the material

Bulk density is a main physical characteristic in designing the logistic system for biomass handling (Bhagwanrao & Singaravelu 2014). The results of bulk density determination of studied materials and fractions before briquetting (in kg.m$^{-3}$) are presented in the graph below (**Figure 30**). The numerical values of the mentioned graph are tabulated in the Annex (**Table II.**)

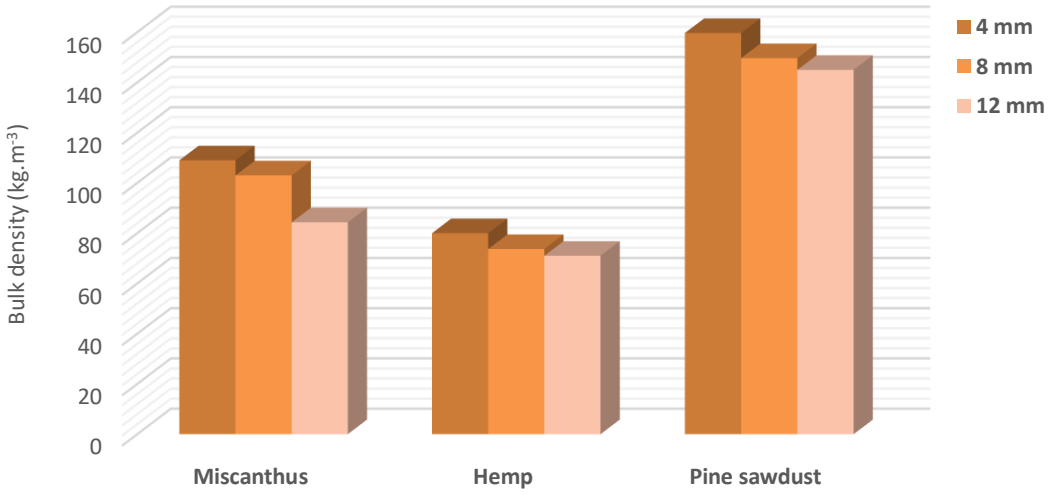


**Figure 30.** Bulk density (kg.m$^{-3}$) of studied materials and fractions

The **bulk densities** of studied materials **increased** according to a power-law relationship **with a decrease of aperture screen size** of grinding mill (McKendry 2002; Oladeji & Enweremadu 2012) as can be clearly seen in the **Figure 30**. The implication of this fact is that the smaller particles are surrounded by less pore spaces and more mass of the material per given volume occurs that is required for densification (Dai et al. 2012).

As it is visible from the **Figure 30**, initial material with the lowest bulk density is the hemp, which shows the minimum density **71.0 kg.m$^{-3}$** for fraction 12 mm and maximum density **80 kg.m$^{-3}$** for fraction 4 mm. Material grinding to smaller fraction may increase the bulk density, but in the same time leads to higher costs for additional milling (Guo et al. 2016). The highest bulk density from the studied materials has pine sawdust with a minimum density **145.0 kg.m$^{-3}$** for fraction 12 mm and maximum **159.67 kg.m$^{-3}$** for fraction 4 mm. Greatly comparable results were obtained by Muntean et al. (2017) for hemp and *Miscanthus* × *giganteus* obtained from the same source as the author of the Thesis and grinded into the same fraction sizes. The bulk density is not only affected by fraction size, but also by *MC*, shape of the particles, particle density and particle texture (Bhagwanrao & Singaravelu 2014).

Bulk density of the feedstock is related to the **energy consumption** during its pressing (Guo et al. 2016) and we can assume that also selected materials with the higher fraction size (12 mm) would have higher energy consumption compare to fractions 8 and 4 mm, as it was reported by Muntean et al. (2017) for the same materials and fractions of *Miscanthus* × *giganteus*, *Miscanthus sinensis*, hemp and apple sawdust.

## 5.5. Particle size and shape characterization

Particle size, shape and PSD are one of the most significant parameters influencing physical and mechanical properties of biomass briquettes (Zhang & Guo 2014). As it defines agglomeration behaviour during densification process (Pietsch 2002) as well as the quality performance of final briquettes (Harun & Afzal 2016), it is important to determine these parameters for ensuring the efficient and quality production.

Firstly, the PSD analyses of studied materials, using conventional sieving method (SA) and novel photo-optical (POA) approach were performed and their results are presented in the following subchapters. And secondly, detailed information about particle size and shape of all individually measured particles from POA is presented as well.

### 5.5.1. Evaluation of particle size distribution

The SA is a **standard approach** (EN ISO 17827-1 2016) for classification of a particular material based on dimensional properties of the sieve through which the material passes; the material is separated by sieves of differently sized apertures into fractions of PSD (Fernlund 1998). And, as it was mentioned in the Methodology (Subchapter 4.2.6.), the PSD from the SA was calculated as percentage of particles' weights retained on each sieve. On the contrary, the POA is a **non-conventional approach** for characterization of particle size and shape and for the classification of particular material based on dimensional properties of **individual particles**. Numbers of analysed particles for each material and their fractions bring precise statistical data, as they were greatly higher than 61000, which is value required to get the mass median diameter within 5% error with 95% probability for a powder having a geometric standard deviation of 1.6 (Masuda & Gotoh 1999; see Subchapter 2.6.1.). The PSD from the POA was calculated as the total percentage of particle number retained on virtual sieves and sorted according to the particles' distinct lengths ($X_{max}$). These virtual sieves corresponded to the sieve sizes used in the sieve method, as described in the Methodology.

***Miscanthus***

PSD of miscanthus material from the **SA** is presented in the chart in **Figure 31** and **Table 13**. The results of **POA** are presented in the **Figure 32** and **Table 14**. Results of PSD analyses were confronted as the percentages of particles' weights retained on the sieves (SA) and the percentages of particle numbers retained on virtual sieves (POA), for each material and fraction separately. In the mentioned Tables, the highlighted (bold) values represent the highest percentage amount/number of the material caught by a sieve during the analyses.

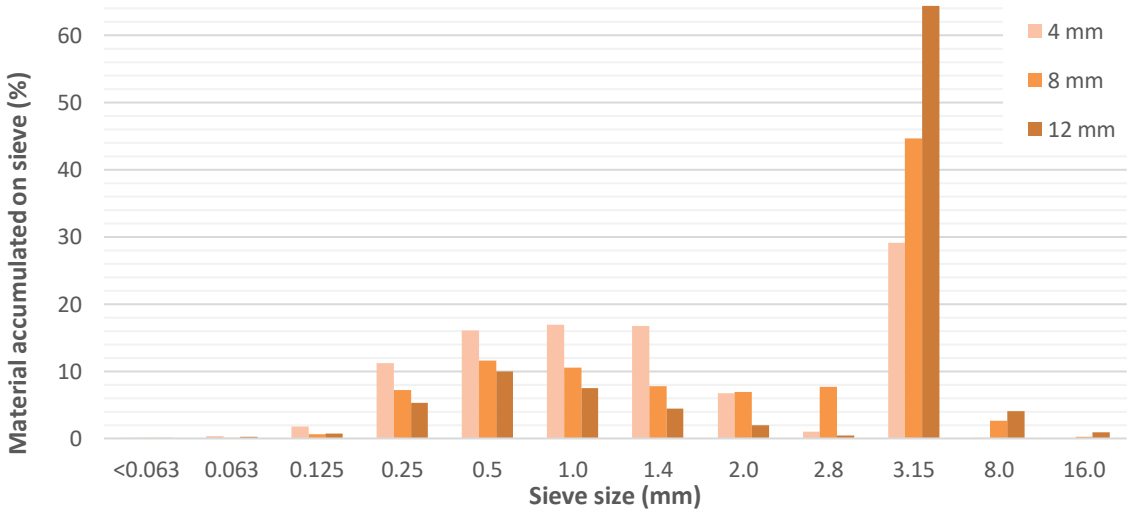


**Figure 31.** PSD of miscanthus via the SA

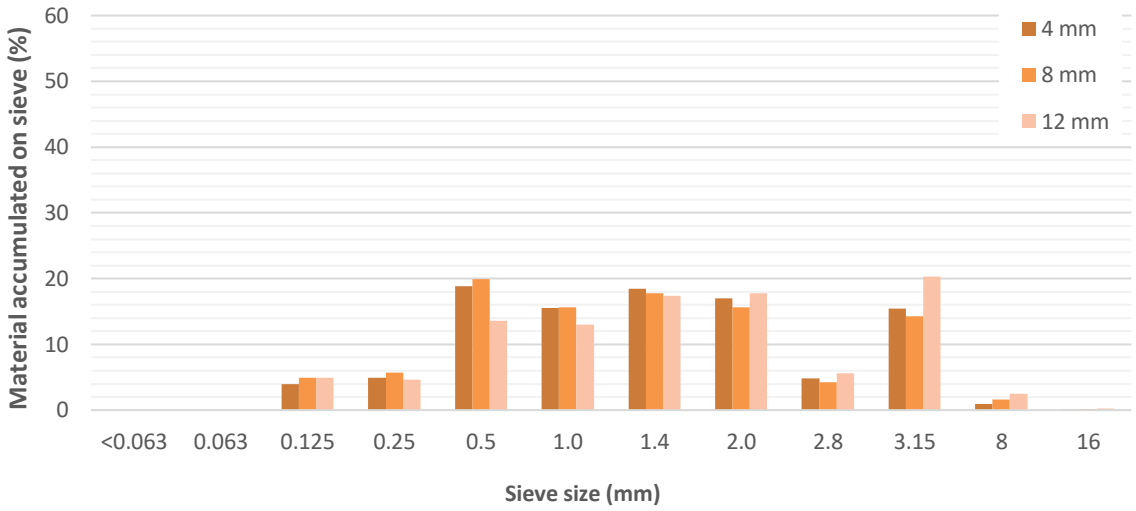


**Figure 32.** PSD of miscanthus via the POA

It is obvious, that in case of **SA**, most of the miscanthus material from all three fractions was captured by the sieve **3.15 mm**; in case of fraction 12 mm it was more than 64%. Then the material was distributed more or less regularly among the sieves of 0.25, 0.5, 1.0 and 1.4 mm. On the other hand, the analysis showed that this material does not contain very fine particles, the sieve 0.125 and less captured infinitesimal amount of the particles.

**Table 13.** Detailed PSD of miscanthus (SA)

| Sieve opening size (mm) | Fraction 4 mm | | | Fraction 8 mm | | | Fraction 12 mm | | |
|---|---|---|---|---|---|---|---|---|---|
| | (g) | (%) | (cum% [a]) | (g) | (%) | (cum% [a]) | (g) | (%) | (cum% [a]) |
| **<0.063** | 0.01 | 0.04 | 0.04 | 0.01 | 0.04 | 0.04 | 0.01 | 0.04 | 0.04 |
| **0.063** | 0.09 | 0.37 | 0.41 | 0.02 | 0.09 | 0.13 | 0.05 | 0.21 | 0.25 |
| **0.125** | 0.42 | 1.74 | 2.15 | 0.14 | 0.62 | 0.75 | 0.17 | 0.72 | 0.97 |
| **0.25** | 2.71 | 11.23 | 13.38 | 1.64 | 7.24 | 7.99 | 1.26 | 5.34 | 6.32 |
| **0.5** | 3.87 | 16.03 | 29.41 | 2.62 | 11.57 | 19.57 | 2.35 | 9.96 | 16.28 |
| **1.0** | 4.09 | 16.94 | 46.35 | 2.38 | 10.51 | 30.08 | 1.76 | 7.46 | 23.74 |
| **1.4** | 4.05 | 16.78 | 63.13 | 1.76 | 7.77 | 37.85 | 1.04 | 4.41 | 28.15 |
| **2.0** | 1.62 | 6.71 | 69.84 | 1.57 | 6.93 | 44.79 | 0.47 | 1.99 | 30.14 |
| **2.8** | 0.24 | 0.99 | 70.84 | 1.75 | 7.73 | 52.52 | 0.11 | 0.47 | 30.61 |
| **3.15** | 7.02 | **29.08** | 99.92 | 10.1 | **44.61** | 97.13 | 15.19 | **64.39** | 95.00 |
| **8 .0** | 0.02 | 0.08 | 100.00 | 0.60 | 2.65 | 99.78 | 0.96 | 4.07 | 99.07 |
| **16.0** | 0.00 | 0.00 | 100.00 | 0.05 | 0.22 | 100.00 | 0.22 | 0.93 | 100.00 |

[a] cumulative %

In contrast, the **POA** showed that the majority of the miscanthus material is regularly distributed among sieves **3.15** and **2.0–0.05 mm**. From the presented comparison, in SA a less amount of particles was captured by the lower sieves and the majortity was cought by one sieve 3.15 mm, which should not occur based on the POA. This is called a **clogging phenomenon**

and it was reported by Igathinathane et al. (2009a), Glé at al. (2013) and Chaloupková et al. (2016). The particles clogged the sieve apertures and the they could not pass further to the smaller sieves.

**Table 14.** Detailed PSD of miscanthus via the POA

| Sieve opening size (mm) | Fraction 4 mm | | | Fraction 8 mm | | | Fraction 12 mm | | |
|---|---|---|---|---|---|---|---|---|---|
| | (N) | (%) | (cum% [a]) | (N) | (%) | (cum% [a]) | (N) | (%) | (cum% [a]) |
| **<0.063** | 0 | 0.00 | 0.00 | 0 | 0.00 | 0.00 | 0 | 0.00 | 0.00 |
| **0.063** | 0 | 0.00 | 0.00 | 0 | 0.00 | 0.00 | 0 | 0.00 | 0.00 |
| **0.125** | 11480 | 3.97 | 3.97 | 8451 | 4.92 | 4.92 | 3293 | 4.95 | 4.95 |
| **0.25** | 14241 | 4.93 | 8.90 | 9881 | 5.75 | 10.67 | 3068 | 4.61 | 9.56 |
| **0.5** | 54597 | **18.88** | 27.78 | 34218 | **19.92** | 30.59 | 9022 | 13.56 | 23.13 |
| **1.0** | 44808 | 15.50 | 43.28 | 26778 | 15.59 | 46.18 | 8682 | 13.05 | 36.18 |
| **1.4** | 53406 | 18.47 | 61.75 | 30610 | 17.82 | 64.00 | 11531 | 17.34 | 53.51 |
| **2.0** | 49026 | 16.96 | 78.71 | 26917 | 15.67 | 79.67 | 11824 | 17.78 | 71.29 |
| **2.8** | 14070 | 4.87 | 83.57 | 269 | 4.23 | 83.90 | 3759 | 5.65 | 76.94 |
| **3.15** | 44558 | 15.41 | 98.98 | 24585 | 14.31 | 98.21 | 13509 | **20.31** | 97.25 |
| **8.0** | 2827 | 0.98 | 99.96 | 2789 | 1.62 | 99.83 | 1666 | 2.50 | 99.75 |
| **16.0** | 108 | 0.04 | 100.00 | 285 | 0.16 | 100.00 | 164 | 0.25 | 100.00 |

[a] cumulative %

### *Hemp*

PSD of hemp from the **SA** is presented in the **Figure 33** and **Table 15**. The PSD results from the **POA** are depicted in the **Figure 34** and **Table 16**. All data are expressed as the total amount of the particles retained on the sieves together with the percentage and cumulative percentage values.

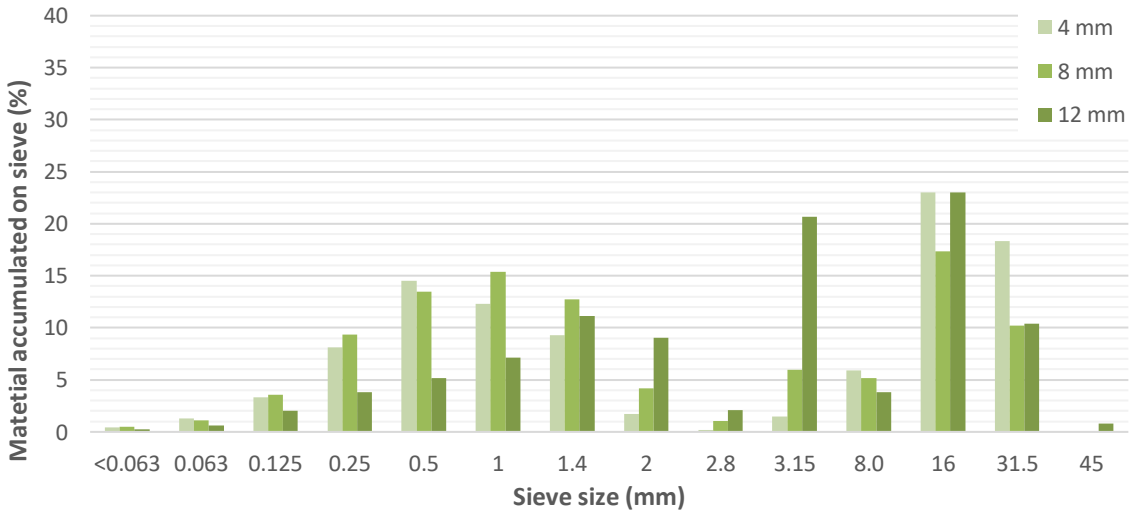


**Figure 33.** PSD of hemp via the SA

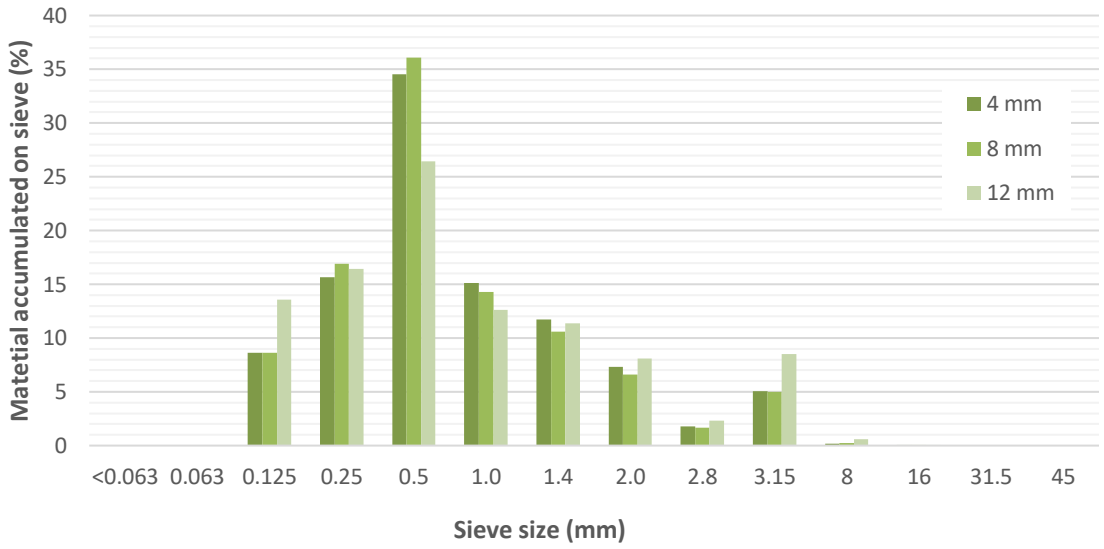


**Figure 34.** PSD of hemp via the POA

As we can see, in case of **SA**, large portion of the hemp material was captured on the sieves with opening size of **31.5** and **16 mm**. Considerable amount of fraction 12 mm was captured by the sieve **3.15 mm**. Due to the fibrous nature of hemp, it is not possible to ground long hemp bast fibres well and they may create tangled masses, which cannot fail through openings and thus stay on the first sieves (Chaloupková et al. 2016), as it happened also in this case (sieves 31.5 and 16 mm). Almost all the rest of the non-fibre part of stem and leaf tissues, i.e. epidermis, cortex, phloem, xylem, and mainly pith, passed through the sieves (however, some of them were caught and tangled by bast fibres on the first sieve, too) and significant amounts of the material were distributed among sieves 0.25 mm and 1.4 mm.

**POA** confirmed what was clear from the visual assessment of SA, that also in this case the **clogging phenomenon** occurred at the sieves **31.5** and **16 mm**. POA distributed the majority of the materials similarly for each fraction on the sieve **0.5 mm** and neighbouring sieves.

As it is evident from the **Figure 33** and **34**, due to the fibrous nature, SA of hemp did not yield absolutely reliable results on real PSD; however, it can be assumed that the material would behave in such manner as in the SA, **fibrous material can cause problems during the grinding and subsequent briquetting**, thus also SA had provided the helpful information about structural composition of the material.

**Table 15.** Detailed PSD of hemp (SA)

| Sieve opening size (mm) | Fraction 4 mm | | | Fraction 8 mm | | | Fraction 12 mm | | |
|---|---|---|---|---|---|---|---|---|---|
| | (g) | (%) | (cum% [a]) | (g) | (%) | (cum% [a]) | (g) | (%) | (cum% [a]) |
| **<0.063** | 0.10 | 0.44 | 0.44 | 0.10 | 0.46 | 0.46 | 0.06 | 0.27 | 0.27 |
| **0.063** | 0.30 | 1.31 | 1.74 | 0.24 | 1.11 | 1.57 | 0.13 | 0.59 | 0.86 |
| **0.125** | 0.76 | 3.31 | 5.05 | 0.77 | 3.56 | 5.13 | 0.45 | 2.03 | 2.88 |
| **0.25** | 1.87 | 8.14 | 13.20 | 2.02 | 9.34 | 14.48 | 0.85 | 3.83 | 6.71 |
| **0.5** | 3.34 | 14.55 | 27.74 | 2.91 | 13.46 | 27.94 | 1.15 | 5.18 | 11.89 |
| **1.0** | 2.83 | 12.33 | 40.07 | 3.33 | 15.40 | 43.34 | 1.58 | 7.12 | 19.01 |
| **1.4** | 2.14 | 9.32 | 49.39 | 2.76 | 12.77 | 56.11 | 2.47 | 11.13 | 30.14 |
| **2.0** | 0.39 | 1.70 | 51.09 | 0.90 | 4.16 | 60.27 | 2.01 | 9.05 | 39.19 |
| **2.8** | 0.04 | 0.17 | 51.26 | 0.22 | 1.02 | 61.29 | 0.46 | 2.07 | 41.26 |
| **3.15** | 0.34 | 1.48 | 52.74 | 1.29 | 5.97 | 67.25 | 4.59 | 20.68 | 61.94 |
| **8.0** | 1.35 | 5.88 | 58.62 | 1.12 | 5.18 | 72.43 | 0.85 | 3.83 | 65.77 |
| **16.0** | 5.29 | **23.04** | 81.66 | 3.75 | **17.35** | 89.78 | 5.11 | **23.02** | 88.78 |
| **31.5** | 4.21 | 18.34 | 100.00 | 2.21 | 10.22 | 100.00 | 2.31 | 10.41 | 99.19 |
| **45.0** | 0 | 0.00 | 100.00 | 0.00 | 0.00 | 100.00 | 0.18 | 0.81 | 100.00 |

[a] cumulative %

**Table 16.** Detailed PSD of hemp via the POA

| Sieve opening size (mm) | Fraction 4 mm | | | Fraction 8 mm | | | Fraction 12 mm | | |
|---|---|---|---|---|---|---|---|---|---|
| | (N) | (%) | (cum% [a]) | (N) | (%) | (cum% [a]) | (N) | (%) | (cum% [a]) |
| **<0.063** | 0 | 0.00 | 0.00 | 0 | 0.00 | 0.00 | 0 | 0.00 | 0.00 |
| **0.063** | 0 | 0.00 | 0.00 | 0 | 0.00 | 0.00 | 0 | 0.00 | 0.00 |
| **0.125** | 22582 | 8.61 | 8.61 | 26395 | 8.62 | 8.62 | 17341 | 13.60 | 13.60 |
| **0.25** | 41044 | 15.66 | 24.27 | 51781 | 16.92 | 25.54 | 20923 | 16.41 | 30.02 |
| **0.5** | 90460 | **34.51** | 58.78 | 110430 | **36.08** | 61.63 | 33715 | **26.45** | 56.46 |
| **1.0** | 39656 | 15.13 | 73.91 | 43687 | 14.27 | 75.90 | 16096 | 12.63 | 69.09 |
| **1.4** | 30781 | 11.74 | 85.65 | 32421 | 10.59 | 86.49 | 14518 | 11.39 | 80.48 |
| **2.0** | 19148 | 7.30 | 92.95 | 20160 | 6.59 | 93.08 | 10313 | 8.09 | 88.57 |
| **2.8** | 4713 | 1.80 | 94.75 | 5166 | 1.69 | 94.77 | 2944 | 2.31 | 90.88 |
| **3.15** | 13346 | 5.09 | 99.84 | 15328 | 5.01 | 99.78 | 10866 | 8.52 | 99.40 |
| **8.0** | 398 | 0.15 | 99.99 | 641 | 0.21 | 99.99 | 725 | 0.57 | 99.97 |
| **16.0** | 15 | 0.01 | 100.00 | 38 | 0.01 | 100.00 | 36 | 0.03 | 100.00 |
| **31.5** | 1 | 0.00 | 100.00 | 1 | 0.00 | 100.00 | 2 | 0.00 | 100.00 |
| **45.0** | 0 | 0.00 | 100.00 | 0 | 0.00 | 100.00 | 0 | 0.00 | 100.00 |

[a] cumulative %

***Pine sawdust***

The size distribution of pine sawdust particles determined by the **SA** is presented in the **Figure 35** and **Table 17**. The PSD results from the **POA** follow in the **Figure 36** and **Table 18**.

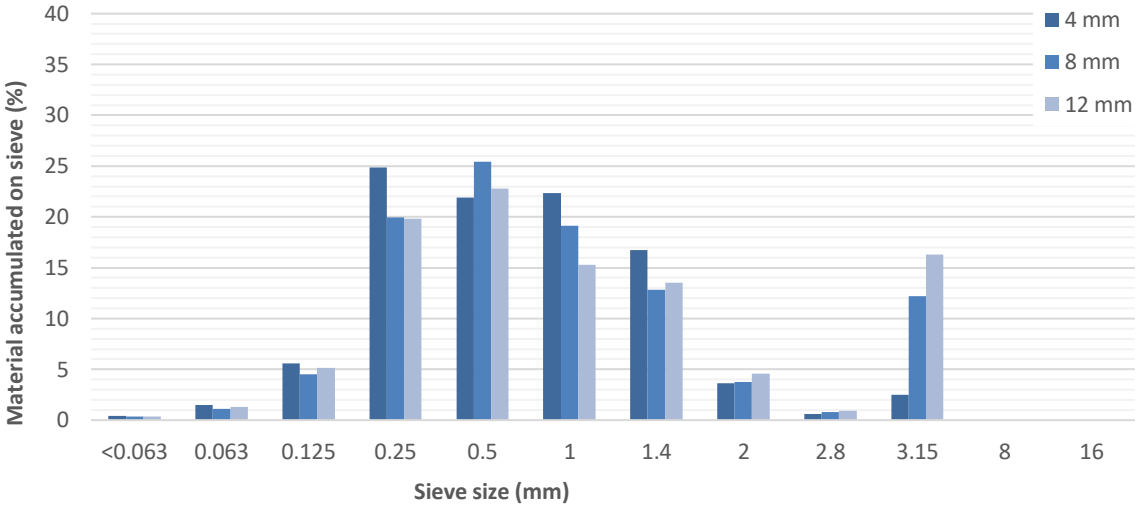


**Figure 35.** PSD of pine sawdust via the SA

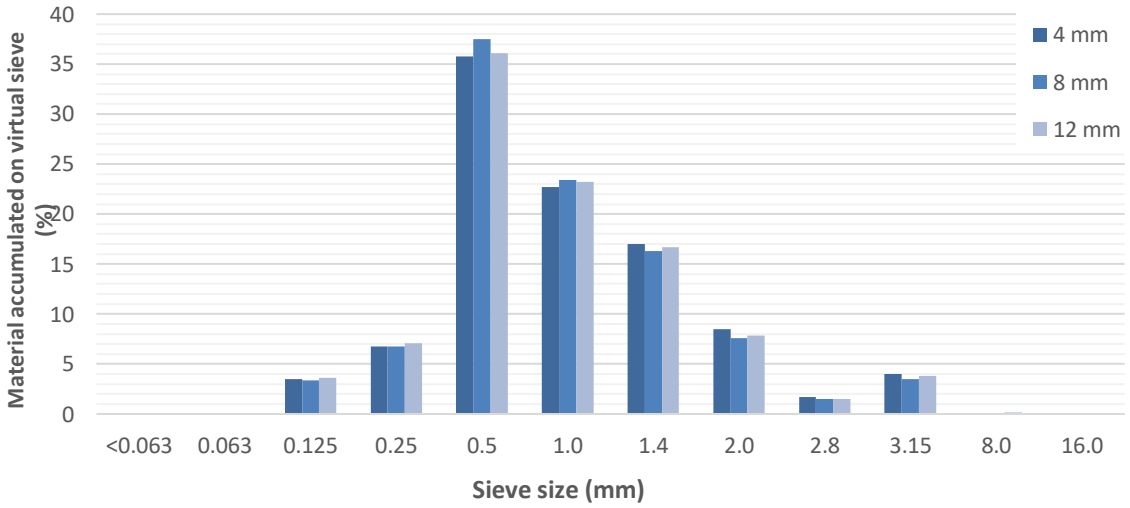


**Figure 36.** PSD of pine sawdust via the POA

In this case, the distribution of all pine sawdust fractions from the SA was more uniform than that for previous materials. And as it can be seen from the results (**Figure 35**, **Table 17**), all fraction samples had very fine particles. Majority of the material comprised of the particles with a size between **0.25** and **1.4 mm**; for 4 mm fraction it was **86%** of the material, for 8 and 12 mm it was 71% and 77%, respectively. Previous study of Chaloupková et al. (2016) also determined that the pine sawdust fraction of 12 mm consisted mainly of the particles smaller than 1.5 mm. The sieves 8 and 16 mm did not capture any material. The minimum of the material

was captured by the sieve 2.8 mm as well as by the last smallest sieve 0.063 mm and the bottom pan. Besides, decreased screens' opening size resulted in decreased particle sizes partly.

**Table 17.** Detailed PSD of pine sawdust (SA)

| Sieve opening size (mm) | Fraction 4 mm | | | Fraction 8 mm | | | Fraction 12 mm | | |
|---|---|---|---|---|---|---|---|---|---|
| | (g) | (%) | (cum% [a]) | (g) | (%) | (cum% [a]) | (g) | (%) | (cum% [a]) |
| **<0.063** | 0.16 | 0.40 | 0.40 | 0.14 | 0.35 | 0.35 | 0.15 | 0.37 | 0.37 |
| **0.063** | 0.59 | 1.48 | 1.88 | 0.44 | 1.10 | 1.44 | 0.53 | 1.32 | 1.69 |
| **0.125** | 2.24 | 2.48 | 2.48 | 1.81 | 4.51 | 5.95 | 2.07 | 5.14 | 6.83 |
| **0.25** | 9.93 | **24.87** | 32.36 | 8.00 | 19.93 | 25.88 | 7.98 | 19.82 | 26.65 |
| **0.5** | 8.74 | 21.89 | 54.24 | 10.22 | **25.45** | 51.33 | 9.17 | **22.77** | 49.42 |
| **1.0** | 8.93 | 22.36 | 76.61 | 7.67 | 19.10 | 70.44 | 6.15 | 15.27 | 64.69 |
| **1.4** | 6.68 | 16.73 | 93.34 | 5.14 | 12.80 | 83.24 | 5.44 | 13.51 | 78.20 |
| **2.0** | 1.44 | 3.61 | 96.94 | 1.52 | 3.79 | 87.02 | 1.84 | 4.57 | 82.77 |
| **2.8** | 0.23 | 0.58 | 97.52 | 0.31 | 0.77 | 87.80 | 0.38 | 0.94 | 83.71 |
| **3.15** | 0.99 | 2.48 | 100.00 | 4.90 | 12.20 | 100.00 | 6.56 | 16.29 | 100.00 |
| **8.0** | 0.00 | 0.00 | 100.00 | 0.00 | 0.00 | 100.00 | 0.00 | 0.00 | 100.00 |
| **16.0** | 0.00 | 0.00 | 100.00 | 0.00 | 0.00 | 100.00 | 0.00 | 0.00 | 100.00 |

[a] cumulative %

**The results of POA** in the **Figure 36** and **Table 18** below showed that the results of all fractions are very similar/more precise. PSD can be described as non-uniform with the finer particles dominated. In the case of POA, most of the material composed of the particles with a size between **0.5 and 1.4 mm**, where more than one third of the material had the length of 0.5 mm.

**Table 18.** Detailed PSD of pine sawdust via the POA

| Sieve opening size (mm) | Fraction 4 mm | | | Fraction 8 mm | | | Fraction 12 mm | | |
|---|---|---|---|---|---|---|---|---|---|
| | (N) | (%) | (cum% [a]) | (N) | (%) | (cum% [a]) | (N) | (%) | (cum% [a]) |
| **<0.063** | 0 | 0.00 | 0.00 | 0 | 0.00 | 0.00 | 0 | 0.00 | 0.00 |
| **0.063** | 0 | 0.00 | 0.00 | 0 | 0.00 | 0.00 | 0 | 0.00 | 0.00 |
| **0.125** | 25599 | 3.48 | 3.48 | 18349 | 3.37 | 3.37 | 19527 | 3.64 | 3.64 |
| **0.25** | 49767 | 6.77 | 10.25 | 36670 | 6.74 | 10.11 | 38071 | 7.10 | 10.74 |
| **0.5** | 263131 | **35.78** | 46.03 | 204136 | **37.49** | 47.60 | 193457 | **36.08** | 46.82 |
| **1.0** | 167081 | 22.72 | 68.74 | 127499 | 23.42 | 71.02 | 124463 | 23.21 | 70.04 |
| **1.4** | 124805 | 16.97 | 85.71 | 88805 | 16.31 | 87.33 | 89291 | 16.65 | 86.69 |
| **2.0** | 62227 | 8.46 | 94.18 | 41271 | 7.58 | 94.91 | 42031 | 7.84 | 94.53 |
| **2.8** | 12419 | 1.69 | 95.86 | 8173 | 1.50 | 96.41 | 8196 | 1.53 | 96.06 |
| **3.15** | 29648 | 4.03 | 99.90 | 18887 | 3.47 | 99.88 | 20253 | 3.78 | 99.84 |
| **8.0** | 747 | 0.10 | 100.00 | 638 | 0.12 | 100.00 | 830 | 0.15 | 99.99 |
| **16.0** | 26 | 0.00 | 100.00 | 23 | 0.00 | 100.00 | 42 | 0.01 | 100.00 |

[a] cumulative %

The **Figures 35–36** also indicated the mentioned **"falling-through" effect** of pine sawdust particles from the SA, which was previously detected by Ulusoy & Igathinathane et al. (2016) and Chaloupková et al. (2016). As it can be seen, starting from the sieve 2.8 mm (more markedly from the sieve 2.0 mm) physically longer particles passed through the sieves with the smaller apertures and passed until the sieve 0.125 mm, where the sieve 0.125 and especially the sieve 0.25 mm captured significantly more material than in a reality should retain. In case of the last sieve (0.063 mm) and the bottom pan it was not possible to compare the results of two methods due to the limited measuring range of the photo-optical analyser.

**Figures 37 and 38** (on the next page) present the cumulative % retained on sieve for SA and POA, respectively, and compares the PSD values for all materials and fractions. Wide PSD is generally required for the material intended for densification (Kirsten et al. 2016). Broad PSD is essential for creation of interlocking bonds and for decrease the pore space between the particles to increase the density (Kirsten et al. 2016). Optimal size distribution reduces the specific energy input during the densification process (Havrland et al. 2011). Wang et al. (2018a) reported that large chopped particles (15 mm) resulted in high briquetting energy consumption compared to smaller fractions (5 and 10 mm). However, Kirsten et al. (2016) found that small particle might also led to high energy consumption. The question of energy consumption and associated costs is inseparable component of socio-economic evaluation of whole biofuel processes and supply chains (Puig-Arnavat et al. 2016; Muazu et al. 2017; Mladenović et al. 2018); the issue is further slightly mentioned in the Subchapter 5.8.1.

From the SA cumulative curves (see **Figure 37**), it can be observed that the **hemp has the widest PSD** curves, on the other hand, the fractions of pine sawdust have more narrow cumulative curves. The curves also clearly show the clogging and falling-down of the particles. From the POA cumulative curves (**Figure 38**), the widest PSD has miscanthus. From the POA curves, it can be seen, that the materials and fractions have similar trend of PSD.

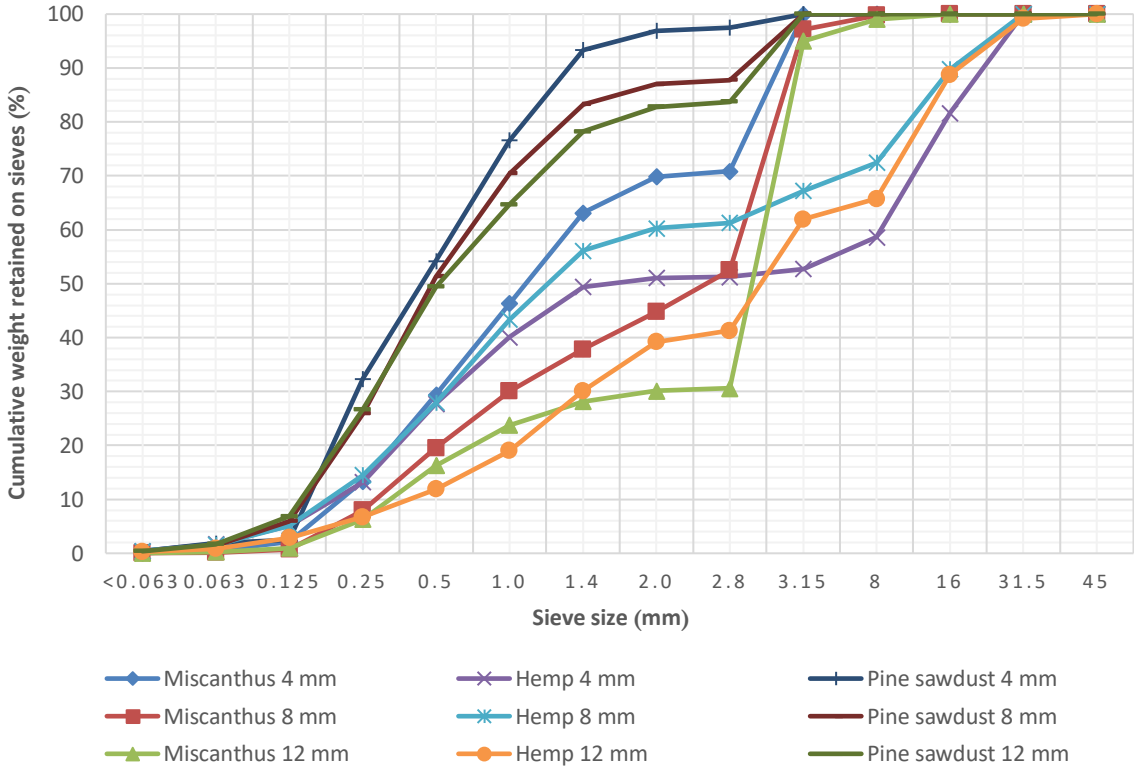


**Figure 37.** Cumulative weights of all materials and fraction retained on sieves (%), SA

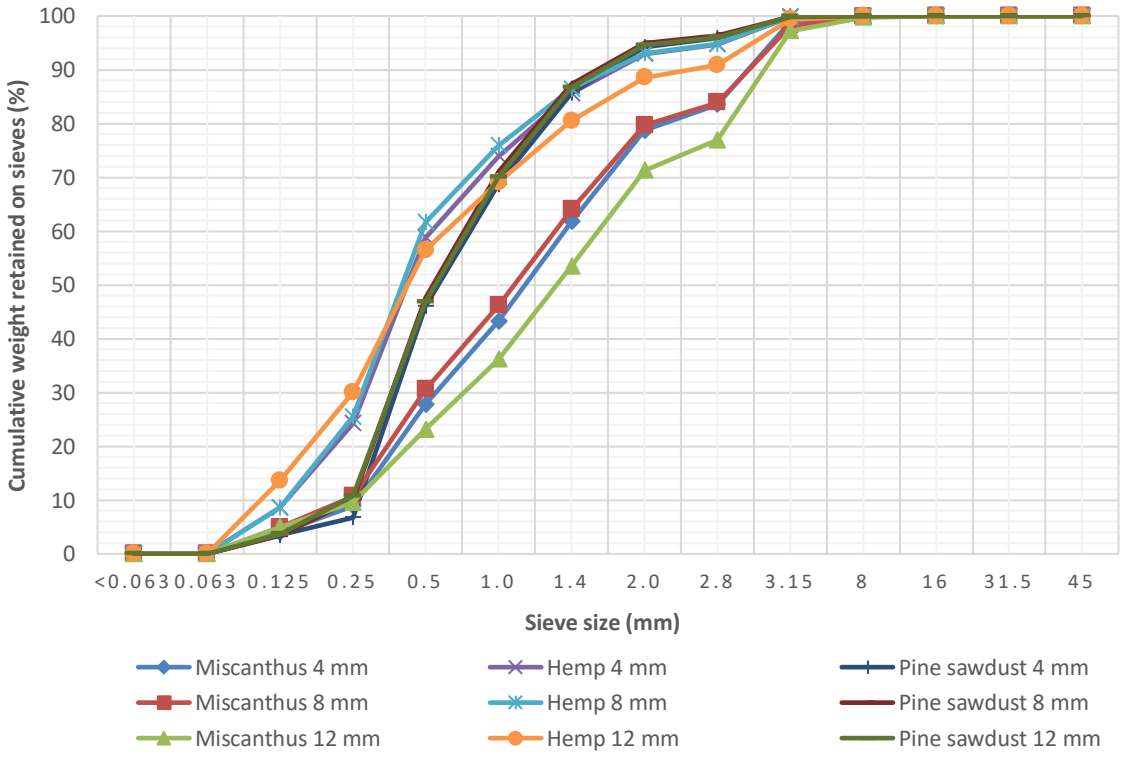


**Figure 38.** Cumulative weights of all materials and fraction retained on sieves (%), POA

Besides the clogging phenomenon and the falling-through effect, the conventional SA is a time-consuming process, particles are not measured individually, and their shape highly affects the final result (Fernlund 1998; Febbi et al. 2015). The SA **considers only one parameter**: general particle shape. This is given by the aperture of a sieve (no detailed individual results of particles' lengths, width or shapes could be obtained), thus it is solely suitable for spherical particles (Igathinathane et al. 2009a). Although biomass particles are characterized by highly irregular sizes and shapes (Guo et al. 2012; Febbi et al. 2015), these irregularities increase errors in the PSD estimation (Shanthi et al. 2014). SA also has limited set of available standard sieves and limited number of sieves held in the shaker. On the other hand, classical SA is an easy, simple, standardized and inexpensive tool (Al-Thyabat & Miles 2006) giving a possibility to physically separate the particle size fractions (Chaloupková et al. 2018b).

Due to mentioned limitations of SA, many authors propounded that more precise results could be acquired by machine vision and image analysis (Igathinathane et al. 2009a; Igathinathane et al. 2009b; Souza & Menegalli 2011; Kumara et al. 2012; Vaezi et al. 2013; Gil et al. 2014; Febbi et al. 2015). In comparison, POA based on a machine vision and an image processing provides more **accurate and precise PSD analysis results**, time savings, particles are examined individually, and it gives an additional information relating to shapes and the number of particles. On the contrary, POA is associated with higher investment costs, only two-dimensional projection of the particles is captured and measured, and the method does not provide the possibility of separation of the particle size fractions (Fernlund 1998; Igathinathane et al. 2009a, Chaloupková et al. 2018b). This shortcoming can be solved by another method of machine vision, which is sensor-based sorting, which enables physical separation of a granular material into predefined classes in real time (Maier 2017); nowadays it is used in the field of waste management (Kępys 2016), food processing (Narendra & Hareesh 2010) and mining industry (Lessard et al. 2014). Also, as it was observed in this study, the POA was limited by the given minimum measuring range.

Regarding to the comparison with other authors, the results of the SA and the advanced POA (employing the photo-optical analyser) were not found to be confronted in any study before, and selected machine vision method was not applied for the studied materials.

## 5.5.2. Particle size and shape characterization

### *Miscanthus*

POA provided also detailed information about particle dimensional characterization by measuring all particles contained in the sample. In the **Table 19**, the descriptive statistics (mean, maximum and minimum and variance values) of miscanthus material are presented.

**Table 19.** Particle characterization of miscanthus

| | Fraction 4 mm | | | | Fraction 8 mm | | | | Fraction 12 mm | | | |
|---|---|---|---|---|---|---|---|---|---|---|---|---|
| | Mean | Min [e] | Max [f] | Var [g] | Mean | Min | Max | Var | Mean | Min | Max | Var |
| $X_{min}$ [a] | 0.50 | 0.09 | 12.80 | 0.16 | 0.55 | 0.09 | 23.27 | 0.24 | 0.61 | 0.09 | 19.12 | 0.27 |
| $L$ [a] | 1.97 | 0.09 | 59.92 | 2.66 | 1.98 | 0.09 | 47.82 | 3.74 | 2.38 | 0.09 | 50.95 | 5.18 |
| $X_{max}$ [a] | 1.99 | 0.13 | 48.67 | 2.63 | 2.01 | 0.13 | 47.83 | 3.73 | 2.40 | 0.13 | 54.80 | 5.18 |
| $W_{max}$ [a] | 0.48 | 0.09 | 13.38 | 0.13 | 0.52 | 0.09 | 16.14 | 0.18 | 0.57 | 0.09 | 18.23 | 0.21 |
| $X_a$ [a] | 0.82 | 0.10 | 8.75 | 0.25 | 0.85 | 0.10 | 12.67 | 0.34 | 0.97 | 0.10 | 13.11 | 0.42 |
| $X$ [a] | 1.80 | 0.09 | 59.92 | 2.33 | 1.79 | 0.09 | 47.23 | 3.18 | 2.15 | 0.09 | 74.79 | 4.72 |
| $X_m$ [a] | 0.53 | 0.09 | 14.20 | 0.27 | 0.58 | 0.09 | 25.94 | 0.38 | 0.64 | 0.09 | 15.83 | 0.41 |
| $C_i$ [d] | 0.63 | 0.07 | 0.97 | 0.03 | 0.65 | 0.10 | 0.97 | 0.02 | 0.63 | 0.06 | 0.97 | 003 |
| $\Psi$ [d] | 0.65 | 0.15 | 0.87 | 0.01 | 0.66 | 0.19 | 0.87 | 0.01 | 0.65 | 0.13 | 0.87 | 0.01 |
| $R_d$ [d] | 0.25 | 0.00 | 0.83 | 0.02 | 0.27 | 0.00 | 0.81 | 0.02 | 0.26 | 0.00 | 0.80 | 0.02 |
| $R_{lw}$ [d] | 5.11 | 1.02 | 87.89 | 19.99 | 4.53 | 1.02 | 107.98 | 15.89 | 4.96 | 1.01 | 77.50 | 20.99 |
| $A_r$ [d] | 4.84 | 1.07 | 71.34 | 17.02 | 4.24 | 1.08 | 337.40 | 13.17 | 4.59 | 1.09 | 82.74 | 15.75 |
| $S_m$ [d] | 0.61 | 0.00 | 1.00 | 0.06 | 0.61 | 0.00 | 1.00 | 0.06 | 0.60 | 0.00 | 1.00 | 0.06 |
| $U_p$ [a] | 4.63 | 0.36 | 108.93 | 14.96 | 4.76 | 0.36 | 194.40 | 24.05 | 5.62 | 0.36 | 91.63 | 27.84 |
| $A_1$ [b] | 0.72 | 0.01 | 60.17 | 1.02 | 0.83 | 0.01 | 126.04 | 2.36 | 1.07 | 0.01 | 110.26 | 3.69 |
| $A_0$ [b] | 2.94 | 0.02 | 141.39 | 19.16 | 3.48 | 0.02 | 852.88 | 63.39 | 4.35 | 0.02 | 193.34 | 55.79 |
| $V_1$ [c] | 0.37 | 0.00 | 462.51 | 2.59 | 0.56 | 0.00 | 953.83 | 24.87 | 0.71 | 0.00 | 209.88 | 8.61 |

[a] unit in mm; [b] $mm^2$; [c] $mm^3$; [d] without unit; [e] ~ minimum; [f] ~ maximum; [g] ~ variance

Diameter of irregular particles is mainly evaluated by $X$, the distance between two furthest points of the particle measured in a given direction (Igathinathane et al. 2009a; Dražić et al. 2016). In case of the studied miscanthus material, mean value of ***X*** for fraction 4, 8 and 12 mm was **1.80, 1.79** and **2.15 mm**, respectively. More useful information is given by **max feret** $\boldsymbol{X_{max}}$ and **min feret** $\boldsymbol{X_{min}}$, since they calculate a diameter of the particle in all directions (Dražić et al. 2016). $X_{max}$ is often associated to the "***length***" of the particle (Pons et al. 1999). It gives the value of the minimum sieve size through which the particle can pass through without any obstacle (Shanthi et al. 2014). Length of the miscanthus particles ranged from its maximum of **54.80 mm** (12 mm) to its minimum of **0.13 mm** (which was given by the measuring possibility of the analyser) and with arithmetic mean of **1.99, 2.01** and **2.40 mm** for 4, 8 and 12 mm. On the contrary, $X_{min}$ is related to the particle "***breadth***" (Pons et al. 1999). $X_{min}$ mean ranged

from 0.50 to 0.61 mm, min 0.09 mm and max values of $X_{min}$ ranged **12.80–23.27 mm**, **0.09 mm** and **10.04 mm**, respectively. Feret diameter as an algorithm for particle dimension is often used to evaluate particle size distribution (Igathinathane et al. 2009a).

***L*, $W_{max}$, $X_m$** and **$X_a$** define particle size in different manners (Pons et al. 1999). Mean value for *L* ranged **1.97–2.38 mm**, for $W_{max}$ **0.48–0.57 mm**, $X_m$ **0.53–0.64 mm** and $X_a$ **0.82–0.97 mm**. Mean $X_m$ is smaller than $X_a$ and both descriptors have smaller mean values than mean *X*; this corresponds with experimental evidence of other studies (Yang 2003).

Shape of particles was defined by **sphericity $\psi$**, **roundness $R_d$** and **circularity $C_i$**, important parameters describing **particle shape** in several studies (Mora & Kwan 2000; Cruz-Matías et al. 2019). They were measured in the range of 0.01–1. $\psi$ describes a compactness of a particle in terms of the surface area (Zhao & Wang 2016) and it is the most dependent on elongation (Olson 2011; Cruz-Matías et al. 2019). $R_d$ is a characteristic affected by a form, it is not a degree of $\psi$ ($\psi$ is a measure of a form) even though $R_d$ is the best manifested by a perfect sphere. $R_d$ is mainly dependent on the sharpness/roughness of angular convexities and concavities of a particle (Cruz-Matías et al. 2019). $R_d$ of the corners is the opposite of the angularity of the corners and plays significant role in the abrasive and perforation features of the particles (Mora & Kwan 2000). Wadell (1932) identified $\psi$ and $R_d$ as two independent aspects of a particle shape, however lately Zhao & Wang (2016) reported their dependency. In general, the particles that have larger $\psi$ values also have larger values of $A_r$ and mean $R_d$ value (Zhao & Wang 2016).

The sphericity index value of a perfect sphere is 1. In case of studied miscanthus the **$\psi$** mean value for all three fractions was **0.65**, thus the particles can be described as irregular (non-spherical) since their average $\psi$ value is smaller than 0.8 (Zhao & Wang 2016). **Figure 39** shows the scatter plot of $\psi$ together with $R_d$ according to Krumbein and Sloss (1963), where it can be seen where the values are mostly accumulated. **$R_d$** of all fractions lies around the value **0.25**, while for an absolutely round and smooth object (i.e. sphere) the value of $R_d$ is 1, for any other object the values is less than 1. According to the classification of Powers (1953), see **Figure 40**, **more than 50%** of particles can be classified as **very angular and angular**.

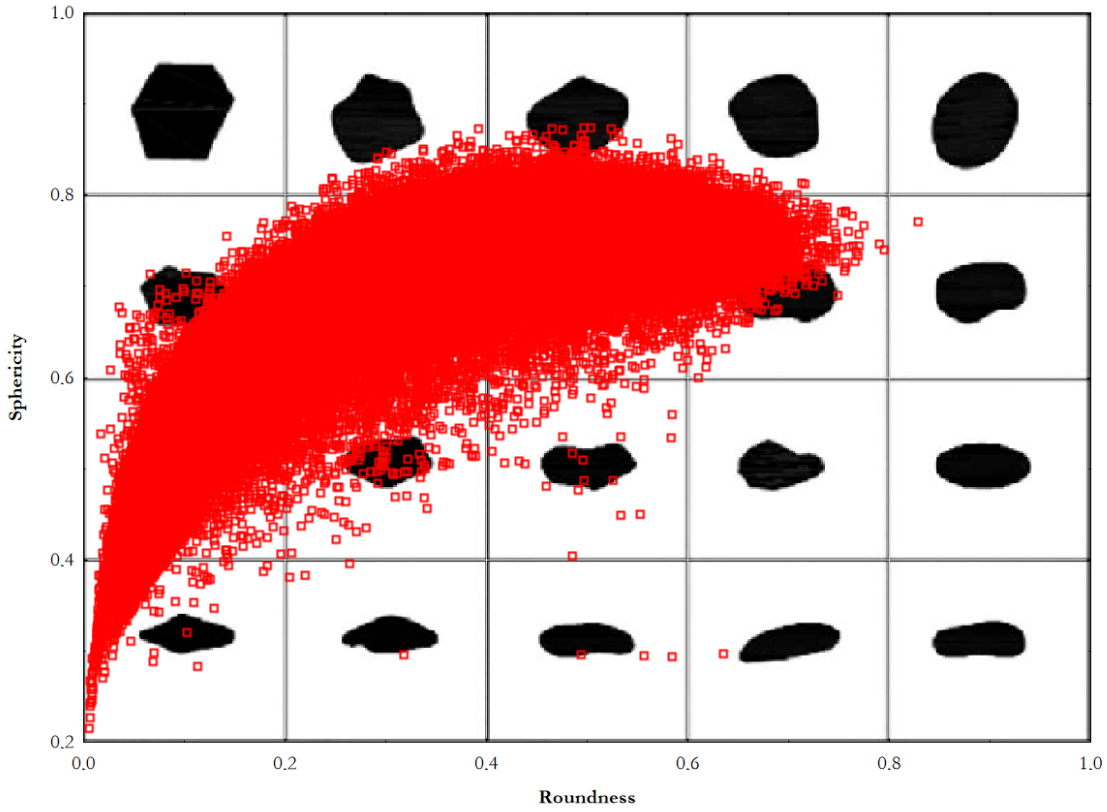


**Figure 39.** Roundness and Sphericity ratios of miscanthus 4 mm
(Background modified according to Krumbein and Sloss 1963)

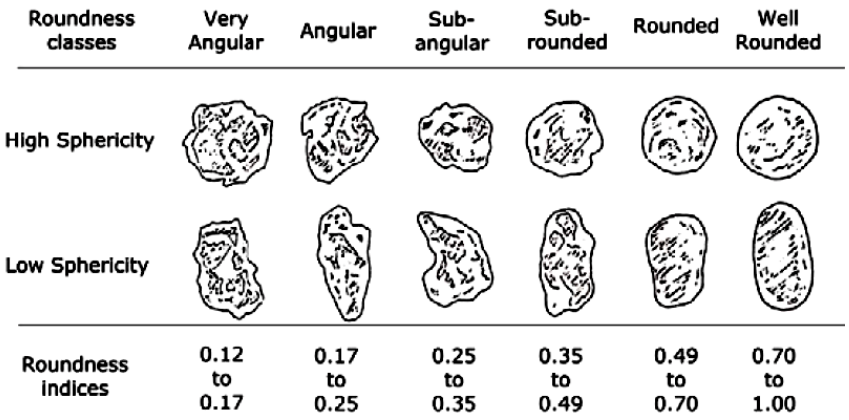


**Figure 40.** Roundness scale for sedimentary particles
Source: Powers (1953)

***Ci*** is a measurement of both the particle form and roughness (Olson 2011). It can also reach values ranging from 1, as it is in case of particle perfectly round and smooth circle, and up to 0, when conversely shape becomes more angular and rougher (Olson 2011). Average *Ci* value of analysed miscanthus was **0.63**, which means that the particles have **moderate surface irregularities**.

Particle shape can be evaluated also in terms of **symmetry $S_m$,** ranging from 0 to 1. Perfectly symmetric objects (like sphere or cube) have $S_m$ equal to 1. In case of measured miscanthus particles, mean $S_m$ was **0.60**, so the particles can be called **moderately asymmetrical** (Yang 2003).

**Length width ratio $R_{lw}$** and **aspect ratio $A_r$** show the degree of particle elongation (Agimelen et al. 2017) based on two particle dimensions (Olson 2011). The ratios can reach values in range of 1–10000 (Haver & Boecker 2014). Value 1 is for object with symmetric shape (e.g. sphere or square) and 10000 theoretically for very elongated and thin objects, however the ratios are suitable only for particles that are not very elongated and curved (EN ISO 9276-6 2008), for example particles of needle-like and acicular shape (Olson 2011), as it was in case of examined miscanthus material. Since biomass particles are in practise non-spherical and irregular (Dai et al. 2012), their ratios normally belong to the range 2–15 (Lu et al. 2010). The measured miscanthus particles have the average value of $R_{lw}$ **4.87** and $A_r$ **4.56**.

Additional information about the particle morphology gave $U_p$, $A_1$, $A_0$ and $V_1$. Despite the fact that surface area, volume and sphericity, representing 3D parameters (Zhao & Wang 2016), were in this study calculated from 2D images, they offered valuable statistical data. 3D imaging could bring more precise results, however, this would be associated with additional costs of equipment, longer analysing time and smaller amount of analysed particles bringing lower statistical confidence (Bagheri et al. 2015).

### *Hemp*

In the **Table 20**, the descriptive statistics (mean, maximum and minimum and variance values) of dimensional characteristics of hemp particles are presented.

In case of hemp, the average values of $X_{max}$ and $X_{min}$ of all fractions are lower than in case of miscanthus, **1.99 mm** and **0.34 mm** respectively. Average $C$ value of analysed hemp was **0.67**. Average $\psi$ and $R_d$ values were **0.67** and **0.30**, respectively. Thus, the particles can be described as **sub-angular** (Powers 1953). Further, average value of all hemp fractions for $R_{lw}$ was **4.60** and for $A_r$ it was **4.57**, which is a slightly higher value than in case of miscanthus, which means that the hemp particles are **more elongated**, however, with more rounded edges. Mean value of $S_m$ was **0.65**, so the hemp particles are more symmetrical than miscanthus and pine sawdust particles.

**Table 20.** Particle characterization of hemp

| | Fraction 4 mm | | | | Fraction 8 mm | | | | Fraction 12 mm | | | |
|---|---|---|---|---|---|---|---|---|---|---|---|---|
| | Mean | Min[a] | Max[b] | Var[c] | Mean | Min | Max | Var | Mean | Min | Max | Var |
| $X_{min}$ [a] | 0.33 | 0.09 | 19.88 | 0.08 | 0.30 | 0.09 | 16.99 | 0.07 | 0.38 | 0.09 | 18.73 | 0.16 |
| $L$ [a] | 1.13 | 0.09 | 35.55 | 1.14 | 1.10 | 0.09 | 35.56 | 1.23 | 1.30 | 0.09 | 33.72 | 2.15 |
| $X_{max}$ [a] | 1.16 | 0.13 | 35.56 | 1.13 | 1.13 | 0.13 | 35.56 | 1.22 | 1.32 | 0.13 | 33.73 | 2.15 |
| $W_{max}$ [a] | 0.32 | 0.09 | 18.57 | 0.07 | 0.30 | 0.09 | 14.40 | 0.06 | 0.37 | 0.09 | 15.86 | 0.14 |
| $X_a$ [a] | 0.51 | 0.10 | 19.17 | 0.13 | 0.48 | 0.10 | 17.18 | 0.12 | 0.57 | 0.10 | 18.43 | 0.27 |
| $X$ [a] | 1.06 | 0.09 | 34.83 | 1.07 | 1.04 | 0.09 | 35.56 | 1.16 | 1.18 | 0.09 | 29.99 | 1.92 |
| $X_m$ [a] | 0.34 | 0.09 | 19.29 | 0.12 | 0.31 | 0.09 | 12.56 | 0.10 | 0.39 | 0.09 | 14.56 | 0.23 |
| $C_i$ [d] | 0.67 | 0.11 | 0.97 | 0.02 | 0.67 | 0.10 | 0.97 | 0.02 | 0.67 | 0.05 | 0.97 | 0.03 |
| $\Psi$ [d] | 0.67 | 0.23 | 0.87 | 0.02 | 0.67 | 0.19 | 0.87 | 0.02 | 0.66 | 0.13 | 0.87 | 0.02 |
| $R_d$ [d] | 0.29 | 0.01 | 0.76 | 0.02 | 0.28 | 0.00 | 0.79 | 0.02 | 0.30 | 0.00 | 0.77 | 0.03 |
| $R_{lw}$ [d] | 4.28 | 1.03 | 143.13 | 14.59 | 4.66 | 1.02 | 33.93 | 23.65 | 4.14 | 1.01 | 99.63 | 15.69 |
| $A_r$ [d] | 4.17 | 1.08 | 111.15 | 12.91 | 4.58 | 1.08 | 33.93 | 22.09 | 3.98 | 1.08 | 109.57 | 13.32 |
| $S_m$ [d] | 0.65 | 0.00 | 1.00 | 0.08 | 0.66 | 0.00 | 1.00 | 0.08 | 0.64 | 0.00 | 1.00 | 0.09 |
| $U_p$ [a] | 2.72 | 0.36 | 226.51 | 6.69 | 2.63 | 0.36 | 157.01 | 6.75 | 3.17 | 0.36 | 147.90 | 13.99 |
| $A_1$ [b] | 0.30 | 0.01 | 288.71 | 0.73 | 0.28 | 0.01 | 91.64 | 0.39 | 0.47 | 0.01 | 266.91 | 2.79 |
| $A_0$ [b] | 1.27 | 0.02 | 267.95 | 5.84 | 1.16 | 0.02 | 536.53 | 7.65 | 1.96 | 0.02 | 614.18 | 31.95 |
| $V_1$ [c] | 0.13 | 0.00 | 343.76 | 0.82 | 0.12 | 0.00 | 651.05 | 2.37 | 0.31 | 0.00 | 287.29 | 5.12 |

[a] unit in mm; [b] $mm^2$; [c] $mm^3$; [d] without unit; [e] ~ minimum; [f] ~ maximum; [g] ~ variance

***Pine sawdust***

**Figure 41** shows the 2D projections of selected pine sawdust particles recorded by the analyser. As it can be seen, the material is composed of un-evenly shaped particles. According to the Gil et al. (2014) the particles can be characterized as **rectangle, rectangle fibrous, hook and fibrous hook**. Owing to the anisotropy of biomass materials, biomass particles have **needle-like shape and large aspect ratio** (Guo et al. 2012). However, presence of fines and more prolonged particles could by caused by application of the hammer mill for grinding (Paulrud et al. 2002).

In the **Table 21**, descriptive statistics of pine sawdust particles are presented. In case of measured pine sawdust particles mean for all fractions $S_m$ was 0.61, so the particles can be described as moderately asymmetrical (Yang 2003). The measured particles can be classified (Powers 1953) as **subangular and subrounded** since the average $R_d$ is **0.35**; approx. 53% of the material belongs to the range of 0.25–0.35 (subangular) and 0.35–0.49 (subrounded). More or less 15% of particles can be called angular and ~14% very angular. Particles of pine sawdust are a bit more rounded than particles of hemp and miscanthus.

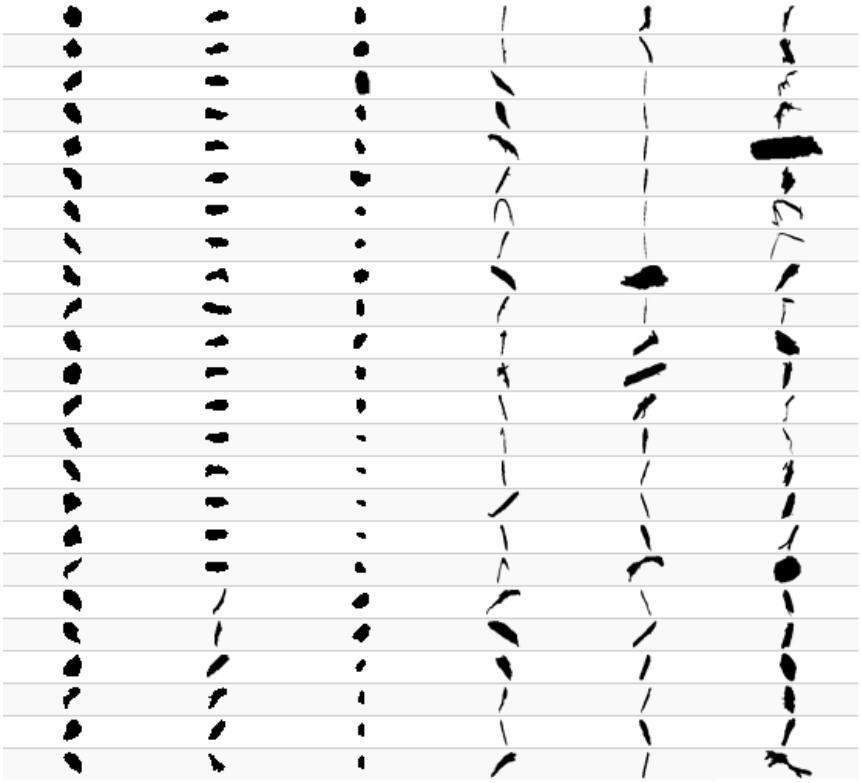

**Figure 41.** 2D projections of selected particles of pine sawdust

**Table 21.** Particle characterization of pine sawdust

| | Fraction 4 mm | | | | Fraction 8 mm | | | | Fraction 12 mm | | | |
|---|---|---|---|---|---|---|---|---|---|---|---|---|
| | Mean | Min [e] | Max [f] | Var [g] | Mean | Min | Max | Var | Mean | Min | Max | Var |
| $X_{min}$ [a] | 0.49 | 0.09 | 66.05 | 0.12 | 0.51 | 0.09 | 10.23 | 0.1 | 0.51 | 0.09 | 10.04 | 0.11 |
| $L$ [a] | 1.25 | 0.09 | 74.86 | 0.89 | 1.21 | 0.09 | 40.33 | 0.83 | 1.23 | 0.09 | 28.26 | 0.90 |
| $X_{max}$ [a] | 1.28 | 0.13 | 72.49 | 0.88 | 1.24 | 0.13 | 40.33 | 0.82 | 1.26 | 0.13 | 28.26 | 0.89 |
| $W_{max}$ [a] | 0.48 | 0.09 | 65.69 | 0.11 | 0.50 | 0.09 | 9.86 | 0.10 | 0.50 | 0.09 | 8.73 | 0.10 |
| $X_a$ [a] | 0.64 | 0.10 | 54.86 | 0.13 | 0.65 | 0.10 | 7.19 | 0.13 | 0.66 | 0.10 | 7.66 | 0.14 |
| $X$ [a] | 1.14 | 0.09 | 77.58 | 0.79 | 1.09 | 0.09 | 40.31 | 0.72 | 1.12 | 0.09 | 28.26 | 0.78 |
| $X_m$ [a] | 0.50 | 0.09 | 78.26 | 0.17 | 0.53 | 0.09 | 8.55 | 0.15 | 0.52 | 0.09 | 12.19 | 0.16 |
| $C_i$ [d] | 0.71 | 0.11 | 20.86 | 0.02 | 0.73 | 0.11 | 0.97 | 0.02 | 0.73 | 0.12 | 0.97 | 0.02 |
| $\Psi$ [d] | 0.69 | 0.10 | 14.27 | 0.01 | 0.70 | 0.23 | 0.87 | 0.01 | 0.70 | 0.24 | 0.87 | 0.01 |
| $R_d$ [d] | 0.33 | 0.00 | 0.89 | 0.03 | 0.35 | 0.01 | 0.81 | 0.02 | 0.35 | 0.01 | 0.81 | 0.02 |
| $R_{bv}$ [d] | 3.41 | 1.01 | 164.39 | 10.63 | 3.01 | 1.01 | 162.31 | 6.74 | 3.04 | 0.09 | 90.67 | 7.03 |
| $A_r$ [d] | 2.61 | 1.04 | 120.65 | 10.54 | 2.50 | 1.09 | 89.08 | 7.93 | 2.93 | 0.10 | 55.02 | 5.77 |
| $S_m$ [d] | 0.61 | 0.00 | 1.00 | 0.05 | 0.61 | 0.00 | 1.00 | 0.04 | 0.62 | 0.00 | 1.00 | 0.04 |
| $U_p$ [a] | 3.11 | 0.36 | 113.55 | 5.27 | 3.04 | 0.36 | 87.15 | 5.13 | 3.08 | 0.36 | 78.25 | 5.52 |
| $A_1$ [b] | 0.21 | 0.00 | 336.03 | 0.80 | 0.43 | 0.01 | 40.58 | 0.39 | 0.45 | 0.01 | 46.11 | 0.47 |
| $A_0$ [b] | 3.11 | 0.02 | 352.10 | 7.70 | 1.98 | 0.02 | 354.94 | 8.88 | 2.04 | 0.02 | 226.91 | 10.02 |
| $V$ | 0.21 | 0.00 | 167.12 | 1.08 | 0.22 | 0.00 | 326.15 | 145.87 | 0.24 | 0.00 | 127.04 | 0.93 |

[a] unit in mm; [b] mm$^2$; [c] mm$^3$; [d] without unit; [e] ~ minimum; [f] ~ maximum; [g] ~ variance

The particles of all three materials can be described as **irregular, slightly elongated with moderate degree of angularity, roughness and asymmetry**. The particles of miscanthus are more elongated than hemp and pine sawdust. The hemp is the most symmetrical from all the materials, however, its value is still described as moderately symmetrical. The real size of all particles was much smaller than grinding size (fraction) and the fine particles were predominated, which is normal in the grinds produced by the hammer mill (Kirsten et al. 2016).

## 5.6. Briquettes properties

**Weight and dimension** of briquettes used in this study are presented in **Table 22** on the next page. It is evident, that the briquettes made of miscanthus had the largest *L* and *D*. On the contrary, the briquettes from hemp had the smallest dimensions. The briquettes with fraction size 4 mm had generally lower *D* than fraction 8 and 12 mm for all materials. All briquettes had slightly larger *D* than diameter defined by the pressing matrix hole of the briquetting machine (matrix diameter 65 mm), which indicated that briquettes slightly expanded after release from the matrix. This is owing to elastic nature of biomass which cause that deformation and densification are not permanent and elastic spring-back occurs after the pressure release (Pietsch 2002). This phenomenon was observed also by Brožek et al. (2012) and Qin et al. (2018).

The *D* of briquettes made of hemp was the closest to the matrix diameter. On the contrary, miscanthus briquettes had the most distant *D* value from the matrix diameter. From the measured values it is possible to find down the **dependence between the briquettes *D* and their ϱ ( $D = -0.015 \times \rho + 80.2$ ; $R^2 = 0.81$)**, that can be seen in the **Figure 42**. This dependency includes all materials and their fractions. With the same type of briquetting machine, similar results were obtained by Brožek et al. (2012) with the briquettes made of birch chips, poplar chips, pine bark, spine sawdust and spruce shavings and they calculated even closer dependence between the briquettes $\varrho$ and their *D* ($D = -0.013 \times \varrho + 77.68$; $R^2 = 0.95$). From this dependence, it is evident that briquettes with higher density raise their *D* less than the briquettes with lower density. The briquettes diameter magnification compared with the matrix diameter is in the range from 3.2 to 5.6% (Brožek et al. 2012). This dependence could be assumed also in our case within visual assessment and manipulation, since the miscanthus briquettes having the largest *D* evinced characteristics of the lowest density and *DU*. However, the briquetting press works in this manner; with each piston stroke the different material amount gets into the pressing chamber. Then the briquette weight and length are dependent on the material amount which gets into the pressing chamber with each piston stroke (Brožek et al. 2012).

**Table 22.** Weight and dimensions of studied briquettes

| | | Miscanthus | | | Hemp | | | Pine sawdust | | |
|---|---|---|---|---|---|---|---|---|---|---|
| Fraction | **No. of briquette** | **Weight** (g) | ***D*** (mm) | ***L*** (mm) | **Weight** (g) | ***D*** (mm) | ***L*** (mm) | **Weight** (g) | ***D*** (mm) | ***L*** (mm) |
| | 1 | 112.35 | 67.35 | 38.34 | 109.35 | 66.42 | 34.12 | 124.75 | 67.45 | 40.97 |
| | 2 | 111.01 | 67.12 | 37.84 | 108.79 | 66.07 | 34.89 | 111.49 | 66.93 | 37.25 |
| 4 mm | 3 | 110.36 | 66.97 | 36.69 | 110.69 | 66.78 | 35.23 | 109.33 | 67.36 | 36.41 |
| | 4 | 113.73 | 67.19 | 37.16 | 112.37 | 67.13 | 37.95 | 103.28 | 67.14 | 34.46 |
| | 5 | 114.99 | 67.71 | 37.98 | 111.53 | 67.03 | 36.13 | 106.44 | 66.87 | 35.59 |
| | **Mean** | **112.49±1.91** [a] | **67.27±0.28** | **37.60±0.67** | **110.55±1.49** | **66.69±0.44** | **35.66±1.47** | **111.06±8.25** | **67.15±0.26** | **36.94±2.48** |
| | 1 | 110.56 | 67.84 | 38.63 | 110.71 | 66.89 | 35.75 | 116.88 | 67.03 | 39.88 |
| | 2 | 117.86 | 68.07 | 40.09 | 116.36 | 67.10 | 39.36 | 121.99 | 66.76 | 41.62 |
| 8 mm | 3 | 114.63 | 67.73 | 39.56 | 112.02 | 67.43 | 36.03 | 118.22 | 66.94 | 39.44 |
| | 4 | 118.34 | 68.16 | 37.12 | 110.41 | 66.72 | 35.63 | 105.77 | 66.90 | 34.85 |
| | 5 | 119.03 | 68.30 | 38.58 | 112.22 | 67.35 | 36.30 | 116.48 | 67.00 | 39.33 |
| | **Mean** | **116.08±3.52** | **68.02±0.23** | **38.80±1.13** | **112.34±2.38** | **67.10±0.30** | **36.61±1.56** | **115.87±6.05** | **66.93±0.11** | **39.02±2.51** |
| | 1 | 118.86 | 68.26 | 38.45 | 113.65 | 67.96 | 37.45 | 135.70 | 67.60 | 45.03 |
| | 2 | 127.15 | 69.14 | 39.14 | 115.36 | 67.24 | 38.95 | 125.27 | 67.69 | 42.88 |
| 12 mm | 3 | 116.87 | 67.76 | 40.21 | 117.12 | 67.81 | 39.47 | 133.56 | 68.28 | 46.18 |
| | 4 | 117.62 | 68.38 | 39.57 | 117.93 | 67.99 | 39.14 | 134.30 | 67.39 | 45.69 |
| | 5 | 118.33 | 68.46 | 42.96 | 118.34 | 68.12 | 39.51 | 107.24 | 67.31 | 34.93 |
| | **Mean** | **119.77±4.20** | **68.40±0.50** | **40.07±1.74** | **116.48±1.95** | **67.82±0.34** | **38.90±0.85** | **127.21±** | **67.65±0.35** | **42.94±4.65** |

[a] ± standard deviation values

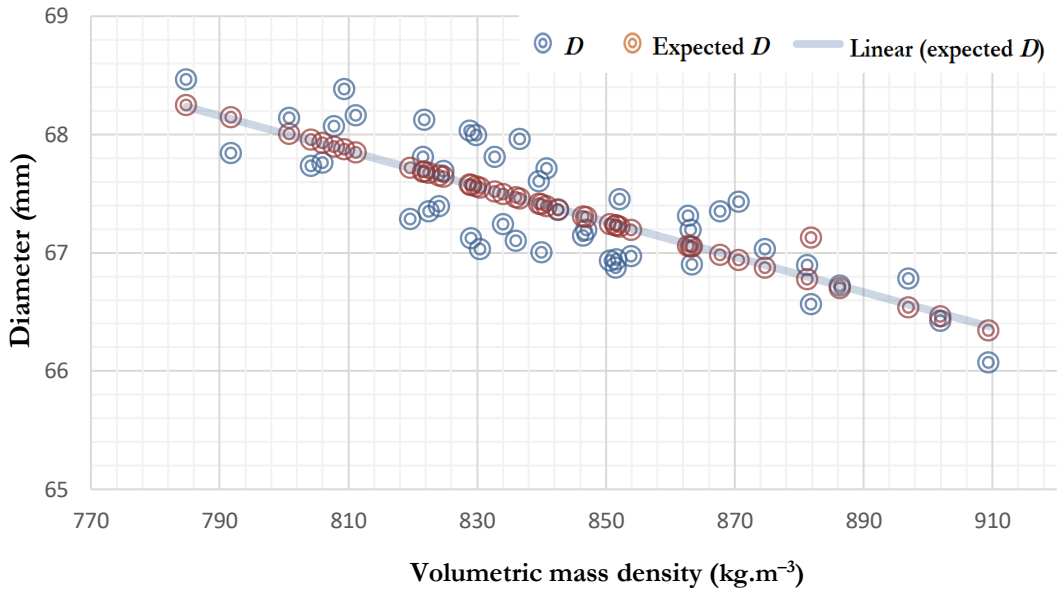


**Figure 42.** Dependence of briquette diameter on its volumetric mass density (all materials and fractions)

## 5.7. Evaluation of briquettes structure

The briquettes structure was evaluated based on the qualitative as well as quantitative assessment. Firstly, the qualitative evaluation was done through visualization of the briquette surface at different locations via microscopy and image analysis software. Secondly, quantitative part was performed based on the particle size measurement at these surface locations together with subsequent statistical analyses, and thus obtained data provided deductions about the concentration of the larger particles on the briquette surface.

### 5.7.1. Characterization of briquette surface structure

The output of the **complex compaction process** is presented in the **Figure 43**, where the images of scanned locations/points (see **Figure 22**, Subchapter 4.2.12.) of the miscanthus' cross-sectional surface are depicted. Process of the structure alteration of the input material was dependent and inseparable associated with the process of applied pressing agglomeration, i.e. pressing of the loose particles of hemp, miscanthus and pine sawdust in the pressing chamber of the briquetting machine BrikStar CS 50 during which external forces and high temperature acted on the mass of particles. The process of material compaction was accompanied by a change in the state of the original material, as it is evident from the comparisons of the **Figure 44**, where the grind fractions of miscanthus before briquetting can be seen (the images are taken with the same magnification 6.5× as all images of briquette structure) and mentioned **Figure 43** with the densified compacts' surface structures.

| | Front side of the briquette | | Rear side of the briquette |
|---|---|---|---|
| **A** |  | **F** |  |
| **B** |  | **G** |  |
| **C** |  | **H** |  |
| **D** |  | **I** |  |
| **E** |  | **J** |  |

**Figure 43.** Images of studied locations of cross-sectional surface of miscanthus briquette (8 mm)

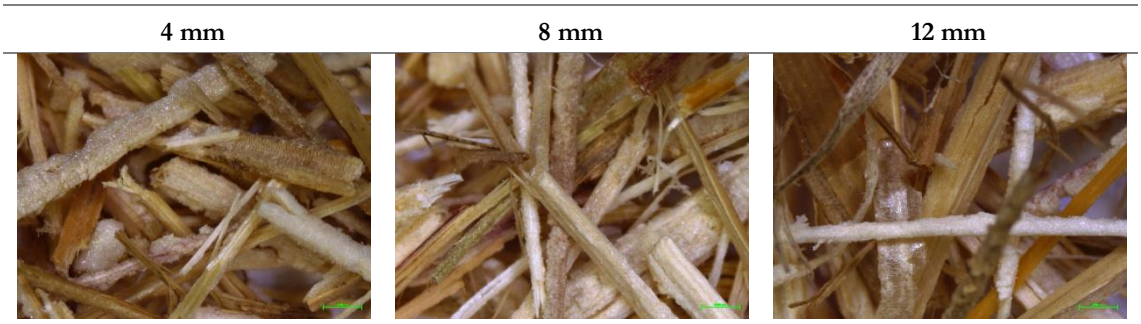


**Figure 44.** Miscanthus particles before densification (magnification 6.5×)

In the first stage, discrete particles did not have a definite and uniform formation, they gradually rearranged due to the application of lower pressures in the beginning to disrupt the unstable packing particle arrangement. Then, elastic and plastic deformation of particles occurred while the pressure increased, when the particles passed through the pre-chamber and the matrix. It resulted in particles' flow into empty spaces, air removal and increased contact and interaction among particles. The particles of the original input materials, mainly fibres of hemp, flat-shaped of pine sawdust and elongated of miscanthus as well as other irregularly shaped particles, were weaved, twisted, and bended about each other and deformed during compaction which led to **mechanical interlocking bonds** between these particles. This process was clearly observed in the images of inner surface obtained from previous study (Chaloupková 2015). Kaliyan and Morey (2010) studied mechanical interlocking of corn stover and switchgrass particles through light microscopy with comparable outputs. On the other hand, Okot et al (2018) observed no evidence of interlocking bonds between particles of corn cobs briquettes by SEM; the main merit attributed to formation of solid bridges.

Besides interlocking mechanisms, in our case, where no binding agents for increase in the briquette strength were applied, binding and adhesion of particular particles in the briquette pressing chamber occurred also due to **secretion and activation of natural binders** (Kaliyan & Morey 2010). During the briquetting process the temperature increases due to the friction caused by the movement of the material pressed through the matrix (Havrland et al. 2011). And when the temperature reaches the specific level which, is called the **glass transition temperature** (*Tg*), these natural binders can be squeezed out of particles (Alaru et al. 2011). *Tg* is the temperature range where a thermosetting polymer changes from a stiffness, rigid or "glassy" state to a more flexible state. Lignin is the only component of biomass that shows glass transition behaviour (Reza et al. 2012), *Tg* is generally in the range of 100−170 °C (Gravitis et al. 2010). The *MC* of a feedstock can significantly influence the glass transition temperature of lignin (Stelte et al. 2011a). For the pressing compaction of a biomass at the *Tg*, a feedstock exhibits inter-diffusion or creation of a solid bridge between the particles. Irvine (1985) observed

for eucalypt and pine sawdust *Tg* of lignin in the temperature range 60–90 °C. However, the low densification temperature (60 °C) used in this study could have decreased the creation of a solid bridge between the particles. As the study of Muntean et al. (2017)[1] showed, the same type of briquetting machine (BrikStar CS 50) reached **temperature**s during densification of miscanthus, hemp and apple wood values from **30 to 59 °C**. The lowest temperatures reached the hemp 51.0, 46.6, 44.1 °C for 4, 8 and 12 mm fraction size and the maximum temperatures for apple wood of 4, 8 and 12 mm 59.0, 57.7 and 54.7 °C, respectively. The higher temperature for wooden material can be explained by its higher content of lignin; higher degree of lignification as compared to herbaceous biomass causes more friction in the press channels (Kirsten et al. 2016).

After densification process, when pressure and temperature were ceased and the briquettes cooled down, the natural binders hardened and formed **solid bonds or bridges** among particles. This mechanism causes high density and strength of the produced briquettes without binding agents' addition (Muntean et al. 2012; Ivanova 2012). As it was mentioned in the Literature review (Subchapter 2.4.3.) the biomass materials contain, in various amounts, natural binders, such as water-soluble carbohydrates, lignin, cellulose, protein, starch and fats (Back 1987; Kaliyan 2008; Chou et al. 2009; Kaliyan & Morey 2010). These secreted natural binders behave as the transparent natural resin coats on the compacted particles and lignin is the only component of biomass that shows glass transition behaviour (Reza et al. 2012). The **glassy coating of lignin** on the compacted particles of pine sawdust is highlighted in the **Figure 45**. In case of studied material, pine sawdust contains high amount of lignin and bonding at lignin and cellulose surface areas was most probably accountable for the major kind of bonding mechanism in the press-drying process (Back 1987).

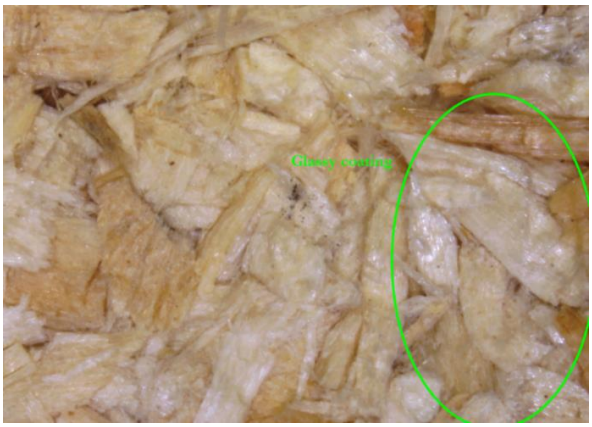


**Figure 45.** Glassy coating on the particles (pine sawdust 4 mm)

[1] A. Muntean is the member of the same research team (Biofuels research group of FTA, CULS) as the Author and his study materials *Miscanthus* × *gig.* and hemp are the same materials as the study materials of the Thesis (the same plantation, harvest year, grinding and briquetting), thus the Author plentifully has drown the data for the discussion

This process of particle agglomeration was reported by Kaliyan and Morey (2010) as well, on example of corn stover and switchgrass briquettes. By using fluorescence microscopy, they found that solid bridges were formed mainly by lignin and protein. Muntean et al. (2012) in their paper also detected lignin secretion as glassy coating on the particle surface by image analysis in case of briquettes made of mixtures of grapevine, straw and corn stalks.

**Figure 47** (on the next page) shows the distribution of secreted natural binders and especially lignin (as previous studies' findings indicates) on miscanthus briquettes' surface via thresholding function, which counterpointed in red colour areas of glassy coating. **Figure 46** below shows the lignin distribution contrasted by RGB image models.

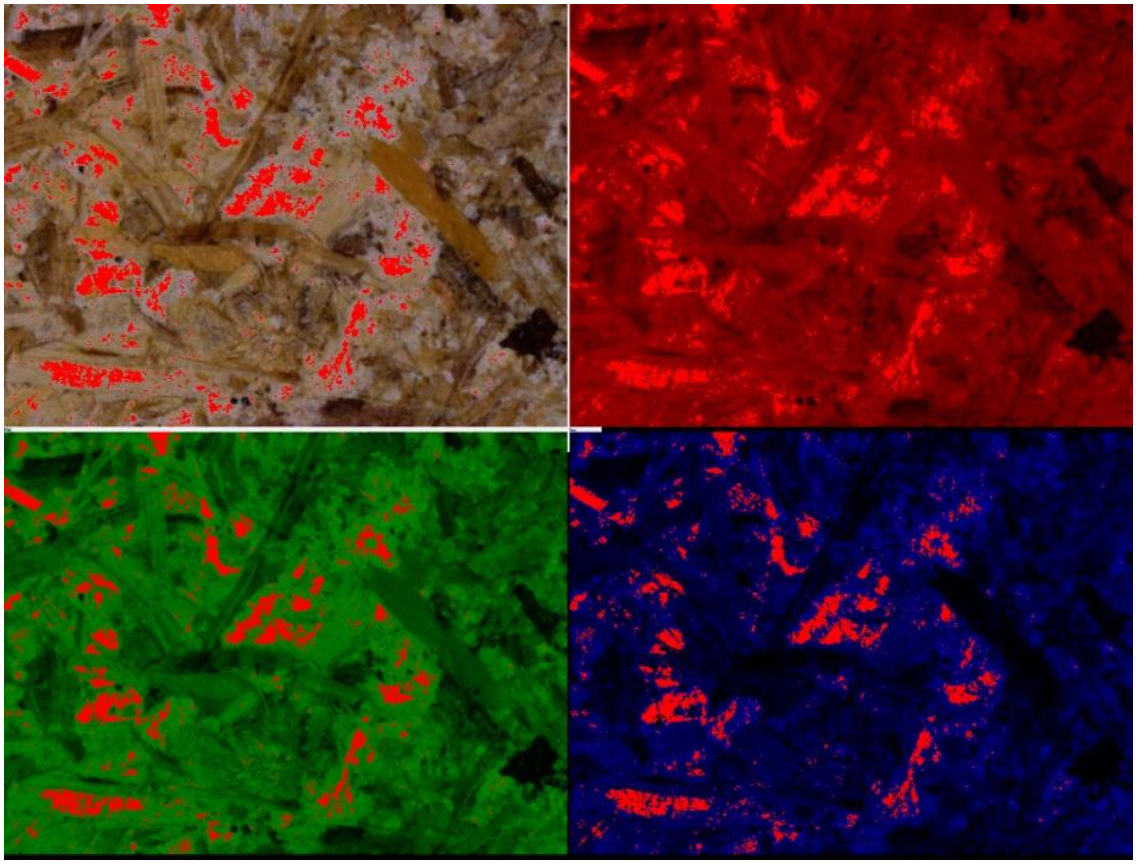

**Figure 46.** Surface structure of miscanthus briquette (8 mm), point J and its RGB models

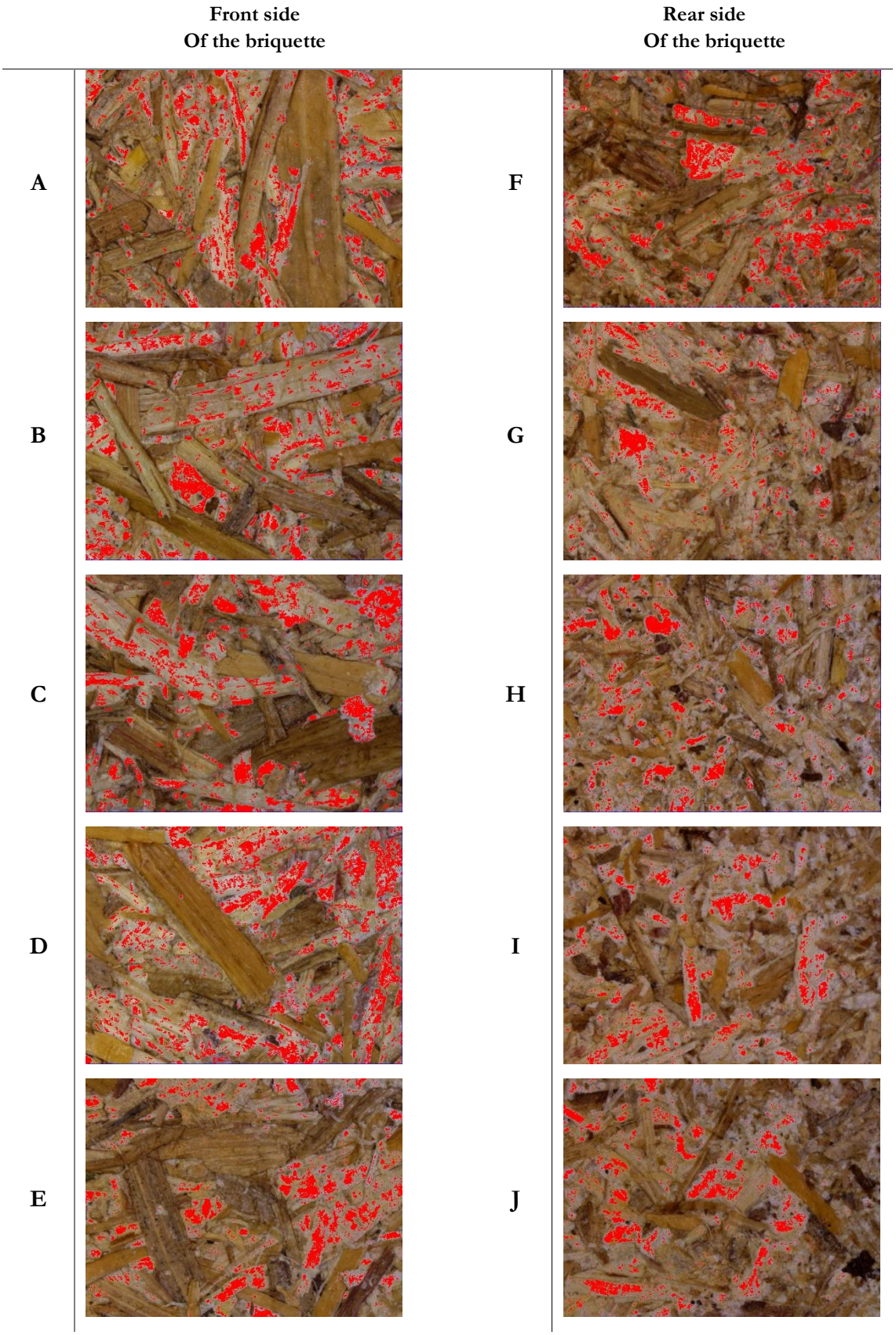


**Figure 47.** Scanned locations of miscanthus briquette (8 mm) with thresholding function highlighting the glassy coat of lignin

As it can be seen (**Figure 47**), the higher excretion of lignin exhibited the pith particles (lighter colour). In case of hemp the excretion pattern was similar, the distribution of the binders was concentrated mainly on non-fibre part of stem and leaf tissues – mainly pith, whereas the bast fibres exhibit no secretion. It can be explained by the composition of bast fibres, since they contain less lignin than pith, approx. 5–9% of total fibre (Capelle 1996; Gutiérrez et al. 2006). The **Figure 48** shows **quantified excretion of lignin** detected by thresholding function, which is expressed as the total are of the glassy coating identified by the thresholding function.

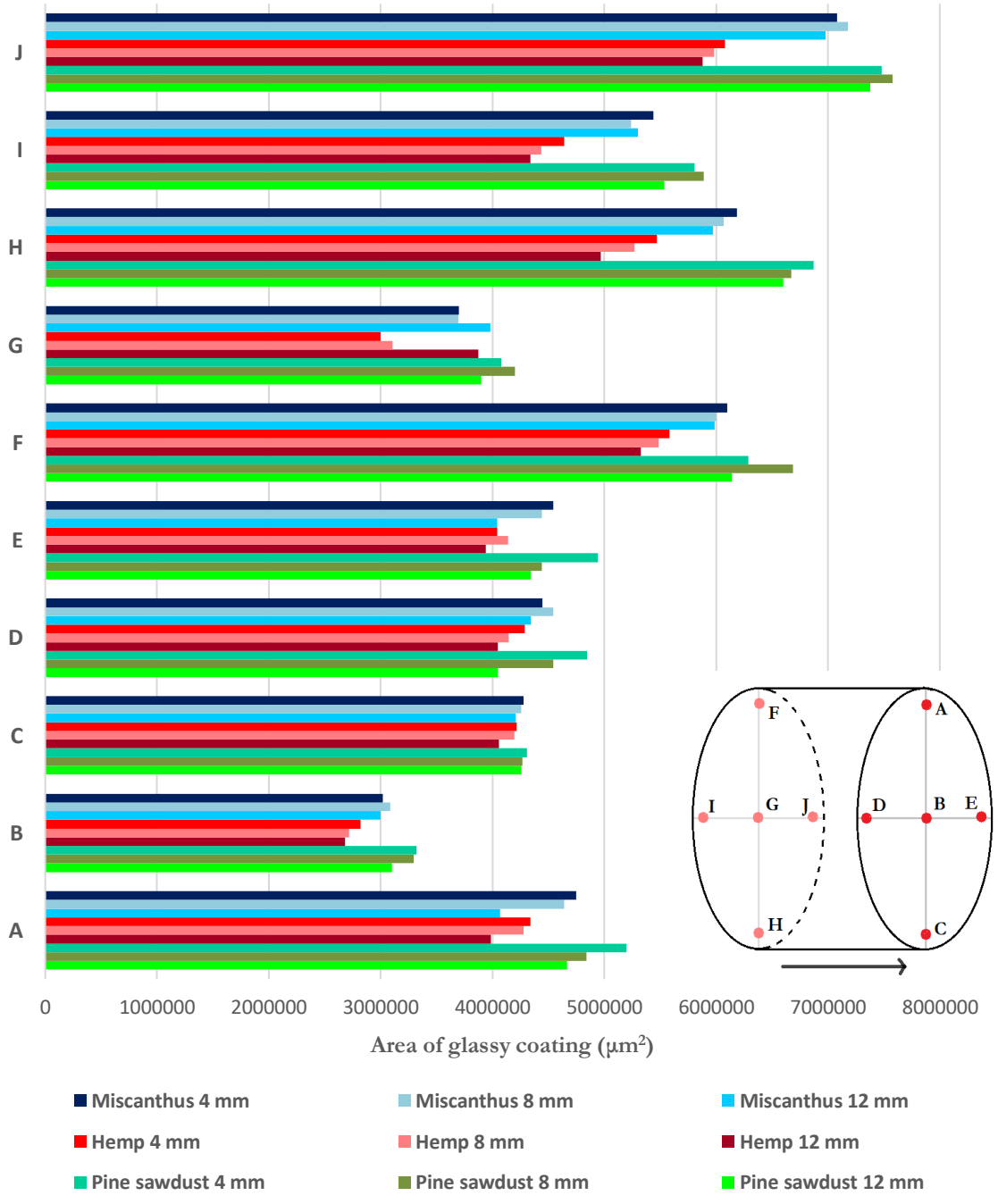


**Figure 48.** Total area of glassy coating on the particles detected by the thresholding function

It can be concluded that in scanned location the **pine sawdust** demonstrated higher amount of lignin excreted compare to miscanthus and hemp. It was confirmed the statement of Kers et al. (2010) that „*the more lignin the material contains the more of it can be released to produce briquettes wit*h higher quality".

Since the smaller particles possess of higher surface area (Sun & Cheng 2002) and during the briquetting of smaller fractions the higher temperatures were reached, it is not surprising that **fraction 4 mm in general exhibited higher excretion of lignin**. Also, it is evident, that the points F, H, I, J from the rear side of the briquette showed higher amount of glassy coating. The points from the middle of the briquette cross-section contained less glassy coating. It could be explained by the increased temperature at the lateral surface of the briquette due to the friction caused by the movement of the material pressed through the matrix (Havrland et al. 2011). The rear side of the briquette is in the contact with the piston, which pushes the material all through the matrix, thus this side of the briquette is exposed to the higher pressure and temperature that results in higher lignin softening.

More precise results could be obtained using UV-fluorescence microscopy to detect natural binders, which generate blue fluorescence for lignin and yellow-green for protein compounds (Rost 1995; Kaliyan & Morey 2010). This method requires higher magnifications than the ones was used in this Thesis, however it do not allow the study of surface areas.

### 5.7.2. Evaluation of particle size on the briquette surface structure

Results of particle size measurements (areas and max feret) on briquette surface structure and related statistical testing, Kruskal-Wallis H test ~ non-parametric variant of ANOVA, are presented below. The squared points in the graphs represent the median values.

First of all, the particle size was compared between materials and fractions. As it can be seen in the **Figure 49–50** from the p-values **(p>0.01)**, there are **statistically significant differences in particles sizes among materials**. From the chart (**Figure 49 and 50**) it is obvious that the hemp material has the largest size, both area and max feret. In case of miscanthus and pine sawdust the situation is different; miscanthus has lower area and higher max feret than pine sawdust. It is due to the fact, that miscanthus has longer and thinner particles than pine sawdust.

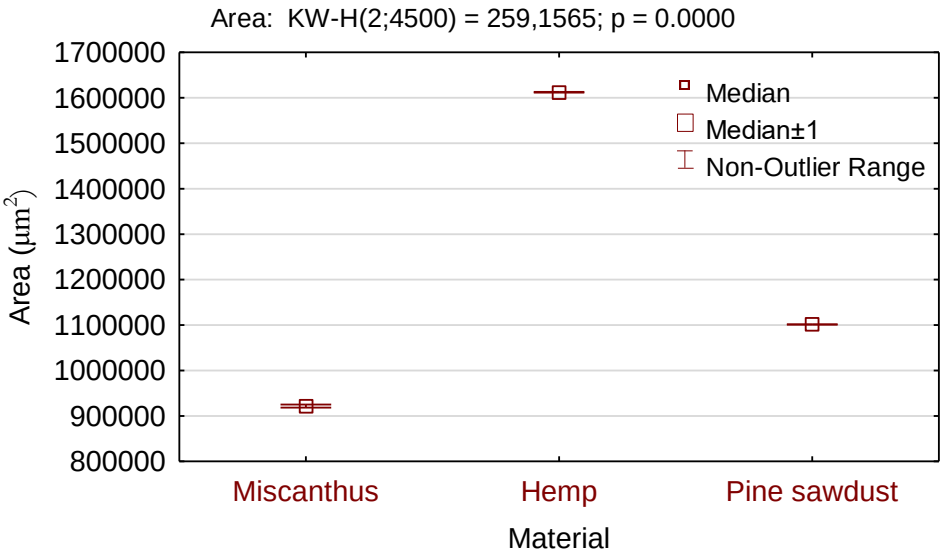


**Figure 49.** Plot of particle size (area) grouped by the material

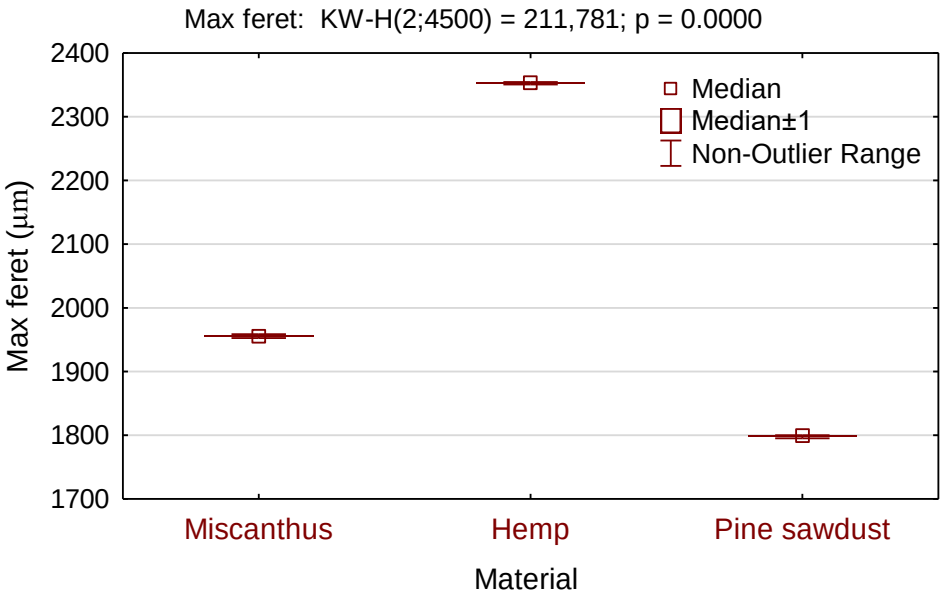


**Figure 50.** Plot of particle size (max feret) grouped by the material

In the **Figures 51** and **52** the particles sizes are grouped by the fraction variable. It is not surprising that there are statistically significant differences among fractions and that with the increasing fraction size the size of the particles increases and that the biggest difference in particles size is between fraction 4 mm and 12 mm. On the other hand, the difference between fraction 8 mm and 12 mm is smaller than between fractions 4 mm and 8 mm.

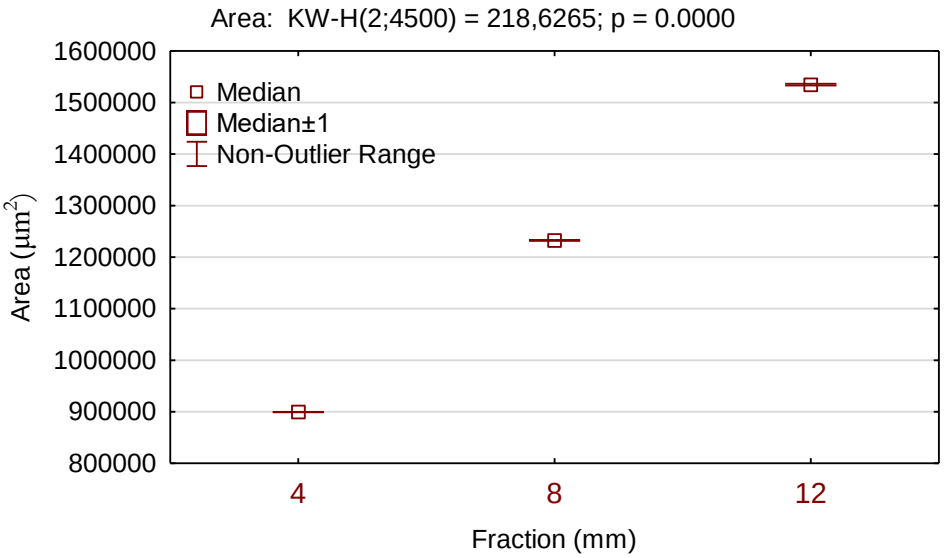


**Figure 51.** Plot of particle size (area) grouped by the fraction

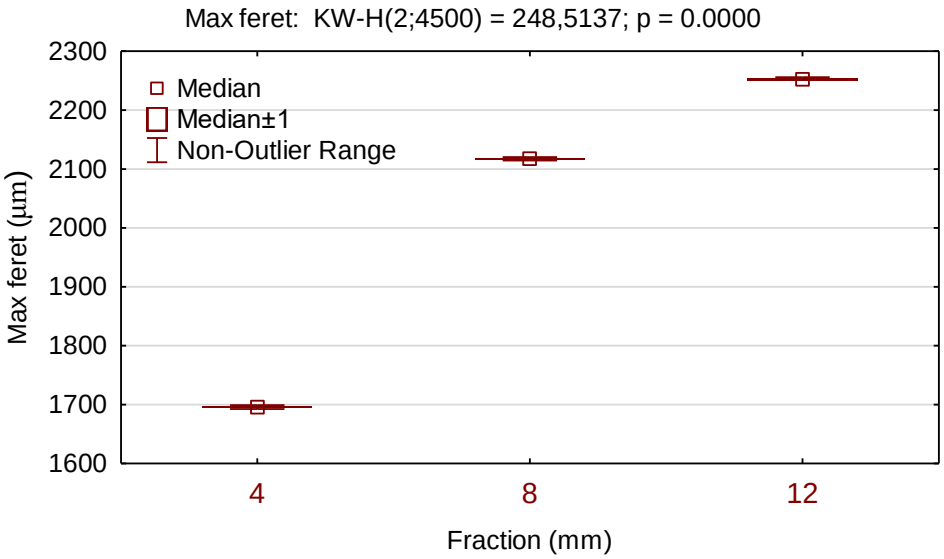


**Figure 52.** Plot of particle size (max feret) grouped by the fraction

Than the particle size was compared among different points (locations) A–J, what had been the main purpose of the particle size measurements. In the **Figures 53–56** results of Kruskal-Wallis tests for area and max feret grouped by material and fraction are graphically presented. Based on the achieved significance level of the Kruskal-Wallis test ($p < 0.01$), it was demonstrated a statistically significant difference (with more than 99% confidence) in particles areas and max feret among specified points within materials and fractions[2].

[2] Based on the fact that the p-value is lower than set significance level (0.05), we rejected the null hypothesis that the area (or max feret) data are equal in terms of medians, and thus alternative hypothesis, that at least two of the medians are different, was accepted.

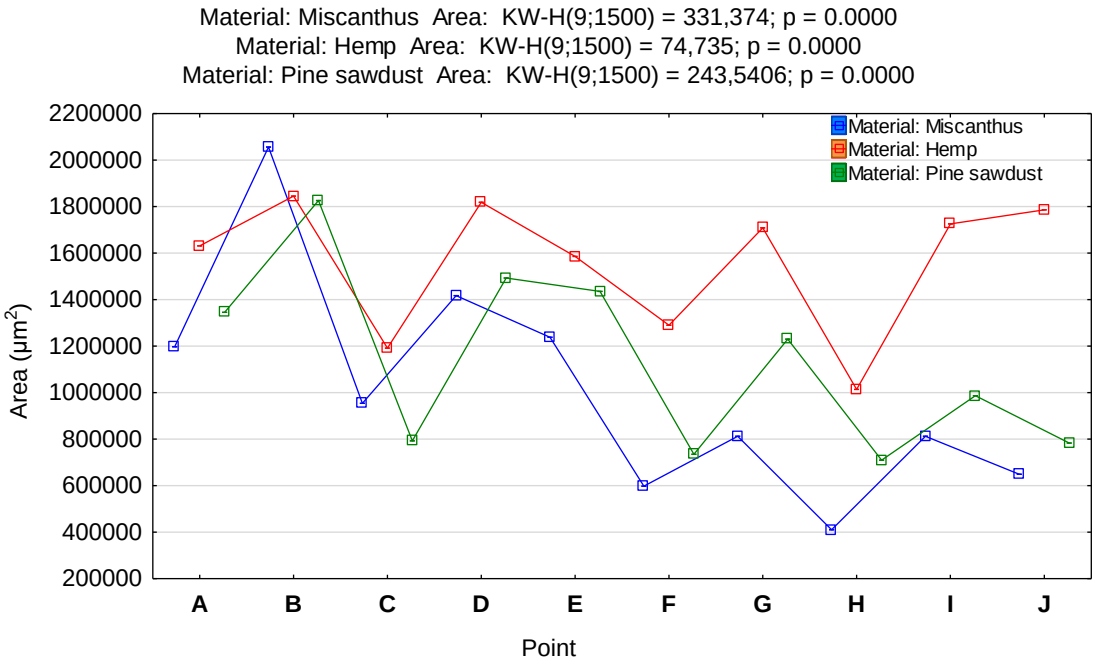


**Figure 53.** Particle size (area) at specified points (locations on the briquette surface) grouped by material

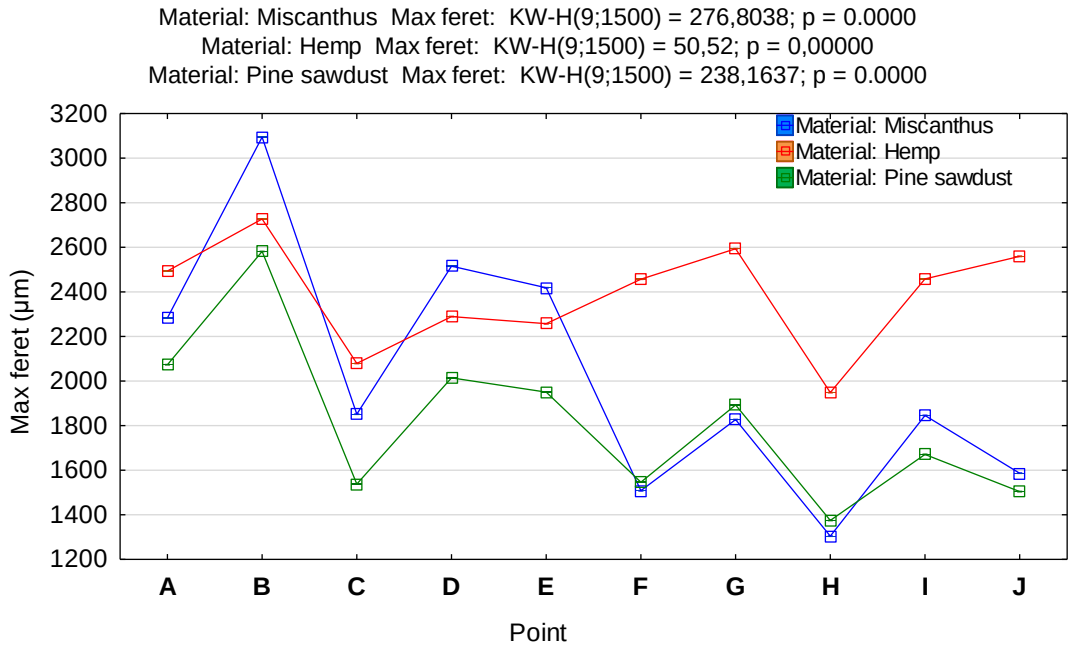


**Figure 54.** Particle size (max feret) at specified points (locations on the briquette surface) grouped by material

From the sum of the ranks for the particular groups it was evident that the particles of **miscanthus** with the largest **area** are concentrated at the point **B** followed by points **D, E, A, C, G, I, J, F** and **H**, and, with the largest max feret at the point B, D, E, A, C, G, I, J, F and H. In case of the pine sawdust the trend was similar, as it is also presented in the **Table 23**, where the locations of the larger particles on the briquette surface are demonstrated. The points located on the front side of the briquette are highlighted in red colour. Which indicates the conclusion, that generally **larger particles were located on the front side**, contrarily **the smaller ones were found on the rear side of the briquettes**.

**Table 23.** Location of the larger particles on the briquette surface ordered from the largest ones

| | | The largest | | | | | | | | | The smallest |
|---|---|---|---|---|---|---|---|---|---|---|---|
| **Miscanthus** | *Area* | **B** | **D** | **E** | **A** | G | I | **C** | J | F | H |
| | *Max feret* | **B** | **A** | **D** | **E** | G | I | F | **C** | J | H |
| **Hemp** | *Area* | **B** | **D** | J | I | G | **A** | **E** | F | **C** | H |
| | *Max feret* | **B** | G | J | **A** | I | F | **D** | **E** | **C** | H |
| **Pine sawdust** | *Area* | **B** | **D** | **E** | **A** | G | I | **C** | J | F | H |
| | *Max feret* | **B** | **A** | **D** | **E** | G | I | F | **C** | J | H |

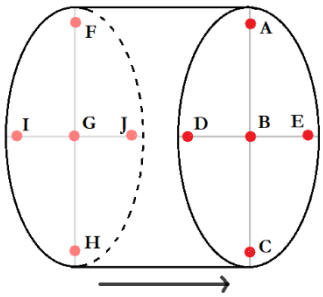


For **hemp** material, the **trend differs**, we can see that the particles with the largest area are located at the point B, followed by D, J, I, G, A, E, F and H and with largest max feret at B as well, but followed by G, J, A, I, F, D, E, C and H. The smallest particles the same as for other studied materials are also concentrated in the bottom of the briquettes. However, the rule that the largest particles are concentrated on the front side as in case of other materials is not true for hemp. **Large particles are distributed more evenly** than in case of other materials, probably due to the presence of fibres and this could influence the lower abrasion of hemp briquettes.

What is common for all materials, that **the biggest particles are located in the middle of front side of the briquette, while the smallest particles on the bottom of rear side**. If we consider the grouping according to the **fraction** instead of material, the situation is similar for all fractions as it can be seen in the **Figures 55 and 56**.

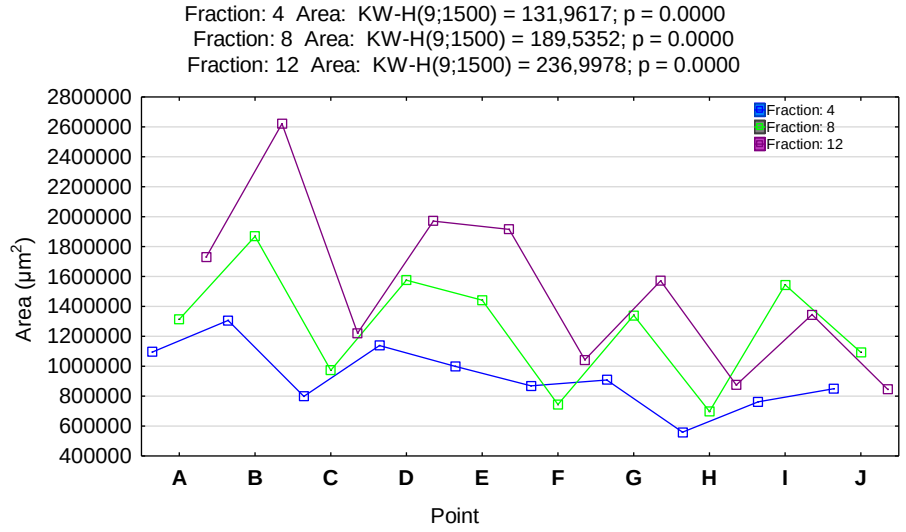


**Figure 55.** Particle size (area) at specified points (locations on the briquette surface) grouped by fraction

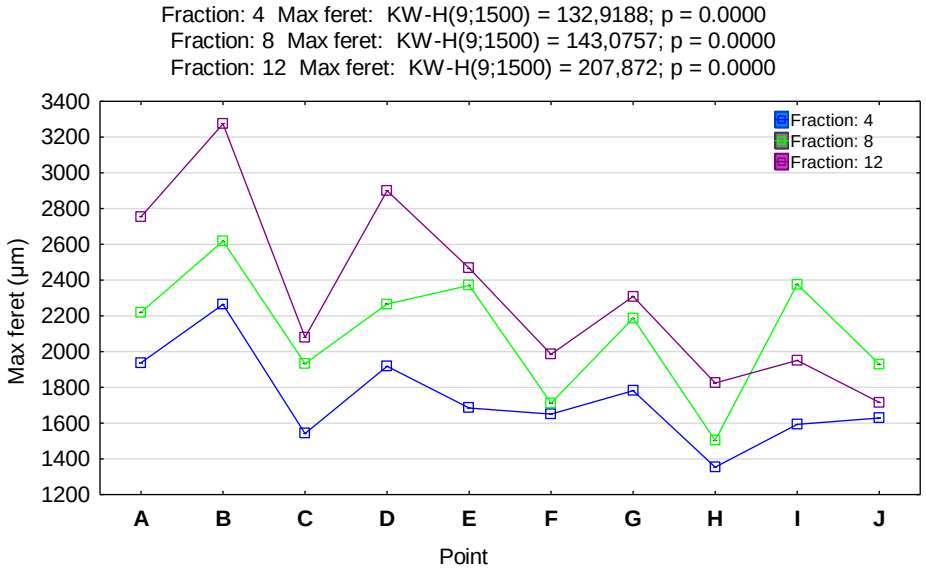


**Figure 56.** Particle size (max feret) at specified points (locations on the briquette surface) grouped by fraction

Based on multiple comparisons and set significance level of 0.05, it was proved, that there is significant difference in areas and max feret mainly between points B and H, which was obvious from the above-mentioned testing (**Figures 53−56**). Further, there is significant difference primarily between B and F, B and D points. It is also evident that there are significant differences in areas between points on the front and their opposite on the rear side of briquettes, i.e. between the point A and its opposite on the other briquette side point F. The same observation is applied for the points B and G, C and H.

As it follows from the results of the analysis, we can conclude that **PSD on the briquette cross-section surface is not uniform**; there are differences between the particle sizes in terms

of length and area on the briquette surface. Chaloupková et al. (2018a) obtained before similar results for the same studied materials grinded into fraction size 12 mm.

In case of **miscanthus and pine sawdust** the pattern is very similar, **generally, the largest particles are on the front side, while the particles with smaller dimension are on the rear side**. In case of **hemp**, the PSD was more uniform, and it can be concluded that **larger particles are located on the front side as well as on the rear side** of the briquettes.

The **non-uniform PSD on the briquette surface leads to the increased abrasion** as the results of *DU* testing showed (Subchapter 5.8.2.). Mixing of the material during the densification could decrease this non-uniformity in the distribution of larger and smaller particles, which could lead to an increase in the quantity of contact points for inter-bonding among particles, and thus, to higher mechanical strength and lower abrasion of the final products during handling and transportation (Wang et al. 2018a). Besides lower abrasion, mixing different sized grinded materials together can lead to lower energy consumption compared to one-sized grinded feedstocks. Generally, the mixing of differently sized materials may potentially leads to lower energy consumption, higher product compressive strength, and higher product density (Wang et al. 2018a).

In most of the studies published so far the image-based analysis has been used for identifying particle size and its distribution from loose aggregate samples (Mora & Kwan 2000; Wang 2006; Womac et al. 2007; Igathinathane et al. 2009a; Igathinathane et al. 2009b; Souza & Menegalli 2011; Kumara et al. 2012; Gil et al. 2014; Pothula et al. 2014; Pons & Dodds 2015; Febbi et al. 2015) before they are densified, in place of direct measurements from the compact's cross-sections image (Ozen & Guler 2014), thus, to compare this part of the Thesis results with other references was not possible.

## 5.8. Evaluation of briquette mechanical quality

The important quality factor of briquettes are their mechanical properties that influence their storage time and handling during which collisions and abrasion of the material occur (Brožek et al. 2012). The most important mechanical parameters are density, mechanical durability and compressive strength. These parameters depend on the used material and its structure and fraction size, *MC* and compaction pressure (Plíštil et al. 2005). Applied compaction pressure was the same for all study materials and their *MC* values were similar, thus factor of material type, structure and particle size is highlighted and discussed together with the results.

### 5.8.1. Volumetric mass density

Volumetric mass density **ϱ** expresses the efficiency of densification process and suitability of feedstock material for briquette production and briquette burning ability (Brunerová 2018). It is influenced by several factors like applied densification technology and applied pressure (Ndiema et al. 2002; Havrland et al. 2011), type of the material (Muazu & Stegemann 2015) and fraction size (Plíštil et al. 2005). In this study, the hydraulic piston press operating with the pressure of 18 MPa and temperature up to 60 °C was applied. The results of density ϱ of studied materials and their fractions are presented in the following **Table 24.**

As it can be seen, the highest ϱ had **hemp briquettes**. They were followed by pine sawdust briquettes and the lowest ϱ value exhibited the miscanthus briquettes.

**Table 24.** Volumetric mass density of studied briquettes

| Fraction | No. of briquette | Miscanthus (kg.m$^{-3}$) | Hemp (kg.m$^{-3}$) | Pine sawdust (kg.m$^{-3}$) |
|---|---|---|---|---|
| | 1 | 822.54 | 901.96 | 852.16 |
| | 2 | 829.12 | 909.47 | 850.70 |
| **4 mm** | 3 | 853.91 | 897.04 | 842.61 |
| | 4 | 863.18 | 881.89 | 846.54 |
| | 5 | 840.83 | 874.77 | 851.58 |
| | **Mean±StD** | **841.92±16.85** | **893.03±14.35** | **848.72±4.06** |
| | 1 | 791.79 | 881.25 | 830.53 |
| | 2 | 807.85 | 836.01 | 847.00 |
| **8 mm** | 3 | 804.24 | 870.63 | 851.71 |
| | 4 | 811.22 | 886.32 | 863.41 |
| | 5 | 832.73 | 867.76 | 840.02 |
| | **Mean±StD** | **809.57±14.89** | **868.39±19.63** | **846.53±12.35** |
| | 1 | 828.89 | 836.60 | 839.64 |
| | 2 | 800.88 | 834.07 | 824.77 |
| **12 mm** | 3 | 806.00 | 821.65 | 819.60 |
| | 4 | 809.41 | 829.90 | 824.09 |
| | 5 | 784.82 | 821.84 | 862.80 |
| | **Mean±StD** | **806.00±15.89** | **828.81±6.88** | **834.18±17.69** |
| **Total** | **Mean±StD** | **819.17±22.28** | **863.41±30.53** | **843.14±13.48** |

Further, it can be observed that **ϱ increases with decreasing fraction size** (see **Table 24**); fraction 4 mm has higher density than fractions 8 and 12 mm. It corresponds with the study of Oladeji and Enweremadu (2012), Mitchual et al. (2013) and Huko et al. (2015). The last mentioned reported the significant dependence of briquette ϱ on their particle size ($R^2 = 0.95$). On the contrary, Helwani et al. (2018) reported the highest ϱ for the briquettes from palm empty

fruit bunches for fraction 8 mm, in comparison with fractions 6 mm and 10 mm. In our study, the differences between fractions are the most noticeable in case of hemp briquettes. In case of pine sawdust, the difference between 4 mm and 8 mm fraction was minimal. In contrast, miscanthus showed similar ϱ values for fractions 8 mm and 12 mm.

According to Oladeji and Enweremadu (2012) and Okot et al. (2018) besides increasing particle size, also **increasing *MC* decreases briquette ϱ** and mechanical strength as well. In this case, the miscanthus had the slightly higher *MC* then other materials and its ϱ is the lowest, pine sawdust fraction 4 mm has a bit higher *MC* than fraction 8 mm and its ϱ was lower. Thus, maybe also the factor of *MC* had the impact on the final ϱ. The briquette ϱ increases with increasing compression force *F* and holding time of the briquette in the pressing chamber (Kaliyan & Morey 2009; Havrland et al. 2011; Tumuluru et al. 2015). Li and Liu (2000) investigated that 10-seconds holding time could result in a 5% increase in briquette density. However, in this case, all briquettes were made under the same operating conditions. A higher level of ϱ provides longer briquette burning and higher amount of produced heat which is greatly demanded (Obernberger & Thek 2004; Križan 2007; Kers et al. 2010). In case of miscanthus, the smallest fraction size 4 mm with the highest ϱ had the lowest value of *DU*. Thus, from all above-mentioned it is visible that the factor of particle size in interaction with other variables has different effects for various material.

On the other hand, increasing ϱ causes the increase of **consumed deformation energy** $E_d$, which means increase of financial expenses (Havrland et at. 2011; Brunerová et al. 2017b). Brunerová et al. (2017b) reported that miscanthus fraction size 8 mm was not possible to press to the briquette (*D*~65 mm) of ϱ 900 kg.m$^{-3}$ and higher, therefore additional $E_d$ should be superfluous. All in all, it is important to set balance in the relation between ϱ and associated $E_d$ (financial expenditures) of the briquette densification process to obtain highest profitability and efficiency (Brunerová et al. 2017b). Several commonly used technical mandatory standards require ϱ of woody briquettes higher than **1000 kg.m$^{-3}$**, for example Austrian ÖNORM M 7135 (2000), EN ISO 13061-2 (2014) and ASAE S269.5 (2012). German standard DIN EN 14961-3 (2011) even requires **ϱ higher than 1120 kg.m$^{-3}$** (Stolarski et al. 2013). All studied material and fractions achieved lower ϱ values, none achieved value higher than 890 kg.m$^{-3}$; pine sawdust, the representative of woody biomass reported even lower value than hemp. Further, it can be mentioned that Plíštil et al. (2005) briquetted nine varieties of energy crops with the same briquetting machine BrikStar CS 50 and did not achieved the limit of 1000 kg.m$^{-3}$ at all. They reported ϱ values of 800–900 kg.m$^{-3}$ for reed canary grass, knotweed, sorghum and other herbaceous crops. The study of Brožek et al. (2012) reported values of ϱ from 692 to 806 kg.m$^{-3}$ for briquettes made of birch chips, poplar chips, pine bark and spruce sawdust.

However, in mentioned investigations the effect of fraction size was not evaluated. Based on the results of other studies, the ϱ in the range of 800−1000 kg.m$^{-3}$ is sufficient for high-quality briquettes on biomass basis, and, their production with higher ϱ is not necessary considering the question of additional energy expenses (Kaliyan & Morey 2009; Brunerová 2018).

Taking into account the energy consumption during the briquetting of different size fractions, it is also important to mention the amount of energy needed for the grinding process itself. Novotný (2017) measured energy consumption during grinding of hemp, *Miscanthus* × *gig.*, *Miscanthus sinensis* and apple wood into the same fraction size (4, 8 and 12 mm) by the same hammer mill as was used in this Thesis, and, the results showed the highest consumption for fraction 4 mm and the lowest for fraction 12 mm, except hemp material. In case of hemp the fraction 8 mm had the highest energy consumption (111.47 kWh.t$^{-1}$) and the lowest fraction 4 mm (65.97 kWh.t$^{-1}$).

### 5.8.2. Mechanical durability

*DU* represents the efficiency of briquettes' compactness created during the densification process (Pietsch 2002; Kaliyan & Morey 2009). The *DU* of studied materials together with other materials grinded into the same size fraction (or similar) is presented in the **Figure 57** and **Table 25.**

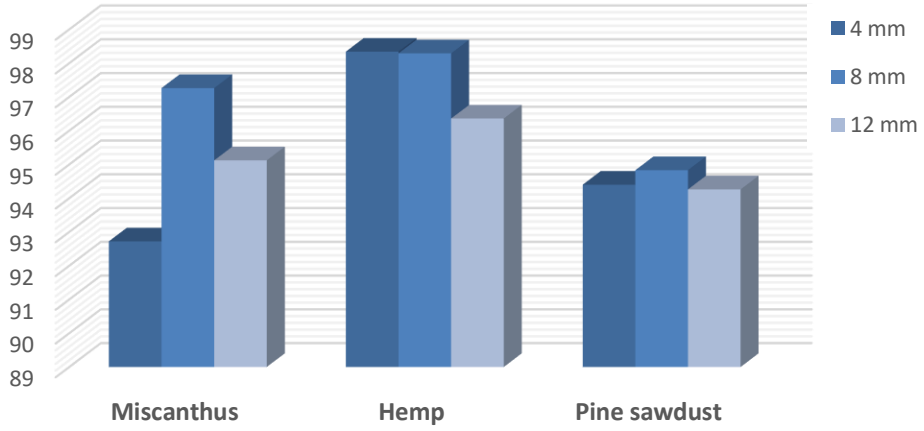


**Figure 57.** *DU* of studied briquettes grouped by the material and fraction

As it can be seen, the **hemp** reported very high *DU* - **more than 98%** for all three fraction sizes and with the highest value for the smallest **fraction 4 mm**, followed closely by the fraction 8 mm and 12 mm. In this case, **lower grind meant higher *DU***. Briquettes produced from **miscanthus**, with fraction size 8 mm and 12 mm although evinced *DU* of better quality than briquettes made from the materials with smaller fraction size 4 mm. It is worth mentioning that in the case of miscanthus, the **lowest fraction size had the lowest *DU***. The similar trend

was observed for briquettes made of **pine sawdust** as well as, the fraction 4 mm had slightly lower *DU* value than fraction 8 mm. Similar results were reported for *Miscanthus sinensis* and apple tree wood (Novotný 2017; Muntean et al. 2017).

**Table 25.** *DU* of studied materials together with *DU* of other materials

| Material | Fraction size | ***DU*** (%) | References |
|---|---|---|---|
| **Miscanthus** [a] | 4 mm | 92.72 | Novotný (2017), Muntean et al. (2017) |
| | 8 mm | **97.26** | Novotný (2017), Muntean et al. (2017) |
| | 12 mm | 95.12 | Novotný (2017), Muntean et al. (2017) |
| **Hemp** [a] | 4 mm | **98.34** | Novotný (2017), Muntean et al. (2017) |
| | 8 mm | 98.29 | Novotný (2017), Muntean et al. (2017) |
| | 12 mm | 96.36 | Novotný (2017), Muntean et al. (2017) |
| **Pine sawdust** | 4 mm | 94.40 | Author (2019) |
| | 8 mm | **94.83** | Author (2019) |
| | 12 mm | 94.26 | Author (2019) |
| **Miscanthus** [b] | 3.8 mm | 89.8 | Ivanova (2012) |
| | 8 mm | 91.9 | Ivanova (2012) |
| **Hemp** [b] | 3.8 mm | 97.7 | Ivanova (2012) |
| ***Miscanthus sinensis*** [b] | 4 mm | 95.80 | Novotný (2017), Muntean et al. (2017) |
| | 8 mm | 95.96 | Novotný (2017), Muntean et al. (2017) |
| | 12 mm | 97.35 | Novotný (2017), Muntean et al. (2017) |
| **Apple wood** [c] | 4 mm | 92.36 | Novotný (2017), Muntean et al. (2017) |
| | 8 mm | 95.13 | Novotný (2017), Muntean et al. (2017) |
| | 12 mm | 95.39 | Novotný (2017), Muntean et al. (2017) |

[a] crops from the same harvest as the study material of the Thesis, [b] plant grew on the field plot of CULS (2010/2011) and grinded by the same hammer mill type as the studied material, [c] branches after pruning

Since the abrasion test of different samples of briquettes followed the same procedure and was applied at the same device, it can be concluded that **particle size has effect on briquette *DU***. Based on previous studies, there is prevailing opinion that finer particles of input material means higher durability and overall quality of solid biofuels (Kaliyan & Morey 2009; Karunanithy et al. 2012; Huko et al. 2015; Ndindeng et al. 2015; Harun & Afzal 2016; Okot et al. 2018). However, in this case of miscanthus and pine sawdust, it was not confirmed. Tendency that briquette quality increases with decreasing of feedstock particle size is restricted (Križan et al. 2018). Very fine grinding has also negative effect on *DU* as well as excessively large particles (Kaliyan & Morey 2009). As the results showed, the fraction size **8 mm** seems to have **the best effect on the *DU*** if all selected materials are considered. The worst mechanical quality provided the fraction size 12 mm, for hemp and pine sawdust briquettes, in case of miscanthus the lowest mechanical properties reported surprisingly fraction 4 mm. Young and Khennas (2013) monitored that particle size 10–15 mm lead to the worse briquette quality. Grover and Mishra

(1996) recommend the size range 6−8 mm for quality briquettes. Comparable results were obtained by Brunerová and Brožek (2016), they found out that the briquettes from pine bark had the best mechanical quality (*DU* and ϱ) with particle size of 6−12 mm, compare to the fraction size <6 mm and >12mm, however, the spruce bark had the best results with the smallest fraction. Okot et al. (2018) produced strong briquettes with particle size <2.36 mm, however the study stated that the durability can be maintained even for higher fractions (<4 mm) if the pressing temperature increases. Huko et al. (2015) reported the best *DU* results for fraction size of 3 mm (~98%) and the lowest *DU* for fraction size of 11 mm (~95%). On the contrary, Tembe et al. (2017) did not report any significant effect of particle size on sawdust briquette durability, nevertheless, all fraction sizes were of lower values (1.70, 2.36, 3.35 mm). Thus, we can see that particle size affect mechanical characteristics of densified biofuels, however, there is no consensus of professional community **which particle size range is optimal**. Even there is no obligatory technical standard specifying this parameter.

In case of this study, the briquettes after abrasion test were examined/observed and it was clearly seen that front side of the briquettes, where the larger particle were located (as confirmed by the measurements), exhibited significantly higher abrasion than the rear side of the briquettes where smaller particle prevailed, as can be seen in the **Figure 58a**. From the visual assessment, this abrasion trend was the same for pine sawdust and miscanthus materials and their fractions. Higher abrasion was concentrated on the edges due to the direct collisions with the wall of durability drum. In the case of hemp, the abrasion of both sides was more uniform (**Figure 58b**), which was caused by the regular distribution of large particles tangled with fibres on briquette surface.


**Figure 58.** Briquettes of pine sawdust and hemp (8 mm) after the abrasion test

As the remarkable fact can be seen the contrast among briquettes made from **hemp** and other materials; it can be probably explained by hemp biomass structure - by better connection of **fibrous particles** (Ivanova et al. 2018). Natural fibers can serve as reinforcing elements with

different mechanical properties, since fibers have high tensile strength compare to other materials (Pickering et al. 2016). Generally, increasing fiber content in the agglomerate enhances the composite's strength significantly (Faruk et al. 2012). However, increased fiber content increases the composite's humidity absorption (Bledzki et al. 2008). Also, the measurements of particle size on the hemp briquette surface showed, that the **particles are distributed more regularly**, than in case of the miscanthus and pine sawdust, which means that the larger particles were not concentrated on the particular points and could not be easily abraded. In case of hemp, the high *DU* can be attributed to its fibrous nature, which enabled the creation of good inter-particle bondings, and not to the content of lignin, since its content was the lowest from the studied materials.

On the other hand, **lignin**-rich composition could have a **positive effect on *DU*** in case of **pine sawdust**, as the lignin content was detected by chemical analysis as well as by the evaluation of the lignin excretion on the surface particles. Contrarily, miscanthus contained higher amount of lignin than hemp, however, its *DU* was lower than *DU* of hemp.

*DU* is a parameter evaluating briquettes strength (Kaliyan & Morey 2009) and stronger briquettes have essentially better quality (Križan et al. 2009). Based on experimental results, it may be concluded that from the viewpoint of *DU* **(DU>95.0%)** the briquettes from **hemp** biomass belong to very **high-quality biofuels** (the highest category DU95.0 according to previously valid standard EN ISO 14961-1 (2010), in actual valid standard there are no categories distinguished and required), followed by the briquettes from miscanthus, fraction 8 and 12 mm. Closely below the highest *DU* category the pine sawdust briquettes were placed. And, still *DU* of miscanthus fraction 4 mm above 90% is considered to be good for transportation and handling purposes (Saikia & Baruah 2013).

### 5.8.3. Compressive strength

The results of compressive strength $\sigma_t$ (N.mm$^{-1}$) of studied materials and their fractions are presented in **Table 26** on the next page.

Generally, the $\sigma_t$ values ranged between 69 **N.mm$^{-1}$** and 110 **N.mm$^{-1}$**; the highest values of $\sigma_t$ reached the **hemp** with more than **85 N.mm$^{-1}$**, followed by **miscanthus (83 N.mm$^{-1}$)** and **pine sawdust (81 N.mm$^{-1}$)**. Regarding to the fraction size, **desceasing fraction size resulted in higher $\sigma_t$.** Bergström et al. (2008) and Križan (2007) also observed that the finer particles led to the higher compression strenght. In case of miscanthus this trend was a bit different, the fraction 8 mm had higher $\sigma_t$ than fraction 4 mm. Comparing the fractions without considering the material type, the highest average $\sigma_t$ value reached **fraction 8 mm**, i.e.

**89.86±19.30 N.mm$^{-1}$**. It was followed by fraction 4 mm with 88.56±23.51 N.mm$^{-1}$. The lowest average $\sigma_t$ was reported for fraction 12 mm − 71.48±24.29 N.mm$^{-1}$. As it can be seen, the $\boldsymbol{\sigma_t}$ values are accompanied by higher variation, which was also reported by Brožek et al. (2012) and Brunerová (2018).

**Table 26.** Compressive strength of studied briquettes

| Fraction size | No. of briquette | Miscanthus (N.mm$^{-1}$) | Hemp (N.mm$^{-1}$) | Pine sawdust (N.mm$^{-1}$) |
|---|---|---|---|---|
| 4 mm | 1 | 49.99 | 99.44 | 77.73 |
| | 2 | 78.50 | 141.60 | 66.23 |
| | 3 | 76.28 | 106.15 | 66.26 |
| | 4 | 117.28 | 107.67 | 70.04 |
| | 5 | 82.30 | 96.15 | 92.76 |
| | **Mean±StD** | **80.87±24.02** | **110.20±18.18** | **92.76±11.18** |
| 8 mm | 1 | 71.78 | 74.65 | 72.22 |
| | 2 | 121.40 | 90.54 | 68.72 |
| | 3 | 111.66 | 74.82 | 90.77 |
| | 4 | 83.96 | 71.05 | 83.79 |
| | 5 | 127.90 | 99.44 | 105.26 |
| | **Mean±StD** | **103.34±24.34** | **76.57±7.99** | **84.15±14.75** |
| 12 mm | 1 | 75.41 | 49.47 | 83.48 |
| | 2 | 80.90 | 85.47 | 95.03 |
| | 3 | 53.11 | 61.69 | 76.25 |
| | 4 | 44.63 | 64.25 | 65.00 |
| | 5 | 70.73 | 71.79 | 98.90 |
| | **Mean±StD** | **70.73±15.41** | **69.00±15.46** | **83.73±13.83** |
| | **Mean±StD** | **83.06±25.84** | **85.26±22.90** | **80.83±13.16** |

Brožek et al. (2012) tested compressive strength (in his tsudy called rupture force) of the briquettes made with the same briquetting machine (BrikStar CS 50) and tested by the same testing machine as in the Thesis. They reported the highest $\boldsymbol{\sigma_t}$ for poplar chips (81.2 N.mm$^{-1}$), lower at briquettes from shavings from 90% spruce and 10% pine (68.6 N.mm$^{-1}$) and spruce sawdust (58.2 N.mm$^{-1}$); on the other hand, relatively low values were determined for briquettes from pine bark (31.5 N.mm$^{-1}$) and birch chips (26.8 N.mm$^{-1}$).

Compare to briquettes made of various materials, Plíštil et al. (2005) reported following $\boldsymbol{\sigma_t}$ values: coriander 30–50 N.mm$^{-1}$, crambe 25–55 N.mm$^{-1}$, saphlor 40–70 N.mm$^{-1}$, sorrel 45–70 N.mm$^{-1}$, sorghum 40–60 N.mm$^{-1}$, reed canary grass 10–35 N.mm$^{-1}$, knotweed 45–80 N.mm$^{-1}$. Brožek (2015; 2016) also determined $\boldsymbol{\sigma_t}$ for waste paper briquettes − 32 N.mm$^{-1}$, for waste wood briquettes (plane tree chips) − 176.1 N.mm$^{-1}$ and 203.4 N.mm$^{-1}$ (depends on feedstock moisture contents) and for waste cardboard briquettes was equal to 153 N.mm$^{-1}$.

Brunerová et al. (2017a) determined $\sigma_t$ of straw and seed pods of poppy – 58.73 N.mm$^{-1}$ and wheat husks – 44.18 N.mm$^{-1}$.

Few authors reported difficulties with the repeatability of the outputs from the compressive strength tests for the same quality of densified biofuels (Li & Liu 2000; Mani et al. 2006; Brožek et al. 2012). During the compression strength test, Li and Liu (2000) noticed that sawdust logs were squeezed (shortened) by approximately one third of the initial size before the final breakage happened. Which means that the compression strength test does not have to exhibit the real compressive strength of the densified biofuels (Kaliyan & Morey 2009). However, as it was stated, this test is still not standardized for densified biofuels.

The comparison of the relation between the briquettes density, mechanical durability and the compressive strength is interesting, too. **Table 27** summarizes the results of compression strength test together with results of *DU* and ϱ presented in the previous Subchapters (5.8.1. and 5.8.2). From the highlighted values we can conclude that hemp briquettes with fraction size 4 and 8 mm achieved very good results of measured mechanical properties.

**Table 27.** Summary of measured mechanical properties of studied briquettes (mean values)

| | | Unit | Miscanthus | Hemp | Pine sawdust |
|---|---|---|---|---|---|
| **4 mm** | ϱ | kg.m$^{-3}$ | 841.92 | **893.03** | 848.72 |
| | DU | % | 92.72 | **98.34** | 94.40 |
| | $\sigma_t$ | N.mm$^{-1}$ | 80.87 | **110.20** | 92.76 |
| **8 mm** | ϱ | kg.m$^{-3}$ | 809.57 | 868.39 | 846.53 |
| | DU | % | 97.26 | 98.29 | 94.83 |
| | $\sigma_t$ | N.mm$^{-1}$ | 103.34 | 76.57 | 84.15 |
| **12 mm** | ϱ | kg.m$^{-3}$ | 806.00 | 828.81 | 834.18 |
| | DU | % | 95.12 | 96.36 | 94.26 |
| | $\sigma_t$ | N.mm$^{-1}$ | 70.73 | 69.00 | 83.73 |

Notes: the bold numbers represent the highest values, the red numbers the lowest values and the underlined ones highlighting the very good results

As we can see, there is no significant dependence between measured mechanical properties. The results also confirmed the statement of Richards (1990) that higher density does not necessarily stand for stronger bonding. Also, according to Brožek et al. (2012) the general dependence between the ϱ and the $\sigma_t$ does not exist.

# 6. Conclusion

Nowadays, there is an important aspect/task related to the efficient production of solid biofuels as a source of energy: to extend and improve existing knowledge on composition and properties of biomass materials and their influence on the quality of final products. This Thesis aimed to evaluate and confront the structure as well as biomass composition of herbaceous, fibrous and wooden biomass grinded into different fraction sizes (4, 8 and 12 mm) and to analyse their influence on quality of produced briquettes. Based on the results of experimental research together with the theoretical base and relevant findings of other authors, following conclusions were formulated.

The results showed that the particles of miscanthus, hemp and pine sawdust are irregular, slightly elongated with moderate degree of angularity, roughness and asymmetry. And these particle characteristics we found to be not suitable for the sieve method, standard approach for the particle size characterization, since the falling-through effect and clogging phenomenon brought to some extend skewed outputs from the analysis. More precise data about particle size and shape were provided by the photo-optical analysis. The bulk densities of studied materials increased according to a power-law relationship with a decrease of aperture screen size of grinding (hammer) mill. Such materials pressed into the briquettes evinced the increasing volumetric mass density with decreasing fraction size; fraction 4 mm had higher density than fraction 8 and 12 mm. It is worth to mention that hemp briquettes had the highest density. Here it was also observed the effect of moisture content, since with increasing water content the briquette volumetric density decreased, as occurred in miscanthus briquettes.

Evaluation of the briquette structure by microscopy technique and image analysis software showed that all scanned points of the briquette surface or better said behavioural pattern of the material at each scanned point has its different attributes that can be explicated by the demeanour of the material mass going through the pressing chamber of the piston briquetting press. The effectiveness of binding mechanisms, i.e. adhesion and bonding between surfaces of input particles, was affected, besides the others, by structural and chemical composition of material, particle size and shape, particle roughness, presence of irregularly shaped particles, like fibres and elongated particles, and presence of air cavities and pores. The surface evaluation showed that the bonding between particles was formed mainly through the inter-locking mechanisms and solid bridges, which were created by hardening of natural binders. It was evident, that the characteristic properties of the briquette surface locations are similar for all briquettes made of different biomass sources. It was observed that the agglomeration and compaction of particles occurred unequally in different zones of the briquette surface and zones

of an interaction of the pressed material with the piston of the briquetting machine. The results for miscanthus and pine sawdust confirmed (Hypothesis 1) that *there are differences in particles size in different briquettes surface locations, larger particles are generally located on the front side of briquettes cross-section and vice versa smaller ones on the rear side, larger particles are centred in the middle of briquette cross-sections and smaller particles are located on the briquette bottom*. The results of hemp were different as they revealed that the particles on hemp briquette surface are more evenly distributed both on front side and rear side, although also in this case the largest particles were located in the middle of the briquette, while the smallest ones on the bottom.

Such irregular particle size distribution on the briquette surface structure was related to the mechanical quality of the briquettes. It was confirmed that *structure of briquettes influences their main mechanical properties* (Hypothesis 2). *Particle size and particle size distribution affect the mechanical stability of briquettes as well as non-uniform distribution of particle sizes on the briquette surface has negative influence on the briquette mechanical strength*. It was not proved the general opinion that finer particles of input material means higher durability and compressive strength. Basically, briquettes with the fraction size of 8 mm demonstrated higher mechanical durability and compressive strength compared to other fractions. Briquettes from the fraction 12 mm exhibited higher uneven distribution of larger particles on the briquette surface structure, which could lead to the higher abrasion of these larger particles concentrated at the specific locations. From the visual assessment, the front side of the briquettes, where the largest particles are concentrated, abraded more that the rear side with the smaller particles.

The last assumption (Hypothesis 3), that *there are links between excretion of binding agents and mechanical strength of the briquettes* was partly verified. According to the studies, the main binding agent in biomass is lignin and the compositional analysis determined that the pine sawdust contains the highest amount of lignin, followed by miscanthus and hemp. The secretion of lignin on the particles surface was observed during the image-based macroscopic analysis and related calculations revealed that the excretion occurred the most on the pine sawdust briquettes that evinced high mechanical durability. On the other hand, the hemp particles exhibited the lowest secretion of lignin during the densification, which corresponded with the results of chemical analysis, while the hemp briquettes (mainly fraction 4 and 8 mm) demonstrated superior mechanical quality compared to the other materials. Thus, the mechanical properties of hemp can be attributed to its fibrous nature than to its ligno-cellulosic composition and ability of lignin to excrete during the densification.

Regarding to the supplementary chemical analyses, the results demonstrated that the miscanthus, hemp and pine sawdust contain low amount of the precursor pollutant elements,

e.g. *N*. The low ash content indicates that the feedstock is unlikely to the encounter operational problems such as slagging and fouling during the thermal conversion. The heating/calorific value of the materials is considerably high, therefore, it should result in good thermal efficiency during thermochemical conversion.

To conclude, the briquette quality is closely associated with the material properties as composition, particle size and shape and particle size distribution. Thus, presented work contributes to the better understanding of linkages between properties of raw input material and final briquetted product. The findings may help to improve regimes, parameters and technological aspects of briquetting equipment to ensure high quality biofuels with appropriate technological and mechanical properties according to the given standards.

# 7. Recommendations for further research

Development of image analysis is still on the rise and it can also find application in the study of physical properties of solid biofuels. Further research on the briquette surface structure based on macroscopic analysis is highly recommended, since, as it was stated, it may help to better understand the interaction of input biomass particles and their behavioural pattern and agglomeration mechanisms within the pressing process and thus it shall contribute to the improvement of the production process of solid biofuels. Extension of the research on more surface zones, including lateral surfaces that are in an interaction with the matrix/die, further on different sources of biomass and fraction size as well as different production conditions (pressure, temperature) is desirable.

Further studying of lignin distribution as well as other natural binders among particles using fluorescence microscopy, which uses ultraviolet light to generate colour fluorescence according to the matter and presence of aromatic molecules in it (Rost 1995), is recommended.

Particle size is related to the process of grinding, on that account it would be useful to analyse different grinding machines and their effect on produced particles size, mainly in case of hemp, since the produced briquettes are of high mechanical quality. This fibrous nature causes difficulties during the grinding and briquetting that are associated with increased energy consumption (Novotný 2017), therefore it would be desired to find out the balance in production technology between costs and quality of final product.

# 8. References


Agarwal AK, Agarwal RA, Gupta T, Gurjar BR. 2017. Introduction to Biofuels. Pages 3-6 in Agarwal AK, Agarwal RA, Gupta T, and Gurjar BR, editors. Biofuels. Technology, Challenges and Prospects. Springer, Singapore.

Agarwal UP. 2006. Raman imaging to investigate ultrastructure and composition of plant cell walls: distribution of lignin and cellulose in black spruce wood (*Picea mariana*). Planta **224**:1141-1153.

Agimelen OS, Mulholland AJ, Sefcik J. 2017. Modelling of artefacts in estimations of particle size of needle-like particles from laser diffraction measurements. Chemical Engineering Science **158**:445-452.

Ahiduzzaman M, Islam Sadrul AKM. 2013. Development of Biomass Stove for Heating up Die Barrel of Rice Husk Briquette Machine. Procedia Engineering **56**:777-781.

Ahmad AA, Zawawi NA, Kasim FH, Inayat A, Khasri A. 2016. Assessing the gasification performance of biomass: A review on biomass gasification process conditions, optimization and economic evaluation. Renewable and Sustainable Energy Reviews **53**:1333-1347.

Akhmedov S, Ivanova T, Krepl V, Muntean A. 2017. Research on solid biofuels from cotton waste biomass– alternative for Tajikistan's energy sector development. Agronomy Research **15**:1846-1855.

Akhtar A, Krepl V, Ivanova T. 2018. Combined overview of combustion, pyrolysis, and gasification of biomass. Energy and Fuels **32**:7294-7318.

Al-Thyabat S, Miles NJ. 2006. An improved estimation of size distribution from particle profile measurements. Powder Technology **166**:152-160.

Al-Widyan MI, Al-Jalil HF, Abu-Zreig MM, Abu-Handeh NH. 2002. Physical Durability and Stability of Olive Cake Briquettes. Canadian Biosystems Engineering **21**:211-224.

Alaru M, Kukk L, Olt J, Menind A, Lauk R, Vollmer E, Astover A. 2011. Lignin content and briquette quality of different fibre hemp plant types and energy sunflower. Field Crops Research **124**:332-339.

Andzs M, Gravitis J, Veveris A. 2013. Extraction of Lignin from Hemp Shives. 9th International Scientific and Practical Conferencec of Environment, Technology, Resourcces, Volume 1, Rēzeknes Augstskola, Rēzekne, Latvia, pp.103-105.

Aniszewska M, Gendek A 2014. Comparison of heat of combustion and calorific value of the cones and wood of selected forest trees species. Forest Research Papers **75**(3):231-236.

Antonyuk S, Tomas J, Heinrich S, Mörl L. 2005. Breakage behaviour of spherical granulates by compression. Chemical Engineering Science **60**:4031-4044.

Antwi-Boasiako C, Acheampong BB. 2016. Strength properties and calorific values of sawdust-briquettes as wood-residue energy generation source from tropical hardwoods of different densities. Biomass and Bioenergy **85**:144-152.

Arregi A, Amutio M, Lopez G, Bilbao J, Olazar M. 2018. Evaluation of thermochemical routes for hydrogen production from biomass: A review. Energy Conversion and Management **165**:696-719.

ASAE S269.5: 2012. densified products for bulk handling - definitions and method. American Society of Agricultural and Biological Engineers, St. Joseph, Michigan, USA.

Back EL. 1987. The bonding mechanism in hardboard manufacture. Holzforschung **41**(4):247-258.

Bagheri GH, Bonadonna C, Manzella I, Vonlanthen P. 2015. On the characterization of size and shape of irregular particles. Powder Technology **270**:141-153.

Bahng M-K, Mukarakate C, Robichaud DJ, Nimlos MR. 2009. Current technologies for analysis of biomass thermochemical processing: A review. Analytica Chimica Acta **651**:117-138.

Bajwa DS, Peterson T, Sharma N, Shojaeiarani J, Bajwa SG. 2018. A review of densified solid biomass for energy production. Renewable and Sustainable Energy Reviews **96**:296-305.

Bao N, Ran X, Wu Z, Xue Y, Wang K. 2017. Design of inspection system of glaze defect on the surface of ceramic pot based on machine vision. 3rd IEEE Information Technology, Networking, Electronic and Automation Control Conference, Chengdu, China, pp. 1486-1492.

Bapat DW, Kulkarni SV, Bhandarkar VP. 1997. Design and operating experience on fluidized bed boiler burning biomass fuels with high alkali ash. 14th International Conference on Fluidized Bed Combustion. ASME, New York, Vancouver, Canada, pp. 165-174.

Batchelor BG, Bruce G. 2012. Machine Vision for Industrial Applications. Pages 1-59 in Batchelor BG, Bruce G, editors. Machine Vision Handbook: Volume 1. Springer, London.

Bergström D, Israelsson S, Öhman M, Dahlqvist S-A, Gref R, Boman C, Wästerlund I. 2008. Effects of raw material particle size distribution on the characteristics of Scots pine sawdust fuel pellets. Fuel Processing Technology **89**:1324-1329.

Bhagwanrao S, Singaravelu M. 2014. Bulk density of biomass and particle density of their briquettes. International Journal of Agricultural Engineering **7**:221-224.

Bitra VSP, Womac AR, Chevanan N, Miu PI, Igathinathane C, Sokhansanj S, Smith DR. 2009a. Direct mechanical energy measures of hammer mill comminution of switchgrass, wheat straw, and corn stover and analysis of their particle size distributions. Powder Technology **193**:32-45.

Bitra VSP, Womac AR, Yang YT, Igathinathane C, Miu PI, Chevanan N, Sokhansanj S. 2009b. Knife mill operating factors effect on switchgrass particle size distributions. Bioresource Technology **100**:5176-5188.

Bledzki AK, Jaszkiewicz A, Murr M, Sperber VE, Lützendgrf R, ReußMann T, Pickering KL. 2008. 4 - Processing techniques for natural- and wood-fibre composites. Pages 163-192 in Pickering KL, editor. Properties and Performance of Natural-Fibre Composites. Woodhead Publishing, Cambridge.

Branca C, Blasi DC, Galgano A. 2017. Experimental analysis about the exploitation of industrial hemp (*Cannabis sativa*) in pyrolysis. Fuel Procecssing Technology **162**:20-29.

Brand MA, Jacinto RC, Antunes R, da Cunha AB. 2017. Production of briquettes as a tool to optimize the use of waste from rice cultivation and industrial processing. Renewable Energy **111**:116-123.

Briklis. 2011. Briquetting Presses BrikStar CS 20, 50, Available from http://www.briklis.cz/en/briquetting-presses-for-wood/brikstar-cs-25-50/ (accessed on November 2015).

Brosse N, Dufour A, Meng X, Ragauskas A. 2012. Miscanthus: A fast-growing crop for biofuels and chemicals production. Biofuels Bioproducts and Biorefining **6**:580-598.

Brown TR, Brown RC. 2013. A Review of Cellulosic Biofuel Commercial-Scale Projects in the United States. Biofuels Bioproducts and Biorefining **7**:10.

Brožek M. 2015. Evaluation of selected properties of briquettes from recovered paper and board. Research in Agricultural Engineering **61**(2): 66-71.

Brožek M. 2016. The Effect of Moisture of the Raw Material on the Properties Briquettes for Energy Use. Acta Universitatis Agriculturae et Silviculturae Mendelianae Brunensis **64**(5):1453-1458.

Brožek M, Nováková A. Kolářová M. 2012. Quality evaluation of briquettes made from wood waste. Research in Agricultural Engineering **58**(1): 30-35.

Brunerová A. 2018. Briquetting of materials suitable for the energy production [PhD Thesis]. Czech University of Life Sciences, Prague.

Brunerová A, Brožek M. 2016. Optimal feedstock particle size and its influence on final briquette quality. 6th International conference of Trends in Agricultural Engineering, Prague, Czech Republic, pp. 95-101.

Brunerová A, Brožek M, Müller M. 2017a. Utilization of waste biomass from post–harvest lines in the form of briquettes for energy production. Agronomy Research **15**: 344-358.

Brunerová A, Brožek M, Šleger V, Nováková A. 2017b. Energy balance of briquette production from various waste biomass. Scientia Agriculturae Bohemica **49**: 236-243.

Brunerová A, Roubík H, Brožek M. 2018. Bamboo Fiber and Sugarcane Skin as a Bio-Briquette Fuel. Energies **11**:1-20.

Brunerová A, Roubík H, Brožek M, Herák D, Šleger V, Mazancová J. 2017c. Potential of Tropical Fruit Waste Biomass for Production of Bio-Briquette Fuel: Using Indonesia as an Example. Energies **10**:1-22.

Burhenne L, Messmer J, Aicher T, Laborie M-P. 2013. The effect of the biomass components lignin, cellulose and hemicellulose on TGA and fixed bed pyrolysis. Analytical and Applied Pyrolysis **101**:177-184.

Calvo H, Moreno-Armendáriz MA, Godoy-Calderón S. 2016. A practical framework for automatic food products classification using computer vision and inductive characterization. Neurocomputing **175, Part B**:911-923.

Capelle A. Hemp: speciality crop for the paper industry. 1996. 3rd National Symposium, Indianapolis, Indiana, USA, 22-25 October, 1996. J. Janick, editor, Progress in New Crops, ASHS Press, Arlington, pp. 384-394.

Cardona J, et al. 2018. Image analysis framework with focus evaluation for in situ characterisation of particle size and shape attributes. Chemical Engineering Science **191**:208-231.

Cardozo E, Erlich C, Alejo L, Fransson TH. 2014. Combustion of agricultural residues: An experimental study for small-scale applications. Fuel **115**:778-787.

Chaloupková V. 2015. Macroscopic analysis of biomass briquettes [MSc Thesis]. Czech University of Life Sciences, Prague.

Chaloupková V, Ivanova T, Havrland B. 2016. Sieve analysis of biomass: Accurate method for determination of particle size distribution. 15th International Scientific Conference of the Engineering for Rural Development, Jelgava, Latvia, pp. 1012-1017.

Chaloupková V, Ivanova T, Ekrt O, Kabutey A, Herák D. 2018a. Determination of Particle Size and Distribution through Image-Based Macroscopic Analysis of the Structure of Biomass Briquettes. Energies **11**(2),331:1-13.

Chaloupková V, Ivanova T, Muntean A. 2018b. Particle size distribution analysis of pine sawdust: comparison of traditional oscillating screen method and photo-optical analysis. Agronomy research **16**(5): 1966-1975.

Channiwala SA, Parikh PP. 2002. A unified correlation for estimating HHV of solid, liquid and gaseous fuels. Fuel **81**:1051-1063.

Chen L, Xing L, Han L. 2009. Renewable energy from agro-residues in China: Solid biofuels and biomass briquetting technology. Renewable and Sustainable Energy Reviews **13**:2689-2695.

Chen W-H, Kuo P-C. 2010. A study on torrefaction of various biomass materials and its impact on lignocellulosic structure simulated by a thermogravimetry. Energy **35**:2580-2586.

Cheng J. 2017. Introduction. Kinetics and Microbiology of Biological Processes. Pages 1-6 and 123-140 in Cheng J, editor. Biomass to Renewable Energy Processes. CRC Press, Boca Raton.

Chin OC, Siddiqui KM. 2000. Characteristics of some biomass briquettes prepared under modest die pressures. Biomass and Bioenergy **18**:223-228.

Chou C-S, Lin S-H, Peng C-C, Lu W-C. 2009. The optimum conditions for preparing solid fuel briquette of rice straw by a piston-mold process using the Taguchi method. Fuel Processing Technology **90**:1041-1046.

Clifton-Brown JC, Stampfl PF, Jones MB. 2004. Miscanthus biomass production for energy in Europe and its potential contribution to decreasing fossil fuel carbon emissions. Global Change Biology **10**:509-518.

Coates W. 2000. Using cotton plant residue to produce briquettes. Biomass and Bioenergy **18**:201-208.

Cox EP. 1927. A Method of Assigning Numerical and Percentage Values to the Degree of Roundness of Sand Grains. Journal of Paleontology **1**:179-83.

Cruz-Matías I, Ayala D, Hiller D, Gutsch S, Zacharias M, Estradé S, Peiró F. 2019. Sphericity and roundness computation for particles using the extreme vertices model. Journal of Computational Science **30**:28-40.

Černá I, Pecen J, Ivanova T, Piksa Z. 2016. The dependence of the durability of digestate briquettes and sorption properties on represented particle sizes. Agronomy Research **14**:1548-1561.

Dai J, Cui H, Grace JR. 2012. Biomass feeding for thermochemical reactors. Progress in Energy and Combustion Science **38**:716-736.

Das L, Liu E, Saeed A, Williams DW, Hu H, Li C, Ray AE, Shi J. 2017. Industrial hemp as a potential bioenergy crop in comparison with kenaf, switchgrass and biomass sorghum. Bioresource Technology **244**:641-649.

Davies ER. 2018. Chapter 1 - Vision, the challenge. Pages 1-15 in Davies ER, editor. Computer Vision (Fifth Edition). Academic Press, London.

Davies RM, Abolude DS. 2013. Ignition and Burning Rate of Water Hyacinth Briquettes. Journal of Scientific Research & Reports **2**:111-120.

De Meyer A, Cattrysse D, Rasinmäki J, Van Orshoven J. 2014. Methods to optimise the design and management of biomass-for-bioenergy supply chains: A review. Renewable and Sustainable Energy Reviews **31**:657-670.

De Oliveira EM, Leme DS, Barbosa BHG, Rodarte MP, Pereira RGFA. 2016. A computer vision system for coffee beans classification based on computational intelligence techniques. Journal of Food Engineering **171**:22-27.

Deac T, Fechete-Tutunaru L, Gaspar F. 2016. Environmental Impact of Sawdust Briquettes Use - Experimental Approach. Energy Procedia **85**:178-183.

Demirbas A. 2005. Fuel and combustion properties of bio-wastes. Energy Sources **27**:451-462.

Demirbas A, Demirbas AS, Demirbas AH. 2004. Briquetting Properties of Biomass Waste Materials. Energy sources **26**:83-91

Dhyani V, Bhaskar T. 2018. A comprehensive review on the pyrolysis of lignocellulosic biomass. Renewable Energy **129**:695-716.

DIN EN 14961-3: 2011. Solid biofuels - fuel specifications and classes - part 3: wood briquettes for non-industrial use. German Institute for Standardisation (Deutsches Institut für Normung), Berlin, Germany (in German).

Dinh TM. 2014. Contribution to the development of precast hempcrete using innovative pozzolanic binder [PhD Thesis], Toulouse: Toulouse University.

Dioguardi F, Mele D. 2015. A new shape dependent drag correlation formula for non-spherical rough particles. Experiments and results. Powder Technology **277**:222-230.

Directive 2009/28/EC. 2009. Available from https://eur-lex.europa.eu/legal-content/EN/ALL/?uri=CELEX%3A32009L0028 (accessed on August 2018).

Directive proposal COM/2016/0767. 2016. Available from https://eur-lex.europa.eu/legal-content/EN/TXT/?uri=CELEX:52016PC0767R%2801%29 (accessed on August 2018).

Dražić S, Sladoje N, Lindblad J. 2016. Estimation of Feret's diameter from pixel coverage representation of a shape. Pattern Recognition Letters **80**:37-45.

Dufossé K, Drewer J, Gabrielle B, Drouet J-L. 2014. Effect of 20-year old *Miscanthus* × *giganteus* stand and its removal on soil characteristics and greenhouse gas emissions. Biomass and Bioenergy **69**:198-210.

Elfasakhany A, Bai XS. 2019. Numerical and experimental studies of irregular-shape biomass particle motions in turbulent flows. Engineering Science and Technology **22**:249-265.

EN ISO 9276-6. 2008. Representation of results of particle size analysis - Part 6: Descriptive and quantitative representation of particle shape and morphology. International Organization for Standardization, Geneva.

EN ISO 13061-2. 2014. Physical and mechanical properties of wood - Test methods for small clear wood specimens - Part 2: Determination of density for physical and mechanical tests. International Organization for Standardization, Geneva.

EN ISO 14780. 2017. Solid biofuels - Sample preparation. International Organization for Standardization, Geneva.

EN ISO 14961-1. 2010. Solid biofuels - Fuel specifications and classes - Part 1: General Requirements. *Superseded by EN ISO 17225-2 2014*. International Organization for Standardization, Geneva.

EN ISO 16559. 2014. Solid biofuels - Terminology, definitions and descriptions. International Organization for Standardization, Geneva.

EN ISO 16948. 2015. Solid biofuels - Determination of total content of carbon, hydrogen and nitrogen. International Organization for Standardization, Geneva.

EN ISO 17225-2. 2014. Solid biofuels - Fuel specifications and classes - Part 1: General Requirements. International Organization for Standardization, Geneva.

EN ISO 17225-2. 2014. Solid biofuels - Fuel specifications and classes - Part 2: Graded wood pellets. International Organization for Standardization, Geneva.

EN ISO 17225-3. 2014. Solid biofuels - Fuel specifications and classes - Part 3: Graded wood briquettes. International Organization for Standardization, Geneva.

EN ISO 17225-6. 2014. Solid biofuels - Fuel specifications and classes - Part 6: Graded non-woody pellets. International Organization for Standardization, Geneva.

EN ISO 17225-7. 2014. Solid biofuels - Fuel specifications and classes - Part 6: Graded non-woody briquettes. International Organization for Standardization, Geneva.

EN ISO 17827-1. 2016. Solid biofuels - Determination of particle size distribution for uncompressed fuels - Part 1: Horizontally oscillating screen using sieve for classification of samples with top aperture of 3,15 mm and above. International Organization for Standardization, Geneva.

EN ISO 17828. 2015. Solid biofuels - Determination of bulk density. International Organization for Standardization, Geneva.

EN ISO 17831-2. 2015. Solid biofuels - Determination of mechanical durability of pellets and briquettes. Briquettes. International Organization for Standardization, Geneva.

EN ISO 18122. 2015. Solid biofuels - Determination of ash content. International Organization for Standardization, Geneva.

EN ISO 18123. 2015. Solid biofuels - Determination of the content of volatile matter. International Organization for Standardization, Geneva.

EN ISO 18125. 2017. Solid biofuels - Determination of calorific value. International Organization for Standardization, Geneva.

EN ISO 18134-2. 2017. Solid biofuels - Determination of moisture content - Oven dry method - Part 2: Total moisture - Simplified method. International Organization for Standardization, Geneva.

Faik A. 2013. "Plant Cell Wall Structure-Pretreatment" the Critical Relationship in Biomass Conversion to Fermentable Sugars. Pages 1-30 in Tingyue G, editor. Green Biomass Pretreatment for Biofuels Production. Springer, New York.

Farrokh NT, Suopajärvi H, Sulasalmi P, Fabritius T. 2019. A thermogravimetric analysis of lignin char combustion. Energy Procedia **158**:1241-1248.

Faruk O, Bledzki AK, Fink H-P, Sain M. 2012. Biocomposites reinforced with natural fibers: 2000–2010. Progress in Polymer Science **37**:1552-1596.

Febbi P, Menesatti P, Costa C, Pari L, Cecchini M. 2015. Automated determination of poplar chip size distribution based on combined image and multivariate analyses. Biomass and Bioenergy **73**:1-10.

Feng C, Yu X, Tan H, Liu T, Hu T, Zhang Z, Qiu S, Chen L. 2013. The economic feasibility of a crop-residue densification plant: A case study for the city of Jinzhou in China. Renewable and Sustainable Energy Reviews **24**:172-180.

Fengel D, Wegner G. 1983. Wood-chemistry, ultrastructure, reactions. Remagen, Kessel Werlag.

Fernlund JMR. 1998. The effect of particle form on sieve analysis: a test by image analysis. Engineering Geology **50**:111-124.

Fournel S, Palacios JH, Morissette R, Villeneuve J, Godbout S, Heitz M, Savoie P. 2015. Influence of biomass properties on technical and environmental performance of a multi-fuel boiler during on-farm combustion of energy crops. Applied Energy **141**:247-259.

Frei M. 2013. Lignin: Characterization of a Multifaceted Crop Component. The Scientific World Journal 2013. Available from http://dx.doi.org/10.1155/2013/436517 (accessed on January 2015).

Fujita M, Harada H. 2000. Ultrastructure and Formation of Wood Cell Wall. Hon DN-S, Shiraishi N editors. Wood and Cellulosic Chemistry. CRC Press, New York.

Gaitán-Alvarez J, Moya R, Puente-Urbina A, Rodriguez-Zuñiga A. 2017. Physical and Compression Properties of Pellets Manufactured with the Biomass of Five Woody Tropical Species of Costa Rica Torrefied at Different Temperatures and Times. Energies **10**:1-17.

Ganesh A, Raveendran K. 2008. Biomass Selection Criteria for Pyrolytic Conversion Processes. Pages 1025-1033 in Bridgwater AV, editor. Progress in Thermochemical Biomass Conversion. Blackwell Science Ltd, Cornwall, GB.

García-Galindo D, et al. 2016. Europruning Project: Summary of Final Results. 24th European Biomass Conference and Exhibition, Amsterdam, Netherlands, pp. 89-102.

Garrido AM, Conesa AJ, Garcia DM. 2017. Characterization and Production of Fuel Briquettes Made from Biomass and Plastic Wastes. Energies **10**:1-12.

Gendek A, Aniszewska M, Malat'ák J, Velebil J. 2018. Evaluation of selected physical and mechanical properties of briquettes produced from cones of three coniferous tree species. Biomass and Bioenergy **117**:173-179.

Ghebre-Sellassie I. 1989. Pharmaceutical pelletization technology. Marcel Dekker, New York.

Gil M, Arauzo I. 2014. Hammer mill operating and biomass physical conditions effects on particle size distribution of solid pulverized biofuels. Fuel Processing Technology **127**:80-87.

Gil M, Teruel E, Arauzo I. 2014. Analysis of standard sieving method for milled biomass through image processing. Effects of particle shape and size for poplar and corn stover. Fuel **116**:328-340.

Gilvari H, de Jong W, Schott DL. 2019. Quality parameters relevant for densification of bio-materials: Measuring methods and affecting factors - A review. Biomass and Bioenergy **120**:117-134.

Girolami A, Napolitano F, Faraone D, Braghieri A. 2013. Measurement of meat color using a computer vision system. Meat Science **93**:111-118.

Gokcol C, Dursun B, Alboyaci B, Sunan E. 2009. Importance of biomass energy as alternative to other sources in Turkey. Energy Policy **37**:424-431.

Gong C, Huang J, Feng C, Wang G, Tabil L, Wang D. 2016. Effects and mechanism of ball milling on torrefaction of pine sawdust. Bioresource Technology **214**:242-247.

Gongal A, Karkee M, Amatya S. 2018. Apple fruit size estimation using a 3D machine vision system. Information Processing in Agriculture **5**:498-503.

Grams J, Kwapińska M, Jędrzejczyk M, Rzeźnicka I, Leahy JJ, Ruppert AM. 2019. Surface characterization of *Miscanthus* × *giganteus* and Willow subjected to torrefaction. Analytical and Applied Pyrolysis **138**:231-241.

Granada E, López González LM, Míguez JL, Moran J. 2002. Fuel lignocellulosic briquettes, die design and products study. Renewable Energy **27**:561-673.

Gravitis J, Abolins J, Tupciauskas R, Vēveris A. 2010. Lignin from steam-exploded wood as binder in wood composites. Environmental Engineering and Landscape Management **18**(2):75-84.

Grover PD, Mishra SK. 1996. Biomass briquetting: technology and practise. FAO, Bangkok.

Guo L, Tabil L, Wang D, Wang G. 2016. Influence of moisture content and hammer mill screen size on the physical quality of barley, oat, canola and wheat straw briquettes. Biomass and Bioenergy **94**: 201-208.

Guo M, Song W, Buhain J. 2015. Bioenergy and biofuels: History, status, and perspective. Renewable and Sustainable Energy Reviews **42**:712-725.

Guo Q, Chen X, Liu H. 2012. Experimental research on shape and size distribution of biomass particle. Fuel **94**:551-555.

Gutiérrez A, Rodríguez IM, del Río JC. 2006. Chemical characterization of lignin and lipid fractions in industrial hemp bast fibers used for manufacturing high-quality paper pulps. Journal of Agricultural and Food Chemistry **54**(6):2138-2144.

Gutzeit E, Voskamp J. 2012. Automatic Segmentation of Wood Logs by Combining Detection and Segmentation. 8th International Symposium on Advances in Visual Computing Symposium, Rethymnon, Crete, pp. 252-261.

Harun NY, Afzal MT. 2016. Effect of Particle Size on Mechanical Properties of Pellets Made from Biomass Blends. Procedia Engineering **148**:93-99.

Haver & Boecker, 2015. Haver CPA 4-2, Haver CPA 4 Conveyor, operating instructions. Computer-supported photo-optical particle analysis. Manual, Haver & Boecker, Oelde.

Havrland B, Pobedinschi V, Vrancean V, Pecen J, Ivanova T, Muntean A, Kandakov A. 2011. Biomass processing to biofuel. Prague-Chisinau, CULS Prague: Power-Print, 86p.

Heidenreich S, Müller M, Foscolo PU. 2016. Advanced Biomass Gasification: New Concepts for Efficiency Increase and Product Flexibility. Academic Press, Cambridge.

Helwani Z, Fatra W, Arifin L, R Othman M, Syapsan 2018. Effect of process variables on the calorific value and compressive strength of the briquettes made from high moisture Empty Fruit Bunches (EFB). Material Science and Engineering **345**:1-10.

Hernández Allica J, Mitre AJ, González Bustamante JeA, Itoiz C, Blanco F, Alkorta I, Garbisu C. 2001. Straw quality for its combustion in a straw-fired power plant. Biomass and Bioenergy **21**:249-258.

Hiloidhari M, Das D, Baruah DC. 2014. Bioenergy potential from crop residue biomass in India. Renewable and Sustainable Energy Reviews **32**: 504-512.

Hodkinson TR, Chase MW, Renvoize SA. 2002. Characterization of a Genetic Resource Collection for *Miscanthus* (*Saccharinae, Andropogoneae, Poaceae*) using AFLP and ISSR PCR. Annals of Botany **89**:627-636.

Holmgren P, Wagner DR, Strandberg A, Molinder R, Wiinikka H, Umeki K, Broström M. 2017. Size, shape, and density changes of biomass particles during rapid devolatilization. Fuel **206**:342-351.

Hu J, Lei T, Wang Z, Yan X, Shi X, Li Z, He X, Zhang Q. 2014. Economic, environmental and social assessment of briquette fuel from agricultural residues in China – A study on flat die briquetting using corn stalk. Energy **64**:557-566.

Huang B, Ma S, Wang P, Wang H, Yang J, Guo X, Zhang W, Wang H. 2018. Research and implementation of machine vision technologies for empty bottle inspection systems. Engineering Science and Technology **21**:159-169.

Huang GX, Chen L, Cao J. 2008. Briquetting mechanism and waterproof performance of bio-briquette. China Coal Society **33**:812-815.

Huhtinen M. 2006. Wood biomass as a fuel. 5EURES Training sessions. Available from M|/5 Eures/Wood Properties PDF.htm (8 of 8)19.1.2006 13:15:40 (accessed on 12 of March 2019).

Huko D, Kamau DN, Ogola WO. 2015. Effects of Varying Particle Size On Mechanical and Combustion Characteristics of Mango Seed Shell Cashew Nut Shell Composite Briquettes. Engineering Science Invention **4**:48-58.

Husain Z, Zainac Z, Abdullah Z. 2002. Briquetting of palm fibre and shell form the processing of palm nuts to palm oil. Biomass and Bioenergy **22**:505-509.

Igathinathane C, Melin S, Sokhansanj S, Bi X, Lim CJ, Pordesimo LO, Columbus EP. 2009a. Machine vision based particle size and size distribution determination of airborne dust particles of wood and bark pellets. Powder Technology **196**:202-212.

Igathinathane C, Pordesimo LO, Columbus EP, Batchelor WD, Sokhansanj S. 2009b. Sieveless particle size distribution analysis of particulate materials through computer vision. Computers and Electronics in Agriculture **66**:147-158.

Igathinathane C, Womac AR, Sokhansanj S. 2010. Corn stalk orientation effect on mechanical cutting. Biosystems Engineering **107**:97-106.

Irvine GM. 1985. The significance of the glass transition of lignin in thermomechanical pulping. Wood Science and Technology **19**:139-149.

Ivanova T. 2012. Research of Energy Plants Processing to Solid Biofuels [PhD Thesis]. Czech University of Life Sciences, Prague.

Ivanova T, Havrland B, Novotny R, Muntean A, Hutla P 2018. Influence of raw material properties on energy consumption during briquetting process. Contemporary Research Trends in Agricultural Engineering. BIO Web of Conferences 10, 02006.

Ivanova T, Mendoza Hernández HA, Bradna J, Fernández Cusimamani E, García Montoya CJ, Armas Espinel AD. 2018. Assessment of Guava (*Psidium Guajava* L.) Wood Biomass for Briquettes' Production. Forests **9**:1-13.

Jenkins BM, Baxter LL, Miles TR. 1998. Combustion properties of biomass. Fuel Processing Technology **54**:17-46.

Jirjis R. 2005. Effects of particle size and pile height on storage and fuel quality of comminuted *Salix viminalis*. Biomass and Bioenergy **28**:193-201.

Jittabut P. 2015. Physical and Thermal Properties of Briquette Fuels from Rice Straw and Sugarcane Leaves by Mixing Molasses. Energy Procedia **79**:2-9.

Johnson R. 2018. Hemp as an Agricultural Commodity. Congressional Research Service. Available from https://fas.org/sgp/crs/misc/RL32725.pdf (accessed on November 2015).

Kadam KL, Forrest LH, Jacobson WA. 2000. Rice straw as a lignocellulosic resource: collection, processing, transportation, and environmental aspects. Biomass and Bioenergy **18**:369-389.

Kaliyan N, Morey RV. 2009. Factors affecting strength and durability of densified biomass products. Biomass and Bioenergy **33**:337-359.

Kaliyan N, Morey RV. 2010. Natural binders and solid bridge type binding mechanisms in briquettes and pellets made from corn stover and switchgrass. Bioresource Technology **101**:1082-1090.

Kaliyan N, Morey RV, Schmidt DR. 2013. Roll press compaction of corn stover and perennial grasses to increase bulk density. Biomass and Bioenergy **55**:322-330.

Kambo HS, Dutta A. 2014. Strength, storage, and combustion characteristics of densified lignocellulosic biomass produced via torrefaction and hydrothermal carbonization. Applied Energy **135**:182-191.

Kang BS, Sim SB, Kim JJ. 2017. Volume and Mass Measurement of a Burning Wood Pellet by Image Processing. Energies **10**:1-13.

Karkania V, Fanara E, Zabaniotou A. 2012. Review of sustainable biomass pellets production – A study for agricultural residues pellets' market in Greece. Renewable and Sustainable Energy Reviews **16**:1426-1436.

Karunanithy C, Wang Y, Muthukumarappan K, Pugalendhi S. 2012. Physiochemical Characterization of Briquettes Made from Different Feedstock. Biotechnology Research International **2012**:1-12.

Kępys W. 2016. Opto-pneumatic Separators in Waste Management. Inżynieria Mineralna **17**:63-67.

Kers J, Kulu P, Aruniit A, Laurmaa V, Križan P, Šoos L, Kask Ü. 2010. Determination of physical, chemical and burning characteristics of polymeric waste material briquettes. Estonian Journal of Engineering **16**:307-316.

Khan AA, Jong de W, Jansens PJ, Spliethoff H. 2009. Biomass combustion in fluidized bed boilers: Potential problems and remedies. Fuel Procecssing Technology **90**(1):21-50.

Kim G-H, Kwon O-H, Myong S-i, Kim S-D. 2016. Development of Plastics Defect Inspection System using Vision System. Control and Automation **9**:51-58.

Kim S, Dale BE. 2015. All biomass is local: The cost, volume produced, and global warming impact of cellulosic biofuels depend strongly on logistics and local conditions. Biofuels, Bioproducts and Biorefining **10**:186-190.

Kirsten C, Lenz V, Schröder H-W, Repke J-U. 2016. Hay pellets - The influence of particle size reduction on their physical–mechanical quality and energy demand during production. Fuel Processing Technology **148**:163-174.

Knoll M, Gerhardter H, Prieler R, Mühlböck M, Tomazic P, Hochenauer C. 2019. Particle classification and drag coefficients of irregularly-shaped combustion residues with various size and shape. Powder Technology **345**:405-414.

Knox JP. 2008. Revealing the structural and functional diversity of plant cell walls. Current opinion in Plant Biology **11**:308-313.

Koerner RM. 1970. Effect of particle characteristics on soil strength. Journal of the Soil Mechanics and Fundations Division, American Society of Civil Engineers **96**:1221-1233.

Kok MV, Özgür E. 2013. Thermal analysis and kinetics of biomass samples. Fuel Processing Technology **106**:739-743.

Kolaříková M. 2017. Evaluation of solid biofuels made of hemp from autumn and spring harvests from two localities - Prague and Chisinau (Moldova) [PhD Thesis]. Czech University of Life Sciences, Prague.

Kolaříková M, Ivanova T, Havrland B, Amonov K. 2014. Evaluation of sustainability aspect – energy balance of briquettes made of hemp biomass cultivated in Moldova. Agronomy Research **12**:519-526.

Kolaříková M, Ivanova T, Hutla P, Havrland B. 2015. Economic evaluation of hemp (*Cannabis sativa)* grown for energy purposes (briquettes) in the Czech Republic. Agronomy Research **13**:328-336.

Kreuger E, Prade T, Escobar F, Svensson SE, Englund JE, Björnsson L. 2011. Anaerobic digestion of industrial hemp–Effect of harvest time on methane energy yield per hectare. Biomass and Bioenergy **35**:893-900.

Kreuger E, Sipos B, Zacchi G, Svensson S-E , Björnsson L. 2011. Bioconversion of industrial hemp to ethanol and methane: The benefits of steam pretreatment and co-production. Bioresource Technology **102**:3457-3465.

Križan P. 2007. Research of factors influencing the quality of wood briquets. Acta Montanistica Slovaca **12**:223-230.

Križan P, Matúš M, Beniak J, Šooš Ľ. 2018. Research of interaction between technological and material parameters during densification of sunflower hulls. 8th TSME-International Conference on Mechanical Engineering. IOP Conf. Series: Materials Science and Engineering 297, Bangkok, Thailand, pp. 1-9.

Križan P, Matúš M, Šooš Ľ, Beniak J. 2015. Behavior of Beech Sawdust during Densification into a Solid Biofuel. Energies **8**(7):6382-6398.

Križan P, Šooš L, Vukelić D. 2009. A study of impact technological parametres on the briquetting process. Facta Universitatis: Working and Living Environmental Protection **6**(1):39-47.

Krumbein WC. 1941. Measurement and geological significance of shape and roundness of sedimentary particles. ournal of Sedimentary Research **11**(2):64-72.

Krumbein WC, Sloss LL. 1963. Stratigraphy and Sedimentation. W.H. Freeman and Company, San Francisco and London.

Krzyżaniak M, Stolarski MJ. 2017. Perennial Grasses for Energy. Pages 131-140 in Abraham MA, editos. Encyclopedia of Sustainable Technologies. Elsevier, Oxford.

Ku Ahmad KZ, Sazali K, Kamarolzaman AA. 2018. Characterization of fuel briquettes from banana tree waste. Materials Today: Proceedings **5**:21744-21752.

Kuang F, Zhou X, Huang J, Wang H, Zheng P. 2019. Machine-vision-based assessment of frictional vibration in water-lubricated rubber stern bearings. Wear **426-427**:760-769.

Kumar M, Turner S. 2015. Plant cellulose synthesis: CESA proteins crossing kingdoms. Phytochemistry **112**:91-99.

Kumar P, Kumar S, Joshi L. 2015. Socioeconomic and Environmental Implications of Agricultural Residue Burning a Case Study of Punjab, India. Concluding Remarks and Policy Recommendations, Socioeconomic and Environmental Implications of Agricultural Residue Burning, pp. 133–139.

Kumara GHAJJ, Hayano K, Ogiwara K. 2012. Image Analysis Technique on Evaluation of Particle Size Distribution of Gravel. GEOMATE **3**:290-297.

Kyzas GZ, Terzopoulou Z, Nikolaidis V, Alexopoulou E, Bikiaris DN. 2015. Low-cost hemp biomaterials for nickel ions removal from aqueous solutions. Molecular Liquids **209**:209-218.

Lavoie J-M, Beauchet R. 2012. Biorefinery of Cannabis sativa using one- and two-step steam treatments for the production of high quality fibres. Industrial Crops and Products **37**:275-283.

Lehtikangas P. 2001. Quality properties of pelletised sawdust, logging residues and bark. Biomass and Bioenergy **20**:351-360.

Lela B, Barišić M, Nižetić S. 2016. Cardboard/sawdust briquettes as biomass fuel: Physical–mechanical and thermal characteristics. Waste Management **47**:236-245.

Lessard J, de Bakker J, McHugh L. 2014. Development of ore sorting and its impact on mineral processing economics. Minerals Engineering **65**:88-97.

Lewandowski I, Scurlock JMO, Lindvall E, Christou M. 2003. The development and current status of perennial rhizomatous grasses as energy crops in the US and Europe. Biomass and Bioenergy **25**:335-361.

Li L, Zhou Y, Cheng X, Sun J, Marita JM, Ralph J, Chiang VL. 2003. Combinatorial modification of multiple lignin traits in trees through multigene cotransformation. Proceedings of the National Academy of Sciences of the United States of America **100**:4939-4944.

Li Y, Liu H. 2000. High-pressure densification of wood residues to form and upgraded fuel. Biomass and Bioenergy **19**:177-186.

Liliedahl T, Sjöström K. 1998. Heat transfer controlled pyrolysis kinetics of a biomass slab, rod or sphere. Biomass and Bioenergy **15**:503-509.

Lisowski A, Klonowski J, Sypula M. 2010. Comminution properties of biomass in forage harvester and beater mill and its particle size characterization. Agronomy Research **8**:459-464.

Lu H, Ip E, Scott J, Foster P, Vickers M, Baxter LL. 2010. Effects of particle shape and size on devolatilization of biomass particle. Fuel **89**:1156-1168.

Lubwama M, Yiga VA. 2017. Development of groundnut shells and bagasse briquettes as sustainable fuel sources for domestic cooking applications in Uganda. Renewable Energy **111**:532-542.

Maier G, et al. 2017. Real-time multitarget tracking for sensor-based sorting. Journal of Real-Time Image Processing 1-12.

Malherbe S, Cloete TE. 2002. Lignocellulose biodegradation: fundamentals and applications. Reviews in Environmental Science and Biotechnology **1**:105-114.

Mani S, Tabil LG, Sokhansanj S. 2004a. Evaluation of compaction equations applied to four biomass species. Canadian Biosystems Engineering **46**:55-61.

Mani S, Tabil LG, Sokhansanj S. 2004b. Grinding performance and physical properties of wheat and barley straws, corn stover and switchgrass. Biomass and Bioenergy **27**:339-352.

Mani S, Tabil LG, Sokhansanj S. 2006. Effects of compressive force, particle size and moisture content on mechanical properties of biomass pellets from grasses. Biomass and Bioenergy **30**:648-654.

Manish R, Venkatesh A, Denis Ashok S. 2018. Machine Vision Based Image Processing Techniques for Surface Finish and Defect Inspection in a Grinding Process. Materials Today: Proceedings **5**:12792-12802.

Manzone M, Paravidino E, Bonifacino G, Balsari P. 2016. Biomass availability and quality produced by vineyard management during a period of 15 years. Renewable Energy **99**:465-471.

Martí-Ferrer F, Vilaplana F, Ribes-Greus A, Benedito-Borrás A, Sanz-Box C. 2005. Flour rice husk as filler in block copolymer polypropylene: Effect of different coupling agents. Applied Polymer **9**:1823-1831.

Masuda H, Gotoh K. 1999. Study on the sample size required for the estimation of mean particle diameter. Advanced Powder Technology **10**:159-173.

Matsumura Y, Minowa T, Yamamoto H. 2005. Amount, availability, and potential use of rice straw (agricultural residue) biomass as an energy resource in Japan. Biomass and Bioenergy **29**:347-354.

Matúš M, Križan P, Šooš L, Beniak J. 2015. Effects of Initial Moisture Content on the Physical and Mechanical Properties of Norway Spruce Briquettes. Environmental and Ecological Engineering 9(10):1227-1233.

McKendry P. 2002. Energy production from biomass (part 1): overview of biomass. Bioresource Technology **83**:37-46.

Melero JA, Iglesias J, Garcia A. 2012. Biomass as renewable feedstock in standard refinery units. Feasibility, opportunities and challenges. Energy and Environmental Sciences **6**:7393-7420.

Miao Z, Phillips J, Grift T, Mathanker S. 2014. Measurement of Mechanical Compressive Properties and Densification Energy Requirement of *Miscanthus* × *giganteus* and Switchgrass. Bioenergy Research **8**:152-164.

Militzer J, Kan JM, Hamdullahpur F, Amyotte PR, Altawee lAM. 1989. Drag coefficient for axisymmetric flow around individual spheroidal particles. Powder Technology **57**:193.

Miranda MT, Arranz JI, Rojas S, Montero I. 2009. Energetic characterization and kinetics of biomass residuals mixtures with lignite. Fuel **82**:1949-1960.

Mitan NMM, Saifulazwan RM, Zainul HNM, Hafizuddin MGM. 2018. Performance of binders in briquetting of durian peel as a solid biofuel. Materials Today: Proceedings **5**:21753-21758.

Mitchual SJ, Frimpong-Mensah K, Darkwa NA. 2013. Effect of species, particle size and compacting pressure on relaxed density and compressive strength of fuel briquettes. Energy and Environmental Engineering **4**:30.

Mladenović M, Paprika M, Marinković A. 2018. Denitrification techniques for biomass combustion. Renewable and Sustainable Energy Reviews **82**:3350-3364.

Molino A, Larocca V, Chianese S, Musmarra D. 2018. Biofuels Production by Biomass Gasification: A Review. Energies **11**:1-31.

Monedero E, Portero H, Lapuerta M. 2018. Combustion of Poplar and Pine Pellet Blends in a 50 kW Domestic Boiler: Emissions and Combustion Efficiency. Energies **11**:1580.

Mora CF, Kwan AKH. 2000. Sphericity, shape factor, and convexity measurement of coarse aggregate for concrete using digital image processing. Cement and Concrete Research **30**:351-358.

Muazu RI, Borrion AL, Stegemann JA. 2017. Life cycle assessment of biomass densification systems. Biomass and Bioenergy **107**:384-397.

Muazu RI, Stegemann JA. 2015. Effects of operating variables on durability of fuel briquettes from rice husks and corn cobs. Fuel Processing Technology **133**:137-145.

Muazu RI, Stegemann JA. 2017. Biosolids and microalgae as alternative binders for biomass fuel briquetting. Fuel **194**:339-347.

Muley PD, Henkel C, Abdollahi KK, Marculescu C, Boldor D. 2016. A critical comparison of pyrolysis of cellulose, lignin, and pine sawdust using an induction heating reactor. Energy Conversion and Management **117**:273-280.

Muntean A, Havrland B, Pobedinsky V, Ivanova T, Grigore M. 2010. Features of bio-briquettes pressing with the piston briquetting press. 9th International Scientific Conference of the Engineering for Rural Development, Jelgava, Latvia, pp. 246-251.

Muntean A, Ivanova T, Havrland B, Pobedinsky V. 2012. Comparative Analysis of Methods for Fuel Briquettes Production. 11th International Scientific Conference of the Engineering for Rural Development, Jelgava, Latvia, pp. 496-499.

Muntean A, Ivanova T, Havrland B, Pobedinsky V, Vrancean V. 2013. Particularities of bio-raw material particle agglomeration during solid fuel pressing process. 12th International Scientific Conference of the Engineering for Rural Development, Jelgava, Latvia, pp. 499-503.

Muntean A, Ivanova1 T, Hutla P, Havrland B. 2017. Influence of raw material properties on the quality of solid biofuel and energy consumption in briquetting process. Agronomy Research **15**:1708-1715.

Murphy C. H. 1984. Handbook of particle sampling and analysis methods. Verlag Chemie International, Michigan, USA.

Narendra VG, Hareesh KS. 2010. Prospects of Computer Vision Automated Grading and Sorting System in Agricultural and Food Products for Quality Evaluation. International Journal of Computer Applications **1**:1-9.

Ndiema CKW, Manga PN, Ruttoh CR. 2002. Influence of die pressure on relaxation characteristics of briquetted biomass. Energy Conversion and Management **43**:2157-2161.

Ndindeng SA, Mbassi JEG, Mbacham WF, Manful J, Graham-Acquaah S, Moreira J, Dossou J, Futakuchi K. 2015. Quality optimization in briquettes made from rice milling by-products. Energy for Sustainable Development **29**:24-31.

Niazmand H, Renksizbulut M. 2003. Surface effects on transient three-dimensional flows around rotating spheres at moderate Reynolds numbers. Computers and Fluids **32**(10):1405-1433.

Novotný R. 2017. Analysis of briquettes' production process from different biomass materials [MSc Thesis]. Czech University of Life Sciences, Prague.

NREL. 2008. Chemical Analysis and Testing Laboratory Analytical Procedures. National Renewable Energy Laboratory: Golden, CO, USA. Available from https://www.nrel.gov/bioenergy/biomasscompositional-analysis.html (accessed on March 2017).

Nzihou A, Stanmore B. 2013. The fate of heavy metals during combustion and gasification of contaminated biomass-A brief review. Hazardous Materials **256-257**:56-66.

Obernberger I, Thek G. 2004. Physical characterisation and chemical composition of densified biomass fuels with regard to their combustion behaviour. Biomass and Bioenergy **27**:653-669.

Obidziński S, Dołżyńska M, Stasieluk W. 2019. Production of fuel pellets from a mixture of sawdust and rye bran. 2nd International Conference on the Sustainable Energy and Environmental Development. IOP Publishing, Krakow, Poland, pp. 1-10.

Oh Y-K, Hwang K-R, Kim C, Kim JR, Lee J-S. 2018. Recent developments and key barriers to advanced biofuels: A short review. Bioresource Technology **257**:320-333.

Okot DK, Bilsborrow PE, Phan AN. 2018. Effects of operating parameters on maize COB briquette quality. Biomass and Bioenergy **112**:61-72.

Oladeji J, Enweremadu C 2012. The Effects of Some Processing Parameters on Physical and Densification Characteristics of Corncob Briquettes. International Journal of Energy Engineering **2**:22-27.

Oladokun O, Ahmad A, Abdullah TAT, Nyakuma BB, Bello AA-H, Al-Shatri AH. 2016. Multicomponent devolatilization kinetics and thermal conversion of Imperata cylindrica. Applied Thermal Engineering **105**:931-940.

Olson E. 2011. Particle Shape Factors and Their Use in Image Analysis–Part 1: Theory. Journal of GXP Compliance **15**(3):85-96.

Ozen M, Guler M. 2014. Assessment of optimum threshold and particle shape parameter for the image analysis of aggregate size distribution of concrete sections. Optics and Lasers in Engineering **53**:122-132.

ÖNORM M 7135 (2000): Compressed wood or compressed bark in natural state - Pellets and briquettes - Requirements and test specifications. Austrian Standard (in German).

Özyuğuran A, Yaman S. 2017. Prediction of Calorific Value of Biomass from Proximate Analysis. Energy Procedia **107**:130-136.

Pace B, Cavallo DP, Cefola M, Colella R, Attolico G. 2015. Adaptive self-configuring computer vision system for quality evaluation of fresh-cut radicchio. Innovative Food Science & Emerging Technologies **32**:200-207.

Pampuro N, Busato P, Cavallo E. 2018. Effect of Densification Conditions on Specific Energy Requirements and Physical Properties of Compacts Made from Hop Cone. Energies **11**:1-10.

Pan L, Sun Y, Xiao H, Gu X, Hu P, Wei Y, Tu K. 2017. Hyperspectral imaging with different illumination patterns for the hollowness classification of white radish. Postharvest Biology and Technology **126**:40-49.

Pari L, Suardi A, Longo L, Carnevale M, Gallucci F. 2018. Jatropha curcas, L. Pruning Residues for Energy: Characteristics of an Untapped By-Product. Energies **11**:1622.

Parikh J, Channiwala SA, Ghosal GK. 2005. A correlation for calculating HHV from proximate analysis of solid fuels. Fuel **84**:487-494.

Patel A, Pravez M, Deeba F, Pruthi V, Singh RP, Pruthi PA. 2014. Boosting accumulation of neutral lipids in Rhodosporidium kratochvilovae HIMPA1 grown on hemp (Cannabis sativa Linn) seed aqueous extract as feedstock for biodiesel production. Bioresource Technology **165**:214-222.

Paulrud S, Mattsson JE, Nilsson C. 2002. Particle and handling characteristics of wood fuel powder: effects of different mills. Fuel Processing Technology **76**:23-39.

Pérez J, Muñoz-Dorado J, de la Rubia T, Martínez J. 2002. Biodegradation and biological treatments of cellulose, hemicellulose and lignin: an overview. Guerrero R, editor. International Microbiology. Springer, New York.

Persson A-L. 1998. Image analysis of shape and size of fine aggregates. Engineering Geology **50**:177-186.

Picchi G, Lombardini C, Pari L, Spinelli R. 2018. Physical and chemical characteristics of renewable fuel obtained from pruning residues. Journal of Cleaner Production **171**:457-463.

Pickering KL, Beckermann GW, Alam SN, Foreman, NJ. 2007. Optimising industrial hemp fibre for composites. Composites Part A: Applied Science and Manufacturing **38**(2):461-468.

Pickering KL, Efendy MGA, Le TM. 2016. A review of recent developments in natural fibre composites and their mechanical performance. Composites Part A: Applied Science and Manufacturing **83**:98-112.

Pickering KL, Priest M, Watts T, Beckermann G, Alam SN. 2005. Feasibility study for NZ hemp fibre composites. Journal of Advanced Materials **37**(3):15-20.

Pidlisnyuk V, Erickson L, Stefanovska T, Popelka J, Hettiarachchi G, Davis L, Trögl J. 2019. Potential phytomanagement of military polluted sites and biomass production using biofuel crop miscanthus x giganteus. Environmental Pollution **249**:330-337.

Pietsch W. 2002. Agglomeration Processes: Phenomena, Technologies, Equipment. Wiley-VCH, Weinheim.

Pietsch W. 2003. An interdisciplinary approach to size enlargement by agglomeration. Powder Technology **130**:8-13.

Pirraglia A, Gonzalez R, Saloni D, Denig J. 2013. Technical and economic assessment for the production of torrefied ligno-cellulosic biomass pellets in the US. Energy Conversion and Management **66**:153-164.

Plíštil D, Brožek M, Malaťák J, Roy A, Hutla P. 2005. Mechanical characteristics of standard fuel briquettes on biomass basis. Research in Agriculture Engineering **51**:66-72.

Poddar S, Kamruzzaman M, Sujan SMA, Hossain M, Jamal MS, Gafur MA, Khanam M. 2014. Effect of compression pressure on lignocellulosic biomass pellet to improve fuel properties: Higher heating value. Fuel **131**:43-48.

Poiša L, Adamovičs A, Jankauskiene Z, Gruzdeviene E. 2010. Industrial hemp (*Cannabis sativa* L.) as a biomass crop // treatment and use of organic residues in agriculture: challenges and opportunities towards sustainable management. 14th Ramiran International Conference of the FAO ESCORENA Network on the Recycling in Agricultural, Lisboa, Portugal, pp. 326-330.

Pons M-N, Dodds J. 2015. Chapter Fifteen - Particle Shape Characterization by Image Analysis. Progress in Filtration and Separation 609-636.

Popp J, Lakner Z, Harangi-Rákos M, Fári M. 2014. The effect of bioenergy expansion: Food, energy, and environment. Renewable and Sustainable Energy Reviews **32**:559-578.

Portugal-Pereira J, Nakatani J, Kurisu K, Hanaki K. 2016. Life cycle assessment of conventional and optimised Jatropha biodiesel fuels. Renewable Energy **86**:585-593.

Pothula AK, Igathinathane C, Kronberg S, Hendrickson J. 2014. Digital image processing based identification of nodes and internodes of chopped biomass stems. Computers and Electronics in Agriculture **105**:54-65.

Powers MC. 1953. A new roundness scale for sedimentary particles. Journal of Sedimentary Research 117-119.

Prade T, Svensson S-E, Andersson A, Mattsson JE. 2011. Biomass and energy yield of industrial hemp grown for biogas and solid fuel. Biomass and Bioenergy **35**:3040-3049.

Prade T, Svensson S-E, Mattsson JE. 2012. Energy balances for biogas and solid biofuel production from industrial hemp. Biomass and Bioenergy **40**:36-52.

Pradhan P, Mahajani SM, Arora A. 2018. Production and utilization of fuel pellets from biomass: A review. Fuel Processing Technology **181**:215-232.

Puig-Arnavat M, Shang L, Sárossy Z, Ahrenfeldt J, Henriksen UB. 2016. From a single pellet press to a bench scale pellet mill - Pelletizing six different biomass feedstocks. Fuel Processing Technology **142**:27-33.

Qin X, Keefe FR, Daugaard ED. 2018. Small Landowner Production of Pellets from Green, Beetle-Killed, and Burned Lodgepole Pine. Energies **11**(3):1-14.

Rady A, Ekramirad N, Adedeji AA, Li M, Alimardani R. 2017. Hyperspectral imaging for detection of codling moth infestation in GoldRush apples. Postharvest Biology and Technology **129**:37-44.

Rahaman SA, Salam PA. 2017. Characterization of cold densified rice straw briquettes and the potential use of sawdust as binder. Fuel Processing Technology **158**:9-19.

Rajaseenivasan T, Srinivasan V, Syed Mohamed Qadir G, Srithar K. 2016. An investigation on the performance of sawdust briquette blending with neem powder. Alexandria Engineering Journal **55**:2833-2838.

Ramírez-Gómez Á, Gallego E, Fuentes JM, González-Montellano C, Ayuga F. 2014. Values for particle-scale properties of biomass briquettes made from agroforestry residues. Particuology **12**:100-106.

Reza MT, Lynam J, Vasquez VR, Coronella CJ. 2012. Pelletization of Biochar from Hydrothermally Carbonized Wood. Environmental Progress **31**(2):225-234.

Ribeiro E, Shah M. 2006. Computer vision for nanoscale imaging. Machine Vision and Applications **17**:147-162.

Richards S. 1990. Physical testing of fuel briquettes. Fuel Processing Technology **25**(2):89-100.

Riguidel F-X, Jullien R, Ristow GH, Hansen A, Bideau D. 1994. Behaviour of a sphere on a rough inclined plane. Journal de Physique I France **4**:261-272.

Roesch H, Dascomb J, Greska B, Krothapalli A, Author C. 2011. Prediction of producer gas composition for small scale commercial downdraft gasifiers. 19th European Biomass Conference and Exhibition, Berlin, Germany, pp. 1594-1601.

Roman KK, Świętochowski A. 2016. X-ray Analysis of Biomass Wood Briquette Structure. Agricultural Engineering **20**(1):147-154.

Rose JW, Cooper JR. 1977. Technical data on fuel, 7th ed. British National Committee of the World Energy Conference, Edinburgh.

Rost FWD. 1995. Fluorescence Microscopy, vol. II. Cambridge University Press, New York.

Rumpf H. 1962. The strength of granules and agglomeration. Pages 379-418 in Knepper WA, editor. Agglomeration. John Wiley, New York.

Rybak W, Morón W, Ferens W. 2019. Dust ignition characteristics of different coal ranks, biomass and solid waste. Fuel **237**(1):606-618.

Rynkiewicz M, Trávníček P, Krčálová E, Mareček J. 2013. Research paper: Influence of annealing temperature of straw briquettes on their density and hardness briquettes. Acta Universitatis Agriculturae Et Silviculturae Mendelianae Brunensis **61**:1377-1382.

Rytioja J, Hildén K, Yuzon J, Hatakka A, de Vries RP, Mäkelä MR. 2014. Plant-Polysaccharide-Degrading Enzymes from Basidiomycetes. Microbiology and molecular biology reviews **78**:614-649.

Saastamoinen JJ. 2006. Simplified model for calculation of devolatilization in fluidized beds. Fuel **85**:2388-2395.

Saikia M, Baruah D. 2013. Analysis of Physical Properties of Biomass Briquettes Prepared by Wet Briquetting Method. Engineering Research and Development **6**:12-14.

Sarkar P, Bosneaga E, Auer M. 2009. Plant cell walls throughout evolution: towards a molecular understanding of their design principles. Journal of Experimental Botany **60**:3615-3635

Sastry KVS, Fuerstenau DW. 1973. Mechanisms of agglomerate growth in green pelletization. Powder Technology **7**:97-105.

Sawadogo M, Tchini Tanoh S, Sidibé S, Kpai N, Tankoano I. 2018. Cleaner production in Burkina Faso: Case study of fuel briquettes made from cashew industry waste. Journal of Cleaner Production **195**:1047-1056.

Scarlat N, Dallemand J-F, Monforti-Ferrario F, Banja M, Motola V. 2015. Renewable energy policy framework and bioenergy contribution in the European Union – An overview from National Renewable Energy Action Plans and Progress Reports. Renewable and Sustainable Energy Reviews **51**:969-985.

Scheller HV, Ulvskov P. 2010. Hemicelluloses. Annual review of plant biology **61**:263-289.

Schmitt VEM, Kaltschmitt M. 2013. Effect of straw proportion and Ca- and Al-containing additives on ash composition and sintering of wood–straw pellets. Fuel **109**:551-558.

Sette Jr. CR, Hansted ALS, Novaes E, Lima PAFe, Rodrigues AC, Santos DRdS, Yamaji FM. 2018. Energy enhancement of the eucalyptus bark by briquette production. Industrial Crops and Products **122**:209-213.

Shah S, Kishen JC. 2011. Fracture properties of concrete–concrete interfaces using digital image correlation. Experimental mechanics **51**:303-313.

Shanthi C, Kingsley Porpatham R, Pappa N. 2014. Image Analysis for Particle Size Distribution. International Journal of Engineering and Technology **6**:1340-1345.

Shaw M. 2008. Feedstock and process variables influencing biomass densification [MSc. Thesis]. University of Saskatchewan, Saskatoon.

Shaw MD, Tabil LG. 2007. Compression and relaxation characteristics of selected biomass grinds. ASAE Annual International Meeting. June 17–20, 2007, Minneapolis: ASAE. Paper No. 076183.

Shekunov BY, Chattopadhyay P, Tong HHY, CHow AHL. 2006. Particle Size Analysis in Pharmaceutics: Principles, Methods and Applications. Pharmaceutical Research **24:**203-227.

Sheng C, Azevedo JLT. 2005. Estimating the higher heating value of biomass fuels from basic analysis data. Biomass and Bioenergy **28**:499-507.

Shuma R, Madyira DM. 2017. Production of Loose Biomass Briquettes from Agricultural and Forestry Residues. Procedia Manufacturing **7**:98-105.

Singh RN. 2004. Equilibrium moisture content of biomass briquettes. Biomass and Bioenergy **26**:251-253.

Sluiter A, Hames B, Ruiz R, Scarlata C, Sluiter J, Templeton D, Crocker D. 2012. Determination of Structural Carbohydrates and Lignin in Biomass. Laboratory Analytical Procedure (LAP), NREL, 18p. Available from https://www.nrel.gov/docs/gen/fy13/42618.pdf (accessed on 15 December 2018).

Smith LN, Zhang W, Hansen MF, Hales IJ, Smith ML. 2018. Innovative 3D and 2D machine vision methods for analysis of plants and crops in the field. Computers in Industry **97**:122-131.

Song Y, Glasbey CA, Horgan GW, Polder G, Dieleman JA, van der Heijden GWAM. 2014. Automatic fruit recognition and counting from multiple images. Biosystems Engineering **118**:203-215.

Souček J. 2008. Drtiče, štěpkovače a řezačky pro úpravu rostlinné biomasy. RIAE, Prague, 55p (in Czech). Available from: http://www.vuzt.cz/svt/vuzt/publ/P2008/049.PDF (accessed on 3 March 2019).

Souza DOC, Menegalli FC. 2011. Image analysis: Statistical study of particle size distribution and shape characterization. Powder Technology **214**:57-63.

Spiers HM. 1962. Technical data on fuel, 6th edition. New York: Wiley.

Srivastava NSL, Narnaware SL, Makwana JP, Singh SN, Vahora S. 2014. Investigating the energy use of vegetable market waste by briquetting. Renewable Energy **68**:270-275.

Steenari B-M, Lundberg A, Pettersson H, Wilewska-Bien M, Andersson D. 2009. Investigation of Ash Sintering during Combustion of Agricultural Residues and the Effect of Additives. Energy & Fuels **23**:5655-5662.

Stelte W, Clemons C, Holm JK, Ahrenfeldt J, Henriksen UB, Sanadi AR. 2011a. Thermal transitions of the amorphous polymers in wheat straw. Industrial Crops and Products **34**:1053-1056.

Stelte W, Holm JK, Sanadi AR, Barsberg S, Ahrenfeldt J, Henriksen UB. 2011b. A study of bonding and failure mechanisms in fuel pellets from different biomass resources. Biomass and Bioenergy **35**:910-918.

Stolarski MJ, Szczukowski S, Tworkowski J, Krzyżaniak M, Gulczyński P, Mleczek M. 2013. Comparison of quality and production cost of briquettes made from agricultural and forest origin biomass. Renewable Energy **57**:20-26.

Strašil Z. 2005. Plodiny pro energetické využití vhodné do marginálních oblastí. Conferencec of Hospodaření v méně příznivých oblastech, VÚRV, Lukavec u Pacova, Czech republic (in Czech), pp. 45-49.

Stupavský V, Holý T. 2010. Brikety z biomasy - dřevěné, rostlinné, směsné brikety. Biom.cz, (in Czech). Available from http://biom.cz/cz/odborne-clanky/brikety-z-biomasy-drevene-rostlinne-smesne-brikety (accessed on April 2015).

Su Q, Kondo N, Li M, Sun H, Al Riza DF, Habaragamuwa H. 2018. Potato quality grading based on machine vision and 3D shape analysis. Computers and Electronics in Agriculture **152**:261-268.

Sun Y, Cheng J. 2002. Hydrolysis of lignocellulosic materials for ethanol production: a review. Bioresource Technology **83**:1-11.

Sunoj S, Igathinathane C, Jenicka S. 2018. Cashews whole and splits classification using a novel machine vision approach. Postharvest Biology and Technology **138**:19-30.

Sutrisno, Anggono W, Suprianto FD, Kasrun AW, Siahaan IH. 2017. The Effects of Particle Size and Pressure on the Combustion characteristics of *Cerbera Manghas* leaf Briquettes. ARPN Journal of Engineering and Applied Sciences **12**:931-936.

Svihus B, Kløvstad KH, Perez V, Zimonja O, Sahlström S, Schüller RB, Jeksrud WK, Prestløkken E. 2004. Physical and nutritional effects of pelleting of broiler chicken diets made from wheat ground to different coarsenesses by the use of roller mill and hammer mill. Animal Feed Science and Technology **117**:281-293.

Szulczewski W, Żyromski A, Jakubowski W, Biniak-Pieróg M. 2018. A new method for the estimation of biomass yield of giant miscanthus (*Miscanthus giganteus*) in the course of vegetation. Renewable and Sustainable Energy Reviews **82**:1787-1795.

Szyszlak-Bargłowicz J, Zarajczyk J. 2009. Timber waste as a source of energy. Commission of Motorization and Power Industry in Agriculture **9**:339–334.

Tan K, Lee WS, Gan H, Wang S. 2018. Recognising blueberry fruit of different maturity using histogram oriented gradients and colour features in outdoor scenes. Biosystems Engineering **176**:59-72.

Tembe ET, Azeh E, Ekhuemelo DO. 2017. Effect of Particle Size on Quality of Briquettes Produced from Sawdust of Daniella oliveiri and Gmelinaarborea in Makurdi, Benue State, Nigeria. Asian Research Journal of Agriculture **3**:1-7.

Temmerman M, Rabier F, Jensen PD, Hartmann H, Böhm T. 2006. Comparative study of durability test methods for pellets and briquettes. Biomass and Bioenergy **30**:964-972.

Thabuot M, Pagketanang T, Panyacharoen K, Mongkut P, Wongwicha P. 2015. Effect of Applied Pressure and Binder Proportion on the Fuel Properties of Holey Bio-Briquettes. Energy Procedia **79**:890-895.

Theis M, Skrifvars B-J, Hupa M, Tran H. 2006. Fouling tendency of ash resulting from burning mixtures of biofuels. Part 1: Deposition rates. Fuel **85**:1125-1130.

Thoreson PC, Webster EK, Darr JM, Kapler JE. 2014. Investigation of Process Variables in the Densification of Corn Stover Briquettes. Energies **7**(6):4019-4032.

Thy P, Jenkins BM, Lesher CE, Grundvig S. 2006. Compositional constraints on slag formation and potassium volatilization from rice straw blended wood fuel. Fuel Processing Technology **87**:383-408.

Timbal J, Bonneau M, Landmann G, Trouvilliez J, Bouhot-Delduc L. 2005. European Non-Boreal Conifer Forests. Pages 131-162 in Andersson FA, Goodall DW. Coniferous Forests. Elsevier, Amsterdam, The Netherlands.

Tortosa Masiá AA, Buhre BJP, Gupta RP, Wall TF. 2007. Characterising ash of biomass and waste. Fuel Processing Technology **88**:1071-1081.

Toscano G, Alfano V, Scarfone A, Pari L. 2018. Pelleting Vineyard Pruning at Low Cost with a Mobile Technology. Energies **11**(9):2477.

Tripathi A, Chhabra RP, Sundararajan T. 1994. Power low fluid flow over spheroidal particles. Industrial & Engineering Chemistry Research **33**:403-410.

Trubetskaya A, Beckmann G, Wadenbäck J, Holm JK, Velaga SP, Weber R. 2017. One way of representing the size and shape of biomass particles in combustion modeling. Fuel **206**:675-683.

Tumuluru JS. 2014. Effect of process variables on the density and durability of the pellets made from high moisture corn stover. Biosystems Engineering **119**:44-57.

Tumuluru JS. 2018. Effect of Moisture Content and Hammer Mill Screen Size on the Briquetting Characteristics of Woody and Herbaceous Biomass. Carbon Resources Conversion **1**:44-54.

Tumuluru JS, Sokhansanj S, Wright CT, Boardman RD, Yancey NA. 2011a. A Review on Biomass Classification and Composition, Co-Firing Issues and Pretreatment Methods. ASABE International Meeting, Paper No. 1110458, Idaho National Laboratory, Idaho.

Tumuluru JS, Tabil LG, Song Y, Iroba KL, Meda V. 2014. Grinding energy and physical properties of chopped and hammer-milled barley, wheat, oat, and canola straws. Biomass and Bioenergy **60**:58-67.

Tumuluru JS, Tabil LG, Song Y, Iroba KL, Meda V. 2015. Impact of process conditions on the density and durability of wheat, oat, canola, and barley straw briquettes. BioEnergy Research **8**:388-401.

Tumuluru JS, Wright CT, Hess JR, Kenney KL. 2011b. A review of biomass densification systems to develop uniform feedstock commodities for bioenergy application. Biofuels, Bioproducts and Biorefining **5**:683-707.

Tumuluru JS, Wright CT, Kenny KL, Hess JR. 2010. A Review on Biomass Densification Technology for Energy Application. Idaho National Laboratory, Idaho.

Tutt M, Olt J. 2011. Suitability of various plant species for bioethanol production. Agronomy Research **9**: 261-267.

Ulusoy U, Igathinathane C. 2016. Particle size distribution modeling of milled coals by dynamic image analysis and mechanical sieving. Fuel Processing Technology **143**:100-109.

Urbanovičová O, Koloman K, Findura P, Jobbágy J, Angelovič M. 2017. Physical and mechanical properties of briquettes produced from energy plants. Acta Universitatis Agriculturae et Silviculturae Mendelianae Brunensis **65**:219-224.

Vaezi M, Pandey V, Kumar A, Bhattacharyya S. 2013. Lignocellulosic biomass particle shape and size distribution analysis using digital image processing for pipeline hydro-transportation. Biosystems Engineering **114**:97-112.

Vassilev SV, Baxter D, Andersen LK, Vassileva CG. 2010. An overview of the chemical composition of biomass. Fuel **89**:913-933.

Vítěz T, Trávníček P. 2010. Particle size distribution of sawdust and wood shavings mixtures. Research in Agricultural Engineering **56**(4):154-158.

Väisänen T, Batello P, Lappalainen R, Tomppo L. 2018. Modification of hemp fibers (Cannabis Sativa L.) for composite applications. Industrial Crops and Products **111**:422-429.

Wadell HA. 1932. Volume, Shape and Roundness of Rock Particles. The Journal of Geology **40**:443-451.

Walpole LJ. 1972. The elastic behaviour of a suspension of spherical particles. The Quarterly Journal of Mechanics and Applied Mathematics **25**(2):153-160.

Wamukonya L, Jenkins B. 1995. Durability and relaxation of sawdust and wheat-straw briquettes as possible fuel for Keny. Biomass and Bioenergy **8**:175-179.

Wanat N, Austruy A, Joussein E, Soubrand M, Hitmi A, Gauthier-Moussard C, Lenain J-F, Vernay P, Munch JC, Pichon M. 2013. Potentials of *Miscanthus×giganteus* grown on highly contaminated Technosols. Journal of Geochemical Exploration **126-127**:78-84.

Wang L, Skjevrak G, Hustad JE, Grønli M, Skreiberg Ø. 2012. Effects of Additives on Barley Straw and Husk Ashes Sintering Characteristics. Energy Procedia **20**:30-39

Wang W. 2006. Image analysis of particles by modified Ferret method - best-fit rectangle. Powder Technology **165**:1-10.

Wang Y, Wu K, Sun Y. 2018a. Effects of raw material particle size on the briquetting process of rice straw. Journal of the Energy Institute **91**:153-162.

Wang Y, Zhou L, Wu Y, Yang Q. 2018b. New simple correlation formula for the drag coefficient of calcareous sand particles of highly irregular shape. Powder Technology **326**:379-392.

Wang Z, Liu R, Sparks T, Liu H, Liou F. 2015. Stereo vision based hybrid manufacturing process for precision metal parts. Precision Engineering **42**:1-5.

Werther J, Saenger M, Hartge E-U, Ogada T, Siagi Z. 2000. Combustion of agricultural residues. Progress in Energy and Combustion Science **26**:1-27.

Whittaker C, Shield I. 2017. Factors affecting wood, energy grass and straw pellet durability - A review. Renewable and Sustainable Energy Reviews **71**:1-11.

Williams O, Newbolt G, Eastwick C, Kingman S, Giddings D, Lormor S, Lester E. 2016. Influence of mill type on densified biomass comminution. Applied Energy **182**:219-231.

Wilk M, Magdziarz A. 2017. Hydrothermal carbonization, torrefaction and slow pyrolysis of *Miscanthus giganteus*. Energy **140**:1292-1304.

Womac AR, Yu M, Igathinathane C, Ye P, Hayes D, Narayan S, Sokhansanj S, Wright L. 2005. Shearing characteristics of biomass for size reduction. ASAE Paper No. 056058, St. Joseph, Michigan.

Wrobel M, Fraczek J, Francik S, Slipek Z, Krzysztof M. 2013. Influence of degree of fragmentation on chosen quality parameters of briquette made from biomass of cup plant *Silphium Perfoliatum* L. 12th International Scientific Conference of the Engineering for Rural Development, Jelgava, Latvia, pp. 653-657.

Xu J, Chang S, Yuan Z, Jiang Y, Liu S, Li W, Ma L. 2015. Regionalized Techno-Economic Assessment and Policy Analysis for Biomass Molded Fuel in China. Energies **8**(12):13846-13863.

Xue S, Lewandowski I, Wang X, Yi Z. 2016. Assessment of the production potentials of Miscanthus on marginal land in China. Renewable and Sustainable Energy Reviews **54**:932-943.

Yaman S, Şahan M, Haykiri-açma H, Şeşen K, Küçükbayrak S. 2000. Production of fuel briquettes from olive refuse and paper mill waste. Fuel Processing Technology **68**:23-31.

Yang H, Yan R, Chen H, Zheng C, Lee DH, Liang DT. 2006. In-Depth Investigation of Biomass Pyrolysis Based on Three Major Components: Hemicellulose, Cellulose and Lignin. Energy & Fuels **20**:388-393.

Yang Z, Peng X-F, Lee D-J, Chen M-Y. 2009. An image-based method for obtaining pore-size distribution of porous media. Environmental Science & Technology **43**:3248-3253.

Yank A, Ngadi M, Kok R. 2016. Physical properties of rice husk and bran briquettes under low pressure densification for rural applications. Biomass and Bioenergy **84**:22-30.

Young P. Kennas S. 2003. Feasibility and Impact Assessment of a Proposed Project to Briquette Municipal Solid Waste for Use as a Cooking Fuel in Rwanda. Intermediate Technology Consultants **1**:1-59.

Yuan H, Pang Y, Wang K, Liu Y, Zuo X, Ma S, Li X. 2010. Ignition and Emission Characteristics of Ignition-assisting Agents for Densified Corn Stover Briquette Fuel. Chinese Journal of Chemical Engineering **18**:687-694.

Yumak H, Ucar T, Seyidbekiroglu N. 2010. Briquetting soda weed (*Salsola tragus*) to be used as a rural fuel source. Biomass and Bioenergy **34**:630-636.

Zainuddin MF, Rosnah S, Noriznan MM, Dahlan I. 2014. Effect of Moisture Content on Physical Properties of Animal Feed Pellets from Pineapple Plant Waste. Agriculture and Agricultural Science Procedia **2**:224-230.

Zeng XY, Ma YT, Ma LR. 2007. Utilization of straw in biomass energy in China. Renewable and Sustainable Energy Reviews **11**:976-987.

Zeng Y, Zhao S, Yang S, Ding A-Y. 2014. Lignin plays a negative role in the biochemical process for producing lignocellulosic biofuels. Current Opinion in Biotechnology **27**:38-45.

Zevenhoven M. 2010. Ash Forming Matter in Biomass Fuels. Department of Chemical Engineering. Process Chemistry Group, Åbo Akademi University, Åbo, Finland.

Zhang G, Sun Y, Xu Y. 2018. Review of briquette binders and briquetting mechanism. Renewable and Sustainable Energy Reviews **82**:477-487.

Zhang J, Guo Y. 2014. Physical properties of solid fuel briquettes made from *Caragana korshinskii* Kom. Powder Technology **256**:293-299.

Zhao B, Wang J. 2016. 3D quantitative shape analysis on form, roundness, and compactness with μCT. Powder Technology **291**:262-275.

Zhao Y, Zhang Y, Zhang H, Wang Q, Guo Y. 2015. Structural characterization of carbonized briquette obtained from anthracite powder. Journal of Analytical and Applied Pyrolysis **112**:290-297.

Zhou Y, Zhang Z, Zhang Y, Wang Y, Yu Y, Ji F, Ahmad R, Dong R. 2016. A comprehensive review on densified solid biofuel industry in China. Renewable and Sustainable Energy Reviews **54**:1412-1428.

Zvicevicius E, Raila A, Bartusevicius V, Endzelis T. 2013. Impact of straw fractional composition on briquette quality. 12th International Scientific Conference of the Engineering for Rural Development, Jelgava, Latvia, pp. 494-498.

# 9. Annex

## List of Annexes

**Annex 1.**



**Annex 2.**

## Annex 1.

**Table I.** Tests of homogeneity of variances: Levene's test

| | Effect: Material<br>Degrees of freedom for all F's: 2, 4497<br>MS | MS | F | p |
|---|---|---|---|---|
| Area | 148698379694269 | 1782367580470.42 | 83.42745 | <0.01 |
| | **Effect: Fraction**<br>**Degrees of freedom for all F's: 2, 4497**<br>**MS** | **MS** | **F** | **p** |
| Area | 270637402852936 | 1697422013733.01 | 159.4403 | <0.01 |
| | **Effect: Point**<br>**Degrees of freedom for all F's: 9, 4490**<br>**MS** | **MS** | **F** | **p** |
| Area | 39765893463968 | 1742542604394.73 | 22.82061 | <0.01 |
| | **Effect: Material**<br>**Degrees of freedom for all F's: 2, 4497**<br>**MS** | **MS** | **F** | **p** |
| Max feret | 55152011 | 755464.0 | 73.00415 | <0.01 |
| | **Effect: Fraction**<br>**Degrees of freedom for all F's: 2, 4497**<br>**MS** | **MS** | **F** | **p** |
| Max feret | 82236508 | 721393.3 | 113.9968 | <0.01 |
| | **Effect: Point**<br>**Degrees of freedom for all F's: 9, 4490**<br>**MS** | **MS** | **F** | **p** |
| Max feret | 10858047 | 729783.6 | 14.87845 | <0.01 |

**Table II.** Bulk density of studied materials and fractions

| | Unit | Miscanthus | Hemp | Pine sawdust |
|---|---|---|---|---|
| **4 mm** | $kg.m^{-3}$ | 109.00 | 80.00 | 159.67 |
| **8 mm** | $kg.m^{-3}$ | 103.00 | 73.70 | 149.67 |
| **12 mm** | $kg.m^{-3}$ | 84.30 | 71.00 | 145.00 |

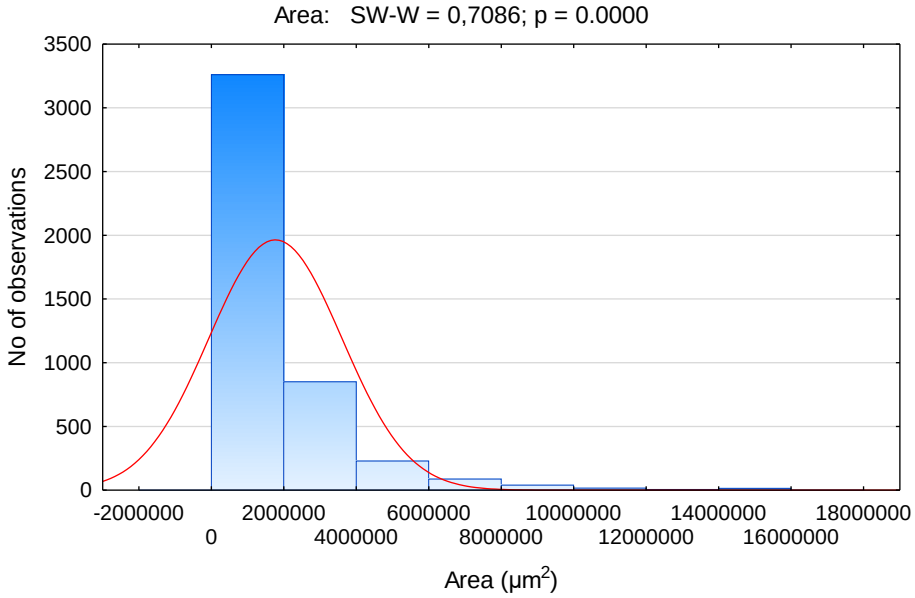


**Figure I.** Histogram of Area variable

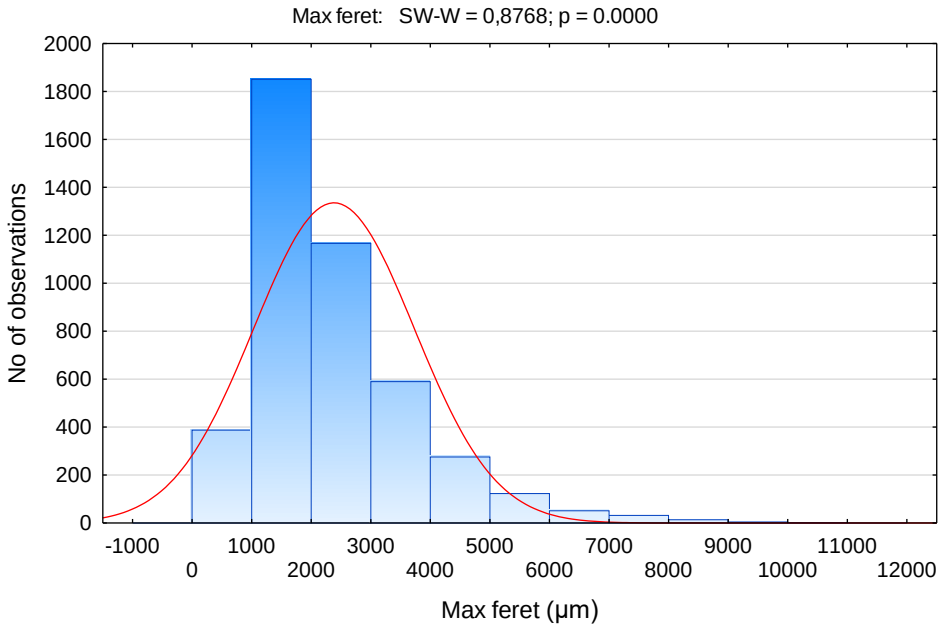


**Figure II.** Histogram of Max feret variable


**Figure III.** Detailed image of area and max feret measurement

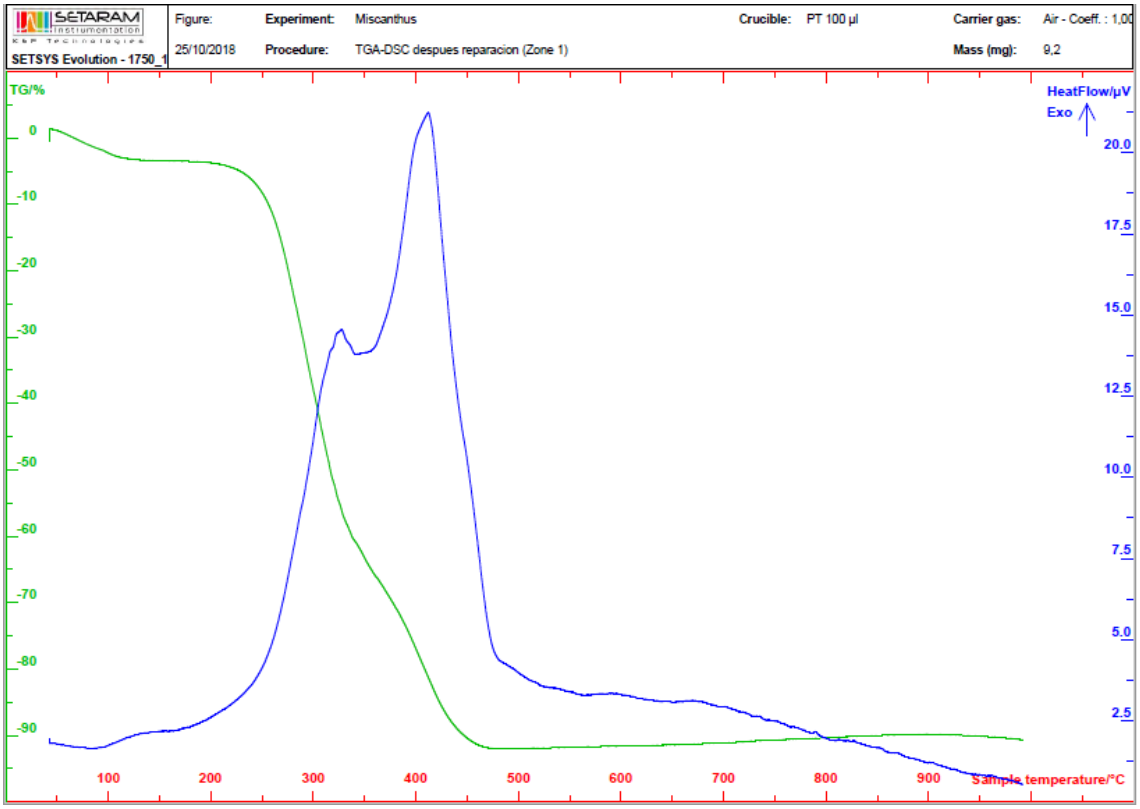


**Figure IV.** TGA graph of miscanthus

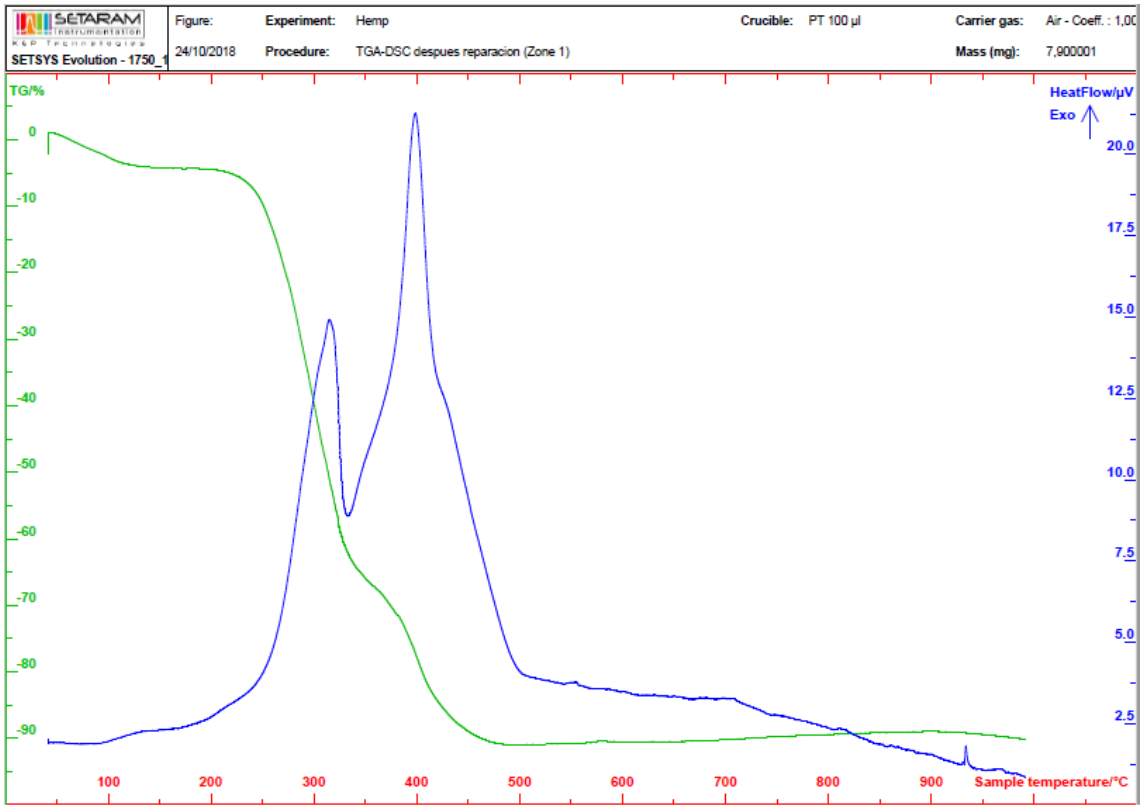


**Figure V.** TGA graph of hemp

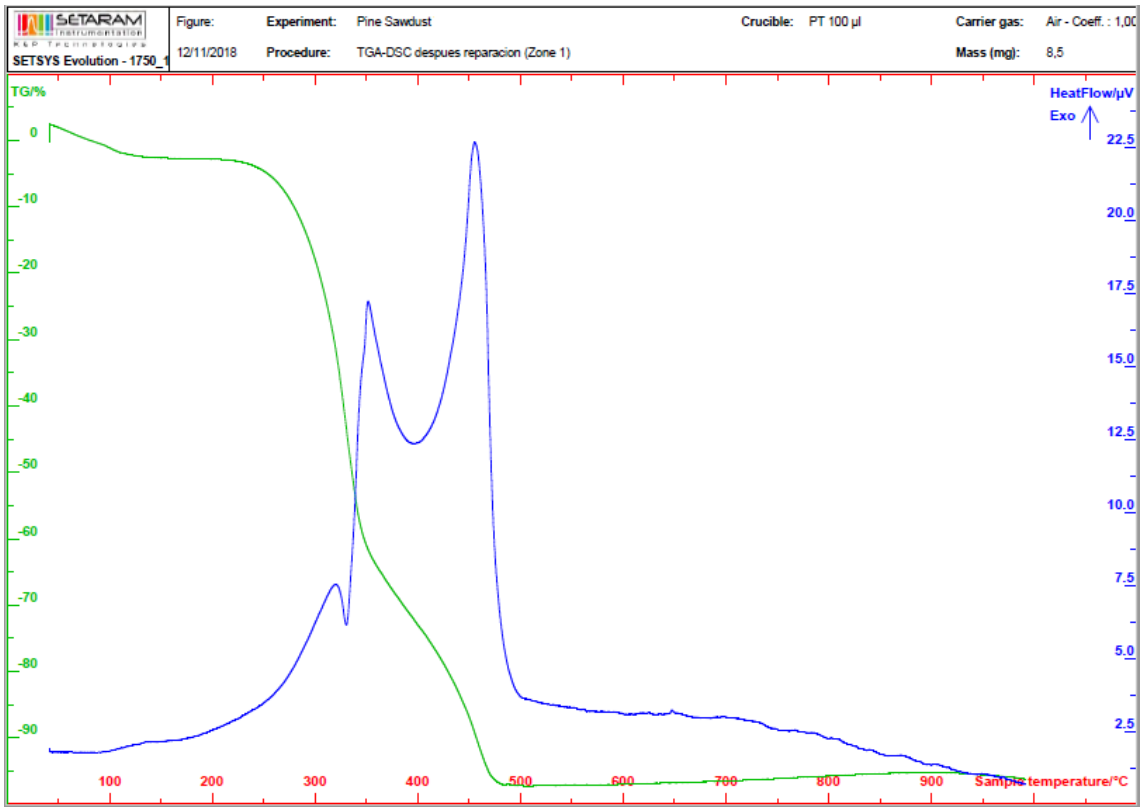


**Figure VI.** TGA graph of pine sawdust

# Annex 2.

## List of Author's publications

### Article with IF index

- **Chaloupková V**, Ivanova T, Ekrt O, Kabutey A, Herák D. 2018. Determination of Particle Size and Distribution through Image-Based Macroscopic Analysis of the Structure of Biomass Briquettes. **Energies** 11(2), 331:1-13.

### Articles with SJR index

- **Chaloupková V**, Ivanova T, Krepl V. 2019. Particle size and shape characterization of feedstock material for biofuel production. **Agronomy Research 17(X):**xxx-ccc, available from https://doi.org/10.15159/ar.19.152.
- **Chaloupková V**, Ivanova T, Muntean A. 2018. Particle size distribution analysis of pine sawdust: comparison of traditional oscillating screen method and photo-optical analysis. **Agronomy Research** 16(5):1966-1975.

### Article in conference proceedings (WoS)

- **Chaloupková V**, Ivanova T, Havrland B. 2016. Sieve Analysis of Biomass: Accurate Method for Determination of Particle Size Distribution. 15th International Scientific Conference of the Engineering for Rural Development, Jelgava, Latvia, pp. 1012-1017.